AFWAL-TR-85-3062

STOCHASTIC CRACK PROPAGATION WITH APPLICATIONS TO DURABILITY AND DAMAGE TOLERANCE ANALYSES

J.N. Yang and W.H. Hsi
School of Engineering and Applied Science
The George Washington University
Washington, D.C. 20052

S.D. Manning
General Dynamics Corporation
Fort Worth Division
Fort Worth, TX 76101

September 1985

FINAL REPORT JUNE 1983 - FEBRUARY 1985

FLIGHT DYNAMICS LABORATORY
AIR FORCE WRIGHT AERONAUTICAL LABORATORIES
AIR FORCE SYSTEMS COMMAND
WRIGHT-PATTERSON AIR FORCE BASE, OHIO 45433

NOTICE

When Government drawings, specifications, or other data are used for any purpose other than in connection with a definitely related Government procurement operation, the United States Government thereby incurs no responsibility nor any obligation whatsoever; and the fact that the government may have formulated, furnished, or in any way supplied the said drawings, specifications, or other data, is not to be regarded by implication or otherwise as in any manner licensing the holder or any other person or corporation, or conveying any rights or permission to manufacture use, or sell any patented invention that may in any way be related thereto.

This report has been reviewed by the Office of Public Affairs (ASD/PA) and is releasable to the National Technical Information Service (NTIS). At NTIS, it will be available to the general public, including foreign nations.

This technical report has been reviewed and is approved for publication.

JAMES L. RUDD
Project Engineer

FRANK D. BOENSCH, Chief
Structural Integrity Branch
Structures & Dynamics Division

FOR THE COMMANDER

ROGER J. HEGSTROM, Colonel, USAF
Chief, Structures & Dynamics Division

"If your address has changed, if you wish to be removed from our mailing list, or if the addressee is no longer employed by your organization please notify AFWAL/FIBEC, *W-PAFB, OH 45433 to help us maintain a current mailing list".*

Copies of this report should not be returned unless return is required by security considerations, contractual obligations, or notice on a specific document.

UNCLASSIFIED

SECURITY CLASSIFICATION OF THIS PAGE

ADA 168040

REPORT DOCUMENTATION PAGE

1a. REPORT SECURITY CLASSIFICATION: Unclassified	1b. RESTRICTIVE MARKINGS:
2a. SECURITY CLASSIFICATION AUTHORITY: N/A	3. DISTRIBUTION/AVAILABILITY OF REPORT: Approved for public release; distribution unlimited.
2b. DECLASSIFICATION/DOWNGRADING SCHEDULE: N/A	
4. PERFORMING ORGANIZATION REPORT NUMBER(S):	5. MONITORING ORGANIZATION REPORT NUMBER(S): AFWAL-TR-85-3062
6a. NAME OF PERFORMING ORGANIZATION: George Washington University; 6b. OFFICE SYMBOL (If applicable):	7a. NAME OF MONITORING ORGANIZATION: Air Force Wright Aeronautical Laboratories Flight Dynamics Laboratory (AFWAL/FIBEC)
6c. ADDRESS (City, State and ZIP Code): School of Engineering and Applied Science Washington, DC 20052	7b. ADDRESS (City, State and ZIP Code): Wright-Patterson AFB, OH 45433
8a. NAME OF FUNDING/SPONSORING ORGANIZATION: Flight Dynamics Laboratory; 8b. OFFICE SYMBOL (If applicable): AFWAL/FIBEC	9. PROCUREMENT INSTRUMENT IDENTIFICATION NUMBER: F33615-83-K-3226
8c. ADDRESS (City, State and ZIP Code): Wright-Patterson AFB, OH 45433	10. SOURCE OF FUNDING NOS.

PROGRAM ELEMENT NO.	PROJECT NO.	TASK NO.	WORK UNIT NO.
61102F	2307	N1	21

11. TITLE (Include Security Classification): See reverse

12. PERSONAL AUTHOR(S): Yang, J.N., Hsi, W.H., and Manning, S.D.

13a. TYPE OF REPORT	13b. TIME COVERED	14. DATE OF REPORT (Yr., Mo., Day)	15. PAGE COUNT
Final	FROM June 83 TO Feb.85	September 1985	268

16. SUPPLEMENTARY NOTATION

17. COSATI CODES			18. SUBJECT TERMS (Continue on reverse if necessary and identify by block number)
FIELD	GROUP	SUB. GR.	

19. ABSTRACT (Continue on reverse if necessary and identify by block number)

Various stochastic models for fatigue crack propagation under either constant amplitude or spectrum loadings have been investigated. These models are based on the assumption that the crack growth rate is a lognormal random process, including the general lognormal random process, lognormal white noise process, lognormal random variable, and second moment approximations, such as Weibull, gamma, lognormal and Gaussian closure approximations. Extensive experimental data have been used for the correlation study with various stochastic models. These include fastener hole specimens under fighter or bomber spectrum loadings and center-cracked specimens under constant amplitude loads. The data sets for the fastener hole specimens cover adequately different loading conditions, environments, load transfers and crack size range. It is shown that the white noise process is definitely not a valid model for fatigue crack propagation.

20. DISTRIBUTION/AVAILABILITY OF ABSTRACT	21. ABSTRACT SECURITY CLASSIFICATION
UNCLASSIFIED/UNLIMITED ☐ SAME AS RPT. ☒ DTIC USERS ☐	Unclassified

22a. NAME OF RESPONSIBLE INDIVIDUAL	22b. TELEPHONE NUMBER (Include Area Code)	22c. OFFICE SYMBOL
J. Rudd	513-255-6104	AFWAL/FIBEC

DD FORM 1473, 83 APR EDITION OF 1 JAN 73 IS OBSOLETE.

Unclassified

SECURITY CLASSIFICATION OF THIS PAGE

BLOCK 11: Title

STOCHASTIC CRACK PROPAGATION WITH APPLICATIONS TO DURABILITY AND DAMAGE TOLERANCE ANALYSES

A method of analysis for the general lognormal random process model has been developed using the Monte Carlo simulation approach. The model is demonstrated to be very flexible and it correlates excellently with all the experimental data considered. Various second moment approximation models are new models proposed in this report. The analysis procedures for these new models are quite simple and their correlations with all the test results are very satisfactory.

The lognormal random variable model is a special case of the lognormal random process model, in which the correlation distance is infinity. The model correlates very well with all the experimental results of fastener hole specimens under spectrum loadings. The lognormal random variable model is recommended for practical applications due to the following reasons: (i) it is mathematically very simple for applications including analysis and design requirements, (ii) it is of conservative nature, (iii) it may reflect closely the crack growth behavior in the real structure in service, and (iv) it does not require the correlation distance parameter, such that a small number of replicate specimens is adequate. In practical applications, test results usually are not plentiful and hence the lognormal random variable model is very appropriate.

In using the base-line crack propagation data for statistical crack growth analyses, the importance of having an equal number of data points for each specimen has been demonstrated. Adjustment is suggested by adding additional data points artificially, if the available data set does not contain an equal number of data points for each specimen. In converting the crack propagation data into the crack growth rate data for analysis purposes, additional undesireble statistical variability is introduced by the data processing procedures. The five point incremental polynomial method is recommended over the direct secant and modified secant methods. This is because the latter two methods introduce much larger additional statistical dispersion into the crack growth rate data.

Based on the recommended lognormal random variable crack growth rate model and the equivalent initial flaw size (EIFS) concept, a stochastic-based initial fatigue quality (IFQ) model has been described and evaluated for the durability analysis of relatively small cracks in fastener holes (e.g., <0.1"). Procedures have been presented and evaluated for optimizing initial flaw size distribution parameters based on pooled EIFS results. Expressions have been developed for predicting the cumulative distribution of crack size at any given time and the cumulative distribution of times to reach any given crack size. The predictions compare well with the actual test results in the small crack size region. However, further research is needed for durability analysis applications in the large crack size region.

A fatigue reliability analysis methodology has been developed for structural components under scheduled inspection and repair maintenance in service. Emphasis is placed on the non-redundant components based on the slow crack growth design requirements. The methodology takes into account the statistical variabilities of the initial fatigue quality, crack propagation rates, service load spectra, nondestructive evaluation (NDE) systems, etc. The significant effect of the NDE system as well as the scheduled inspection maintenance on the fatigue reliability of structural components have been illustrated. An example is worked out to demonstrate the application of the methodology developed.

TABLE OF CONTENTS

TABLE OF CONTENTS

TABLE OF CONTENTS

List of Tables

List of Figures

List of Figures
(continued)

List of Figures
(continued)

List of Figures
(continued)

List of Figures
(continued)

List of Figures
(continued)

List of Figures
(continued)

List of Figures
(continued)

List of Figures
(continued)

List of Figures
(continued)

List of Figures
(continued)

List of Figures
(continued)

List of Figures
(continued)

CHAPTER 1

INTRODUCTION

From the fracture mechanics standpoint, fatigue failure of a metallic component results from the propagation of a dominant crack to its critical size. Hence, the crack propagation analysis is one of the major tasks in the design and life prediction of fatigue-critical structures, such as airframes, gas turbine engine components, and helicopter structures, just to mention a few. Durability and damage tolerance are two major design requirements for aircraft structures, in which the prediction of fatigue crack growth damage accumulation is one of the most important tasks [Refs. 1-6].

Experimental test results indicate that the fatigue crack propagation involves considerable statistical variability. Such a variability should be taken into account appropriately in the analysis and design of fatigue-critical components. As a result, probabilistic approaches to deal with the fatigue crack propagation have received considerable attention recently, and some statistical models have been proposed in the literature [e.g., Refs. 7-28].

Unfortunately, the statistical variability of the crack growth rate seems to vary with respect to many parameters, such as materials, amounts of load transfer in fastener holes, types of specimens, magnitude of constant amplitude loads,

types of spectrum loadings, ranges of crack size, environmental conditions, etc. For instance, the crack growth rate dispersion for specimens under constant amplitude loadings differs from that under spectrum loadings. The variability in crack growth damage accumulation for fastener hole specimens with natural cracks (starting from time to crack initiation) differs also from that of preflawed specimens. For practical analysis and design purposes, test results as close to the service loading environments as possible are highly desirable, and the statistical model should be established based on the correlation with test data thus obtained.

From the standpoint of practical applications, any stochastic model for the fatigue crack propagation should be as simple as possible while maintaining a reasonable accuracy for the prediction of the fatigue crack growth damage accumulation. The purposes of this report are as follows: (i) to investigate and examine simple stochastic models proposed in the literature for practical applications, (ii) to propose several new stochastic crack propagation models and to demonstrate their validity by correlating with extensive experimental test results, (iii) to recommend a most appropriate stochastic model for practical applications in aircraft structures, (iv) to investigate factors affecting the accuracy of stochastic crack propagation analysis, including the data processing procedures for obtaining the crack growth rate data and the number of fractographic data points for each specimen, (v) to apply the recommended stochastic crack growth model to

possible durability analysis of aircraft structures, and (vi) to investigate possible applications to probabilistic damage tolerance analysis as well as the fatigue reliability analysis of non-redundant structural components under scheduled inspection and repair maintenance.

On the basis of fracture mechanics, the stochastic crack propagation model should be built upon the crack growth rate descriptions. Hence the fracture mechanics parameters and the model statistics should be estimated from available crack growth rate data. Base-line crack growth rate data are obtained from the measurements of crack size versus cycle (or flight hour) using various data reduction methods, such as the direct secant, modified secant, and 5, 7 and 9 point incremental polynomial methods. Unfortunately, different data processing procedures result in different statistical dispersion for the crack growth rate data [e.g., 29-36]. Furthermore, bias in determining the crack growth rate parameters using the derived crack growth rate data may be induced by unequal number of data points associated with each test specimen. As a result, the effects of the data processing procedure and the number of data points (measurements) for each specimen on the overall probabilistic prediction of crack growth damage accumulation are investigated.

Metallic airframes contain thousands of fastener holes which are susceptible to fatigue cracking in service. The accumulation of relatively small fatigue cracks in fastener holes (e.g., 0.03" - 0.05") must be accounted for in the

design of aircraft structures to assure that the structure will be durable and can be economically maintained [2,4 and 5]. In this report an initial fatigue quality (IFQ) model, based on stochastic crack growth and the equivalent initial flaw size (EIFS) concept, is described and evaluated for the durability analysis of relatively small fatigue cracks in fastener holes (e.g. $\leq$ 0.10"). Procedures and concepts are also described and evaluated for optimizing the equivalent initial flaw size (EIFS) distribution parameters based on pooled EIFS results. Fatigue crack growth results for 7475-T7351 aluminum fastener holes under fighter and bomber load spectra are used to evaluate the proposed IFQ model and model calibration procedures. The cumulative distribution of crack size at any given time and the cumulative distribution of the time-to-crack initiation (TTCI) at any given crack size are predicted using the derived EIFS distribution and a stochastic crack growth approach. Predictions compared well with actual test results in the small crack size region. The methods described are promising for durability analysis application.

Based on a stochastic crack propagation model and the distribution of the equivalent initial flaw size (EIFS), a fatigue reliability analysis methodology is presented for non-redundant structural components under scheduled inspection and repair maintenance in service. Emphasis is placed on the airframe components in which fastener holes are critical locations. The significant effect of the nondestruc-

tive evaluation (NDE) system as well as the scheduled inspection maintenance on the fatigue reliability of structural components is illustrated. A numerical example for the crack propagation in fastener holes of a F-16 lower wing skin is presented to demonstrate the application of the developed analysis methodology.

In Chapter 2 the validity and practicality of simple stochastic crack growth models proposed in the literature are investigated using extensive fatigue crack growth data of fastener hole specimens. While the general lognormal random process model has been proposed in the literature [Refs. 16-21,25-26], the method of analysis has not been established, and its advantage has not been demonstrated by experimental test results. These tasks are accomplished in Chapter 2. In Chapter 3, several new stochastic models using the second moment approximation approach are proposed, investigated, and verified by experimental test results using fastener hole specimens. In Chapter 4 stochastic crack growth behavior in center-cracked specimens are investigated using various models studied in Chapters 2 and 3. In Chapter 5 the effect of data processing procedures and the required number of fractographic readings for each specimen on the stochastic crack growth analysis results are investigated. Chapter 6 presents the applications of a recommended stochastic crack growth model to durability analysis. In Chapter 7, possible applications of a recommended stochastic crack growth model to the fatigue

reliability analysis of structural components under scheduled inspection and repair maintenance are presented. Conclusions and recommendations are made in Chapter 8.

CHAPTER 2

STOCHASTIC MODELS FOR FATIGUE CRACK PROPAGATION

2.1 Stochastic Crack Propagation Model

Various fatigue crack growth rate functions have been proposed in the literature [e.g., Refs. 37-42]. These functions can be represented by a general form

$$\frac{da(t)}{dt} = L(\Delta K, K_{max}, R, S, a) \tag{1}$$

in which $L(\Delta K, K_{max}, R, S, a)$ = a non-negative function, t = time or cycle, a(t) = crack size at t, ΔK = stress intensity factor range, K_{max} = maximum stress intensity factor, R = stress ratio, and S = maximum stress level in the loading spectrum.

Some commonly used crack growth rate functions, such as Paris-Erdogan model [41], Forman model [42], and hyperbolic sine model [16,25-26], are given in the following

$$\frac{da(t)}{dt} = L = C(\Delta K)^n \tag{2}$$

$$\frac{da(t)}{dt} = L = \frac{C(\Delta K)^n}{(1-R)K_c - \Delta K} \tag{3}$$

$$\frac{da(t)}{dt} = L = 10**\{C_1 \sinh[C_2(\log\Delta K + C_3)] + C_4\} \tag{4}$$

in which ** represents the exponent and the arguments of L have been omitted for brevity. In the above equation, C, n,

C_1, C_2, C_3 and C_4 are constants to be determined from baseline crack propagation data.

For crack propagation in fastener holes under spectrum loading, the following crack growth rate equation proposed recently appears to be reasonable [Refs. 6,43-47],

$$\frac{da(t)}{dt} = L = Qa^b(t) \tag{5}$$

in which $Q = C_5 S^\gamma$; C_5, b and γ are constants depending on the characteristics of the spectrum loading and the materials of fastener specimens.

The crack growth rate models described above are deterministic in nature. In order to take into account the statistical variability of the crack growth rate, Eq. (1) is randomized as follows [Refs. 16-21],

$$\frac{da(t)}{dt} = X(t)L(\Delta K, K_{max}, R, S, a) \tag{6}$$

in which the additional factor X(t) is a non-negative stationary stochastic process with a median value equal to unity. Thus, the deterministic crack growth rate function given by Eq. (1) represents the median crack growth rate behavior, and the random process X(t) [Refs. 16-21] accounts for the statistical variability of the crack growth rate.

To take into account the statistical variability of fatigue crack growth damage accumulation, Bogdanoff and Kozin [e.g., Refs. 10-13] have proposed that the crack size a(t) is a discrete Markov chain. Such a stochastic process, however, is based on the crack size a(t) rather than the crack growth rate da(t)/dt. Based on the stochastic crack growth

rate model given by Eq. (6), Lin and Yang proposed that X(t) followed a continuous Markov process [e.g., Refs. 18-20]. Further, Yang et al. considered a special case in which X(t)=X is a random variable for fastener hole specimens under spectrum loadings [Refs. 21-26].

2.2 Fatigue Crack Growth Data in Fastener Holes

To show the statistical variability of the crack growth damage accumulation, crack propagation time histories for five data sets are shown in Figs. 1-5*. These test results were obtained from fractographic data of 7475-T7351 aluminum fastener hole specimens subjected to spectrum loadings. The first two data sets shown in Figs. 1-2 are referred to as WPB and XWPB, respectively, in which the letters W, P and B indicate that the specimens are drilled with a Winslow Spacematic drill (W), using a proper drilling technique (P), and subjected to a given B-1 bomber load spectrum (B). The additional symbol X associated with the XWPB data set denotes the fasteners having a 15% load transfer, whereas the WPB fasteners transfer no load. Specimens for both data sets from Ref. 48 had a width 1.50 inches. All fastener holes were not intentionally flawed so that natural fatigue cracks were obtained and the time-to-crack initiation varied from one specimen to another [see Refs. 44-48].

The fractographic data have been censored to include only those corner cracks propagating from 0.004 inch to 0.04 inche for the WPB data set and from 0.004 inch to 0.07 inch for the XWPB data set. This censoring procedure is necessary

*Figures and tables are located in the back of the report.

to normalize the data to zero life at 0.004 inch, and to obtain homogeneous data sets as shown in Figs. 1-2. The resulting WPB and XWPB data sets include 16 and 22 specimens, respectively.

Fastener hole specimens used in Ref. 48 were too narrow to acquire fatigue crack growth data, without significant edge effects included, for large fatigue cracks. To generate fractographic data for crack growth damage accumulation in the large crack size region, General Dynamics/Fort Worth Division recently fatigue tested eight dog-bone specimens of 7475-T7351 aluminum with a 3.0 inch width and a 0.375 inch thickness in the test section. These tests were conducted to acquire natural fatigue cracks in fastener holes greater than 0.60 inch. Each specimen contained a 0.25 inch nominal diameter straight-bore center hole with a NAS6204 (0.25 inch diameter) steel protruding head bolt installed with a "finger-tight" nut. All fastener holes were drilled with a modified spacematic drill without deburring holes [see Ref. 28].

Four specimens were tested under a fighter spectrum, referred to as the WWPF data set and four other specimens were tested under a B-1 bomber spectrum, referred to as the WWPB data set; the first letter W refers to a wide (i.e., 3.0 inch) specimen. Fastener holes were not intentionally pre-flawed so that natural fatigue cracks could be obtained. The fractographic data for each specimen in the WWPB and WWPF data sets were normalized to a zero life at crack sizes of 0.008 inch and 0.017 inch , respectively, to obtain

homogeneous crack growth data bases, in which each specimen starts with the same initial crack size. The normalized crack growth results for the two data sets are presented in Figs. 3 and 4.

Recently, 10 dog-bone specimens (7075-T7651 aluminum) were fatigue tested in a 3.5% NaCl solution using a fighter spectrum (hi-lo 400 hour block). Tests and fractographic results were documented in Ref. 49. Test specimens were 2 inches wide and 0.3 inch thick in the test section and included a center hole (open with a nominal diameter of 7/16 inch). All fastener holes were polished to obtain at least 8 microinches finish in the bore of the hole to minimize the effects of initial hole quality variation. An environmental chamber containing 3.5% NaCl solution was mounted on the test specimen. All spectrum fatigue tests were run continuously until specimen failure or to a specified time. Servo-controlled hydraulically actuated load frames were used. Two different loading frequencies were used; fast = 8,000 flight hours per 2 days and slow = 8,000 flight hours per 16 days. A fractographic evaluation of the largest fatigue crack for each specimen was performed to determine the crack growth behavior in terms of crack size versus flight hours.

Fastener holes were not intentionally preflawed in any of the 10 specimens so that natural fatigue cracks could be obtained, and the time-to-crack-initiation varied from one specimen to another. The fractographic data for each

specimen were normalized to a zero life at a crack length of 0.01 inch to obtain a homogeneous crack growth data base in which each specimen starts with the same initial crack size. The normalized crack growth results, presented in Fig. 5, are referred to as the CWPF data set. It is observed that the statistical dispersion of the crack growth damage accumulation is very large; a typical phenomenon of corrosion-fatigue cracking in fastener holes.

For detailed descriptions of the geometries of test specimens, loading spectra, fractographic readings of crack sizes, crack geometries, etc., refer to References 6, 44-47 for the WPB and XWPB data sets, to Reference 28 for the WWPF and WWPB data sets, and to Reference 49 for the CWPF data set.

2.3 Lognormal Crack Growth Rate Model and Analysis Procedures

Since X(t) should be non-negative, it was proposed to be a stationary lognormal random process by Yang, et al. [Refs. 16-21]. The validity of the proposed lognormal random process will be verified later. The lognormal random process, X(t), is defined by the fact that it's logarithm is a normal (or Gaussian) random process, i.e., Z(t) is a normal random process, where

$$Z(t) = \log X(t) \tag{7}$$

The stationary normal random process $Z(t)$ is defined by the mean value μ_z and the autocorrelation function $R_{zz}(\tau)$. The autocorrelation function between $Z(t)$ and $Z(t+\tau)$ is given by

$$R_{zz}(\tau) = E[Z(t)Z(t+\tau)] \tag{8}$$

in which $E[\ ]$ is the ensemble average of the bracketed quantity. Because the process $Z(t)$ is stationary, the autocorrelation function $R_{zz}(\tau)$ depends only on the time difference τ.

The Fourier transform of the autocorrelation function, denoted by $\Phi_{zz}(\omega)$, is referred to as the power spectral density, [e.g., 50-51],

$$\Phi_{zz}(\omega) = \frac{1}{2\pi}\int_{-\infty}^{\infty} R_{zz}(\tau)e^{-\underline{i}\omega\tau}d\tau \tag{9}$$

in which $\underline{i} = \sqrt{-1}$ and ω = frequency in radians per second.

The mean value, μ_z, of $Z(t)$ is equal to the logarithm of the median value, $\tilde{X}$, of $X(t)$. Since the median value $\tilde{X}$ of $X(t)$ is equal to unity, the mean value μ_z of $Z(t)$ is equal to zero, i.e., $\mu_z = \log \tilde{X} = 0.0$. Hence $Z(t)$ is a stationary normal random process with zero mean, and it is completely defined by the autocorrelation function $R_{zz}(\tau)$. The standard deviation σ_z is a special case of $R_{zz}(\tau)$, in which $\tau = 0$, i.e.,

$$\sigma_z = \sqrt{R_{zz}(0)} \tag{10}$$

Consider the fatigue crack propagation in fastener holes subjected to spectrum loading, such that Eq. (5) applies, i.e.,

$$\frac{da(t)}{dt} = X(t)Qa^b(t) \tag{11}$$

Taking the logarithm of both sides of Eq. (11), one obtains

$$Y = bU + q + Z(t) \tag{12}$$

in which

$$Y = \log \frac{da(t)}{dt} \quad , \quad U = \log a(t) \quad , \quad q = \log Q \tag{13}$$

The relationship between the log crack growth rate, $Y = \log[da(t)/dt]$, and the log crack size, $U = \log[a(t)]$, for the test results shown in Figs. 1 to 5, are obtained herein using the 5 point incremental polynomial method [e.g., 36,69]. The results are presented in Figs. 6 to 10 by dots. In Figs. 6 to 10 note that the test results scatter around a straight line, indicating the validity of Eqs. (5) and (11).

Crack growth rate data have also been derived from Figs. 1 to 5 using the modified secant method [7,8]. However, the modified secant method is not recommended, because it introduces larger statistical dispersion of the crack growth rate than the five point incremental polynomial method. This will be discussed later. It is important to emphasize that the statistical dispersion of the crack growth rate data depends not only on the inherent material crack

resistant variability but is also influenced significantly by the following factors; (i) the data reduction procedure used, such as the secant method, the method of incremental polynomial, etc., and (ii) the statistical error in crack size measurements as well as the crack size measurement interval. The results of such investigations along with other relevant factors will be presented later.

Since Z(t) at time (or cycle) t is a normal random variable, it follows from Eq. (12) that the log crack growth rate Y = log[da(t)/dt] is also a normal random variable, conditional on a given crack size a(t). The mean value, μ_y, and standard deviation, σ_y, of Y are given by

$$\mu_y = bU + q \tag{14}$$

$$\sigma_y = \sigma_z \tag{15}$$

The crack growth rate parameters b and Q, as well as the standard deviation, σ_z, of Z(t), conditional on the crack size a(t), can be obtained from the test results of the crack growth rate versus the crack size using Eq. (12) and the linear regression analysis [Refs. 17,21]. With the crack growth rate data shown as dots in Figs. 6 to 10, the method of linear regression is employed to estimate b, Q and σ_z. The results are presented in Table 1. Also displayed in Figs. 6-10 as straight lines are the mean values of the crack growth rate μ_y given by Eq. (14). Since Y and Z are normal random variables, and Eq. (12) is linear, the linear regres-

sion analysis is identical to the method of least-squares or the method of maximum likelihood.

To show the validity of the lognormal crack growth rate model, i.e., X(t) is a stationary lognormal random process with a median of unity, it is necessary to demonstrate that Z(t) follows the normal distribution with zero mean, i.e.,

$$F_{Z(t)}(z) = p[Z(t) \leq z] = \Phi(z/\sigma_z) \tag{16}$$

in which $\Phi(\ )$ is the standardized normal distribution function and σ_z has been estimated in Table 1.

Sample values of Z(t), denoted by z_j, are computed from the sample values of Y and U, denoted by (y_j, u_j), using Eq. (12)

$$z_j = y_j - bu_j - q \qquad \text{for } j=1,2,\ldots,n \tag{17}$$

where b and q have been estimated by the linear regression analysis in Table 1 and n is the total number of test data.

Sample data, z_j (j=1,2,...,n), associated with Figs. 6-10 are computed from Eq. (17) and plotted on the normal probability paper in Figs. 11-15, where the sample values, z_j, are arranged in an ascending order, viz, $z_1 \leq z_2 \leq \ldots \leq z_n$. The distribution function corresponding to z_j is $j/(n+1)$. Hence, on the normal probability paper z_j is plotted against $\Phi^{-1}[j/(n+1)]$ with $\Phi^{-1}(\ )$ being the inverse standardized normal distribution function. A straight line shown in Figs. 11-15 denotes the normal distribution for Z with σ_z being given in Table 1. It is observed that the

sample values of Z scatter around the straight line, indicating that the normal distribution is very reasonable.

Kolmogorov-Smirnov tests for goodness-of-fit [52,53] were performed to determine the observed K-S statistics. The results show that the normal distribution is acceptable at least at a 20% level of significance for all data sets, indicating an excellent fit for the normal distribution.

The crack growth rate da(t)/dt follows the lognormal distribution, and the coefficient of variation, denoted by V, is related to σ_z through the following relation

$$V = \left[e^{(\sigma_z \ell n 10)^2} - 1 \right]^{1/2} \tag{18}$$

The coefficient of variation, V, of the crack growth rate for WPB, XWPB, WWPF, WWPB and CWPF data sets are also shown in Table 1.

Experimental study of the measurement of crack propagation at microscopic level indicates that the fatigue crack propagates successively creating striations randomly spaced. It is suggested that the spacing of such striations is somehow related to the rate of crack propagation. Considerable statistical dispersion of the spacing of striations has been observed [Ref. 27]. Moreover, the striation spacings are correlated and its correlation decays as the distance in space increases [Ref. 27]. Thus, it is reasonable to assume that the autocorrelation function $R_{zz}(\tau)$ of the normal random process Z(t) is an exponentially decaying function of the time difference, τ, i.e.,

$$R_{zz}(\tau) = \sigma_z^2 \, e^{-\xi|\tau|} \tag{19}$$

in which ξ^{-1} is the measure of the correlation distance for $Z(t)$.

The power spectral density $\Phi_{zz}(\omega)$ corresponding to Eq. (19) is obtained as

$$\Phi_{zz}(\omega) = \frac{1}{2\pi} \int_{-\infty}^{\infty} \sigma_z^2 \, e^{-\xi|\tau|} \, e^{-i\omega\tau} \, d\tau = \frac{2\xi}{\xi^2+\omega^2} \sigma_z^2 \tag{20}$$

Both the autocorrelation function and the power spectral density of $Z(t)$ given by Eqs. (19) and (20) are shown in Fig. 16 for two values of ξ^{-1}.

Within the class of random process $Z(t)$ or $X(t)$, two extreme cases should be considered, because of mathematical simplicity. At one extreme when $\xi \to \infty$, the autocorrelation function becomes a Dirac delta function,

$$R_{zz}(\tau) = \sigma_z^2 \delta(\tau) \tag{21}$$

indicating that the random process $Z(t)$ or $X(t)$ is totally uncorrelated at any two time instants. Such a random process is referred to as the white noise process.

At another extreme as $\xi \to 0$, the autocorrelation function $R_{zz}(\tau)$ becomes a constant, i.e.,

$$R_{zz}(\tau) = \sigma_z^2 \tag{22}$$

indicating that the random process $Z(t)$ or $X(t)$ is totally correlated at any two time instants. Hence $Z(t)$ or $X(t)$ becomes a random variable, and the crack propagation model is referred to as the lognormal random variable model.

In reality, the stochastic behavior of crack propagation lies between the two extreme cases described above.

Although the general lognormal random process model for X(t) was proposed by Yang, et al. [Refs. 16-21], the analysis and verification of the model using available data sets were not carried out, because they found that the random variable model is adequate for the fastener hole specimens subjected to bomber or fighter loading spectra. In this report, the analysis of the general lognormal random process model is performed using the method of Monte Carlo simulation. Further, the correlation studies between such a model and the test results are also conducted.

2.4 Lognormal Random Process Model

In the prediction of fatigue crack growth damage accumulation in fastener holes, two statistical distributions are most important: The distribution of the crack size a(t) at any service time t, and the distribution of service life to reach any given crack size, including the critical crack size. Integrating Eq. (11) from zero to t, one obtains

$$a(t) = \frac{a_0}{[1 - cQa_0^c \Lambda(t)]^{1/c}} \tag{23}$$

in which $a_0 = a(0)$ is the initial crack size and

$$c = b - 1 \tag{24}$$

$$\Lambda(t) = \int_0^t X(\tau)d\tau \tag{25}$$

When X(t) is either a lognormal random process or a lognormal white noise, the distribution function of the crack size, a(t), at any service time t is not amenable to analytical solution. As a result, the method of Monte Carlo simulation is used herein. The stationary Gaussian random process $Z(t) = \log X(t)$, Eq. (7), can be simulated using the following expression [e.g., Refs. 54-55]

$$Z(t) = \sqrt{2\Delta\omega}\ \mathrm{Re}\left\{\sum_{k=1}^{M} \sqrt{4\Phi_{zz}(\omega_k)}\ e^{\pm i(\omega_k t+\phi_k)}\right\} \tag{26}$$

in which Re{ } represents the real part of the complex quantity in the bracket, and ϕ_k (k=1,2,...,M) are statistically independent and identically distributed random variables with the uniform distribution in $[0,2\pi]$, i.e.,

$$\begin{aligned} f_{\phi_k}(x) &= \frac{1}{2\pi} && \text{for } 0 \le x \le 2\pi \\ &= 0 && \text{elsewhere} \end{aligned} \tag{27}$$

where $f_{\phi_k}(x)$ is the probability density function of the random variable ϕ_k (k=1,2,...,M). In Eq. (26), the power spectral density $\Phi_{zz}(\omega)$ for $\omega \ge 0$ is evaluated at an equally spaced interval $\Delta\omega$ with $\omega_k = k\Delta\omega > 0$.

The well-known Fast Fourier Transform (FFT) technique can be applied by letting

$$\omega_k = k\Delta\omega \quad , \quad t = j\Delta t \quad \text{and} \quad \Delta\omega\Delta t = 2\pi/M \tag{28}$$

such that Eq. (26) becomes [54,55]

$$Z(j\Delta t) = \sqrt{2\Delta\omega}\ \mathrm{Re}\left\{\sum_{k=1}^{M}\left[\sqrt{4\Phi_{zz}(k\Delta\omega)}\ e^{\underline{i}\phi_k}\right]e^{\underline{i}jk\,2\pi/M}\right\} \tag{29}$$

Thus, when applying the FFT technique, the stationary Gaussian random process $Z(t)$ is evaluated at equally spaced discrete time points $t_j = j\Delta t$ for $j=1,2,\ldots,M$. The total number of sample points, M, must be an integer power of 2 based on the FFT algorithm.

Sample functions of the crack size $a(t)$ versus the service time t can be simulated conveniently using the efficient FFT technique. The Monte Carlo simulation procedures are summarized in the following:

(i) Simulate a sample function, say the jth sample function, of stationary Gaussian random process $Z_j(t)$ using Eq. (29) and the FFT technique.

(ii) Compute the corresponding sample function of the stationary lognormal random process $X_j(t)$

$$X_j(t) = (10)^{**}Z_j(t) \tag{30}$$

(iii) Compute the sample function $\Lambda_j(t)$ as a function of time t using Eq. (25), i.e.,

$$\Lambda_j(t) = \int_0^t X_j(\tau)\,d\tau \tag{31}$$

(iv) Compute the sample function of the crack size $a_j(t)$ as a function of time t using Eq. (23), i.e.,

$$a_j(t) = \frac{a_0}{[1 - cQa_0^c \Lambda_j(t)]^{1/c}} \tag{32}$$

(v) Repeat procedures (i) to (iv) for N times, i.e., j=1,2,...,N, to obtain N sample functions of the crack size a(t) as a function of the service time t.

(vi) Sample values of the random time, $T(a_1)$, to reach any specific crack size a_1 is obtained from sample functions a(t) versus t by drawing a horizontal line through the crack size $a(t) = a_1$. The simulated distribution function of $T(a_1)$ is established from the sample values thus obtained.

(vii) Sample values of the crack size $a(\tau)$ at any service time τ is obtained from sample functions of a(t) versus t by drawing a vertical line through $t = \tau$, and the distribution function of $a(\tau)$ is established from the corresponding sample values.

2.5 Lognormal White Noise Model

As described previously, the stationary Gaussian random process Z(t) is a Gaussian white noise when its autocorrelation function is a Dirac delta function given by Eq. (21). The corresponding power spectral density $\Phi_{zz}(\omega)$ is constant, i.e.,

$$R_{zz}(\tau) = \sigma_z^2 \delta(\tau) \quad ; \quad \Phi_{zz}(\omega) = \sigma_z^2/2\pi \tag{33}$$

With the constant power spectral density as well as the values of b, Q, and σ_z given in Table 1, sample functions of the crack growth damage accumulation a(t) for WPB and XWPB fastener holes are simulated and presented in Figs. 17-18.

The following conclusions are derived from a comparison between the simulation results, Figs. 17-18, and the experimental test data given in Figs. 1-2. (i) The Gaussian white noise model correlates very well with the experimental data only for the mean (average) crack growth behavior, and (ii) the model introduces very little statistically dispersion for the crack growth damage accumulation. As a result, the Gaussian white noise model is unconservative and unrealistic for engineering applications. No further study will be made of this model.

It is interesting to note that Virkler, Hillberry and Goel [Refs. 7 - 8] have undertaken simulation studies of fatigue crack propagation , which amount to the white noise assumption, although the method of Monte Carlo simulation they used is different from what is described above. They also arrived at the same conclusions [Refs. 7 - 8]. The fact that the white noise model results in a small statistical dispersion for the crack growth damage accumulation can be shown in the following.

Equation (25) can be written as follows:

$$\Lambda(n\Delta t) \cong \sum_{j=1}^{n} X(j\Delta t)\Delta t \tag{34}$$

Being a Gaussian white noise, $Z(j\Delta t)$ and $Z(k\Delta t)$ are statistically independent for $j \neq k$. Hence, $X(j\Delta t) = (10)^{**}Z(j\Delta t)$ and $X(k\Delta t) = (10)^{**}Z(k\Delta t)$ are also statistically independent. It follows from Eq. (34) that $\Lambda(n\Delta t)$ is the sum of independent random variables $X(j\Delta t)$ $(j=1,2,\ldots,n)$, in which each random variable has an identical median value (unity) and standard deviation. By virtue of the central limit theorem, the statistical dispersion of $\Lambda(t)$ diminishes as n increases, and hence $\Lambda(t)$ approaches to the mean value. Then, it follows from Eq. (23) that the statistical dispersion of the crack growth damage accumulation $a(t)$ is extremely small.

2.6 Lognormal Random Variable Model

For the other extreme case in which $\xi \to 0$, the lognormal random process $X(t)$, or the normal random process $Z(t)$, is completely correlated at any two time instants. Under this circumstance, the lognormal random process $X(t)$ becomes a lognormal random variable X, and the normal random process $Z(t)$ becomes a normal random variable Z, i.e.,

$$X(t) = X \quad , \quad Z(t) = Z \tag{35}$$

where

$$Z = \log X \tag{36}$$

Such a model is referred to as the lognormal random variable model and it has been investigated in Refs. 16, 17, 21, 25 and 26.

For the lognormal random variable model, the statistical distribution of the crack growth damage accumulation can be derived analytically as follows.

Equation (11) is now simplified as

$$\frac{da(t)}{dt} = XQa^{b}(t) \tag{37}$$

and the integration of Eq. (37) yields

$$a(t) = \frac{a_0}{[1-XcQta_0^c]^{1/c}} \tag{38}$$

in which $a_0 = a(0)$ is the initial crack size and $c = b - 1$ is given by Eq. (24).

Let z_γ be the γ percentile of the normal random variable Z. Then, it follows from Eq. (16) that

$$\gamma\% = P[Z > z_\gamma] = 1 - \Phi[z_\gamma/\sigma_z] \tag{39}$$

or, conversely,

$$z_\gamma = \sigma_z \, \Phi^{-1}(1 - \gamma\%) \tag{40}$$

in which $\Phi^{-1}(\,)$ is the inverse standardized normal distribution function.

The γ percentile of the random variable X, denoted by x_γ, follows from Eq. (36) as

$$x_\gamma = (10)^{z_\gamma} \tag{41}$$

and the γ percentile of the crack size, $a_\gamma(t)$, at t flight hours follows from Eqs. (38) and (41) as

$$a_\gamma(t) = \frac{a_0}{[1 - x_\gamma c Q t a_0^c]^{1/c}} \tag{42}$$

Various γ percentiles of the crack size $a_\gamma(t)$ versus flight hours t have been computed from Eqs. (39)-(42), using the parameter values given in Table 1 for the WPB, XWPB, WWPF, WWPB and CWPF data sets. The results are presented in Figs. 19-23 in which the initial crack sizes, $a_0 = a(0)$, for each data set are, respectively, 0.004, 0.004, 0.017, 0.008 and 0.01 inch. For example, the curve associated with $\gamma = 10$ in these figures indicates that the probability is 10% that a specimen randomly chosen will have a crack growing faster than that shown by the curve. Another interpretation is that on the average 10% of the total specimens will have a crack growing faster than that indicated by the 10% curve, when the total number of specimens is large.

Thus, the distribution function of the crack size, a(t), as a function of service life t (flight hours) has been established by Eqs. (39)-(42) and shown in Figs. 19-23. On the basis of the lognormal random variable model, the distribution of the crack size at any service time t, and the distribution of service life to reach any specific crack size, including the critical crack size, can be derived analytically as follows:

The distribution function of the lognormal random variable X is given by

$$F_X(x) = P[X \leq x] = \Phi[\log x/\sigma_z] \tag{43}$$

in which σ_z has been obtained from the linear regression analysis of the crack growth rate data shown in Table 1 for various data sets.

The distribution function of the crack size, a(t), at any service life, t, can be obtained from that of X given by Eq. (43) through the transformation of Eq. (38). The results are given as follows:

$$F_{a(t)}(x) = P[a(t) \leq x] = \Phi\left[\frac{\log\left(\frac{a_0^{-c} - x^{-c}}{cQt}\right)}{\sigma_z}\right] \tag{44}$$

Let $T(a_1)$ be a random variable denoting the time to reach any given crack size a_1. Then $T(a_1)$ can be obtained from Eq. (38) by setting $a(t) = a_1$ and $t = T(a_1)$, respectively, i.e.,

$$T(a_1) = \frac{1}{cQX}\left[a_0^{-c} - a_1^{-c}\right] \tag{45}$$

Thus, the distribution of $T(a_1)$ can be obtained from that of X given by Eq. (43) through the transformation of Eq. (45). The results can be expressed as follows:

$$F_{T(a_1)}(\tau) = P[T(a_1) \leq \tau] = 1 - \Phi\left(\frac{\log \eta}{\sigma_z}\right) \tag{46}$$

where

$$\eta = \frac{1}{cQ\tau}\left[a_0^{-c} - a_1^{-c}\right] \tag{47}$$

In the durability analysis, the extent of cracking in a structural component can be measured by the probability that a crack size may exceed any specific value x_1 at any point in time τ, referred to as the probability of crack exceedance. The probability of crack exceedance, denoted by $p(x_1,\tau)$, is the complement of the distribution function of the crack size $a(\tau)$, i.e.,

$$p(x_1,\tau) = P[a(\tau)>x_1] = 1 - F_{a(\tau)}(x_1)$$
$$= 1 - \Phi\left[\frac{\log\left(\frac{a_0^{-c} - x_1^{-c}}{cQ\tau}\right)}{\sigma_z}\right] \qquad (48)$$

in which Eq. (44) has been used.

It is observed from Eqs. (44) and (48) that the distribution functions of the crack size at any given number of flight hours and the time to reach any specific crack size, as well as the probability of crack exceedance derived above, require only the crack growth rate parameters b and Q as well as the model statistics σ_z. They are determined from the linear regression analysis of the crack growth rate data presented in Table 1.

2.7 Correlation With Experimental Results

2.7.1 Lognormal Random Variable Model

Based on the lognormal random variable model, the distribution of the crack size, a(t), as a function of flight

hours, t, can be expressed in terms of various γ percentiles. The results for WPB, XWPB, WWPF, WWPB, and CWPF fastener holes are shown in Figs. 19-23, respectively. A visual comparison between Figs. 1-5 and 19-23 indicates a good correlation between experimental results and the lognormal random variable model.

Using Eqs. (46)-(47) the distribution functions for the random number of flight hours to reach various crack sizes a_1 are shown in Figs. 24-28 as solid curves for different fastener holes (a_1 = 0.01, 0.02 and 0.04 inch for WPB fastener holes; a_1 = 0.008, 0.025, and 0.07 inch for XWPB fastener holes; a_1 = 0.05, 0.15 and 0.51 inch for WWPF fastener holes; a_1 = 0.025, 0.1 and 0.57 inch for WWPB fastener holes; a_1 = 0.04, 0.08 and 0.35 inch for CWPF fastener holes). The corresponding experimental results obtained from Figs. 1-5 are plotted in Figs. 24-28 as circles. Figures 24-28 demonstrate a good correlation between the lognormal random variable model (solid curves) and experimental results.

The plot for the probability of crack exceedance is referred to as the crack exceedance curve. The crack exceedance curves based on the statistical model, Eq. (48), for various fastener holes at different service times (flight hours) are shwon in Figs. 29-33 as solid curves. Also shown in these figures as circles are the corresponding test results obtained from Figs. 1-5. Again, the correlation between the lognormal random variable model and the test results is very good.

In computing the crack growth rate data, da/dt, from the fractographic results, various data processing procedures can be used. These include the secant method, the modified secant method, and the 3, 5, 7 and 9 point incremental polynomial methods [Refs. 7,8,29,34-36]. For the statistical analysis of crack propagation, the incremental polynomial method is considered superior to the secant or modified secant method, because the latter introduces additional dispersion into the crack growth rate data. Both the direct secant and modified secant methods have been employed in the theoretical model; however, the correlation with the experimental results is not as good as that presented above. Further investigation will be made in later chapters.

The number of crack growth data measurements during expermental tests, i.e., the crack size a(t) versus the flight hour t, usually is not equal for each specimen. Frequently, more data points are measured for specimens with slower crack growth rates than those with faster crack growth rates. Consequently, more crack growth rate data associated with the slow crack growth specimens would have been used in the regression analysis to determine the crack growth rate parameters b and Q. As a result, the estimated parameter values of b and Q tend to be biased to the slow crack growth damage accumulation. This clearly violates the statistical implication that each specimen is statistically independent with the same weight. To compensate for such an error, interpolations have been conducted for fast crack growth specimens and

additional crack growth rate data points have been added artificially so that the number of crack growth rate data points for each specimen is roughly the same. This approach eliminates the estimation bias for the crack growth rate parameters. This aspect will be discussed further in the following chapters.

2.7.2 General Lognormal Random Process Model

When X(t) is a stationary lognormal random process with a median value of unity, the process Z(t) = log X(t) is a stationary normal (Gaussian) random process with zero mean and an autocorrelation function $R_{zz}(\tau)$ given by Eq. (19) or a power spectral density $\Phi_{zz}(\omega)$ given by Eq. (20). With such a stochastic model, the statistical distribution of the crack growth damage accumulation is not amenable to analytical solution. Hence, the method of Monte Carlo simulation has been employed, and the simulation procedures have been described previously.

For any general random process model, an additional parameter appearing in the autocorrelation function should be estimated from the experimental test results. For instance, the parameter ξ^{-1} in Eqs. (19) and (20), which is a measure of the correlation distance, referred to as the correlation parameter, should be estimated. Estimating such a correlation parameter is quite involved and may require many sample functions of the test results. Since the objective herein is to investigate the ability of the proposed stochastic

model in describing the statistical fatigue crack propagation behavior, no effort is made to establish analysis procedures for the determination of such a parameter.

Different values of the correlation parameter, ξ^{-1}, were used and the corresponding simulation results were examined. As expected, the statistical scatter of the crack growth damage accumulation increases as the correlation parameter, ξ^{-1}, increases and vice versa. A value for the correlation parameter, ξ^{-1}, that results in a good correlation with the experimental test results is chosen to demonstrate the validity of the lognormal random process model.

The best parameter value, ξ^{-1}, associated with each data set is shown in Table 2. Using the Monte Carlo simulation procedures developed and described previously, and using the power spectral density given by Eq. (20), sample functions of the crack size a(t) versus the flight hour t have been simulated, and some of these results are presented in Figs. 34-38. Although over 150 sample functions of a(t) have been simulated for each case, only the first 50 sample functions are depicted in these figures so that each figure will not be too crowded. The total number of simulated sample functions for each data set is given in Table 2. In the simulation process using a FFT technique that is very efficient, the total number of discrete points, M, for each sample function of a(t) is 2,048 with Δt = 60 flight hours except the CWPF data set in which Δt = 20 flight hours (see Table 2.)

It is observed that the simulated sample functions of the crack growth damage accumulation a(t) presented in Figs. 34-38 closely resemble those of the experimental test results given in Figs. 1-5. The simulation results for the distribution function, $F_{T(a_1)}(t)$, of the random time, $T(a_1)$, to reach some specific crack sizes are presented in Figs. 39-43 as solid curves (empirical distribution) for various data sets. Also shown in these figures as stars are the experimental test results obtained from Figs. 1-5. The probabilities of crack exceedance at some specific service times are displayed in Figs. 44-48 as solid curves, whereas the corresponding test results for different fastener holes obtained from Figs. 1-5 are shown as stars. Figures 39 to 48 show that the correlation between the lognormal random process model and the experimental results is excellent.

CHAPTER 3

SECOND MOMENT APPROXIMATION

The most important statistics for a random variable such as the crack size a(t), are a few lowest cumulants. Frequently, the distribution function of a random variable is not amenable to analytical solution, but a few lowest cumulants of such a random variable can be obtained easily. In this case, the distribution may be approximated by a particular function with an acceptable level of accuracy when the few lowest cumulants are incorporated in the particular distribution. Since the first two cumulants, i.e., the mean value and standard deviation, of the crack size a(t) at any service life t can be determined analytically, the distribution function of a(t) will be fitted by different functions. Several possible distribution functions will be studied from which a most suitable one may be chosen for a(t). This approach is referred to as the second moment approximation.

Again, the crack propagation in fastener holes is considered such that the following crack growth rate equation holds,

$$\frac{da(t)}{dt} = X(t)L(a) = X(t)Qa^{b}(t) \qquad (49)$$

in which X(t) is a stationary lognormal random process and

$$L(a) = Qa^{b}(t) \tag{50}$$

3.1 Cumulant - Neglect Closure

A random process, say W(t), can be described by its log-characteristic functional which has a series expansion as follows [Ref. 20]:

$$\begin{aligned} \ell n\, E\{\exp[\underline{i}\int\theta(t)W(t)dt]\} &= \underline{i}\int\theta(t)\kappa_1[W(t)]dt \\ &+ \frac{\underline{i}^2}{2}\iint\theta(t_1)\theta(t_2)\kappa_2[W(t_1),W(t_2)]dt_1dt_2 \\ &+ \frac{\underline{i}^3}{3!}\iiint\theta(t_1)\theta(t_2)\theta(t_3)\kappa_3[W(t_1),W(t_2),W(t_3)] \\ &\cdot dt_1dt_2dt_3 + \cdots\cdots \end{aligned} \tag{51}$$

where $E\{\ \}$ = an ensemble average, $\underline{i} = \sqrt{-1}$, $\kappa_n[\ ]$ = nth cumulant of n random variables, each integration extends over the entire domain on which W(t) is defined, and $\theta(t)$ belongs to a set of functions for which all the integrals on the right-hand side exist and the series converges. It can be shown that the first cumulant is equal to the mean and the second and third cumulants are equal to the second and third central moments, respectively. In the special case $\theta(t) = \Sigma\theta_j\delta(t-t_j)$ where θ_j are constants, a log-characteristic functional becomes a log-characteristic function. In general, the number of terms in Eq. (51) is infinite, in which case an approximation is obtained when the series is truncated, or when cumulants higher than a given order are

set to zero. This general scheme is called the cumulant-neglect closure. However, retaining only the first cumulant is trivial since it reduces to the deterministic description $W(t) = E[W(t)]$. The special case of Gaussian closure is equivalent to neglecting the third and higher cumulants and allowing the random process to assume any value in $(-\infty,\infty)$.

Now, Eq. (49) can be simplified by a change of variable [Ref. 20]:

$$W(t) = \int_{a_0}^{a(t)} \frac{dv}{L(v)} \tag{52}$$

in which $a_0 = a(0)$ is the initial crack size. Then Eq. (49) becomes

$$\frac{dW(t)}{dt} = X(t) \tag{53}$$

If $F_{a(t)}(x)$ and $F_{W(t)}(x)$ denote the distribution functions of $a(t)$ and $W(t)$, respectively, then it follows from Eq. (52) that they are related through

$$F_{a(t)}(x) = F_W[y(x)]$$

$$y(x) = \int_{a_0}^{x} \frac{dv}{L(v)} = (a_0^{-c} - x^{-c})/cQ \tag{54}$$

Hence, the distribution of $a(t)$ can be derived once the distribution function of $W(t)$ is obtained.

Integration of Eq. (53) from 0 to t yields

$$W(t) = \int_0^t X(\tau)d\tau \tag{55}$$

It is obvious from Eq. (55) that W(t) is a stationary random process, representing the integration of a stationary log-normal random process.

While the distribution function of W(t) is difficult to obtain, the cumulants of W(t) can be derived from that of X(t) through the following relation

$$\kappa_n[W(t_1),W(t_2),\ldots,W(t_n)] = \int_0^{t_1} d\tau_1 \int_0^{t_2} d\tau_2 \ldots \int_0^{t_n} \kappa_n[X(\tau_1),X(\tau_2),\ldots,X(\tau_n)]d\tau_n \tag{56}$$

The first cumulant $\kappa_1[W(t)]$ is the mean value given by

$$\mu_W = E[W(t)] = \int_0^t E[X(\tau)]d\tau = \mu_X t \tag{57}$$

in which μ_X is the mean value of the stationary lognormal random process X(t).

The second cumulant $\kappa_2[W(t_1),W(t_2)]$ at the same time instant $t_1=t_2=t$ is the variance $E[\{W(t)-\mu_W\}^2] = \sigma_W^2$ given by

$$\sigma_W^2 = \int_0^t\int_0^t E[\{X(\tau_1)-\mu_X\}\{X(\tau_2)-\mu_X\}]d\tau_1 d\tau_2$$

$$= \int_0^t\int_0^t \mathrm{cov}[X(\tau_1),X(\tau_2)]d\tau_1 d\tau_2 \tag{58}$$

From the physical standpoint, the covariance function, $\mathrm{cov}[X(\tau_1),X(\tau_2)]$, of the crack growth rate should decrease

as the difference between two time instants τ_1 and τ_2 increases. Thus, an exponentially decaying function is proposed herein

$$\text{cov}[X(\tau_1),X(\tau_2)] = \sigma_X^2 \, e^{-\zeta|\tau_1-\tau_2|} \tag{59}$$

in which σ_X is the standard deviation of X(t), and ζ^{-1} is a constant, that is a measure of the correlation distance. As $\zeta^{-1} \to 0$, the correlation distance approaches zero signifying a white noise process for X(t). The solution for the white white noise process, presented in the previous chapter, is shown to be unreasonable. On the other hand, as $\zeta^{-1} \to \infty$ X(t) is completely correlated and hence it is a random variable. The solution for the random variable model has been presented previously.

Substituting Eq. (59) into Eq. (58) and carrying out the integration, one obtains

$$\sigma_W = \sqrt{2} \, (\sigma_X/\zeta)[e^{-\zeta t} + \zeta t - 1]^{1/2} \tag{60}$$

Thus, the mean value μ_W and standard deviation σ_W of the stationary random process W(t) are expressed in terms of the mean value, μ_X, the standard deviation, σ_X, and the correlation parameter ζ of the lognormal random process X(t), see Eqs. (57) and (60). Both μ_X and σ_X can be determined from experimental test results as follows.

Taking the logarithm of both sides of Eq. (49), one obtains

$$Y = bU + q + Z(t) \tag{61}$$

in which

$$Y = \log \frac{da(t)}{dt} \quad , \quad U = \log a(t) \quad , \quad q = \log Q \tag{62}$$

$$Z(t) = \log X(t) \tag{63}$$

where $Z(t)$ is a stationary Gaussian (or normal) random process with zero mean, i.e., $\mu_Z = 0$, and standard deviation σ_Z. The crack growth rate parameters b and Q as well as the standard deviation σ_Z of $Z(t)$ can be determined from the baseline crack growth rate data using Eq. (61) and the linear regression analysis as described previously.

From the properties of lognormal random variable, the mean value, μ_X, and standard deviation, σ_X, of $X(t)$ are related to μ_Z and σ_Z in the following [e.g., Refs. 52,53]

$$\mu_X = \exp\left[\frac{1}{2} (\sigma_Z \ell n 10)^2\right] \tag{64}$$

$$\sigma_X = \mu_X \left[e^{(\sigma_Z \ell n 10)^2} - 1\right]^{1/2} \tag{65}$$

in which the property that $\mu_Z = 0$ has been used.

Substituting Eqs. (64) and (65) into Eqs. (57) and (60), one obtains the mean value, μ_W, and standard deviation, σ_W, of the stationary random process $W(t)$ as follows

$$\mu_W = t \exp\left[\frac{1}{2} (\sigma_Z \ell n 10)^2\right] \tag{66}$$

$$\sigma_W = \frac{\sqrt{2}(e^{-\zeta t}+\zeta t - 1)^{1/2}}{\zeta} \exp\left[\frac{1}{2}(\sigma_Z \ell n 10)^2\right]\left[e^{(\sigma_Z \ell n 10)^2}-1\right]^{1/2} \tag{67}$$

The coefficient of variation of W(t), denoted by V_W, is given by

$$V_W = \sigma_W/\mu_W = \frac{\sqrt{2}(e^{-\zeta t}+\zeta t - 1)^{1/2}}{\zeta t}\left[e^{(\sigma_Z \ell n 10)^2} - 1\right]^{1/2} \tag{68}$$

3.2 Gaussian Closure Approximation

As mentioned before, the log-characteristic function of the random process W(t) can be expressed by an infinite series involving all the cumulants as shown in Eq. (51). An approximation can be made by a truncation of the series or by setting all cumulants higher than a given order to zero. This general scheme is referred to as the cumulant-neglect closure [Ref. 20].

A special case of the cumulant-neglect closure is called Gaussian closure, assuming that W(t) is a Gaussian (normal) random variable, which is equivalent to neglecting the third and higher order cumulants, and allowing W(t) to take values in $(-\infty,\infty)$ [Ref. 20].

With the Gaussian closure approximation, the distribution function, $F_{W(t)}(x) = P[W(t) \leq x]$, of W(t) is given by

$$F_{W(t)}(x) = \phi\left[\frac{x-\mu_W}{\sigma_W}\right] \quad ; \quad -\infty < x < \infty \tag{69}$$

in which μ_W and σ_W are given by Eqs. (66) and (67), respectively. The relation between the crack size a(t) and W(t)

is obtained by substituting Eq. (50) into Eq. (52) and carrying out the integration; with the results

$$W(t) = (Qc)^{-1}[a_0^{-c} - a^{-c}(t)] \tag{70}$$

in which $c = b - 1$.

Hence, the distribution function of the crack size a(t) at any service life t can be obtained from that of W(t) given by Eq. (54) as follows:

$$F_{a(t)}(x) = F_{W(t)}[(Qc)^{-1}(a_0^{-c} - x^{-c})]$$

$$= \Phi\left[\frac{(Qc)^{-1}(a_0^{-c} - x^{-c}) - \mu_W}{\sigma_W}\right] \quad ; \quad -\infty<x<\infty \tag{71}$$

in which Eq. (69) has been used.

Equation (71) admits all values for the crack size a(t), including those values smaller than a_0. To compensate the error thus introduced, the crack size should be restricted only to those values larger than a_0, denoted by a*(t). The distribution function of the crack size a*(t) can be obtained through the normalization process as follows;

$$F_{a^*(t)}(x) = P[a^*(t)\leq x] = 1-P[a^*(t)>x] = 1-P[a(t)>x|a(t)>a_0]$$

$$= 1 - \frac{P[a(t)>x]}{P[a(t)>a_0]} = 1 - \frac{1-F_{a(t)}(x)}{1-F_{a(t)}(a_0)}$$

$$= \frac{F_{a(t)}(x) - F_{a(t)}(a_0)}{1 - F_{a(t)}(a_0)} \quad ; \quad x \geq a_0 \tag{72}$$

Substitution of Eq. (71) into Eq. (72) yields

$$F_{a^*(t)}(x) = \left[\Phi\left(\frac{(Qc)^{-1}(a_0^{-c} - x^{-c}) - \mu_W}{\sigma_W}\right) - \Phi\left(\frac{-\mu_W}{\sigma_W}\right)\right] \Bigg/ \left[1 - \Phi\left(\frac{-\mu_W}{\sigma_W}\right)\right] \quad ; \quad x \geq a_0 \tag{73}$$

Such a normalized distribution, $F_{a^*(t)}(x)$, is nearly equal to the unnormalized one, $F_{a(t)}(x)$, except for very small t.

From an application point of view, the probability distribution of fatigue life (or crack propagation life) is also of great interest. Let $T(a_1)$ be the random time at which a given crack size a_1 is reached. Since the event $\{T(a_1) \leq t\}$ is the same as the event $\{a(t) > a_1\}$, the distribution function of $T(a_1)$, denoted by $F_{T(a_1)}(t)$, can be computed as follows

$$F_{T(a_1)}(t) = 1 - F_{a^*(t)}(a_1) \tag{74}$$

in which the normalization procedure is used. Without normalization, one obtains

$$F_{T(a_1)}(t) = 1 - F_{a(t)}(a_1) \tag{75}$$

The probability that a crack size will exceed x_1, at any service time τ, referred to as the probability of crack

exceedance, is given by

$$p(x_1,\tau) = P[a^*(\tau)>x_1] = 1 - F_{a^*(\tau)}(x_1) \qquad (76)$$

in which $F_{a^*(\tau)}(x_1)$ is given by Eq. (73) with t and x being replaced by τ and x_1, respectively.

3.3 Weibull Approximation

The distribution function of the crack size a(t) has been derived from that of W(t) in Eq. (54). While the distribution of W(t) is unknown, the mean value μ_W and standard deviation σ_W have been obtained in Eqs. (66) and (67). Moreover it is obvious from Eq. (52) that W(t) is a non-negative random variable, since L(a) in Eq. (50) is a non-negative function of the crack size a. Thus, various distribution functions which are defined in the positive domain, such as Weibull, lognormal, gamma, etc., will be investigated for approximating that of W(t).

Instead of truncating the third and higher order cumulants, the distribution of W(t) is approximated herein by the Weibull distribution. Note that the higher order cumulants of the Weibull random variable are not zero. Consequently, the Weibull approximation implies that the higher order cumulants of W(t) are approximated by those of the Weibull. Then, the distribution function of W(t) is given by

$$F_{W(t)}(x) = 1 - \exp\{-(x/\beta)^{\alpha}\} \quad ; \quad x \geq 0 \qquad (77)$$

in which α and β are the shape parameter and scale parameter, respectively. Both α and β are related to the mean value, μ_W, and coefficient of variation, V_W, of W(t) through the following [Ref. 53]

$$V_W = \left[\Gamma(1 + \frac{2}{\alpha}) - \Gamma^2(1 + \frac{1}{\alpha})\right]^{1/2} \Big/ \Gamma(1 + \frac{1}{\alpha}) \tag{78}$$

$$\mu_W = \beta\Gamma(1 + \frac{1}{\alpha}) \tag{79}$$

in which $\Gamma(\ )$ is the gamma function. Thus, the shape parameter α is determined from Eq. (78) and then the scale parameter β is computed from Eq. (79).

The distribution function of the crack size a(t) is obtained from that of W(t) given by Eq. (77) through the transformation of Eq. (70); with the results

$$F_{a(t)}(x) = 1 - \exp\{-[(a_0^{-c} - x^{-c})/cQ\beta]^{\alpha}\} \quad ; \quad x \geq a_0 \tag{80}$$

The distribution function of the propagation life, $T(a_1)$, to reach any given crack size a_1 is equal to $1 - F_{a(t)}(a_1)$, i.e.,

$$F_{T(a_1)}(t) = \exp\{-[(a_0^{-c} - x^{-c})/cQ\beta]^{\alpha}\} \tag{81}$$

and the probability of crack exceedance is given by

$$p(x_1,\tau) = 1 - F_{a(\tau)}(x_1) \tag{82}$$

It is important to note that both the distribution functions of a(t) and $T(a_1)$, given by Eqs. (80)-(81), as well

as the probability of crack exceedance, Eq. (82), are implicit functions of the service life t. This is because α and β are functions of V_W and μ_W, see Eqs. (78)-(79), that in turn are functions of t as given by Eqs. (66)-(68).

3.4 Lognormal Approximation

With the lognormal approximation, the distribution function of W(t) is expressed as

$$F_{W(t)}(x) = \Phi\left(\frac{\log x - \mu_{\log W}}{\sigma_{\log W}}\right) \quad ; \quad x \geq 0 \tag{83}$$

in which $\mu_{\log W}$ and $\sigma_{\log W}$ are the mean value and standard deviation of logW, which are related to μ_W and V_W in the following [e.g., Refs. 52-53]

$$\sigma_{\log W} = [\ell n(1 + V_W^2)]^{1/2} / \ell n 10 \tag{84}$$

$$\mu_{\log W} = \ell n \left[\frac{\mu_W}{(1+V_W^2)^{1/2}}\right] \Big/ \ell n 10 \tag{85}$$

where μ_W and V_W are given by Eqs. (66) and (68), respectively.

Thus, the distribution functions of the crack size a(t) at any service time t and the propagation life, $T(a_1)$, to reach any given crack size a_1 can be derived through Eqs. (54) and (83) as follows

$$F_{a(t)}(x) = \Phi\left[\frac{\log(a_0^{-c} - x^{-c}) - \log Qc - \mu_{\log W}}{\sigma_{\log W}}\right] \; ; \quad x \geq a_0 \tag{86}$$

and

$$F_{T(a_1)}(t) = 1 - F_{a(t)}(a_1) \tag{87}$$

The crack exceedance probability $p(x_1,\tau)$ is obtained from Eq. (82) where $F_{a(\tau)}(x_1)$ is given by Eq. (86) with t and x being replaced by τ and x_1, respectively.

3.5 Gamma Approximation

With the gamma approximation, the distribution function of W(t) is expressed as

$$F_{W(t)}(x) = \gamma(\eta,\lambda x)/\Gamma(\eta) \tag{88}$$

in which $\gamma(\eta,\lambda x)$ is the incomplete gamma function, and $\Gamma(\eta)$ is the complete gamma function given by

$$\gamma(\eta,\lambda x) = \int_0^{\lambda x} y^{\eta-1}\, e^{-y}\, dy \tag{89}$$

$$\Gamma(\eta) = \int_0^{\infty} y^{\eta-1}\, e^{-y}\, dy \tag{90}$$

The η and λ are related to the mean value, μ_W, and coefficient of variation, V_W, as follows [Ref. 53]:

$$\eta = 1/V_W^2 \tag{91}$$

$$\lambda = 1/(V_W^2 \mu_W) \tag{92}$$

where μ_W and V_W are expressed in terms of σ_z, and ζ and t in Eqs. (66) and (68), respectively.

The distribution function of the crack size a(t) at any service time is obtained as

$$F_{a(t)}(x) = \gamma[\eta, \lambda(cQ)^{-1}(a_0^{-c} - x^{-c})]/\Gamma(\eta) \quad ; \quad x \geq a_0 \tag{93}$$

and the distribution function of the propagation life, $T(a_1)$, to reach any given crack size a_1 is given by

$$F_{T(a_1)}(t) = 1 - F_{a(t)}(a_1) \tag{94}$$

The probability of crack exceedance can be obtained from Eq. (82) in which $F_{a(\tau)}(x_1)$ is given by Eq. (93) with t and x being replaced by τ and x_1, respectively.

3.6 Correlation Between Second Moment Approximations and Experimental Results

Unlike the general lognormal random process model in which the correlation parameter ξ^{-1} is a measure of the correlation distance for the Gaussian random process Z(t), the correlation parameter ζ^{-1} in the present case is a measure of the correlation distance for the lognormal random process X(t). Again, no effort is made to establish procedures for determining ζ^{-1} from experimental results. Hence, an appropriate value of ζ^{-1} that results in the best correlation with the experimental results is chosen by scanning different values of ζ^{-1}. It is found that within

the same data set, the parameter value ζ^{-1} providing the best correlation varies slightly among various approximations. As a result, a suitable value of ζ^{-1} for each approximation in each data set is shown in Table 3.

With the parameter values, b, Q, and σ_Z given in Table 1 as well as the value of ζ^{-1} given in Table 3, the distribution function, $F_{T(a_1)}(t)$, for the random time $T(a_1)$ to reach any specific crack size a_1, has been derived in Eqs. (74), (81), (87) and (94) for various approximations. The results for different fastener holes are presented in Figs. 49(a) to 53(a) as dotted and solid curves for Weibull and gamma approximations, respectively. With Gaussian closure and lognormal approximations, the results are presented in Figs. 49(b)-53(b), respectively, by dotted and solid curves. Also shown in these figures as circles are the experimental results obtained from Figs. 1-5. Furthermore, based on various approximations the corresponding probabilities of crack exceedance, $p(x_1,\tau)$, at any specific service life, τ, are depicted in Figs. 54-58 as dotted and solid curves. The corresponding experimental results obtained from Figures 1-5 are shown in these figures as circles.

Figures 49 to 58 demonstrate that the correlations between all the second moment approximations and the experimental data are very satisfactory.

CHAPTER 4

FATIGUE CRACK PROPAGATION IN CENTER-CRACKED SPECIMENS

So far, emphasis has been placed on the crack growth damage accumulation in fastener holes subjected to spectrum loadings, which is the main subject of this report. It should be emphasized that the statistical model for the fatigue crack propagation given in Eq. (6) is quite general and it can be applied to other materials, crack geometries, fatigue loading, and environments. The log-normal random variable model has been recently applied to super-alloys used in jet engine components, such as IN100, Titanium, Waspaloy, etc., in high temperature environments [Refs. 26-27]. All the test data studied in Refs. 16, 26-27 were obtained using compact tension specimens under either constant-amplitude or spectrum loadings. The log-normal random variable model was shown to be quite reasonable for constant amplitude cyclic loadings. Likewise, it was demonstrated that the statistical model can be used to predict the fatigue crack propagation under spectrum loading using the base-line constant-amplitude test results [Refs. 26-27].

A literature survey has been made to investigate available fatigue crack propagation data. Unfortunately, most of the test results do not have enough replicates for a meaningful statistical analysis as well as model varification, except

one data set generated in Refs. 7 and 8. This data set, consisting of crack growth damage accumulation in the large crack size region, will be studied in this chapter.

Crack propagation experimental results of sixty-four (64) center-cracked specimens, made of 2024-T3 aluminum and subjected to a constant amplitude cyclic loading, were reported in Refs. 7 and 8. The time histories of half crack length, a(t), plotted against the number of cycles, t, are shown in Fig. 59 [after Ref. 7]. The initial half crack length of each specimen was 9 mm and the tests were terminated when each half crack length reached 49.8 mm. The maximum cyclic load was 5.2 kips (23.35 kN) and the stress ratio was 0.2. Data for the crack growth rate, da/dt, versus the stress intensity range, ΔK, were obtained from the test results using the seven point incremental polynomial method. The results were shown as dots in Refs. 7 and 8.

4.1 Synergistic Sine Hyperbolic Crack Growth Rate Function

The log crack growth rate data is not linearly related to the log stress intensity range, ΔK. As a result, the following synergistic sine hyperbolic function was shown to be very reasonable for the crack growth rate [Refs. 16, 25 and 26],

$$\frac{da(t)}{dt} = (10)^{C_1 \sinh[C_2(\log\Delta K + C_3)]+C_4} \tag{95}$$

in which a(t) is the half crack length, ΔK is the stress intensity range, C_1 is a material constant, and C_2, C_3 and

C_4 are parameters. Based on Eq. (6), the randomized form for Eq. (95) is given by

$$\frac{da(t)}{dt} = X(t)\,(10)^{C_1 \sinh[C_2(\log\Delta K + C_3)]+C_4} \tag{96}$$

in which X(t) is a stationary lognormal random process with a median value of unity.

Taking logarithms on both sides of Eq. (96) one obtains

$$Y = \log \frac{da(t)}{dt} = C_1 \sinh[C_2(\log\Delta K + C_3)]+C_4+Z(t) \tag{97}$$

where $Y = \log[da(t)/dt]$ is the log crack growth rate and

$$Z(t) = \log X(t) \tag{98}$$

is a stationary Gaussian (normal) random process with zero mean and standard deviation σ_Z.

The stress intensity range, ΔK, for the center-cracked specimen is given by

$$\Delta K = \frac{\Delta P}{Bw}\sqrt{\pi a(t)\sec[\pi a(t)/w]} \tag{99}$$

in which ΔP = load range = 4.16 kips, B = thickness of specimen = 0.1 inch, and w = width of specimen = 6.0 inch.

The log crack growth rate data versus log ΔK were given in Refs. 7 and 8. From these data, the method of maximum likelihood can be applied to estimate the parameters C_2, C_3, C_4, and the standard deviation σ_Z as described in detail in Refs. 25-26; with the results, C_2=3.4477, C_3 = -1.3902, C_4 = -4.5348 and σ_Z = 0.0823. The material constant C_1 for aluminum

is 0.5, i.e., $C_1 = 0.5$. The autocorrelation function $R_{zz}(\tau)$ and the power spectral density $\Phi_{zz}(\omega)$ of the stationary Gaussian random process Z(t) are given by Eqs. (19) and (20), respectively.

4.2 Lognormal Random Process Model and Correlation With Experimental Results

For the Gaussian white noise model, Monte Carlo simulations have been conducted in Refs. 7 and 8 as well as in the present study. The simulation results are shown in Fig. 60. Similar to Fig. 7, the Gaussian white noise model results in very little statistical dispersion for the crack growth damage accumulation, and hence it is not a valid model.

At the other extreme, the lognormal random variable model, i.e., X(t) = X and Z(t) = Z = log X is applied as follows. The γ percentile of the log crack growth rate $Y_\gamma(\Delta K, C_i)$, (i=1,2,3,4) follows from Eq. (97) as

$$Y_\gamma(\Delta K, C_i) = C_1 \sinh[C_2(\log \Delta K + C_3)] + C_4 + z_\gamma \qquad (100)$$

in which z_γ is the γ percentile of Z given by Eq. (40). The γ percentile of the crack growth rate becomes

$$\left[\frac{da(t)}{dt}\right]_\gamma = (10) ** Y_\gamma(\Delta K, C_i) \qquad (101)$$

Then, the γ percentile of the crack size after t cycles, denoted by $a_\gamma(t)$, is computed by numerically integrating

the γ percentile crack growth rate, yielding

$$a_\gamma(t) = a_0 + \sum_{j=1}^{m} \Delta a_j(\gamma) \tag{102}$$

$$\Delta a_j(\gamma) = \left[\frac{da(t)}{dt}\right]_\gamma \Delta t_j \tag{103}$$

in which $a_0 = a(0)$ is the initial crack size and

$$t = \sum_{j=1}^{m} \Delta t_j \tag{104}$$

The cycle-by-cycle numerical integration given by Eqs. (102)-(103) is deterministic and straightforward. Hence, by varying the value of the γ percentile, one obtains from a cycle-by-cycle integration a set of crack growth curves a(t), i.e., the crack size versus the number of cycles for each γ value. The results were shown in Ref. 26, in which a much larger statistical dispersion than the experimental results was observed.

After constructing a series of crack growth damage accumulation curves $a_\gamma(t)$ for many values of γ, one can establish (i) the distribution function $F_{T(a_1)}(t)$ of the number of load cycles $T(a_1)$ to reach any crack size a_1 by drawing a horizontal line through a_1, and (ii) the distribution function $F_{a(t)}(x)$ of the crack size a(t) at any number of load cycles t by drawing a vertical line through t. Then, the probability

of crack exceedance is obtained as $p(x_1,\tau) = 1 - F_{a(\tau)}(x_1)$.

The distribution functions for the random number of load cycles $T(a_1)$ to reach half crack lengths a_1 = 21 and 49.8 mm are presented in Figs. 61(a)-61(b) as solid curves, whereas the probability of crack exceedance at t = 150,000 cycles is displayed as a solid curve in Fig. 62. The corresponding experimental results obtained from Fig. 59 are shown in these figures as circles. It is observed from Figs. 61-62 that the lognormal random variable model is too conservative in such a situation.

For the lognormal random process model, sample functions of the normal random process Z(t) and the lognormal random process X(t) have been simulated using the Fast Fourier transform (FFT) technique previously described. Then, the corresponding sample function of the crack size, a(t), versus the number of load cycles, t, can be obtained from Eq. (96) using a cycle-by-cycle numerical integration procedure. The correlation parameter ξ^{-1} is chosen to be 9,524 cycles and the simulation results of a(t) versus t are presented in Fig. 63. A comparison between Figs. 59 and 63 indicates that the simulated sample functions resemble closely those of the experimental results.

The simulated distribution functions for the number of load cycles to reach some specific half crack lengths and the probability of crack exceedance at t = 150,000 cycles are presented in Figs. 64 and 65 as solid curves. Also shown in these figures as circles are the experimental results obtained from Fig. 59. It is observed from Figs. 64 and 65 that

the correlation between the lognormal random process model and the experimental results is very satisfactory.

4.3 Second Moment Approximation

The mean value, μ_x, and standard deviation, σ_x, of the stationary lognormal random process X(t) are related to the standard deviation σ_z of the normal random process Z(t) through Eqs. (64) and (65) as follows

$$\mu_x = \exp\left[\tfrac{1}{2}(\sigma_z \ell n 10)^2\right] \quad ; \quad \sigma_x = \mu_x\left[e^{(\sigma_z \ell n 10)^2} - 1\right]^{1/2} \tag{105}$$

The covariance function of the lognormal random process X(t) is given by Eq. (59), whereas the mean value, μ_W, standard deviation, σ_W, and coefficient of variation, V_W, of the random process W(t) are given by Eqs. (66) to (68) in terms of σ_z and ζ. The random process W(t) is defined by Eq. (52) as

$$W(t) = \int_{a_0}^{a(t)} \frac{dv}{L(v)} \tag{106}$$

in which it follows from Eqs. (95) and (96) that

$$L(v) = 10**\{C_1 \sinh[C_2(\log \Delta K + C_3)] + C_4\} \tag{107}$$

where $\Delta K = \Delta K(v)$ is given by Eq. (99) with a(t) being replaced by v, i.e.,

$$\Delta K = \frac{\Delta P}{Bw}\sqrt{\pi v \sec[\pi v/w]} \tag{108}$$

The distribution function of the crack size, a(t), after any number of load cycles, t, can be derived from that of W(t) through the transformation of Eq. (106) as follows

$$F_{a(t)}(x) = P[a(t) \leq x] = P[W(t) \leq y(x)] = F_{W(t)}[y(x)] \qquad (109)$$

in which $F_{W(t)}[y(x)]$ is the distribution function of W(t) evaluated at y(x) where

$$y(x) = \int_{a_0}^{x} \frac{dv}{L(v)} \qquad (110)$$

Hence, it follows from Eqs. (109) and (110) that

$$F_{a(t)}(x) = F_{W(t)}\left[\int_{a_0}^{x} \frac{dv}{L(v)}\right] \qquad (111)$$

in which L(v) is given by Eqs. (107) and (108).

The probability of crack exceedance $p(x_1,t)$, i.e., the probability that $a(\tau)$ will exceed any crack size x_1, is given by

$$p(x_1,\tau) = 1 - F_{W(\tau)}\left[\int_{a_0}^{x_1} \frac{dv}{L(v)}\right] \qquad (112)$$

Let $T(a_1)$ be the random number of load cycles when the crack size a(t) reaches a specific value a_1. Since the event $\{a(t) > a_1\}$ is the same as the event $\{T(a_1) \leq t\}$, the distribution function of $T(a_1)$ is given by

$$F_{T(a_1)}(t) = 1 - F_{a(t)}(a_1) \tag{113}$$

where $F_{a(t)}(a_1)$ is given by Eq. (111) in which x is replaced by a_1.

4.4 Gaussian Closure, Weibull, Gamma and Lognormal Approximations

Various approximations presented in Chapter 3, i.e., Gaussian closure approximation, Weibull approximation, lognormal approximation and gamma approximation, will be studied in the following.

(i) For the Gaussian closure approximation, the distribution of W(t) is assumed to be Gaussian given by Eq. (69) and the truncated distribution function, $F_{a^*(t)}(x)$, of the crack size a(t) is given by Eq. (72)

$$F_{a^*(t)}(x) = \frac{F_{a(t)}(x) - F_{a(t)}(a_0)}{1 - F_{a(t)}(a_0)} \quad ; \quad x \geq a_0 \tag{114}$$

in which

$$F_{a(t)}(x) = \Phi\left[\frac{\int_{a_0}^{x} \frac{dv}{L(v)} - \mu_W}{\sigma_W}\right] \tag{115}$$

where Eqs. (111) and (69) have been used, and

$$F_{a(t)}(a_0) = \Phi(-\mu_W/\sigma_W) \tag{116}$$

The distribution function of the random number of load cycles to reach any given crack size a_1, is given by Eq. (74), i.e.,

$$F_{T(a_1)}(t) = 1 - F_{a^*(t)}(a_1) \tag{117}$$

where $F_{a^*(t)}(a_1)$ is given by Eqs. (114)-(116) with x being replaced by a_1.

(ii) In the case of Weibull approximation, both the distribution functions $F_{a(t)}(x)$ and $F_{T(a_1)}(t)$ can be obtained from Eqs. (77) and (110)-(113) as follows:

$$F_{a(t)}(x) = 1 - \exp\left\{-\left[\int_{a_0}^{x} \frac{dv}{L(v)} \Big/ \beta\right]^{\alpha}\right\}; \quad x \geq a_0 \tag{118}$$

$$F_{T(a_1)}(t) = \exp\left\{-\left[\int_{a_0}^{a_1} \frac{dv}{L(v)} \Big/ \beta\right]^{\alpha}\right\} \tag{119}$$

in which α and β are obtained from Eqs. (78) and (79) in terms of V_W and μ_W.

(iii) For the lognormal approximation, the distribution functions of a(t) and $T(a_1)$ can easily be obtained from Eqs. (83), (110)-(113) as follows:

$$F_{a(t)}(x) = \Phi\left[\frac{\log\int_{a_0}^{x} \frac{dv}{L(v)} - \mu_{\log W}}{\sigma_{\log W}}\right]; \quad x \geq a_0 \tag{120}$$

$$F_{T(a_1)}(t) = 1 - \Phi\left[\frac{\log\int_{a_0}^{a_1} \frac{dv}{L(v)} - \mu_{\log W}}{\sigma_{\log W}}\right] \tag{121}$$

in which $\mu_{\log W}$ and $\sigma_{\log W}$ are given by Eqs. (84) and (85).

(iv) For the gamma approximation, the distribution functions of both $a(t)$ and $T(a_1)$ can easily be obtained from Eqs. (88) and (110)-(113) in the following

$$F_{a(t)}(x) = \gamma\left(\eta, \lambda\int_{a_0}^{x} \frac{dv}{L(v)}\right)\Big/\Gamma(\eta) \tag{122}$$

$$F_{T(a_1)}(t) = 1 - \left[\gamma\left(\eta, \lambda\int_{a_0}^{a_1} \frac{dv}{L(v)}\right)\Big/\Gamma(\eta)\right] \tag{123}$$

in which $\gamma(\ )$ and $\Gamma(\ )$ are the incomplete and complete gamma functions, respectively, and η and λ are given by Eqs. (91) and (92) in terms of V_W and μ_W.

The probability of crack exceedance $p(x_1,\tau)$ is given by

$$p(x_1,\tau) = 1 - F_{a(\tau)}(x_1) \tag{124}$$

in which $F_{a(\tau)}(x_1)$ is given by Eqs. (122), (120) and (118) for the gamma, lognormal and Weibull approximations, respectively. For the Gaussian closure approximation, however, $F_{a(\tau)}(x_1) = F_{a^*(\tau)}(x_1)$ is given by Eq. (114).

4.5 Correlation With Experimental Results

In addition to the crack propagation parameter values C_1, C_2, C_3, C_4 and the model statistics σ_z obtained previously, the correlation parameter ζ^{-1} is needed. In the present study, a value of ζ^{-1} is selected which gives a good correlation with the experimental results. With ζ^{-1} = 15,380 cycles, the distribution functions for the random number of load cycles to reach half crack lengths 13, 21 and 49.8 mm are presented in Fig. 66. The results of Weibull and gamma approximations are shown in Fig. 66(a) by dashed and solid curves, respectively. The results of Gaussian closure and lognormal approximations are presented in Fig. 66(b), respectively, by dashed and solid curves. Also shown in Fig. 66 as circles are the experimental test results obtained from Fig. 59 for comparison. The probability of crack exceedance based on various approximations are depicted in Fig. 67 as solid and dashed curves. The corresponding experimental results obtained from Fig. 59 are shown in the figures as circles. Figures 66 and 67 show that the correlations between various second moment approximations and the experimental results are very satisfactory.

CHAPTER 5

FACTORS AFFECTING STOCHASTIC PREDICTION OF FATIGUE CRACK PROPAGATION

5.1 Fatigue Crack Growth Analysis Procedures

In the deterministic crack growth analysis, the following procedures in four steps are used: (i) Experimental results for the crack size, a(t), versus cycles t (or flight hours), are measured. These test results are referred to as the primary data. (ii) The crack growth rate data are derived from the primary data in terms of ΔK, log ΔK or log a(t), etc. using various data processing procedures. (iii) An appropriate crack growth rate function, L, is chosen and best-fitted to the derived crack growth rate data to estimate the pertinent parameters. (iv) The crack growth rate function and the associated parameters obtained are used to predict the crack growth damage accumulation under different loading conditions either analytically or numerically. A schematic illustration of the deterministic crack growth analysis is shown in Fig. 69.

In the case of probabilistic analysis, primary data of many replicate specimens are needed. In addition, the statistical variability of crack growth data should be determined. Then, the statistical distribution of the crack growth damage accumulation can be predicted. The analysis procedures have been described in the previous chapters.

From the deterministic analysis standpoint, various kinds of error may be introduced in the sequential steps of fatigue crack growth analysis described above. For instance, measurement errors in primary data for the crack size, a(t), may result from the instrumentation precision and sensitivity. The measurement error may be manifested by other factors, such as the incremental measurement interval, Δa [e.g., Refs. 31-33].

In the second step above, various data processing procedures may be employed, including the direct secant and modified secant methods, as well as the methods of 3, 5, 7 and 9 point incremental polynomial. However, each procedure results in different crack growth rate data. In the third step, bias in determining the crack growth rate parameters may be induced by the number of data points associated with each test specimen. Finally, prediction errors may be introduced by the crack growth rate function used. From the standpoint of stochastic crack growth analysis, the statistical variability of the crack growth damage accumulation is very important, yet it may be influenced by various factors described above. As a result, the problems mentioned above should be investigated.

In this chapter, only the following two subjects will be studied: (1) possible bias in estimating the crack growth rate parameters due to unequal number of fractographic data (readings) for each test specimen, and (2) the effect of data processing procedure on the accuracy of the

stochastic crack propagation prediction. Various factors affecting the stochastic crack growth analysis will be reported elsewhere.

5.2 Equal Number of Data Points for Each Test Specimen

Since fatigue crack propagation involves considerable statistical variability, some specimens may have short fatigue lives while others may have longer lives. Therefore, more crack size measurements (readings) may be taken for slow crack growth specimens than for fast ones. This is particularly true for the fractographic readings of fastener holes where fatigue tests are conducted on specimens without an intentional preflaw. In fact, all the fractographic data sets investigated in this report do not have an equal number of data points for each specimen.

When such primary data are processed and the resulting crack growth rate data are pooled together for the linear regression analysis, see Figs. 5-10, the estimated crack propagation parameters, such as b and Q, are biased to the slow crack growth rate side. This is because more data points are usually measured for the slow crack growth specimens. As such, it clearly violates the statistical premise that each specimen (a sample) is of equal weight. Consequently, the resulting statistical fatigue crack propagation predictions are biased toward the unconservative side, i.e., the stochastic model tends to predict a longer propagation life or smaller crack size.

To circum ent such an error due to an unequal number of measurements for each specimen, additional data points for the primary data, i.e., a(t) versus t, can be added artificially to the fast crack growth specimens. The idea is to equalize the number of data points for each specimen. In most cases the artificial points can be determined by interpolation. However circumstances may arise where additional data points are needed outside the region of available primary data, and extrapolation procedures may not be satisfactory. In this case, it is suggested that the primary data for a particular specimen be best-fitted using the crack propagation model. Then the additional data points outside the available primary data region are obtained from the model.

To demonstrate such a crucial point, consider the CWPF data set. Crack growth rate data derived directly from the fractographic readings using the five point incremental polynomial method are used to estimate the crack propagation parameters b and Q, as well as the standard deviation of the log crack growth rate, σ_z. The results are presented in Table 4. Also shown in the table are the corresponding values from Table 1 in which additional data points have been added artificially to those specimens with fast crack growth rates to equalize the number of a(t) versus t data points. Based on the lognormal random variable model, the distribution functions for the random time to reach some specific crack sizes are shown in Fig. 28 as dashed curves.

Also shown in the figure as solid curves are the corresponding results with added data points. The circles shown in the figure are the experimental results. As expected, the dashed curves are biased toward slow crack growth and hence their correlations with the experimental results are not as good as the solid curves.

5.3 Data Processing Procedures

As described in the previous chapters, the fatigue crack growth rate parameters as well as the statistics of the stochastic model are determined from the crack growth rate data. The former represents the median crack growth behavior that can be used for deterministic crack propagation analysis. The latter is influenced exclusively by the statistical variability of the crack growth rate data. Since, however, the crack growth rate data are derived from the primary data, their median behavior and statistical dispersion are affected by several important factors;

(i) The inherent variability of the crack growth resistance in materials,

(ii) The variability of fatigue loadings and environments,

(iii) Measurement errors in the primary data,

(iv) The incremental measurement interval Δa in the primary data, and

(v) The data processing procedures in deriving the crack growth rate data from the primary data.

The purpose of establishing the stochastic fatigue crack growth model is to account for (i) and (ii) above, although the consideration of loading and environmental variabilities is beyond the scope of the present study. Hence, the influence by factors (iii), (iv) and (v) should be minimized.

Various data processing procedures, including the direct secant method, modified secant method, and 3, 5, 7 and 9 point incremental polynomial methods, have been proposed in the literature [Refs. 8,29,34-36,69]. All the data sets studied in this report, including the center-cracked specimens, have been analyzed using each data processing technique. The statistical variability of the crack growth rate data varies depending on the data processing method used. It is found that the secant method introduces a much larger additional statistical dispersion for the crack growth rate data than any of the incremental polynomial methods. This is not surprising because the incremental polynomial method tends to smooth out the data. The induced undesirable statistical variability of the crack growth rate data reduces slightly as more points are used in the incremental polynomial, such as 9 or 7 points. While it may be desirable to use the 7 or 9 point incremental polynomial method, the limited amount of data available may inhibit its application. As a result, the five point incremental polynomial method appears to be quite reasonable.

Again, the CWPF data set is considered for illustrative purposes. With the application of the modified secant method, the estimated parameters b and Q, the standard deviation, σ_z, and the coefficient of variation, V, of the crack growth rate are shown in Table 4 for comparison. Based on the lognormal random variable model and the modified secant method, the distribution functions of the random time to reach some specific crack sizes are displayed in Fig. 28 as dotted curves. It is observed from Fig. 28 that the modified secant method introduces a larger statistical dispersion and hence its correlation with the experimental tests results (circles) is not as good as the five point incremental polynomial method (solid curves). Similar behaviors have been observed in all other data sets. Finally, poorer correlation is obtained using the direct secant method than the modified secant method. It is concluded that, for the stochastic crack growth analysis, the method of five point incremental polynomial is superior to both the direct secant and modified secant methods.

CHAPTER 6

A STOCHASTIC INITIAL FATIGUE QUALITY MODEL FOR FASTENER HOLES AND DURABILITY ANALYSIS

6.1 Introduction

Metallic airframes contain thousands of fastener holes which are susceptible to fatigue cracking in service. The accumulation of relatively small fatigue cracks in fastener holes (e.g., 0.03" - 0.05") must be accounted for in the design of aircraft structures to assure that the structures will be durable and can be economically maintained [2-5].

A durability analysis methodology has recently been developed for quantifying the extent of fatigue damage in fastener holes as a function of time and applicable design variables [6,43-47]. This methodology is based on the fracture mechanics philosophy, combining a probabilistic format with a deterministic crack growth approach. The initial fatigue quality (IFQ) of fastener holes is treated as a random variable and is represented by an equivalent initial flaw size (EIFS) distribution. The existing durability analysis methodology has been demonstrated for making crack exceedance predictions in the small crack size region (e.g., <0.10") for full-scale aircraft structure under both fighter and bomber load spectra [6,45-47,64].

Further research is now being conducted [66] to: (1) extend the present durability analysis methodology to the large crack size region (e.g., >0.10"), (2) refine the methods for determining a generic EIFS distribution, (3) develop procedures for optimizing the equivalent initial flaw size distribution (EIFSD) parameters, and (4) develop a better understanding of the effects of crack growth rate dispersion on the EIFS distribution and on the accuracy of crack exceedance predictions in both the small and large crack size regions.

In the current durability analysis methodology [6,60, 64,44], the EIFS is determined by back-extrapolating available fractographic results [e.g., 48] to time zero using a single deterministic crack growth equation, referred to as the EIFS master curve,

$$da(t)/dt = Q[a(t)]^b \qquad (125)$$

in which $da(t)/dt$ = crack growth rate, $a(t)$ = crack size at any time t and Q and b are empirical constants which are dependent upon the load spectrum and other design parameters.

The crack growth rate, however, involves statistical variability, which is not accounted for in back-extrapolation. Hence, the statistical distribution of EIFS thus established contains the statistical dispersion of the crack growth rate in the very small crack size region. This approach is quite reasonable if the resulting EIFS distri-

bution is employed to predict the statistical crack growth damage accumulation in service using a deterministic service crack growth master curve in the small crack size region. This has been demonstrated in Refs. 6, 44, 60 and 64. The main advantage of such an approach is that the durability analysis procedure can be simplified mathematically.

Another possible approach is to obtain the EIFS values by back-extrapolating available fractographic results stochastically. Thus, the statistical dispersion of the crack growth rate in the small crack size region is filtered out, and the resulting EIFS distribution represents the true initial fatigue quality (IFQ). Such an EIFS distribution will have a smaller dispersion than that obtained using a deterministic EIFS crack growth master curve. This EIFS model is referred to as the stochastic-based initial fatigue quality model. In predicting the statistical crack growth damage accumulation in service using the stochastic-based EIFS model, however, the stochastic crack growth rate equation should be used. As a result, the feasibility of such a stochastic approach depends essentially on the establishment of a reasonable but simple stochastic crack propagation model.

The objectives of this chapter are to: (1) develop the durability analysis methodology using the stochastic-based IFQ model, and (2) evaluate proposed EIFS data pooling methods and procedures for optimizing the EIFS distribution parameters.

Analytical expressions are derived for the cumulative distributions of the time to initiate a crack of any size, and the crack size at any service life. These expressions are based on a stochastic transformation of the cumulative distribution of EIFS and the theorem of total probability. Actual crack propagation results for two fractographic data sets (7475-T7351 aluminum fastener hole specimens; fighter and bomber load spectra) in the small crack size region are used in the investigation [48]. A correlation study is performed to compare the results of the stochastic-based IFQ model with actual fractographic results. Very reasonable correlations were obtained. The proposed procedures for EIFS data pooling and for optimizing the EIFS distribution parameters are promising for future durability analysis applications.

6.2 Application of Lognormal Random Variable Model

The investigation of various stochastic crack growth rate models presented in the previous chapters is aimed at possible applications to durability and damage tolerance analyses as well as the inspection and repair maintenance problems. From the standpoint of practical applications, the lognormal random variable model appears to be most appropriate because of the following reasons: (i) It is the simplest mathematical model for which the analytical solution is possible for many problems. Likewise, it can easily be understood by engineers. (ii) The correlation with crack propagation data in fastener holes is very reasonable, and

the model always results in a slight conservative prediction. (iii) The model does not need the correlation parameter for the crack growth rate, thus eliminating the requirement for extensive test results. A few crack propagation parameters and the model statistics can be estimated from a limited amount of base-line test results, which is usually the case in practical applications. (iv) The model can be extended easily to incorporate other statistical uncertainties involved in the crack growth damage accumulation. This includes the statistical variability of stress intensity factor, applied stresses, crack modeling, etc., as will be described later [e.g., Refs. 22-24]. As a result, the lognormal random variable model will be used in the following two chapters.

The lognormal random variable model for fastener holes under fighter or bomber load spectra is given by Eq. (37) as

$$da(t)/dt = XQ[a(t)]^b \tag{126}$$

in which X is a lognormal random variable with a median of 1.0. Such a model has been demonstrated to be very reasonable, and it simplifies the stochastic crack growth analysis significantly.

Taking the logarithm of both sides of Eq. (126) yields

$$Y = bU + q + Z \tag{127}$$

where

$$\left.\begin{aligned} Y &= \log da(t)/dt \quad , \quad U = \log a(t) \\ q &= \log Q \quad , \quad Z = \log X \end{aligned}\right\} \tag{128}$$

Since X is a lognormal random variable with a median of 1.0, it follows from Eq. (128) that Z = log X is a normal random variable with zero mean and standard deviation σ_z. The crack growth rate parameters b and Q as well as the standard deviation, σ_z, of Z can be estimated from the log crack growth rate, log[da(t)/dt] = Y, versus log crack length, log a(t) = U, data, denoted by (Y_i, U_i) for i = 1, 2, ...,n, using Eq. (127) and the linear regression analysis. Since Eq. (127) is linear, the results obtained from the method of linear regression are identical to those of the method of least-squares or the method of maximum likelihood. Expressions for b, Q and σ_z are given by

$$\left.\begin{aligned} b &= \frac{n\Sigma U_i Y_i - (\Sigma U_i)(\Sigma Y_i)}{n\Sigma U_i^2 - (\Sigma U_i)^2} \\ Q &= 10^{\lambda} \;;\quad \lambda = \frac{\Sigma Y_i - b\Sigma U_i}{n} \\ \sigma_z &= \left\{\frac{\Sigma[Y_i - (q - bU_i)]^2}{n-1}\right\}^{\frac{1}{2}} \end{aligned}\right\} \qquad (129)$$

in which n = number of samples (i.e., crack growth rate data) and the other terms have been previously defined.

6.3 Stochastic Crack Growth Analysis

Expressions are derived for predicting the cumulative distributions of crack size at any given time t and of TTCI for any given crack size a_1. Essential elements of the stochastic crack growth approach are described in Fig. 69 and details are provided later.

6.3.1 Equivalent Initial Flaw Size (EIFS) Concept

An equivalent initial falw size (EIFS) is a hypothetical initial falw assumed to exist in a structural detail which characterizes the equivalent effect of actual flaws produced by the manufacturing process. Such flaws must be consistently defined so that the EIFSs for different fractographic specimens are on the same baseline. EIFSs are defined by back-extrapolating suitable fractographic results to time zero (Fig. 69, Frame A). The objective is to define a statistical distribution of EIFS and then to verify that the derived distribution will provide reasonable predictions for the cumulative distributions of TTCI and a(t) (Fig. 69, Frame D and Fig. 70).

6.3.2 Analysis Procedures

1. EIFS is a random variable and each individual value is determined by back-extrapolating fractographic results for each individual crack (or specimen).
2. The population of EIFSs is fitted by a suitable cumulative distribution, denoted as $F_{a(0)}(x)$ (Fig. 69, Frame B).
3. A stochastic crack growth law, such as Eq. (126), which accounts for the statistical dispersion of the crack growth rate (Fig. 69, Frame C), provides the basis for growing flaws backward and forward.
4. A stochastic transformation of $F_{a(0)}(x)$ is made using the crack growth law, Eq. (126), to obtain

expressions for the cumulative distributions of crack size, $F_{a(t)}(x)$, and of TTCI, $F_{T(a_1)}(t)$, Fig. 70.

6.3.3 Crack Size-Time Relationships

Two different crack size-time relationships can be obtained by integrating Eq. (126), considering b = 1 and b ≠ 1, from t = 0 to any time t. The resulting expressions for b = 1 and b ≠ 1 are shown in Eqs. (130) and (131), respectively,

$$a(t) = a(0)\exp[XQt] \quad ; \quad b = 1 \tag{130}$$

$$a(t) = \{[a(0)]^{-c} - cQtX\}^{-1/c} \quad ; \quad b \neq 1 \tag{131}$$

where, a(t) = crack size at any time t, a(0) = crack size at t = 0 (EIFS), Q = crack growth rate constant, c = b - 1, and X = lognormal random variable with median of 1.0

6.3.4 Cumulative Distribution of EIFS

Various distribution functions defined in the positive domain may be used to fit the EIFS values, such as the Weibull, lognormal, beta, etc. The following distribution function, which is derived based on the three-parameter Weibull distribution for TTCI and the deterministic crack growth law of Eq. (125) with b = 1, will be used herein;

$$f_{a(0)}(x) = \exp\left\{-\left[\frac{\ell n(x_u/x)}{\phi}\right]^{\alpha}\right\} \quad ; \quad 0 \leq x \leq x_u$$
$$= 1.0 \quad ; \quad x \geq x_u \tag{132}$$

in which $F_{a(0)}(x) = P[a(0) \leq x]$ is the cumulative distribution of EIFS, indicating the probability that the EIFS, a(0), will be smaller or equal to a value x. In Eq. (132), x_u = upperbound of EIFS and α and ϕ are two empirical constants [6]. In the original derivation of Eq. (132) in Ref. 6, the notation "Qβ" was used instead of "ϕ". To distinguish between the deterministic and stochastic crack growth approaches, the notation "ϕ" is used herein. The expression given by Eq. (132) is considered to be reasonable for the distribution of the stochastic-based EIFS.

6.3.5 Cumulative Distribution of Crack Size

The conditional distribution function of the crack size a(t), denoted by $F_{a(t)}(x|z) = P[a(t) \leq x | X=z]$, given that the lognormal random variable X takes a value z, can be obtained from Eq. (132) through a transformation of Eqs. (130) and (131) for b = 1 and b ≠ 1, respectively. Then, the unconditional cumulative distribution of crack size a(t), $F_{a(t)}(x)$ = $P[a(t) \leq x]$, is obtained from the conditional one, $F_{z(t)}(x|z)$, using the theorem of total probability. The results for $F_{a(t)}(x)$ are shown in Eqs. (133) and (134) for b = 1 and b ≠ 1, respectively.

$$F_{a(t)}(x) = \int_0^\infty \exp\left\{-\left[\frac{Qzt + \ell n(x_u/x)}{\phi}\right]^\alpha\right\} f_X(z)dz \; ; \qquad (133)$$

for $b = 1$

$$F_{a(t)}(x) = \int_0^\infty \exp\left\{-\left[\frac{c\ell nx_u + \ell n(x^c + cQtz)}{c\phi}\right]^\alpha\right\} f_X(z)dz \; ; \qquad (134)$$

for $b \neq 1$

In Eqs. (133) and (134), $f_X(z)$ is the lognormal probability density function of X given by

$$f_X(z) = \frac{\log e}{\sqrt{2\pi}\, z\sigma_z} \exp\left\{-\frac{1}{2}\left(\frac{\log z}{\sigma_z}\right)^2\right\} \qquad (135)$$

in which σ_z is the standard deviation of the normal random variable $Z = \log X$ given in Eq. (128).

6.3.6 Cumulative Distribution of TTCI

Let $T(a_1)$ be the random time to initiate a crack size a_1. Then, the distribution of $T(a_1)$, denoted by $F_{T(a_1)}(t) = P[T(a_1) \leq t]$, can be derived from that of a(t) as follows. Since the event $\{T(a_1) \leq t\}$ is the same as the event $\{a(t) > a_1\}$, one has

$$F_{T(a_1)}(t) = 1 - F_{a(t)}(a_1) \qquad (136)$$

Substituting Eqs. (133) and (134) into Eq. (136), one obtains for $b = 1$ and $b \neq 1$, respectively,

$$F_{T(a_1)}(t) = 1 - \int_0^\infty \exp\left\{-\left[\frac{Qzt + \ell n(x_u/a_1)}{\phi}\right]^\alpha\right\} f_X(z)dz \; ; \qquad (137)$$

for $b = 1$

$$F_{T(a_1)}(t) = 1 - \int_0^\infty \exp\left\{-\left[\frac{c\ell n x_u + \ell n(a_1^c + cQtz)}{c\phi}\right]^\alpha\right\} f_X(z)dz \; ; \qquad (138)$$

for $b \neq 1$

in which $f_X(z)$ is given by Eq. (135).

Equations (133)-(134) and (137)-(138) are not amenable to analytical integrations. However, these equations can easily be solved by a straight-forward numerical integration.

6.4 Determination of EIFS Distribution Parameters

Procedures are described and discussed for determining EIFS values based on the stochastic crack growth approach and fractographic data. EIFS pooling concepts and justification are considered and procedures are described for optimizing the EIFS distribution parameters in Eq. (132), i.e., x_u, α and ϕ. For brevity, the discussion is limited to the $b = 1$ case.

6.4.1 Stochastic-Based EIFS

EIFS values are determined by back-extrapolating suitable fractographic data based on fatigue cracking results in fastener holes without intentional initial flaws. Such data are currently available for both straight-bore and countersunk fastener holes [e.g., 48,65].

When the deterministic crack growth approach is used [6,67,68] to determine EIFSs, the same EIFS master curve is used to back-extrapolate to time zero for each fatigue crack in the fractographic data set. In this case the statistical dispersion of the crack growth rate is included in the resulting EIFS values.

When the crack growth rate is treated as a stochastic process, such as Eq. (126), the fractographic results should be back-extrapolated to time zero using the applicable crack growth records for a given fractographic sample (specimen). A stochastic-based EIFS value is obtained for each fractographic sample in the data set. In this case, the statistical dispersion of the crack growth rate is reflected in the random variable X and hence it is filtered out from the EIFS.

A stochastic-based EIFS value can be obtained for a given fractographic sample, say jth specimen, based on

$$a_j(0) = a_j(t)\exp[-X_j Qt] \tag{139}$$

in which X_j is the jth sample value of the lognormal random variable X, and $a_j(0)$ and $a_j(t)$ are the corresponding jth sample values of EIFS and the crack size at time t, respectively.

Using the least squares criterion, one obtains the expression for $a_j(0)$,

$$a_j(0) = \exp\left\{\frac{[\Sigma \ell n a_j(t_i)](\Sigma t_i^2) - (\Sigma t_i)[\Sigma (t_i)\ell n a_j(t_i)]}{N\Sigma t_i^2 - (\Sigma t_i)^2}\right\} \tag{140}$$

in which $a_j(t_i)$ = crack size of jth specimen at time t_i and N = number of $[a_j(t_i),t_i]$ pairs for the jth fractographic sample. Thus, using Eq. (140), $a_j(0)$ can be determined directly from $[a_j(t_i),t_i]$ pairs without computing the X_jQ value in Eq. (139).

It has been shown that the range of the fractographic crack size used affects the EIFS values [64]. Therefore, EIFS values should be determined using fractographic results in the same crack size range. For example, the upper and lower bounds of the crack size range is denoted by a_u and a_ℓ as shown in Fig. 69, Frame A.

6.4.2 EIFS Pooling Concepts

For practical durability analysis, an EIFS distribution is needed to represent the initial fatigue quality variation of the fastener holes. Ideally, such a distribution can be determined for a given material, fastener hole type (e.g., straight-bore or countersunk) and drilling procedure from fractographic results reflecting different test variables (e.g., stress level, % bolt load transfer and load spectra). The resulting EIFS distribution can be used to perform durability analyses for other conditions. In other words, an EIFS distribution (EIFSD), based on different fractographic results, is sought which is suitable for a broad range of durability analysis applications (e.g., different stress levels, % bolt load transfer and load spectra).

One way to justify using a given equivalent initial flaw size distribution (EIFSD) for a general durability analysis

is to define the EIFSD parameters using pooled EIFS values obtained from different fractographic data sets. For example, fractographic results are available for the same material, fastener hole type/fit and drilling procedure for different stress levels, % bolt load transfer and load spectra [48,65]. If compatible EIFSs can be determined for different fractographic data sets, then the EIFSs can be pooled to determine the EIFSD parameters. Pooling the EIFSs is very desirable because this increases the sample size and therefore the confidence in the EIFSD parameters. Also, since different fractographic data sets are used to determine the EIFSD parameters, it forces the derived EIFSD to cover a wider range of variables.

6.4.3 Optimization of EIFS Distribution Parameters

Once the EIFSs have been determined for selected fractographic data sets, they can be pooled and the parameters x_u, α, and ϕ can be optimized to "best fit" the pooled EIFSs to the theoretical cumulative distribution, $F_{a(0)}(x)$, shown in Eq. (132). The optimization procedure described below is intended for Eq. (132) but the same ideas can be applied to other $F_{a(0)}(x)$ distributions.

In Eq. (132), x_u defines the EIFS upper bound limit, i.e., the maximum initial flaw size in $F_{a(0)}(x)$. A value of $x_u = 0.03"$ is assumed to be a reasonable upper bound limit for the EIFSD. This limit is arbitrarily based on the typical economical repair limit for fastener holes [6,43,67, 68]. Another reason for limiting x_u to <0.03" is to

eliminate the probability of exceeding a crack size of 0.03" at time zero. This is equivalent to assuming that no fastener hole will have an initial flaw size >0.03". If a larger x_u limit is used, then the probability of exceeding an initial flaw size of 0.03" will not be zero, which implies that some fastener holes could have an initial flaw size greater than the economical repir limit before the structure enters into service.

The EIFSD parameters x_u, α and ϕ in Eq. (132) are optimized using the following iterative procedure.

1. Assume a value of x_u: largest EIFS $\leq x_u \leq$ 0.03".

2. Compute α and ϕ by least-squares fitting the pooled EIFSs to $F_{a(0)}(x)$ given in Eq. (132). Equation (132) is transformed into the following linear least-squares fit form,

$$W = \alpha V + B \tag{141}$$

where

$$W = \ell n \{- \ell n F_{a(0)}(x)\}; \quad V = \ell n\{\ell n(x_u/x)\}$$
$$B = -\alpha \ell n \phi \tag{142}$$

Let x_i (i=1,2,...,N) be the ith smallest EIFS sample value with N being the pooled sample size of EIFS values. The distribution function corresponding to x_i is given by $F_{a(0)}(x_i) = i/(N+1)$. Then the parameters α and ϕ in Eq. (141) can be determined using the following least-squares fit equations,

$$\alpha = \frac{N\Sigma V_i W_i - (\Sigma V_i)(\Sigma W_i)}{N\Sigma V_i^2 - (\Sigma V_i)^2} \quad ; \quad \phi = \exp\left(\frac{\alpha\Sigma V_i - \Sigma W_i}{\alpha N}\right) \tag{143}$$

where V_i and W_i are the sample values of V and W associated with x_i and $F_{a(0)}(x_i)$, respectively, as defined in Eq. (142).

3. Compute the goodness-of-fit of the established $F_{a(0)}(x)$ for the given x_u, α and ϕ. The standard error and Kolmogorov-Smirnov statistics (K-S value) are two reasonable measures of goodness-of-fit tests. The standard error, denoted by σ_E, is expressed as

$$\sigma_E = \left\{\frac{\Sigma\left[\frac{k}{N+1} - F_{a(0)}(x_k)\right]^2}{N}\right\}^{1/2} \tag{144}$$

in which all the EIFS sample values are arranged in an ascending order $(x_1, x_2, \ldots, x_k, \ldots, x_N)$, k = rank of EIFS value and N = total No. of pooled EIFS samples.

Let $S_N(x)$ be the empirical distribution of the EIFS values defined as follows; $S_N(x) = 0$ for $x < x_1$; $S_N(x) = k/N$ for $x_k \leq x < x_{k+1}$; $S_N(x) = 1$ for $x > x_N$. Then, the K-S statistics, denoted by D_{max}, is the maximum absolute difference between the empirical distribution $S_N(x)$ and the theoretical $F_{a(0)}(x)$ values given by

$$D_{max} = \max_x \left| S_N(x) - F_{a(0)}(x) \right| \tag{145}$$

4. Steps 1-3 are repeated to minimize the standard error σ_E and K-S value D_{max}.

6.4.4 Determination and Normalization of Forward Crack Growth Rate Parameters

The statistical distribution of the crack growth damage in service, such as $F_{a(t)}(x)$ and $F_{T(a_1)}(t)$ given by Eqs. (133)-(138), is derived using the EIFS distribution, $F_{a(0)}(x)$, and the forward stochastic crack growth rate equation, Eq. (126). The parameters b, Q and σ_z appearing in Eq. (126) have been obtained in Eq. (129) when the fractographic data for the applicable service environment are available. When the fractographic results are not available, however, these parameters should be determined from the general crack growth computer program. This subject will be discussed in another document.

When pooled EIFS results are used to determine x_u, α and ϕ in Eq. (132), the Q value for a given fractographic data set should be normalized to the same baseline as the EIFSD. This is needed to assure that $F_{a(t)}(x)$ and $F_{T(a_1)}(t)$ predictions for a given data set are consistent with the basis for the EIFSD.

Let $(x_u,\alpha,\phi)_{\text{data set}}$ and $Q_{\text{data set}}$ be, respectively, the EIFSD parameters and the forward crack growth rate parameter using a given fractographic data set alone (without pooling procedures). Then, the normalized Q values for such a given data set, denoted by $\hat{Q}_{\text{data set}}$, in the forward crack growth analysis is suggested to be

$$\hat{Q}_{\text{Data Set}} = \frac{\phi_{\text{Pooled}}}{\phi_{\text{Data Set}}} \left(Q_{\text{Data Set}} \right) \tag{146}$$

Thus, when pooled EIFS results are used, the Q value appearing in Eqs. (133)-(138) for a given fractographic data set should be replaced by $\hat{Q}_{\text{data set}}$. This approach will be illustrated in the following correlation study.

6.5 Correlation With Test Results

Fatigue crack growth results are available for fatigue cracking in fastener holes without the presence of intentional initial flaws [e.g., 48]. Two fractographic data sets from Ref. 48 will be used to evaluate: (1) the stochastic-based IFQ model developed, (2) the proposed EIFS data pooling procedure, (3) the procedure for optimizing the EIFSD parameters and (4) the effectiveness of the derived EIFSD and stochastic crack growth approach for making $F_{a(t)}(x)$ and $F_{T(a_1)}(t)$ predictions. The distribution of the crack size, $F_{a(t)}(x)$, will be considered at two different service times and that of TTCI, $F_{T(a_1)}(t)$, will be considered at crack sizes a_1 = 0.03", 0.05" and 0.10". Predicted results will be compared with actual fractographic data.

6.5.1 Fractographic Data Sets

Two fractographic data sets, identified as "WPF" and "WPB", reflect 7475-T7351 aluminum, replicate dog-bone specimens with a 1/4" diameter straight-bore, centered hole containing an unloaded protruding head steel bolt (NAS6204)

with a clearance fit. The "WPF" and "WPB" data sets were fatigue tested in a lab. air environment using a fighter spectrum and bomber spectrum, respectively. A maximum gross section stress of 34 ksi was selected for each spectrum. The test specimens were fatigue tested without intentional flaws in the fastener hole and natural fatigue cracks were allowed to occur. Following the fatigue test, the largest fatigue crack in each fastener hole was evaluated fractographically. Fractographic results (i.e., a(t) versus t records) were presented in Ref. 48. The number of fatigue cracks used in this invstigation is 33 for the WPF data set and 32 for the WPB data set.

6.5.2 EIFS Parameters

EIFSs for each fatigue crack in the WPF and WPB data sets were computed using Eq. (140) and the fractographic results in the crack size range from 0.01" to 0.05". The ranked EIFSs for the WPF and WPB data sets are summarized in Table 5 in an ascending order of crack size.

EIFSD parameters x_u, α and ϕ were determined using the EIFS values for the WPF, WPB and combined WPF and WPB data sets. Different values were assumed for x_u and the corresponding α, ϕ, standard error σ_E and D_{max} (K-S) values were determined using Eqs. (142)-(145), respectively. The results are summarized in Table 6.

6.5.3 Goodness-of-Fit Plots

EIFSD parameters based on x_u = 0.03" were used to make predictions for $F_{a(t)}(x)$ and $F_{T(a_1)}(t)$ based on Eqs. (133)

and (137), respectively. The upper bound value of $x_u = 0.03$" was used because the standard error, σ_E, and the K-S value, D_{max}, "indicators" for the EIFSD goodness-of-fit shown in Table 6 were smaller than those values for $x_u < 0.03$".

The forward crack growth parameter Q in Eqs. (126), (133) and (137) and the standard deviation of the crack growth rate, σ_z, were estimated for each data set (i.e., WPF and WPB) using the applicable log da(t)/dt versus log a(t) data and Eq. (129) with b = 1. Crack growth rates, da(t)/dt, were determined for each fatigue crack in each fractographic data set based on the 5-point incremental polynomial method [69]. A typical plot of log da(t)/dt versus log a(t) is shown in Fig. 71 for the WPF data set.

Normalized Q values, denoted by $\hat{Q}$, were determined for each data sets using Eq. (146) for individual and pooled EIFS data sets with the following results: $\hat{Q} = 2.708 \times 10^{-4}$ (WPF) and $\hat{Q} = 1.272 \times 10^{-4}$ (WPB). Results of Q, $\hat{Q}$ and σ_z are summarized in Table 7.

With the durability analysis approach using the stochastic -based EIFS model described above and the parameters presented in Table 7 for the six cases considered, the distributions of the crack size at any service life, $F_{a(t)}(x)$, and the TTCI at any crack size can be predicted theoretically, using Eqs. (133) and (137), respectively.

The cumulative distribution of crack size at two different service times (WPF at 9,200 and 14,800 flight hours, and WPB at 29,109 and 35,438 flight hours) are plotted in Figs.

72-77 as a solid curve for the theoretical predictions. The experimental results are also plotted in these figures using selected symbols. For example, in Fig. 72 the results for t = 0, 9,200 and 14,800 flight hours are denoted by an open circle, a star and a square, respectively. In Figs. 73 and 74, an open circle and a solid circle denote the EIFS values at t = 0 for the WPF and WPB data sets, respectively.

Plots fo theoretical predictions of the cumulative distribution of TTCI at crack sizes 0.03", 0105" and 0.1" are shown as solid curves in Figs. 78-80 and Figs. 81-83 for the WPF and WPB data sets, respectively. The corresponding ranked TTCI test results are displayed in these figures as a circle, star and square, respectively. Symbols for the WPF data set are open and those for the WPB data set are solid.

The following observations are based on Figs. 72-77:

1. The theoretical predictions for $F_{a(t)}(x)$ generally fit the overall test results better when the EIFSs for a given data set are sued (e.g., see Fig. 72 and 75).

2. When the EIFSD parameters are based on the pooled EIFSs for the WPF and WPB data sets, the theoretical predictions for $F_{a(t)}(x)$ for a given data set generally correlate better with the ranked experimental results when the crack growth parameter Q is normalized using Eq. (146). For example, compare the plots shown in Figs. 73 and 74 and Figs. 76 and 77 for the WPF and WPB data sets, respectively.

3. The upper tail of $F_{a(t)}(x)$ (i.e., largest crack sizes) is of most interest for durability analysis. For all

the cases considered herein the theoretical predictions for crack exceedance (i.e., $p(i,\tau) = 1-F_{a(\tau)}(x_1)$) in the upper tail generally fit the ranked experimental results very well. In Fig. 76 the theoretical predictions for $F_{a(t)}(x)$ for the WPB data set are conservative in the upper tail (i.e., the predicted crack exceedance is larger than the ranked test results). In this case, the Q value is not normalized. The goodness-of-fit improves significantly when Q is normalized.

4. It is interesting to note that reasonable $F_{a(t)}(x)$ predictions are obtained for crack sizes larger than the fractographic crack size range used to determine the EIFSD parameters (i.e., 0.01"-0.05"). This is encouraging.

The following observations are based on Figs. 78-83.

1. The lower tail (i.e., smallest TTCIs) of the TTCI cumulative distribution, $F_{T(a_1)}(t)$, is generally the area of most interest for durability analysis. As shown in Figs. 78-83, the theoretical predictions for $F_{T(a_1)}(t)$ correlate very well with the ranked experimental results.

2. The overall fit is generally improved when Q is normalized. For example, compare results for Fig. 79 and 80 and Fig. 82 and 83 for the WPF and WPB data sets, respectively.

3. Reasonable $F_{T(a_1)}(t)$ predictions for the WPF and WPB data sets are obtained in the lower tail for $a_1 = 0.10"$, see Figs. 80 and 83. Thus, reasonable $F_{T(a_1)}(t)$ predictions are obtained for a crack size outside the fractographic crack size range used to define the EIFSD parameters.

6.6 Conclusions for Stochastic IFQ Model for Durability Analysis

Expressions have been developed for predicting the cumulative distribution of crack size at any given time, and the cumulative distribution of times to reach any given crack size using the stochastic-based EIFS model. These expressions, based on a stochastic crack growth approach, have been evaluated for the durability analysis of fastener holes in the small crack size region (e.g., < 0.10"). The analytical expressions for $F_{a(t)}(x)$ and $F_{T(a_1)}(t)$ are derived based on a stochastic transformation of the theoretical EIFSD. EIFS data pooling concepts and procedures for optimizing the distribution parameters have been presented and evaluated.

Theoretical predictions for $F_{a(t)}(x)$ and $F_{T(a_1)}(t)$ compared reasonably well with ranked experimental results when both the WPF and WPB data sets were considered separately. Overall fits based on pooled EIFS values for both WPF and WPB data sets were improved when the normalized crack growth parameters were used. EIFS distributions based on normalized crack growth results need to be investigated further for a wide range of practical durability analysis situations.

The upper tail of the EIFSD is of most interest for durability analysis because the large initial flaws are more apt to cause crack exceedance problems than the smaller

initial flaw sizes. The EIFSD can be force-fitted to the upper tail of the EIFS population. This may provide an even better fit of the EIFSD to the tail area of most interest [70]. This aspect needs to be investigated further.

The EIFS pooling concepts and procedures for optimizing EIFS distribution parameters are promising for determining a reasonable EIFSD for practical durability analyses. Further research is needed to determine the EIFSD parameters based on pooled EIFSs for several fractographic data sets and to evaluate the accuracy and limits of the durability analysis predictions in the small crack size region (e.g., < 0.10").

A parallel investigation to the one described herein has been performed using the deterministic crack growth approach [66]. The results of this investigation will be reported in the future. Based on the results for the stochastic and deterministic crack growth approaches, it is concluded that either approach is satisfactory for the durability analysis of aluminum alloys in the small crack size region. However, since the deterministic crack growth approach is mathematically simpler, this approach is recommended for use in the small crack size region. Further research is needed to show that the deterministic crack growth approach is also satisfactory for other alloys in the small crack size region. Also, the deterministic and stochastic crack growth approaches need to be investigated for durability analysis applications in the large crack size region.

CHAPTER 7

FATIGUE RELIABILITY OF STRUCTURAL COMPONENTS UNDER SCHEDULED INSPECTION AND REPAIR MAINTENANCE

Fatigue cracking is one of the most important damage modes in aircraft structures. To prevent catastrophic failure, fatigue-critical components, such as wings, fuselages, gas turbine engine disks, etc., are usually subjected to scheduled inspection or proof test maintenance. In order to establish an optimal inspection and repair or proof test maintenance in terms of, for instance, minimum life-cycle-cost criteria, the effect of scheduled maintenance on the component reliability should be determined [Refs. 22-24,43, 71 - 78]. In such a reliability analysis, however, many quantities involving statistical variabilities should be considered, for instance, the initial fatigue quality, crack propagation rate, service loading spectra, nondestructive evaluation (NDE) systems, etc.

Under scheduled inspection and repair maintenance in service, a fatigue reliability analysis methodology is presented for non-redundant fatigue-critical airframe components, in which fastener holes are critical locations. Various statistical variables mentioned above have been taken into account. The fatigue reliability is shown to be influenced significantly by the scheduled inspection maintenance as well as the capability of the NDE system employed.

Both the fatigue reliability in service and the average number of fastener holes to be repaired are presented in this chapter. These are important inputs for the life-cycle-cost analysis of airframe structures. A numerical example for the crack propagation in fastener holes of an F-16 lower wing skin has been worked out to demonstrate the application of the analysis methodology.

7.1 Formulation

For simplicity of presentation, service inspection maintenance is assumed to be periodic with the inspection interval, τ, as shown in Fig. 84. A fastener hole is repaired when a crack is detected. After repair, the fatigue quality is assumed to be renewed, in the sense that the crack size distribution is identical to that of the new fastener hole.

One important quantity in the fatigue reliability analysis is the initial fatigue quality (IFQ) that defines the initial manufactured state of a structural detail or component prior to service. For aluminum alloys used in airframe structures, it has been shown in Chapter 6 that the initial fatigue quality can be represented by the equivalent initial flaw size (EIFS). The equivalent initial flaw size is determined by back extrapolation of fractographic data obtained from laboratory tests.

The cumulative distribution, $F_{a(0)}(x) = P[a(0) \leq x]$, of the EIFS, $a(0)$, is suggested to have the following form in Chapter 6:

$$F_{a(0)}(x) = \exp\left\{-\left[\frac{\ell n(x_u/x)}{\phi}\right]^{\alpha}\right\} \quad ; \quad 0 \leq x \leq x_u$$
$$= 1.0 \quad ; \quad x > x_u \tag{147}$$

in which x_u is the upper bound, and α and ϕ are parameters. After the distribution of the EIFS is defined, the entire fatigue process can be described by the stable crack propagation until fracture.

The lognormal random variable model for the crack growth rate is employed for predicting the statistical crack growth damage accumulation,

$$\frac{da(t)}{dt} = XQ[a(t)]^b \tag{148}$$

in which X is a random variable introduced to take into account various contributions to the crack growth rate variability in service. It is expressed as

$$X = H_1 H_2 S^v \tag{149}$$

in which H_1, H_2 and S are random variables denoting the contributions to the statistical variability of the crack growth rate from various sources. H_1 represents the material crack growth resistance variability, H_2 represents the crack geometry variability or stress intensity factor variability, and S represents the variability of service loading spectrum with respect to the nominal design loading spectrum, and v is a constant [Refs. 6,22-23].

All the random variables H_1, H_2 and S are assumed to follow the lognormal distribution with a median of 1.0. Then, it follows from Eq. (149) that X is a lognormal random variable with a median of 1.0. Hence,

$$Z = \log X \tag{150}$$

is a normal random variable with a mean value $\mu_z = 0$ and standard deviation σ_z given by

$$\sigma_z = [\sigma_{H_1}^2 + \sigma_{H_2}^2 + v^2\sigma_s^2]^{1/2} \tag{151}$$

in which σ_{H_1}, σ_{H_2} and σ_s are the standard deviations of H_1, H_2 and S, respectively.

Since X is a lognormal random variable with a median of 1.0, the distribution function $F_X(z) = P[X \leq z]$ is given by

$$F_X(z) = \Phi\left(\frac{\log z}{\sigma_z}\right) \tag{152}$$

in which σ_z is the standard deviation of $Z = \log X$ given by Eq. (151), and the corresponding probability density function of X, denoted by $f_X(z)$, is given by

$$f_X(z) = \frac{\log e}{\sqrt{2\pi}\, z\, \sigma_z} \exp\left\{-\frac{1}{2}\left[\frac{\log z}{\sigma_z}\right]^2\right\}; \quad 0 \leq z \tag{153}$$

Current nondestructive evaluation (NDE) systems are not capable of repeatedly producing correct indications when applied to flaws of the same length. As a result, the probability of detection (POD) for all cracks of a given length has been used in the literature to define the capability of

a particular NDE system in a given environment.

The probability of detection (or POD curve) of an NDE system can be expressed as

$$F_D(a) = POD(a) = \frac{\exp(\alpha^* + \beta^* \ell n a)}{1 + \exp(\alpha^* + \beta^* \ell n a)} \; ; \quad 0 \leq a \qquad (154)$$

in which $F_D(a) = POD(a)$ is the probability of detecting the crack size "a", and α^* and β^* are constants. Equation (154) is referred to as the log odd function [e.g., Refs. 79-80].

Let a_c be the critical crack size at which failure of a non-redundant structured component occurs. Without the inspection and repair maintenance, the probability of failure in any service time interval (0,T), denoted by p(T), can be obtained from Eq. (138) of Chapter 6 by replacing a_1 and t by a_c and T, respectively, as follows

$$p(T) = 1 - \int_0^\infty \exp\left\{-\left[\frac{c\ell n x_u + \ell n(a_c^c + cQTz)}{c\phi}\right]^\alpha\right\} f_X(z)\,dz \qquad (155)$$

With the implementation of scheduled inspection and repair maintenance procedures, the structural reliability depends on the NDE capability and the frequency of inspection (or service inspection interval τ). The solution is derived in the following.

7.1.1 In the First Service Interval $(0,\tau)$

The crack size $a(\tau)$ at the end of the first service interval prior to inspection maintenance is related to EIFS, $a(0)$, through the integration of Eq. (148) from $t = 0$ to τ,

$$a(\tau) = \frac{a(0)}{[1 - a^c(0)cQ\tau X]^{1/c}} \tag{156}$$

in which $c = b - 1$ and both $a(0)$ and X are random variables.

Let $f_{a(\tau)}(x|z)$ be the conditional probability density function of the crack size $a(\tau)$ given $X = z$. Then, $f_{a(\tau)}(x|z)$ can be obtained from the distribution of $a(0)$ given by Eq. (147) through the transformation of Eq. (156); with the result

$$f_{a(\tau)}(x|z) = f_{a(0)}[Y(x;\tau,z)]J(x;\tau,z) \tag{157}$$

in which

$$Y(x;\tau,z) = \frac{x}{(1 + x^c cQ\tau z)^{1/c}} \tag{158}$$

$$J(x;\tau,z) = \frac{1}{(1 + x^c cQ\tau z)^{1/c + 1}} \tag{159}$$

The unconditional probability density function of $a(\tau)$ is obtained from the conditional one using the theorem of total probability,

$$f_{a(\tau)}(x) = \int_0^\infty f_{a(0)}[Y(x;\tau,z)]J(x;\tau,z)f_X(z)dz \tag{160}$$

in which the probability density function of the lognormal random variable X, denoted by $f_X(z)$, is given by Eq. (153), and $f_{a(0)}(x)$ is the probability density function of EIFS, $a(0)$, obtained from Eq. (147) as $f_{a(0)}(x) = dF_{a(0)}(x)/dx$, i.e.,

$$f_{a(0)}(x) = \frac{\alpha}{\phi x}\left[\frac{\ell n(x_u/x)}{\phi}\right]^{\alpha-1} \exp\left\{-\left[\frac{\ell n(x_u/x)}{\phi}\right]^{\alpha}\right\} \quad ; \ 0 \leq x \leq x_u$$
$$= 0 \quad ; \ x > x_u \tag{161}$$

The probability of failure in the first service interval $(0,\tau)$ for one fastener hole, denoted by p(1), is the probability that the crack size $a(\tau)$ will be greater than the critical crack size a_c, i.e.,

$$p(1) = \int_{a_c}^{\infty} f_{a(\tau)}(x)\,dx \tag{162}$$

in which $f_{a(\tau)}(x)$ is obtained in Eq. (160). It is mentioned that the probability of failure, p(1), in the first service interval can also be computed from Eq. (155) in which T is replaced by τ.

A fastener hole is repaired when a crack is detected during the inspection maintenance. The probability of repairing a fastener hole (or the probability of detecting a crack in the fastener hole), during the first inspection maintenance at τ, denoted by G(1), is given by

$$G(1) = \int_0^{a_c} f_{a(\tau)}(x) F_D(x)\,dx \tag{163}$$

in which $F_D(x)$ is the probability of detecting a crack size x given by Eq. (154).

After the first inspection maintenance at τ, the probability density of the crack size $a(\tau^+)$ is modified, because of possible repair,

$$f_{a(\tau^+)}(x) = G(1) f_{a(0)}(x) + F_D^*(x) f_{a(\tau)}(x) \quad ; \quad x<a_c \tag{164}$$

in which the first term is contributed by the renewal population (repaired fastener hole) with probability G(1) and $F_D^*(x)$ is the probability of not detecting (missing) a crack of size x during inspection,

$$F_D^*(x) = 1 - F_D(x) \tag{165}$$

where $F_D(x)$ is give by Eq. (154).

The corresponding conditional probability density function of the crack size after inspection, $a(\tau^+)$, under the condition that X = z, denoted by $f_{a(\tau^+)}(x|z)$, can be shown, using Eqs. (157) and (164), as follows,

$$f_{a(\tau^+)}(x|z) = G(1) f_{a(0)}(x) + F_D^*(x) f_{a(0)}[Y(x;\tau,z)] J(x;\tau,z) \tag{166}$$

7.1.2 In the Second Service Interval $(\tau,2\tau)$

The crack size $a(2\tau)$ at the end of the second service interval 2τ for the original population (fastener holes without being repaired at τ) is related to a(0) through Eq. (156) with τ being replaced by 2τ,

$$a(2\tau) = \frac{a(0)}{[1 - a^c(0) c Q 2\tau X]^{1/c}} \tag{167}$$

The conditional probability density function of $a(2\tau)$ given X = z, denoted by $f_{a(2\tau)}(x|z)$, is contributed by two

populations; the original population (fastener holes) that is not repaired at τ, and the fastener holes repaired at τ, referred to as the renewal population, with probability G(1), see Eq. (163). Through the transformation of random variables, the results can be obtained from Eq. (166) by the following replacements, $x \to Y(x;\tau,z)$, $Y(x;\tau,z) \to Y(x;2\tau,z)$, $J(x;\tau,z) \to J(x;2\tau,z)$, $f_{a(0)}(x) \to f_{a(0)}[Y(x;\tau,z)]J(x;\tau,z)$; with the result

$$f_{a(2\tau)}(x|z) = G(1) f_{a(0)}[Y(x;\tau,z)]J(x;\tau,z) + F_D^*[Y(x;\tau,z)] \cdot f_{a(0)}[Y(x;2\tau,z)]J(x;2\tau,z) \tag{168}$$

in which an additional condition is imposed on F_D^*, i.e., $F_D^*(Y) = 0$ for $Y > a_c$. In Eq. (168), $Y(x;\tau,z)$ is the crack size at τ which grows to x at 2τ. Therefore, if $Y(x;\tau,z)$ is greater than a_c, the component would have failed in the previous service interval already. The unconditional probability density function is given by

$$f_{a(2\tau)}(x) = \int_0^\infty F_D^*[Y(x;\tau,z)] f_{a(0)}[Y(x;2\tau,z)]J(x;2\tau,z) \cdot f_X(z)\,dz + G(1)\int_0^\infty f_{a(0)}[Y(x;\tau,z)]J(x;\tau,z) f_X(z)\,dz \tag{169}$$

The probability of failure in the second service interval $(\tau,2\tau)$ for a fastener hole is equal to the probability that $a(2\tau)$ is greater than the critical crack size a_c, i.e.,

$$p(2) = \int_{a_c}^\infty f_{a(2\tau)}(x)\,dx \tag{170}$$

and the probability that a fastener hole will be repaired at 2τ is given by

$$G(2) = \int_0^{a_c} f_{a(2\tau)}(x) F_D(x)\, dx \tag{171}$$

7.1.3 In the nth Service Interval $[(n-1)\tau, n\tau]$

Owing to crack propagation, the crack size and its probability density in a fastener hole increase as a function of service time. Meanwhile, the probability density is also subjected to modifications during each inspection and repair maintenance. Following a similar procedure described above, the probability density function of the crack size, $a(n\tau)$, at $n\tau$ right before the nth inspection maintenance, can be obtained in a recurrent form,

$$f_{a(n\tau)}(x) = \int_0^{\infty} f_{a(n\tau)}(x|z) f_X(z)\, dz \tag{172}$$

where $f_{a(n\tau)}(x|z)$ is the conditional probability density of $a(n\tau)$, under the condition that $X = z$,

$$f_{a(n\tau)}(x|z) = \left\{ \sum_{m=1}^{n-1} F_D^*[Y(x;m\tau,z)] \right\} f_{a(0)}[Y(x;n\tau,z)] \cdot J(x;n\tau,z) + \sum_{k=1}^{n-1} G(n-k)\bar{A}_k \quad ; \quad \text{for } n=2,3,\ldots \tag{173}$$

in which the first term is contributed by the original population introduced at $t = 0$ (i.e., fastener hole without being repaired), and the second summation term is contributed

by the renewal populations (repaired fastener holes) introduced at n-kth inspection maintenance (k=1,2,...,n-1).

In Eq. (173), G(n-k) is the probability of repairing a fastener hole at (n-k)τ (i.e., at n-kth inspection maintenance), and

$$\bar{A}_k = \left\{ \sum_{m=1}^{k-1} F_D^*[Y(x;m\tau,z)] \right\} f_{a(0)}[Y(x;k\tau,z)]J(x;k\tau,z) \quad (174)$$

in which $Y(x;m\tau,z)$ and $J(x;k\tau,z)$ are given by Eqs. (158) and (159) with τ being replaced by $m\tau$ and $k\tau$, respectively, i.e.,

$$Y(x;m\tau,z) = \frac{x}{(1 + x^c cQm\tau z)^{1/c}} \quad (175)$$

$$J(x;k\tau,z) = \frac{1}{(1 + x^c cQk\tau z)^{1/c+1}} \quad (176)$$

It should be mentioned that in Eq. (174), $\sum_{m=1}^{k-1} F_D^*[Y(x;m\tau,z)] = 1$ for $k = 1$ and $F_D^*[Y] = 0$ for $Y > a_c$.

The probability of failure in the nth service interval $[(n-1)\tau,n\tau]$, denoted by p(n), is obtained as

$$p(n) = \int_{a_c}^{\infty} f_{a(n\tau)}(x)dx \quad ; \text{ for } n=2,3,... \quad (177)$$

and the probability of repairing a fastener hole, G(n), during the nth inspection maintenance is given by

$$G(n) = \int_0^{a_c} f_{a(n\tau)}(x)F_D(x)dx \; ; \text{ for } n=2,3,... \quad (178)$$

Equations (172)-(178) are the recurrent solutions for n = 2,3,..., where the solutions for n = 1 are given by Eqs. (160)-(163).

The cumulative probability of failure for a fastener hole in n service intervals $(0,n\tau)$, denoted by $P(n\tau)$, is given by

$$P(n\tau) = 1 - \prod_{j=1}^{n} [1 - p(j)] \tag{179}$$

When the fatigue-critical component consists of M fastener holes and the component will fail if one or more fasteners fail, then the cumulative probability of failure of the entire component in the service interval $(0,n\tau)$, denoted by $P_M(n\tau)$, is given by

$$P_M(n\tau) = 1 - [1 - P(n\tau)]^n \tag{180}$$

When the stress level in each fastener hole is not identical, the probability of failure in each fastener hole varies. In such a case, the cumulative probability of failure in $(0,n\tau)$ for the mth fastener hole, denoted by $p(n\tau,m)$, can be obtained in a similar manner, e.g., Eq. (179). Then, the cumulative probability of failure of the entire component consisting of M fastener holes is obtained as

$$P_M(n\tau) = 1 - \prod_{m=1}^{M} [1 - P(n\tau,m)] \tag{181}$$

7.2 Demonstrative Example

Fatigue crack growth damage accumulation in fastener holes of a F-16 lower wing skin shown in Fig. 85 is considered. Extensive investigations indicate that the initial fatigue quality of aluminum fastener holes can be represented by the distribution of the equivalent initial flaw size (EIFS).

The distribution function of EIFS for countersunk fastener holes in lower wing skins subjected to F-16 load spectra is given by Eq. (147) with $\alpha = 1.823$, $x_u = 0.03$ in. and $\phi = 1.928$ [Ref. 6]. The lower wing skin is divided into ten (10) stress regions, Fig. 85. In each stress region, the maximum stress level in each fastener hole is approximately identical. The stress region No. 7 near the cut-out is subjected to the highest maximum stress level of 32.4 ksi (223.5 MPa) in the F-16 400 hour spectrum [Ref. 6]. This stress region containing eight (8) fastener holes is assumed to be safety critical. The crack propagation parameters in this stress region are found to be $Q = 1.3504 \times 10^{-4}$, $b = 1.01$, Eq. (148). The coefficient of variation of the crack growth rate is $V_X = 30\%$ and hence $\sigma_Z = \sqrt{\ell n(1+V_X^2)}/\ell n10 = 0.1276$. One design life for the aircraft is 8,000 flight hours, and the reliability of such a critical stress region up to two life times, i.e., 16,000 flight hours, will be investigated. The critical crack size a_c is assumed to be 0.2 inch.

Fastener holes are repaired when cracks are detected. Hence, the cost of repair depends on the size of the detected crack. When the crack size in fastener holes is smaller than 0.03 inches to 0.05 inches, depending on the location of the fastener holes, repair can be made by reaming the fastener hole to the next hole size. This is the most economic repair procedure. When the crack size is larger, a retrofit repair procedure may be needed, in which case the cost of repair is much higher.

Assuming that the crack size is divided into r regions, i.e., $(0,a_1)$, $(a_1,a_2),\ldots,(a_{r-1},a_r)$, and the cost of repairing a crack in each region varies. Then, the probability of repairing a crack in the kth region during the nth inspection maintenance, denoted by G(n;k), is obtained as [Ref. 81]

$$G(n;k) = \int_{a_{k-1}}^{a_k} f_{a(n\tau)}(x) F_D(x)\,dx \quad ; \quad \text{for } n=1,2,\ldots \tag{182}$$

in which $f_{a(n\tau)}(x)$ is given by Eqs. (160) and (172), and $F_D(x)$ is given by Eq. (154). It follows from Eq. (178) that the probability of repairing a crack of any size, G(n), during the nth inspection maintenance is

$$G(n) = \sum_{k=1}^{r} G(n;k) \tag{183}$$

It should be noted that G(n) can also be interpreted as the average percentage of fastener holes to be repaired

during the nth inspection maintenance. For simplicity of presentation, only the results of G(n) will be presented in this example.

The probability of failure depends on the inspection interval τ and the capability of the NDE system employed. Four (4) probability of detection (POD) curves shown in Fig. 86 will be considered. The parameter values of α^* and β^* appearing in Eq. (154) for these four POD curves are as follows: (i) $\alpha^* = 55.28$ and $\beta^* = 16.4$ for the No. 1 POD curve, (ii) $\alpha^* = 66.6$ and $\beta^* = 23.4$ for the No. 2 POD curve, (iii) $\alpha^* = 28.94$ and $\beta^* = 11.73$ for the No. 3 POD curve, and (iv) $\alpha^* = 13.44$ and $\beta^* = 3.95$ for the No. 4 POD curve.

Without inspection maintenance, the cumulative probabilities of failure for one hole and for the entire stress region containing eight fastener holes are plotted as a solid curve and a dashed curve, respectively, in Fig. 87. These curves are designated by zero. It is observed that the probability of failure increases drastically as the service life increases, a typical fatigue failure mode.

Under periodic inspection maintenance using the No. 1 POD curve shown in Fig. 86 , the cumulative probabilities of failure for one hole and for the entire stress region are computed and displayed in Fig. 87 as solid curves and dashed curves, respectively. The numerical value designated for each curve in the figure denotes the number of inspection maintenances in 16,000 flight hours. For instance, the curve designated by 1 indicates the cumulative failure

probability with an inspection interval of 8,000 flight hours (1 inspection in 16,000 flight hours). It is observed from Fig. 87 that the probability of failure is reduced drastically as the number of inspection maintenances increases.

The average percentage of fastener holes to be repaired during each inspection maintenance, as well as the total average percentage of fastener holes to be repaired in 16,000 flight hours are presented in Table 8. From Table 8 the total average percentage of fastener holes to be repaired increases as the number of inspection maintenances increases. This trend has been expected since higher component reliability is achieved through higher percentage of repairs.

Suppose the capability of the NDE system is represented by No. 2 POD curve as shown in Fig. 86. The cumulative probabilities of failure under various number of inspection maintenances are presented in Fig. 88. The average percentage of fastener holes to be repaired is shown in Table 8. Since the capability of the No. 2 POD curve is not as good as that of the No. 1 POD curve, the cumulative probability of failure shown in Fig. 88 is higher than that displayed in Fig. 87. However, the average percentage of repair is lower using the No. 2 POD curve.

Both No. 1 and No. 2 POD curves are narrow-banded, indicating that the NDE system involves less uncertainty in crack detection. Now consider the No. 3 and No. 4 POD curves, respectively, for the NDE system. Since these POD curves are wide-banded, the NDE system involves considerable statistical uncertainty in crack detections. By use of the No. 3 POD curve, the cumulative probabilities of failure are displayed in Fig. 89. The average percentage of fastener holes to be repaired during each inspection maintenance and the total average percentage of fastener holes to be repaired in 16,000 flight hours are shown in Table 8. The results using the No. 4 POD curve are presented in Fig. 90 and Table 8. Again, the inspection maintenance is capable of significantly reducing the probability of failure for components in service.

A comparison between the results obtained using the No. 2 POD curve (narrow-banded) and the No. 4 POD curve (wide-banded) indicates that although the No. 4 POD curve is capable of detecting a smaller crack with a 50% probability, it has a higher probability of missing large cracks, and hence the probability of failure is higher. Likewise, many small cracks may be detected by the No. 4 POD curve, leading to an unnecessary repair. It is observed from Table 8 and Figs. 87 to 90 that the narrow-banded POD curve is superior to the wide-banded POD curve in terms of the probability of failure and the average percentage of fastener holes to be repaired.

7.3 Conclusion

A method has been developed for the fatigue reliability analysis of some types of airframe structures under scheduled inspection and repair maintenance. It is shown that the scheduled inspection maintenance can be used to drastically reduce the fatigue failure probability. The significant effect of the NDE system on the component reliability is also demonstrated. The analysis methodology presented may be applied to the probabilistic damage tolerance analysis in the future.

CHAPTER 8

CONCLUSIONS AND RECOMMENDATIONS

Various stochastic models for fatigue crack propagation under either constant amplitude or spectrum loadings have been investigated. These models are based on the assumption that the crack growth rate is a lognormal random process, including the general lognormal random process, lognormal white noise process, lognormal random variable and second moment approximations, such as Weibull, gamma, lognormal and Gaussian closure approximations. It is shown in this report that (i) the white noise process is definitely not a valid model for fatigue crack propagation, and (ii) all other stochastic models considered correlate very well with the experimental results of fastener hole specimens.

In the development of stochastic crack propagation models, the main contribution of this report are given in the following: (i) Although the concept of the general lognormal random process model has been proposed in the literature by Yang et al. [Refs. 16-21,25-26], the analysis procedures have not been worked out and the advantage of the model has not been demonstrated by experimental results. In this report a method of analysis for the general lognormal random process model has been developed using the Monte Carlo

simulation approach, and a correlation study for such a model with extensive test results has been conducted, (ii) the accuracy of the lognormal random variable model has been improved herein using an equal number of data points for each specimen and the incremental polynomial method for deriving the crack growth rate data, and (iii) various second moment approximations are new models proposed and verified by experimental data in this report.

Experimental data used for the correlation study with various stochastic models include fastener hole specimens under fighter or bomber spectrum loadings and center-cracked specimens under constant amplitude loads. The fastener hole specimens consist of WPB, XWPB, WWPF, WWPB and CWPF data sets. Basically, the WPB and the XWPB data sets involve fatigue crack propagation in the very small crack size region, whereas the WWPF and WWPB data sets cover the entire crack size region, i.e., from the very small cracks to large cracks. The CWPF data set involves crack propagation in a salt water corrosive environment. Therefore, the data sets for the fastener hole specimens used in the present study cover adequately different loading conditions, environments, load transfers and crack size range. It should be emphasized that, unlike the center-cracked specimens, the fastener hole specimen are not intentionally preflawed, i.e., the specimen starts with the crack initiation stage.

The general lognormal random process model is not amenable to the analytical close-form solution. A method of analysis

is developed using the Monte Carlo simulation approach. The model is demonstrated to be very flexible and it correlates excellently with all the experimental data considered. The second moment approximation models are new models proposed in this report. The analysis procedures for these new models are quite simple and their correlations with all the test results are very satisfactory. This indicates that as long as the first two central moments of the crack size distribution can be estimated reasonably well, the model will have very good correlation with the experimental test results, with the possible exception of the tail portion of the distribution as will be discussed later.

The lognormal random variable model is a special case of the lognormal random process model, in which the correlation distance is infinity. As a result, it is always conservative in predicting the crack growth damage accumulation, in the sense that the statistical dispersion based on the model is the largest among the class of lognormal random processes. Further, it is less flexible than the lognormal random process model and the second moment approximation models because its correlation distance is fixed to be infinity.

The lognormal random variable model correlates very well with all the experimental results of fastener hole specimens under spectrum loadings. However, for crack propagation in the large crack size region in center-cracked specimens (CCT data set) under constant amplitude loading,

the model is rather conservative in the sense that it predicts larger statistical dispersion. Note that the statistical dispersion of the CCT data set is much smaller than that of all the fastener hole specimen data sets under spectrum loadings, and such a small statistical variability may not reflect the real situation of structural details experienced in the field. Laboratory test results of full-scale articles [e.g., 6,45], as well as the results of tear-down inspections [e.g., 82], indicate that the statistical variability of the crack growth damage accumulation is much larger than that of the CCT data set. Consequently, it is expected that the lognormal random variable model may reflect the field situation more realistically.

The lognormal random variable model is very attractive for practical applications due to the following reasons: (i) it is mathematically very simple for practical applications including analysis and design requirements, (ii) it is of conservative nature, (iii) it may reflect closely the crack growth behavior in the real structure in service, and (iv) it does not require the correlation distance parameter, such that a small number of replicate specimens is adequate. In practical applications, test results usually are not plentiful and hence the model is very attractive.

The general lognormal random process model and the second moment approximation models are quite flexible and they are capable of describing fatigue crack propagation behavior very well. However, these models require a corre-

lation distance parameter, the determination of which may need a large number of sample functions for the primary data. It is mentioned that the information similar to the correlation distance is required in all advanced stochastic fatigue crack propagation models proposed in the literature [Refs. 10-12,18-19].

For the crack propagation in fastener holes, in which extensive data have been used for model verifications, the lognormal random variable model is recommended. The advantages of such a model for practical applications to analysis and design have been described previously. Although the second moment approximation models and the lognormal random process model correlation equally well with the experimental results, the second moment approximation models are recommended, because their applications are simpler than the simulation approach employed for the lognormal random process model.

In using the base-line crack propagation data (or primary data) for crack growth analyses, the importance of having an equal number of data points for each specimen has been demonstrated. Adjustment is suggested by adding additional data points artificially, if the available data set does not contain an equal number of data points for each specimen. In converting the primary data into the crack growth rate data for analysis purposes, additional undesirable statistical variability is introduced by the data processing procedures. The five point incremental polynomial method is recommended

over the direct secant and modified secant methods. This is because the latter two methods introduce much larger additional statistical dispersion into the crack growth rate data than the former.

Based on the recommended lognormal random variable crack growth rate model and the equivalent initial flaw size (EIFS) concept, a stochastic-based initial fatigue quality (IFQ) model has been described and evaluated for the durability analysis of relatively small cracks in fastener holes (e.g., <0.1"). Procedures have been presented and evaluated for optimizing initial flaw size distribution parameters based on pooled EIFS results. Expressions have been developed for predicting the cumulative distribution of crack size at any given time and the cumulative distribution of times to reach any given crack size. The predictions compare well with the actual test results in the small crack size region. However, further research is needed to compare the durability analysis results based on the deterministic crack growth approach [Refs. 6,64,45-47]. Likewise, research is needed for durability analysis applications in the large crack size region.

A fatigue reliability analysis methodology has been developed for structural components under scheduled inspection and repair maintenance in service. Emphasis is placed on the non-redundant components based on the slow crack growth design requirements. The methodology takes into account the statistical variabilities of the initial

fatigue quality, crack propagation rates, service load spectra, nondestructive evaluation (NDE) systems, etc. The significant effect of the NDE system as well as the scheduled inspection maintenance on the fatigue reliability of structural components have been illustrated. A numerical example for the crack propagation in fastener holes of a F-16 lower wing skin is worked out to demonstrate the application of the developed analysis methodology.

The stochastic crack growth models investigated in this report are aimed at the prediction of the global behavior of the entire population. As such, the accuracy of the predicted upper or lower tail of the distribution of either the crack size at any service time or the propagation life to reach a specific crack size may be sacrificed. The durability requirement of aircraft structures deals with the small crack size in which the extent of cracking and the economical life are of major concern [Refs. 6,45-47]. Under this circumstance, the prediction of the entire crack population, rather than the lower tail, should be made. Note that the lower tails of the distributions shown in Figs. 24 and 25 for the WPB and XWPB data sets, respectively, should not be interpreted as early failure, because the corresponding crack size is very small. Thus, the present investigation for the stochastic crack growth models is applicable to the durability analysis of aircraft structures.

The damage tolerance requirement, however, is dealing with the safety of flight and hence the crack propagation

in the large crack size region [Refs. 1-3]. In this case, the lower tail portion of the distribution of the propagation life, representing the early failure, is of major concern. As a result, any stochastic model should be capable of accurately predicting the lower tail portion of the propagation life distribution. The stochastic models investigated in this report may be applicable to the damage tolerance analysis; however, further effort is needed to demonstrate their applicability. Another alternate approach for these stochastic models is to estimate the corresponding crack growth rate parameters only from a certain percentage, say 5%, of the test results with high crack growth rate. Further investigation is needed to verify such a possibility. Another problem of future research in the damage tolerance analysis is the stochastic approach to take into account the outliers resulting in an early failure.

Finally, the stochastic models for crack propagation presented in this report are based on the crack growth rate equation. As such, only the crack growth rate data are required to estimate the crack growth rate parameters and the model statistics. How the crack size a(t) varies as a function of the propagation life t is not needed. Likewise, the crack growth rate data generated under nonhomogeneous conditions can be pooled together to increase the sample size [16,25,26]. This is consistent with the fracture mechanics approach, and hence is referred to as the fracture mechanics-based stochastic model. Any stochastic model,

which is based on the data of the crack size a(t) versus the propagation life t for estimating the model parameters, is not consistent with fracture mechanics.

Table 1: Linear Regression Estimate of b, Q, σ_z and Coefficient of Variation, V, of Crack Growth Rate

Data Set	b	Q (10^{-3})	σ_z	V (%)	a(0) (in)	a_F (in)
WPB	0.9413	0.116	0.0702	16.3	0.004	0.04
XWPB	1.0144	0.284	0.1093	25.6	0.004	0.07
WWPF	1.1226	0.414	0.0774	17.9	0.017	0.51
WWPB	1.0125	0.237	0.1102	25.8	0.008	0.57
CWPF	1.3721	2.128	0.2020	49.2	0.010	0.35

* a(0) = initial crack size, a_F = final crack size

Table 2: Correlation Parameter ξ^{-1} and Number of Simulated Sample Functions for Each Data Set

	WPB	XWPB	WWPF	WWPB	CWPF
ξ^{-1} (Flight Hours)	6,670	10,000	8,330	11,100	2,860
No. of Simulated Samples	160	176	180	180	200

TABLE 3: Correlation Parameter ζ^{-1} in Flight Hours for Various Data Sets and Approximations

Data Set \ Approximation	Flight Hours			
	Gaussian Closure	Weibull	Gamma	Lognormal
WPB	7,042	7,143	7,143	7,194
XWPB	10,530	10,530	10,530	10,360
WWPF	38,460	38,460	38,460	38,460
WWPB	11,630	11,760	11,760	11,760
CWPF	4,500	5,556	4,000	5,000
CCT	15,380*	15,380*	15,380*	15,380*

* Cycles

TABLE 4: Linear Regression Estimate of b, Q, σ_z and Coefficient of Variation, V, of Crack Growth Rate for CWPF Fastener Holes Using Various Data Processing Procedures

	b	Q (10^{-3})	σ_z	V (%)
5 Point Incremental Polynomial Method (raw data)	1.385	2.120	0.219	53.9
5 Point Incremental Polynomial Method (added data)*	1.372	2.128	0.202	49.2
Modified Secant Method	1.393	2.142	0.231	57.2

* Equalized the number of a(t) versus t values for each specimen in the data set.

Table 5: EIFSs For Data Sets WPF and WPB Based on Stochastic Crack Growth

RANK	WPF EIFS (Inch)	WPB EIFS (Inch)
1	.000218	.0000605
2	.000368	.0001240
3	.000385	.0001255
4	.000387	.0001652
5	.000459	.0001825
6	.000478	.0001872
7	.000485	.0001910
8	.000494	.0002105
9	.000523	.0002238
10	.000534	.0002458
11	.000582	.0002638
12	.000624	.0002658
13	.000629	.0002747
14	.000656	.0002969
15	.000714	.0003361
16	.000913	.0003386
17	.000962	.0003656
18	.000994	.0003822
19	.001000	.0003882
20	.001025	.0003963
21	.001040	.0004342
22	.001056	.0004421
23	.001075	.0004506
24	.001325	.0004665
25	.001390	.0005016
26	.001466	.0005073
27	.001797	.0007059
28	.001871	.0007586
29	.001890	.0008675
30	.002410	.0010270
31	.002441	.0010310
32	.003407	.0020770
33	.003864	---

NOTE: Fractographic Crack Size Range Used: $0.01'' \leq a(t) \leq 0.05''$

Table 6: Summary of EIFSD Parameters Based on Stochastic Crack Growth

DATA SET(s)	x_u (Inch)	α	ϕ	STD. ERROR	MAX. DIFF. (K-S)
WPF (N = 33)	.030	5.409	3.801	.0323	.0829
	.020	4.705	3.392	.0330	.0886
	.013	3.939	2.956	.0349	.0969
	.010	3.458	2.691	.0371	.1039
	.0039	.928	2.039	.1331	.2575
WPB (N = 32)	.030	6.684	4.775	.0367	.1075
	.020	6.013	4.367	.0372	.1106
	.013	5.287	3.935	.0383	.1149
	.010	4.835	3.671	.0396	.1186
	.0039	3.079	2.739	.0541	.1446
	.0030	2.479	2.478	.0677	.1620
	.0027	2.193	2.414	.0774	.1729
WPF + WPB (N = 65)	.030	5.240	4.319	.0231	.0562
	.020	4.633	3.908	.0237	.0601
	.013	3.968	3.472	.0256	.0663
	.010	3.547	3.206	.0279	.0720
	.0039	1.199	2.556	.1186	.2135

NOTE: Fractographic Crack Size Range Used: $0.01" \leq a(t) \leq 0.05"$

Table 7: Summary of Parameters Used in Correlation Plots

Case	EIFS Basis	u_x (INCH)	$\alpha(4)$	$\phi(4)$	$Qx10^4$	$\sigma_z(5)$	b	t (FLT HRS)	t (FLT HRS)
I	WPF	0.03	5.409	3.801	2.383	0.0839	1.0	9200	14800
II	WPF + WPB	↓	5.240	4.319	2.383	↓	↓	↓	↓
III	WPF + WPB	↓	5.240	4.319	2.708*	↓	↓	↓	↓
IV	WPB	↓	6.684	4.775	1.406	0.0669	↓	29109	35438
V	WPF + WPB	↓	5.240	4.319	1.406	↓	↓	↓	↓
VI	WPF + WPB	↓	5.240	4.319	1.272*	↓	↓	↓	↓

Note: (1)* Normalized Q value, $\hat{Q}$ (Ref. Eq. (146))

(2) Fractographic crack size range used: $0.01" \leq a(t) \leq 0.05"$

(3) a_1 = 0.03", 0.05", 0.10"

(4) Ref. Eqs. (142) and (143)

(5) Ref. Eq. (129)

Table 8: Average Percentage of Repair

NUMBER OF INSPECTIONS	INSPECTION INTERVAL, HOURS	AVERAGE PERCENTAGE OF REPAIR i th INSPECTION MAINTENANCE					TOTAL
		1	2	3	4	5	
No. 1 POD CURVE							
1	8,000	25.54					25.54
2	5,333	12.17	29.19				41.36
3	4,000	6.74	19.26	23.78			49.78
No. 2 POD CURVE							
1	8,000	8.45					8.45
2	5,333	1.46	18.61				20.07
3	4,000	0.24	8.21	18.27			26.72
4	3,200	0.03	3.50	11.49	15.85		30.87
No. 3 POD CURVE							
1	8,000	2.62					2.62
2	5,333	0.17	9.53				9.70
3	4,000	0.01	2.61	12.19			14.81
4	3,200	0.00	0.68	5.63	11.93		18.24
5	2,666	0.00	0.17	2.45	7.11	10.95	20.68
No. 4 POD CURVE							
1	8,000	28.13					28.13
2	5,333	16.02	29.42				45.44
3	4,000	11.00	20.57	24.77			56.34
4	3,200	8.45	15.40	19.40	21.01		64.26
5	2,666	7.00	12.20	15.66	17.46	18.23	70.55

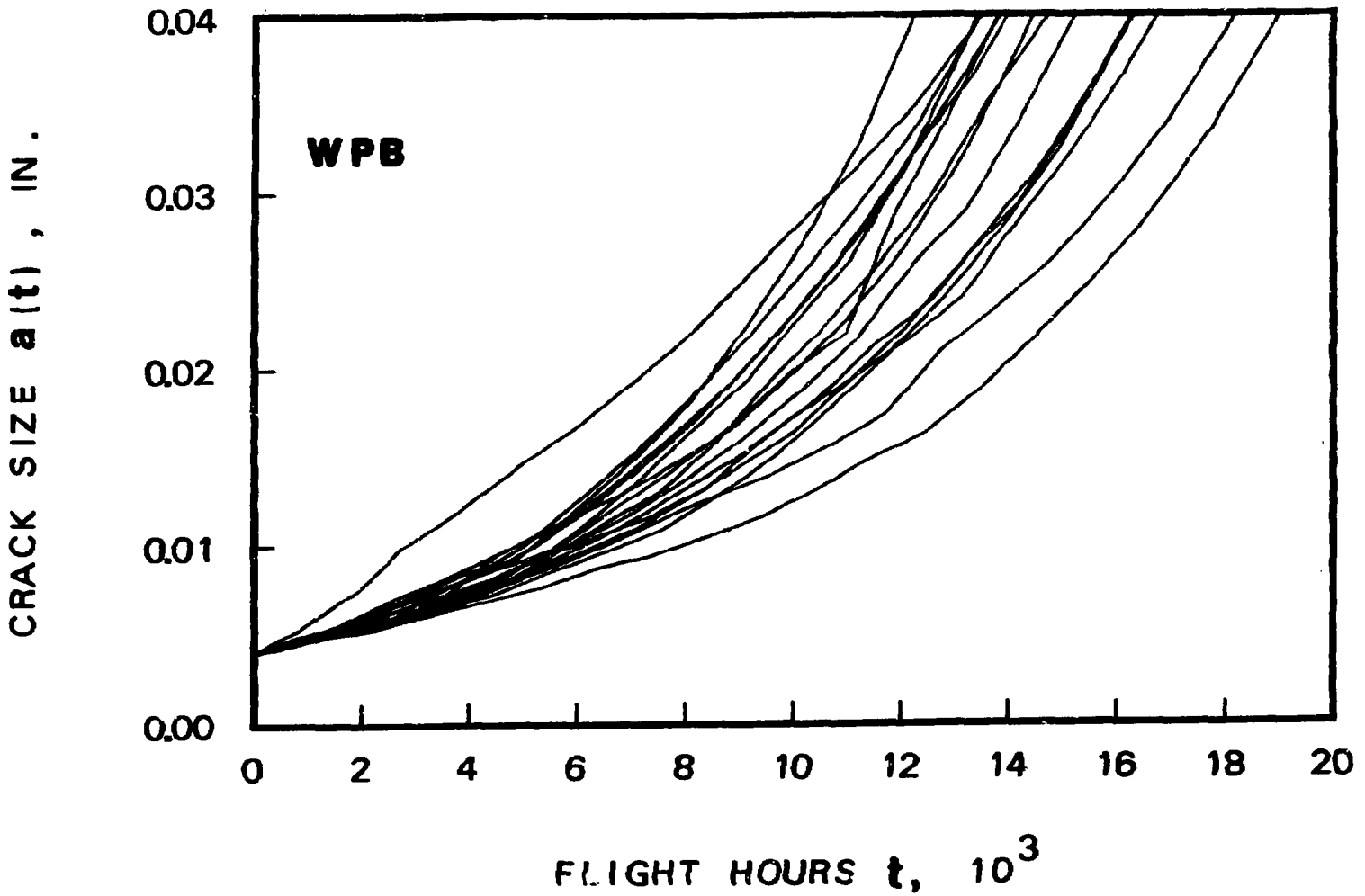

Fig. 1: Actual Crack Propagation Time Histories of Fastener Hole Specimens for WPB Data Set.

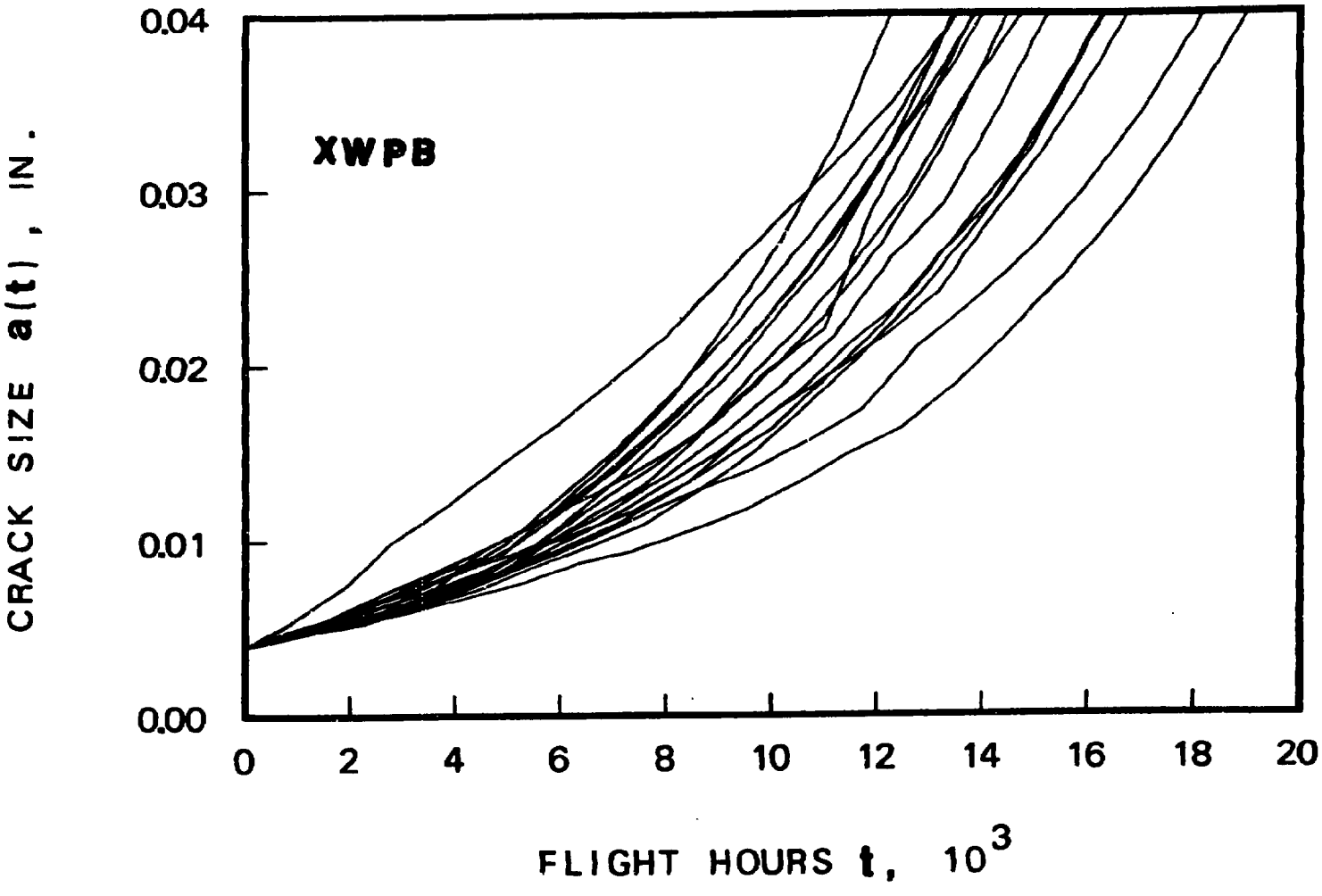

Fig. 2: Actual Crack Propagation Time Histories of Fastener Hole Specimens for XWPB Data Set.

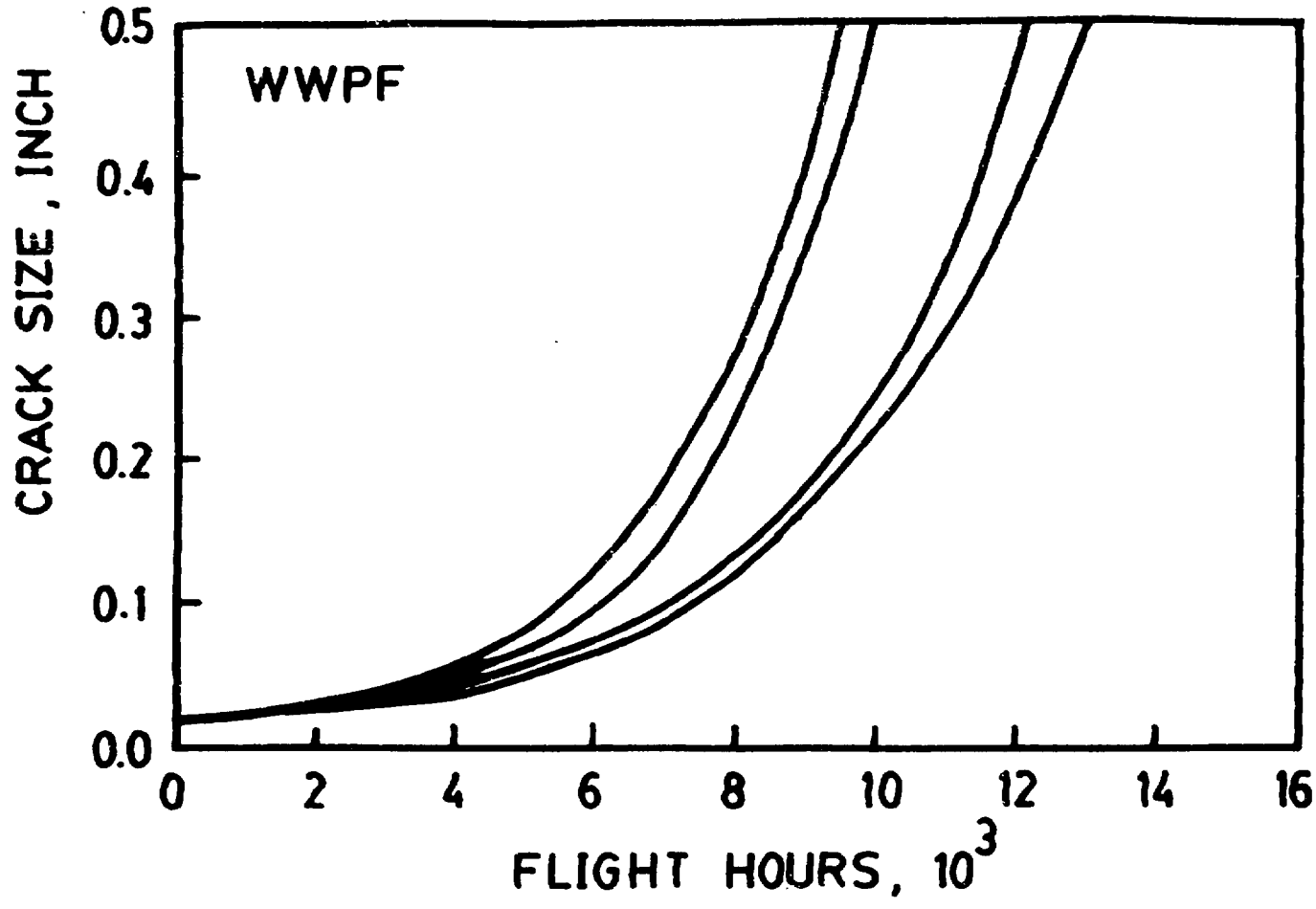

Figure 3: Actual Crack Propagation Time Histories of Fastener Hole Specimens for WWPF Data Set

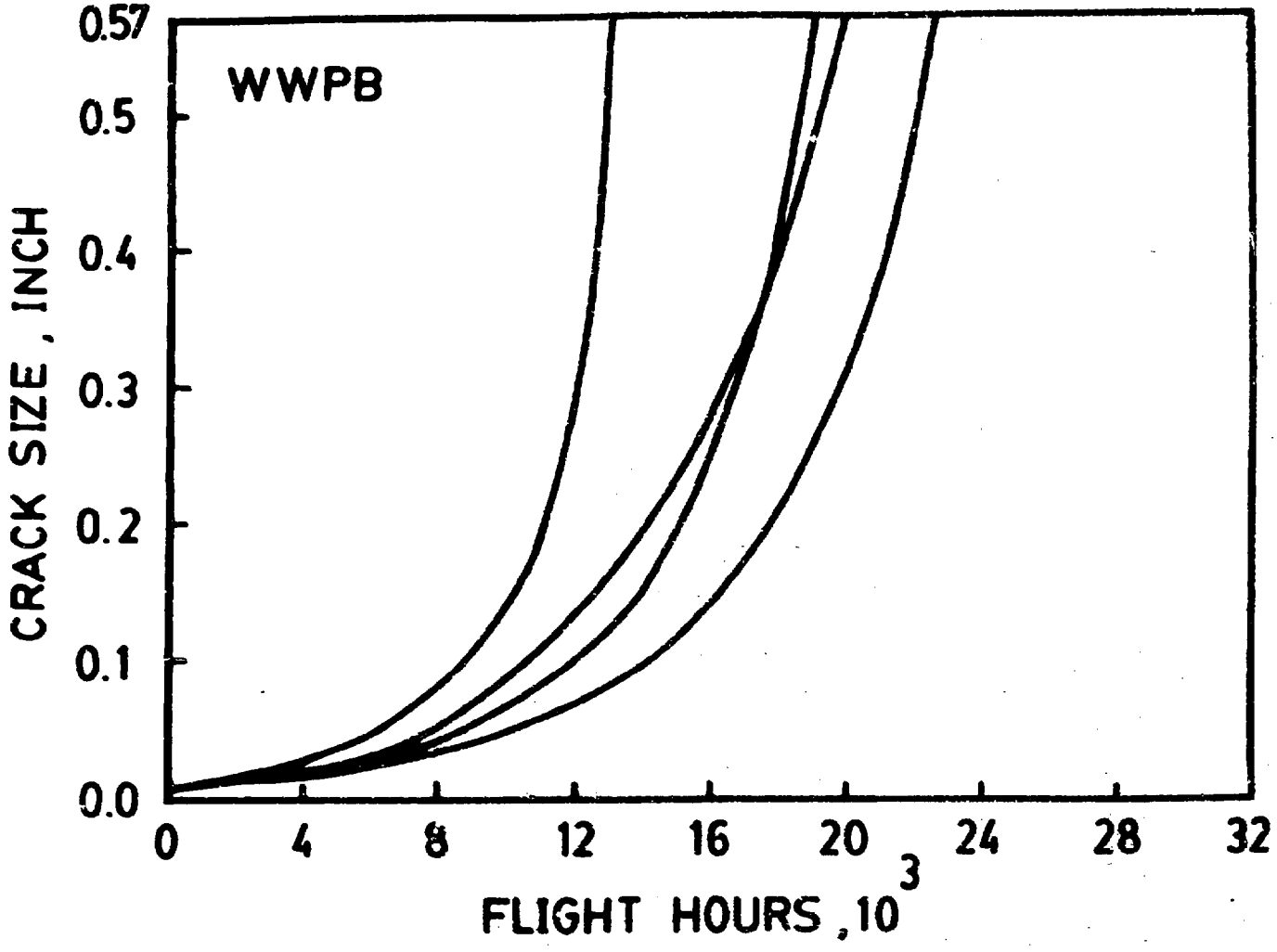

Figure 4: Actual Crack Propagation Time Histories of Fastener Hole Specimens for WWPB Data Set

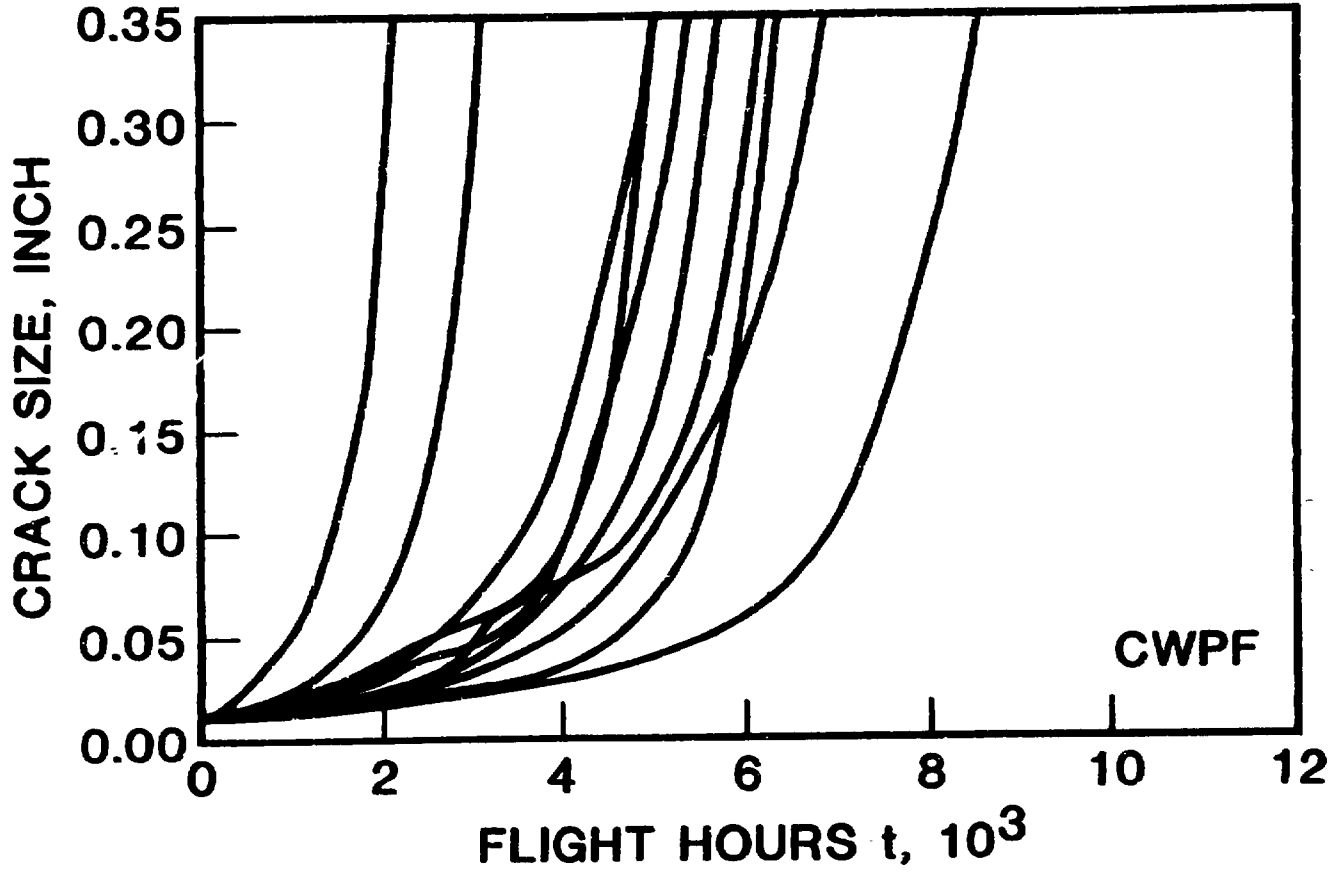

Figure 5: Actual Crack Propagation Time Histories of Fastener Hole Specimens for CWPF Data Set

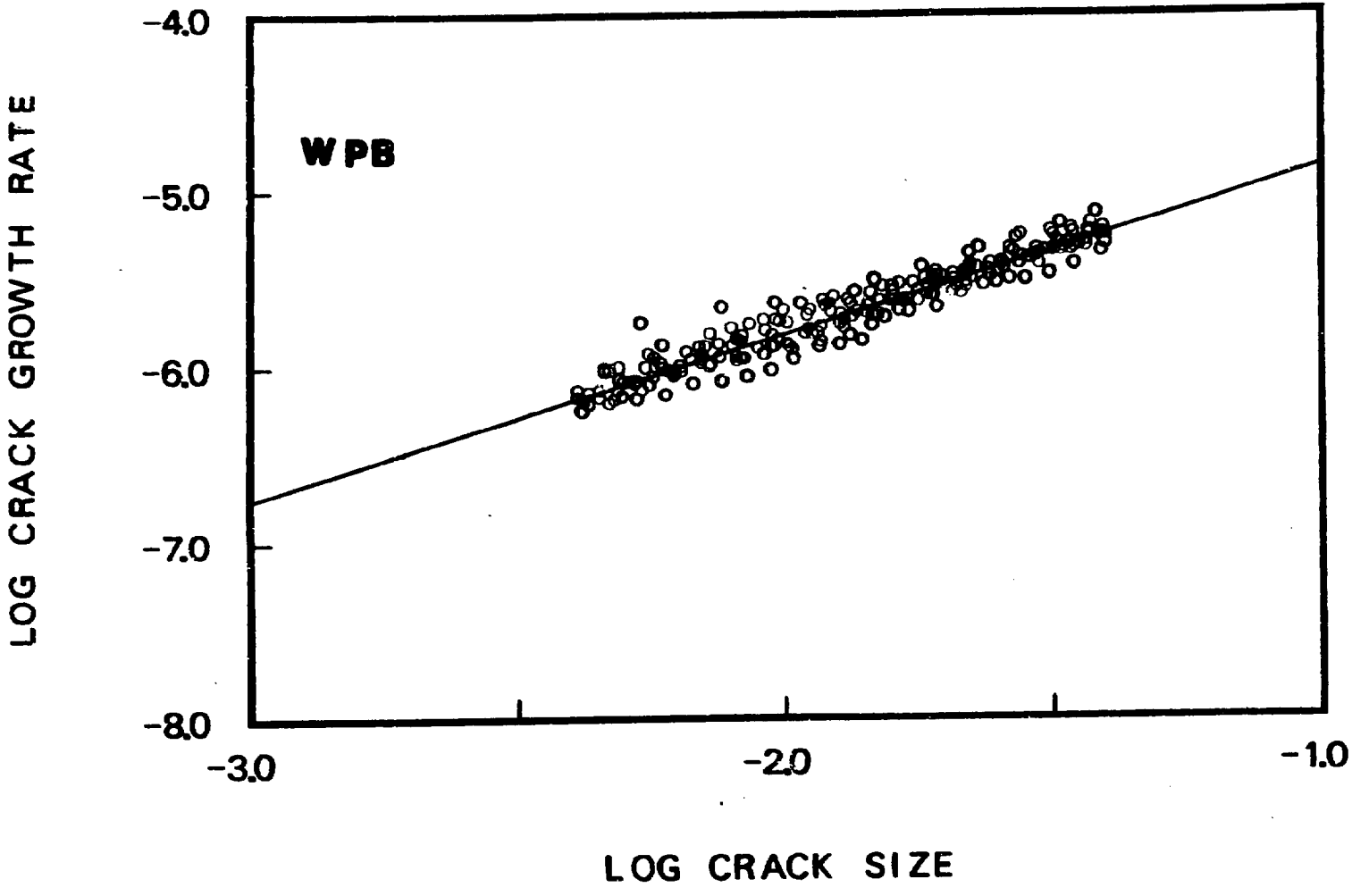

Figure 6: Crack Growth Rate as Function of Crack Size for WPB Data Set Using 5 Point Incremental Polynomial Method.

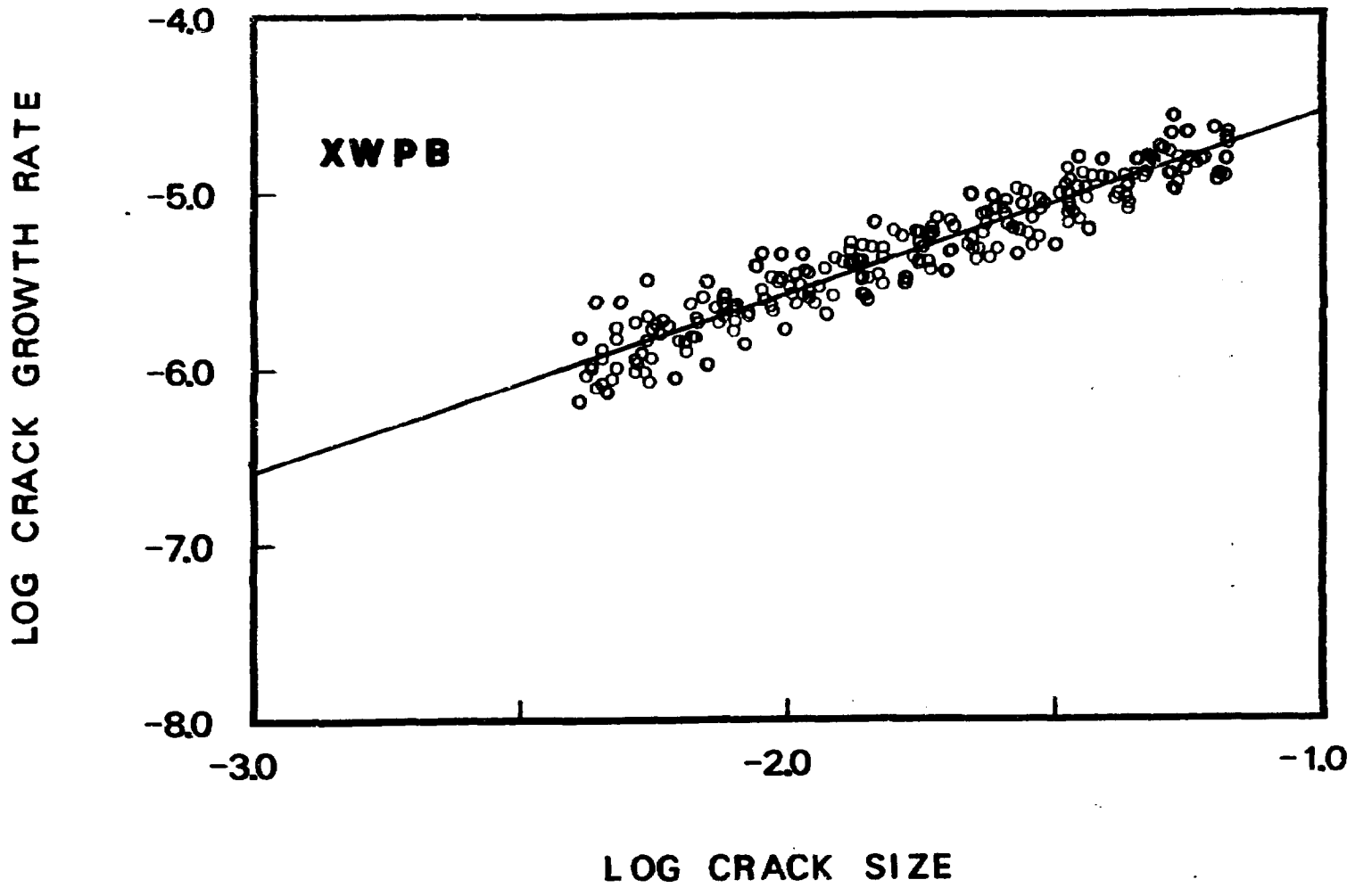

Figure 7: Crack Growth Rate as Function of Crack Size for XWPB Data Set Using 5 Point Incremental Polynomial Method.

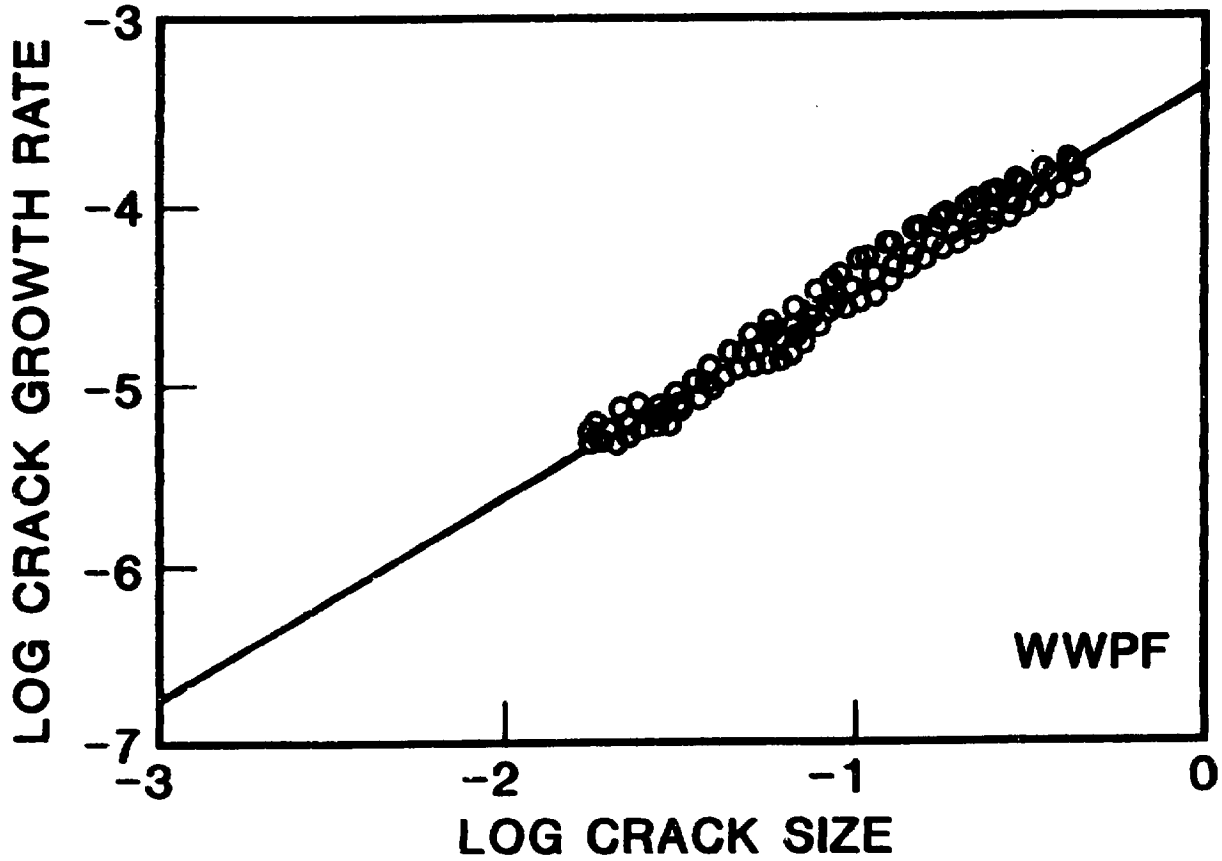

Figure 8: Crack Growth Rate as Function of Crack Size for WWPF Data Set Using 5 Point Incremental Polynomial Method

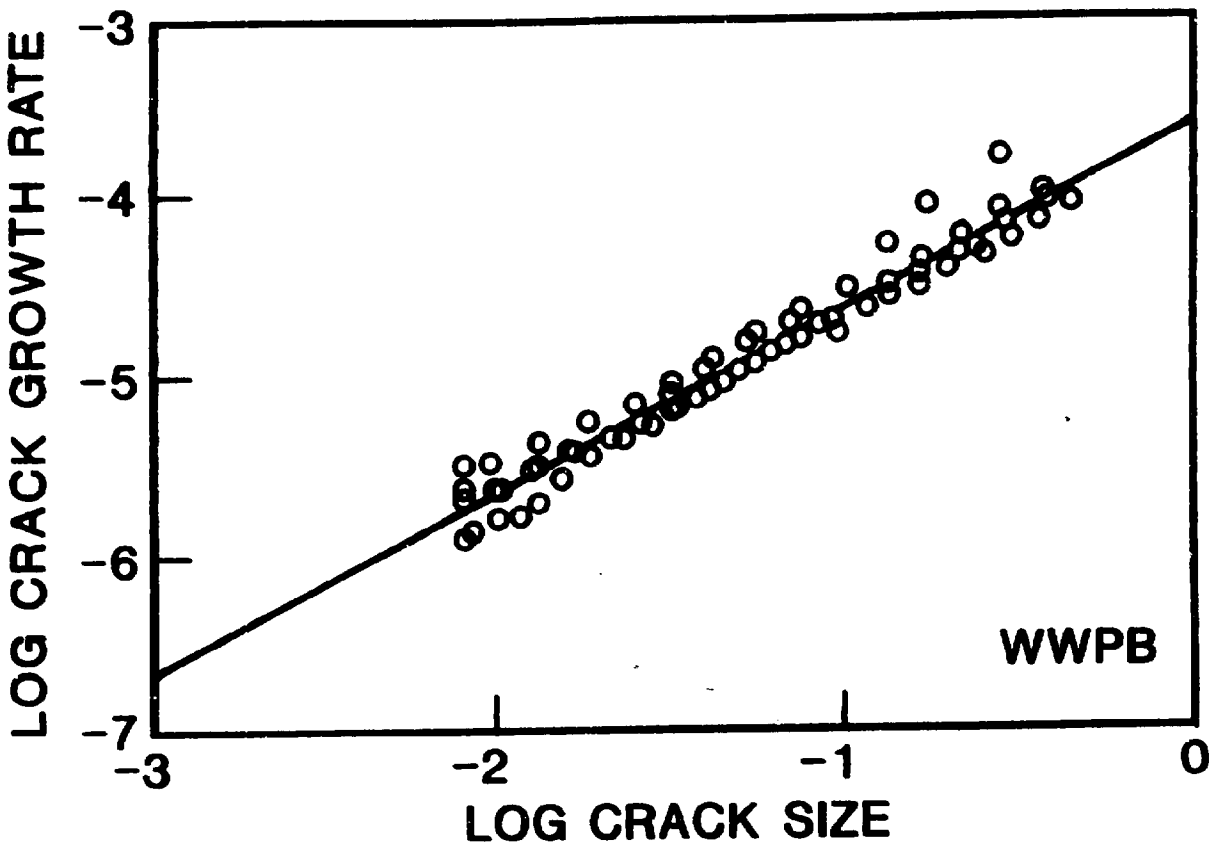

Figure 9: Crack Growth Rate as Function of Crack Size for WWPB Data Using 5 Point Incremental Polynomial Method

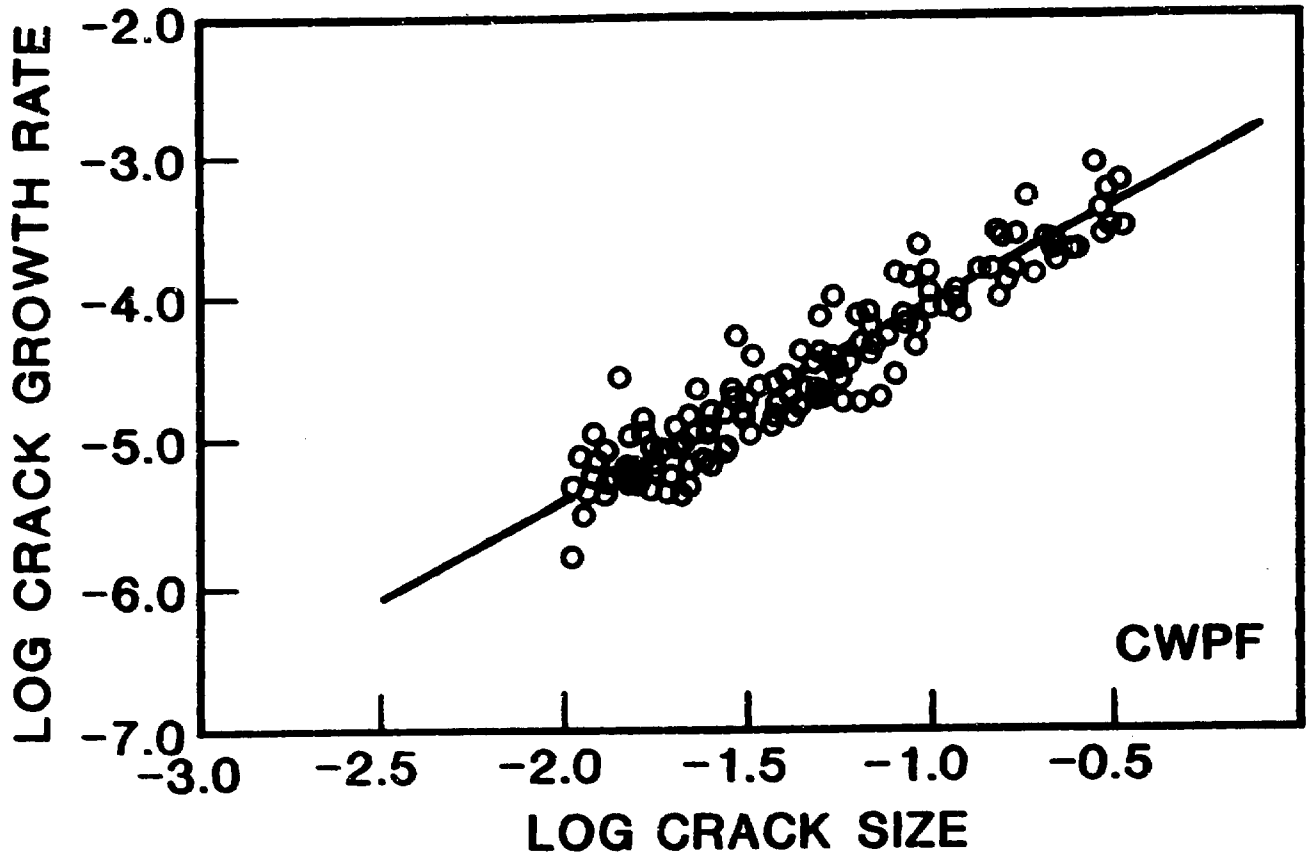

Figure 10: Crack Growth Rate as Function of Crack Size for CWPF Data Set Using 5 Point Incremental Polynomial Method

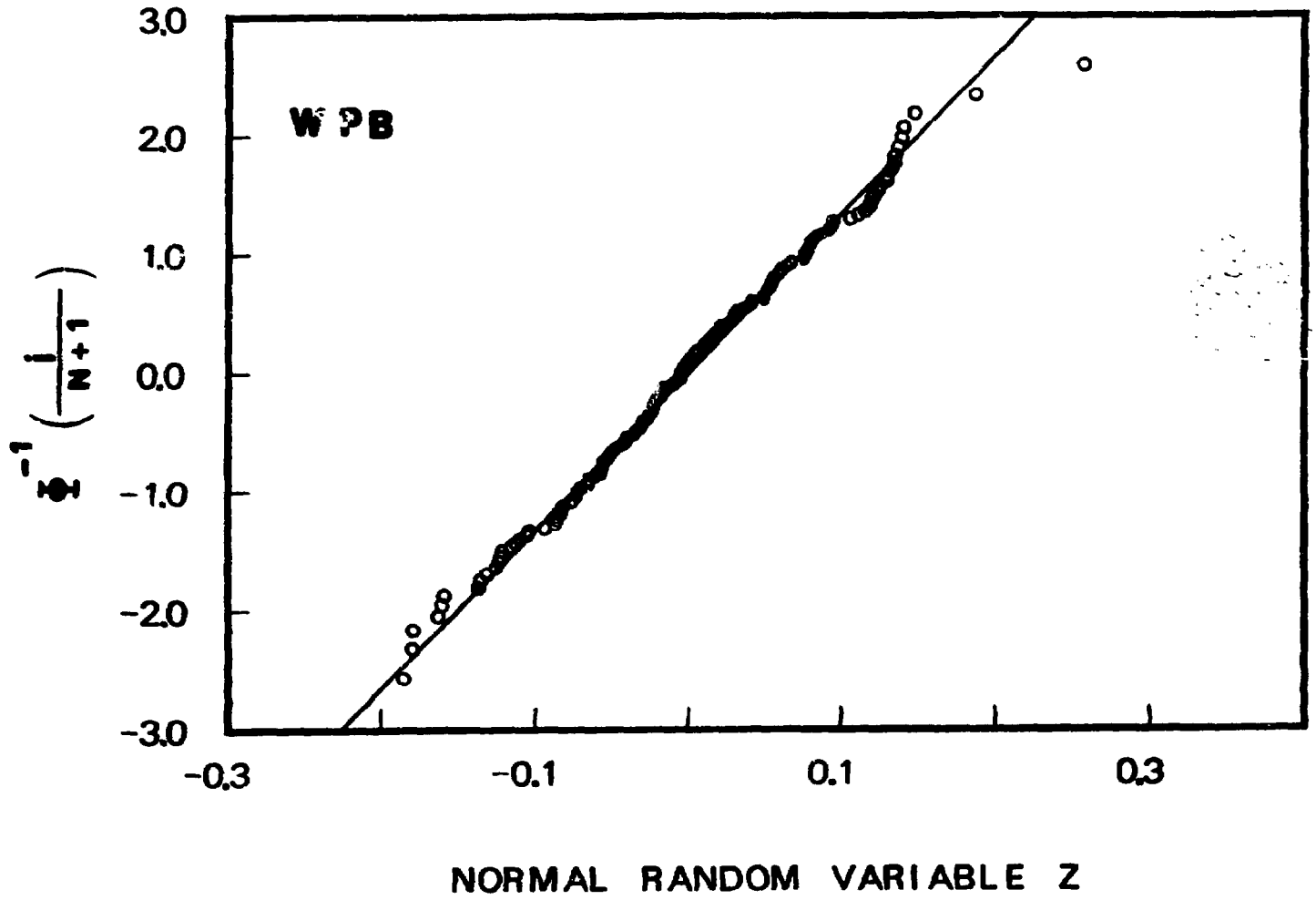

Figure 11: Normal Probability Plot of Z(t) for WPB Data Set.

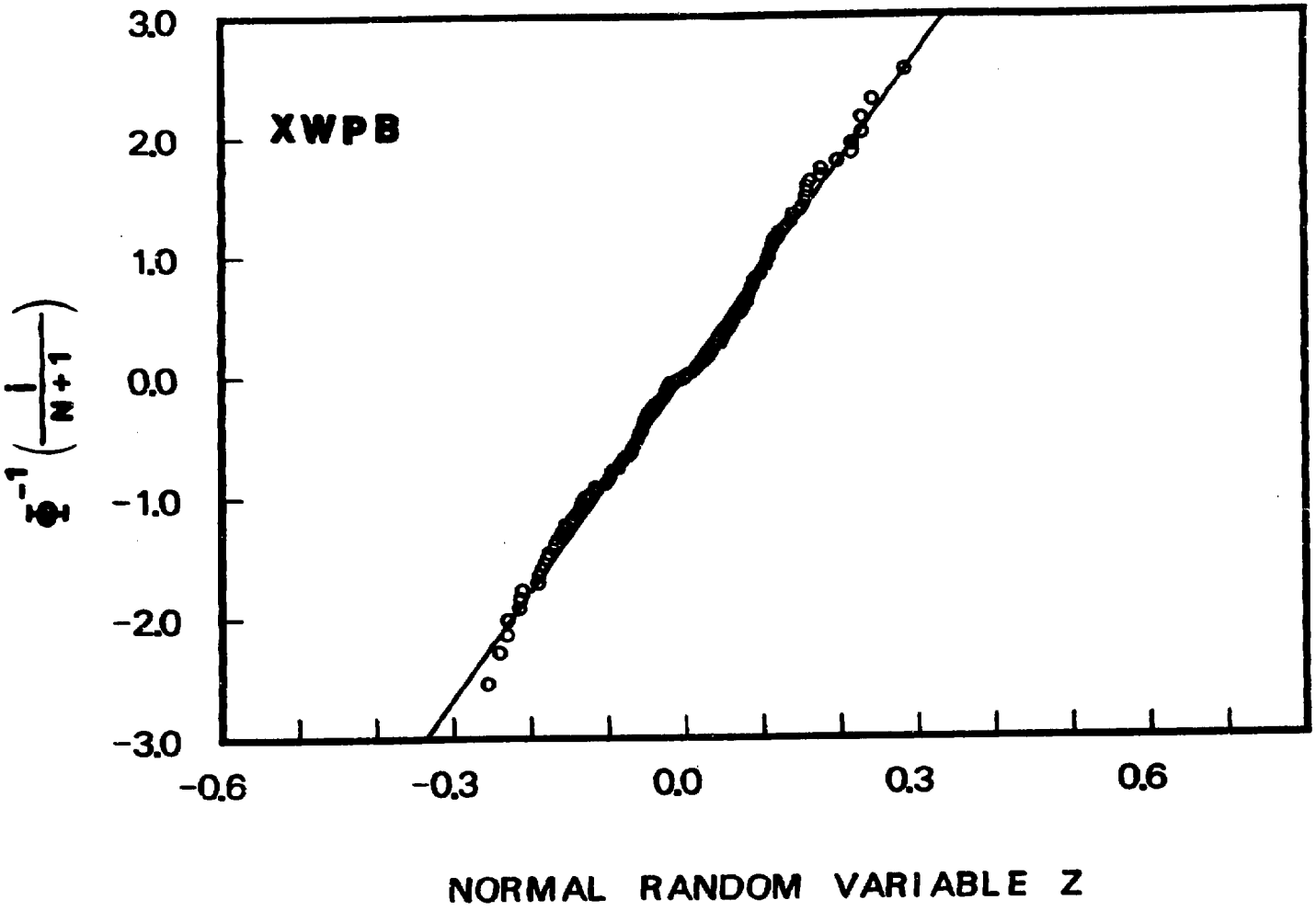

Figure 12: Normal Probability Plot of Z(t) for XWPB Data Set.

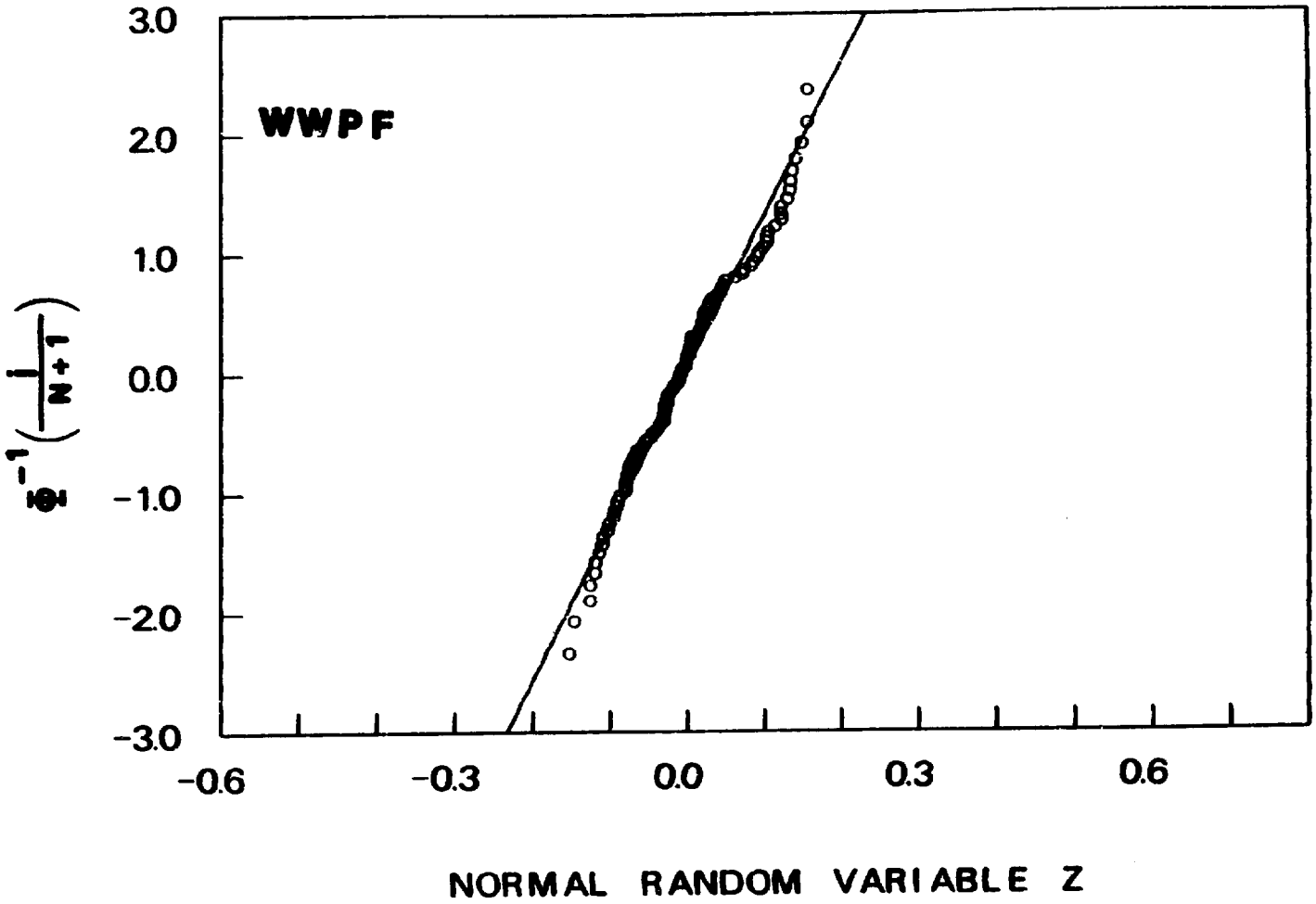

Figure 13: Normal Probability Plot of Z(t) for WWPF Data Set

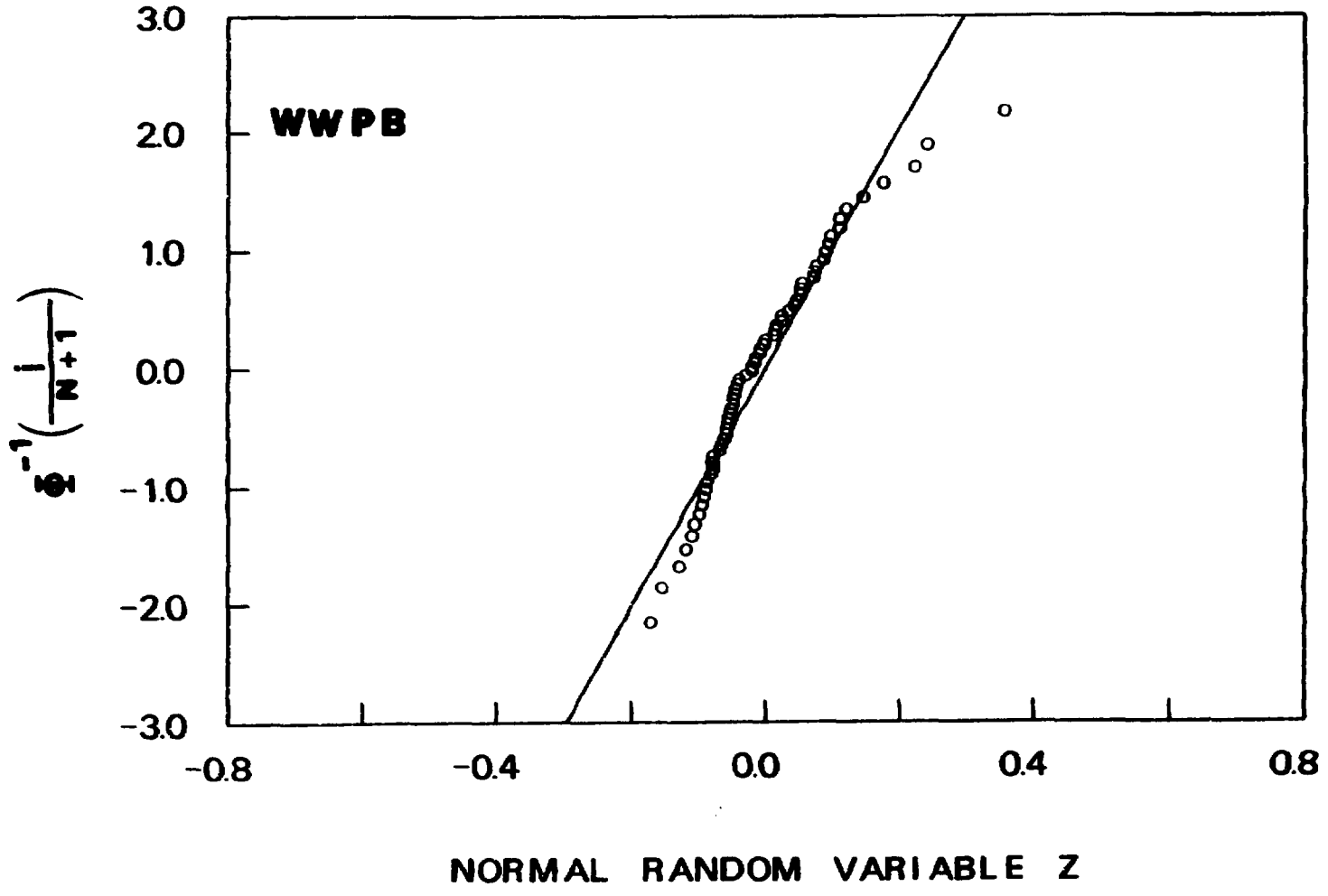

Figure 14: Normal Probability Plot of Z(t) for WWPB Data Set

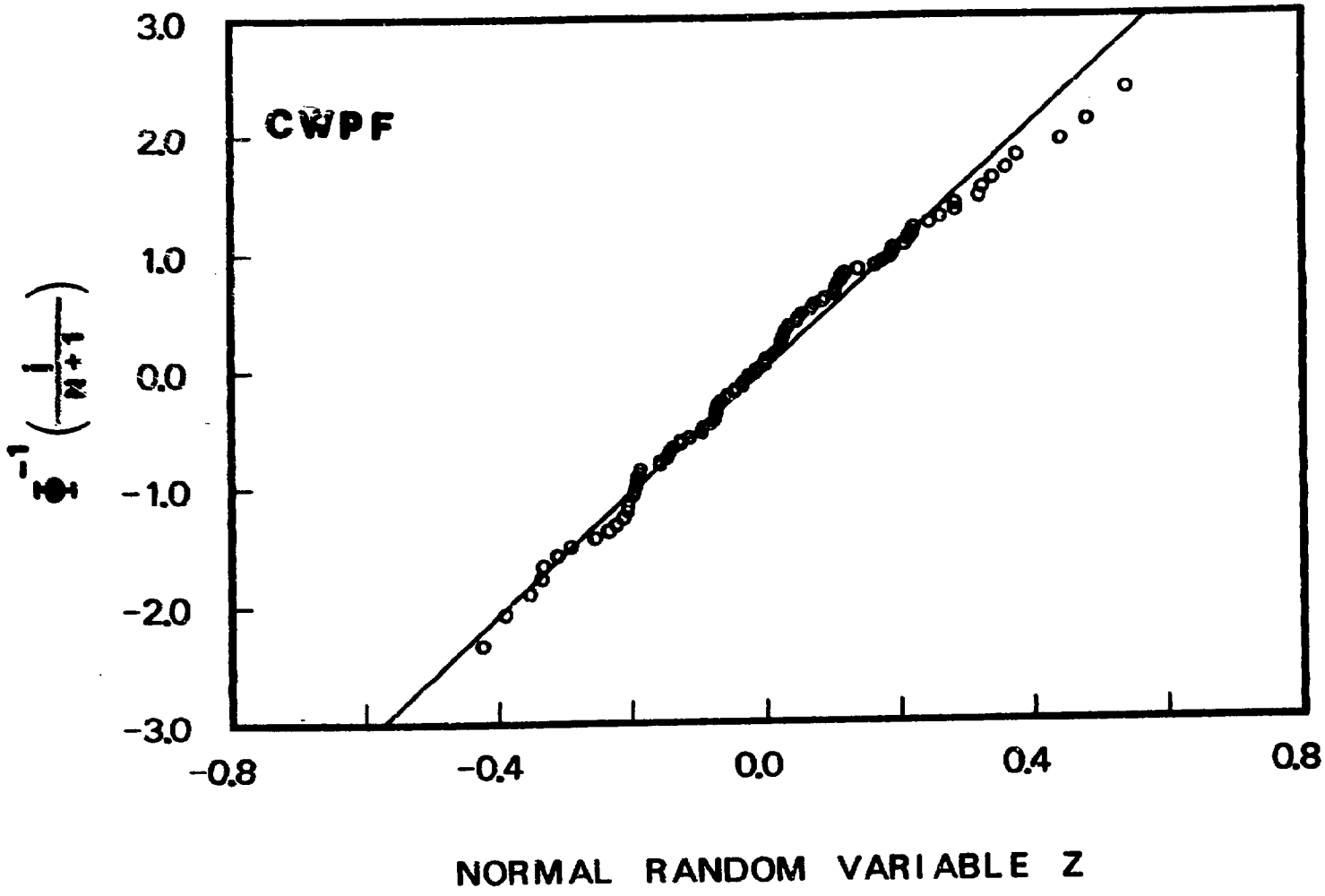

Figure 15: Normal Probability Plot of Z(t) for CWPF Data Set.

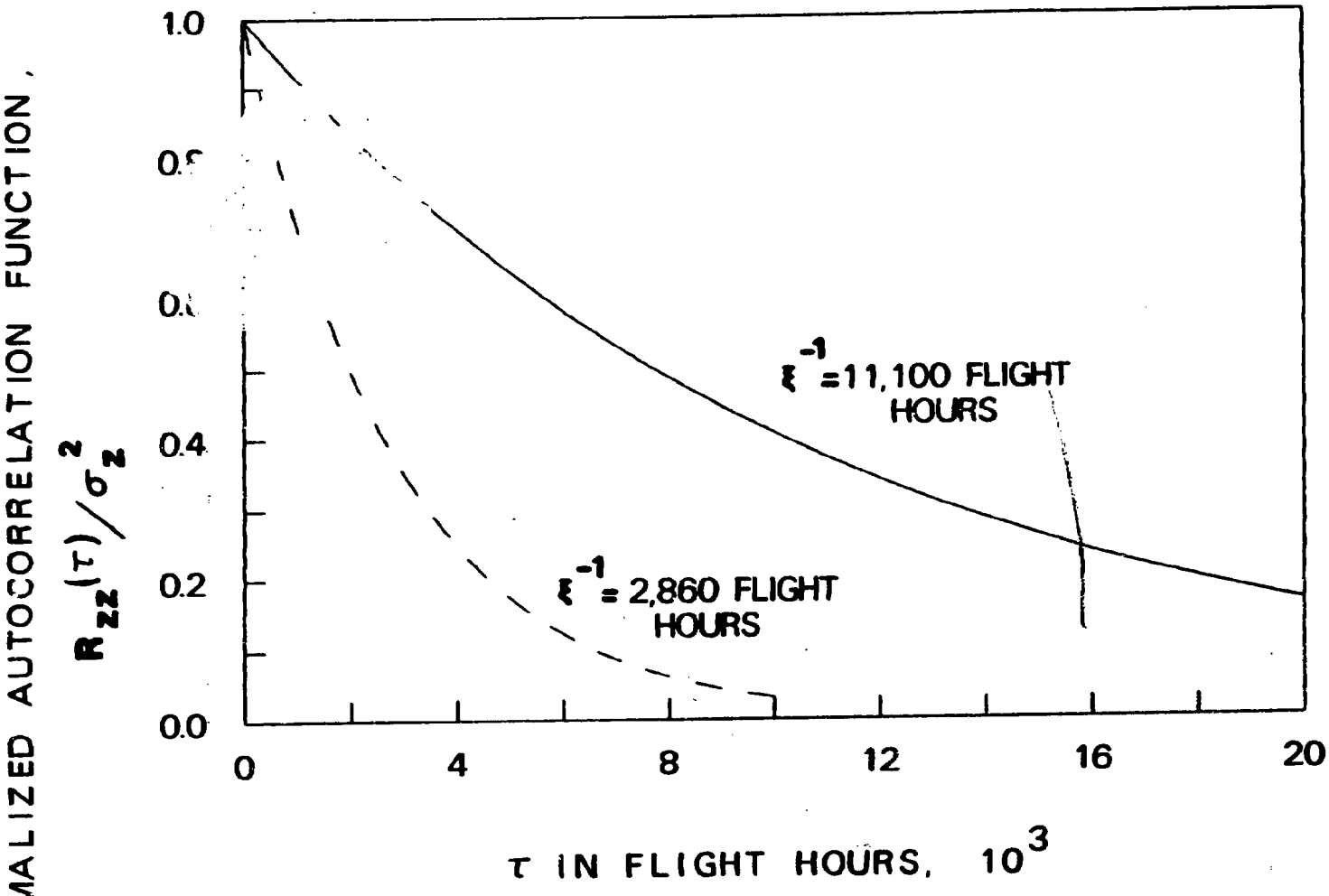

Figure 16(a): Autocorrelation Function $R_{zz}(\tau)$ for Stationary Normal Random Process Z(t); Dash Curve for ξ^{-1} = 2,860 Flight Hours and Solid Curve for ξ^{-1} = 11,100 Flight Hours

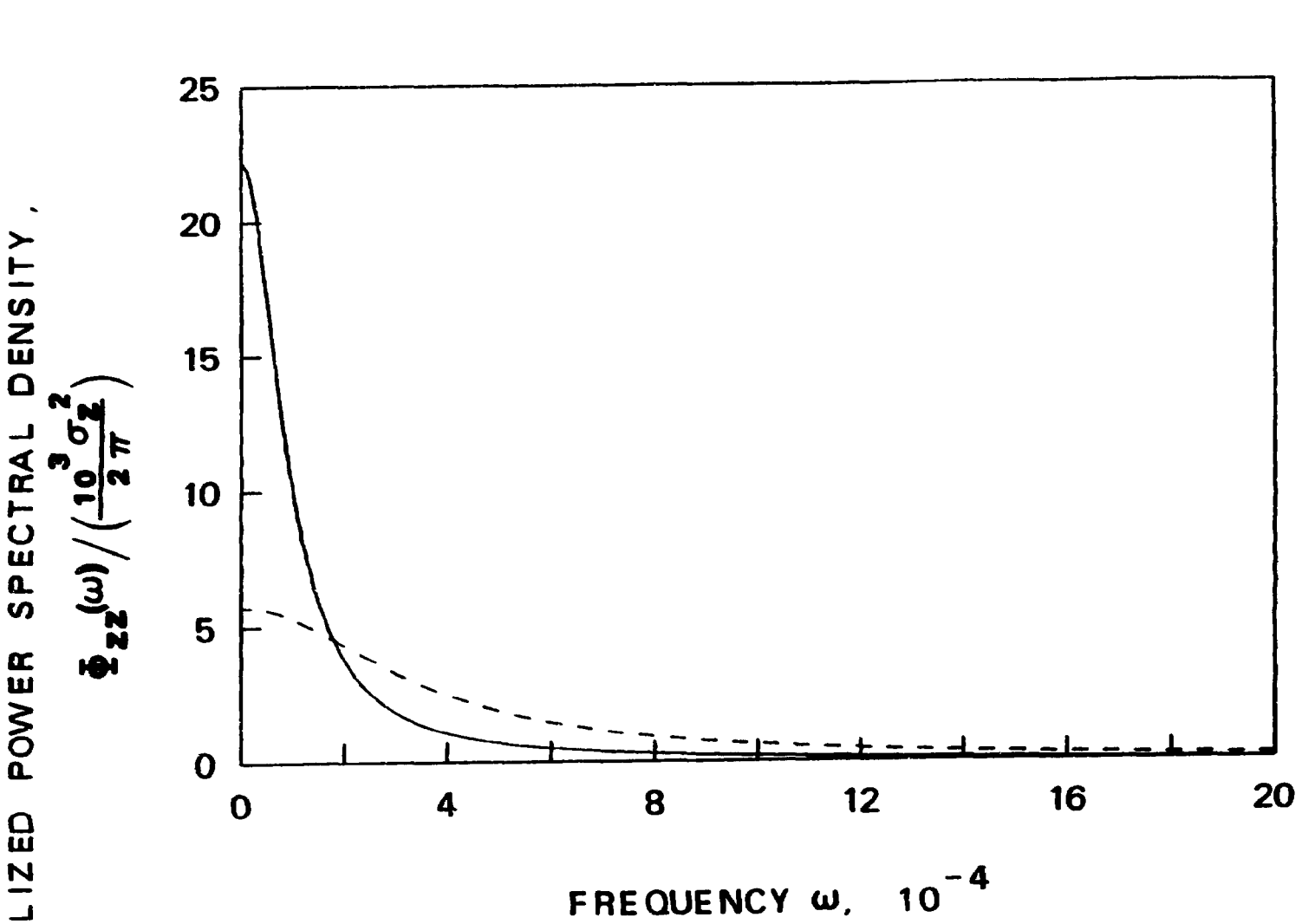

Figure 16(b): Power Spectral Density $\Phi_{zz}(\omega)$ for Stationary Normal Random Process Z(t): Dash Curve for ξ^{-1} = 2,680 Flight Hours and Solid Curve for ξ^{-1} = 11,100 Flight Hours

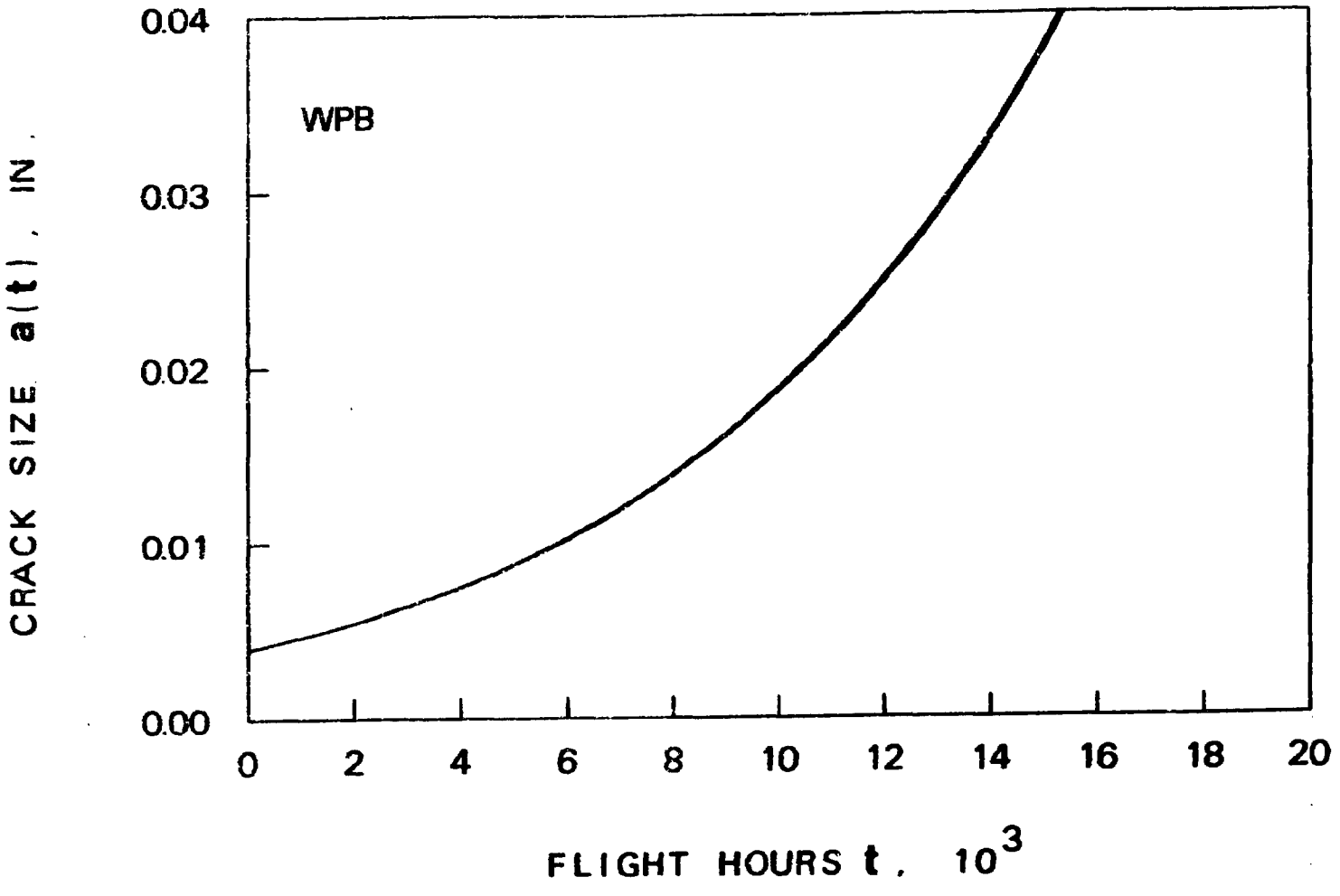

Figure 17: Simulated Crack Propagation Time Histories for WPB Data Set Based on White Noise Model

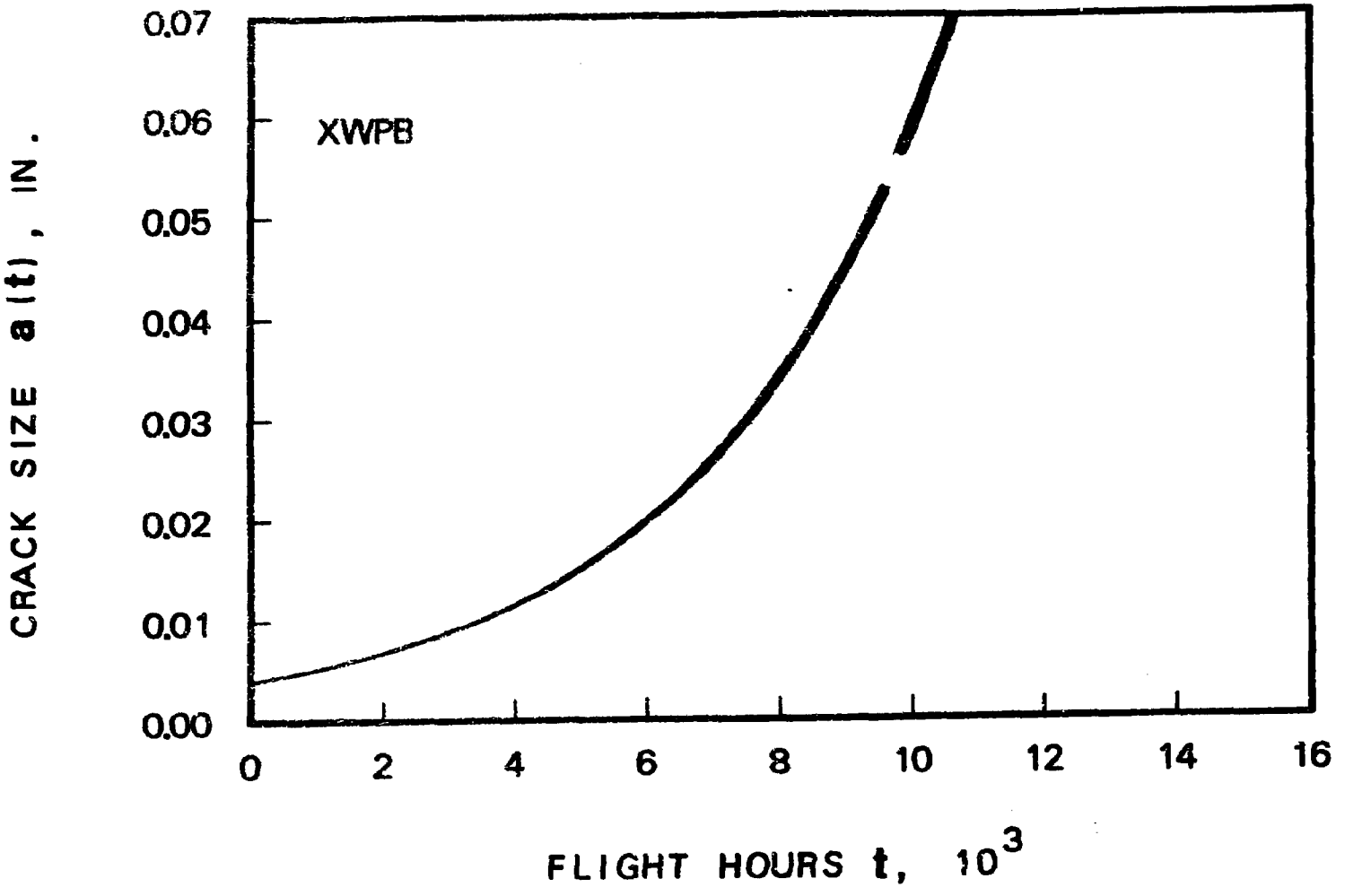

Figure 18: Simulated Crack Propagation Time Histories XWPB Data Set Based on White Noise Model.

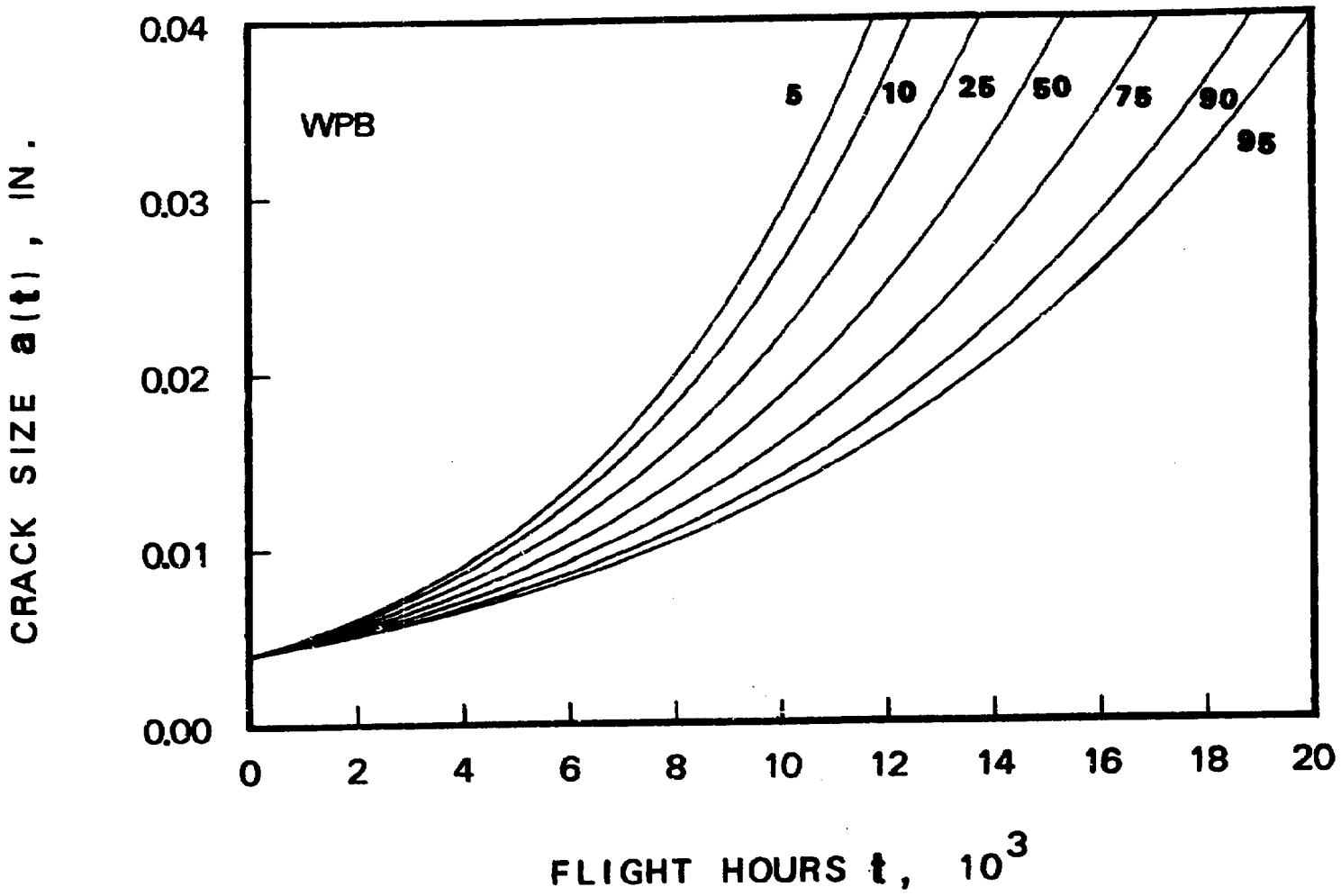

Figure 19: Percentiles of Crack Size a(t) as Function of Service Time t Based on Lognormal Random Variable Model for WPB Fastener Holes.

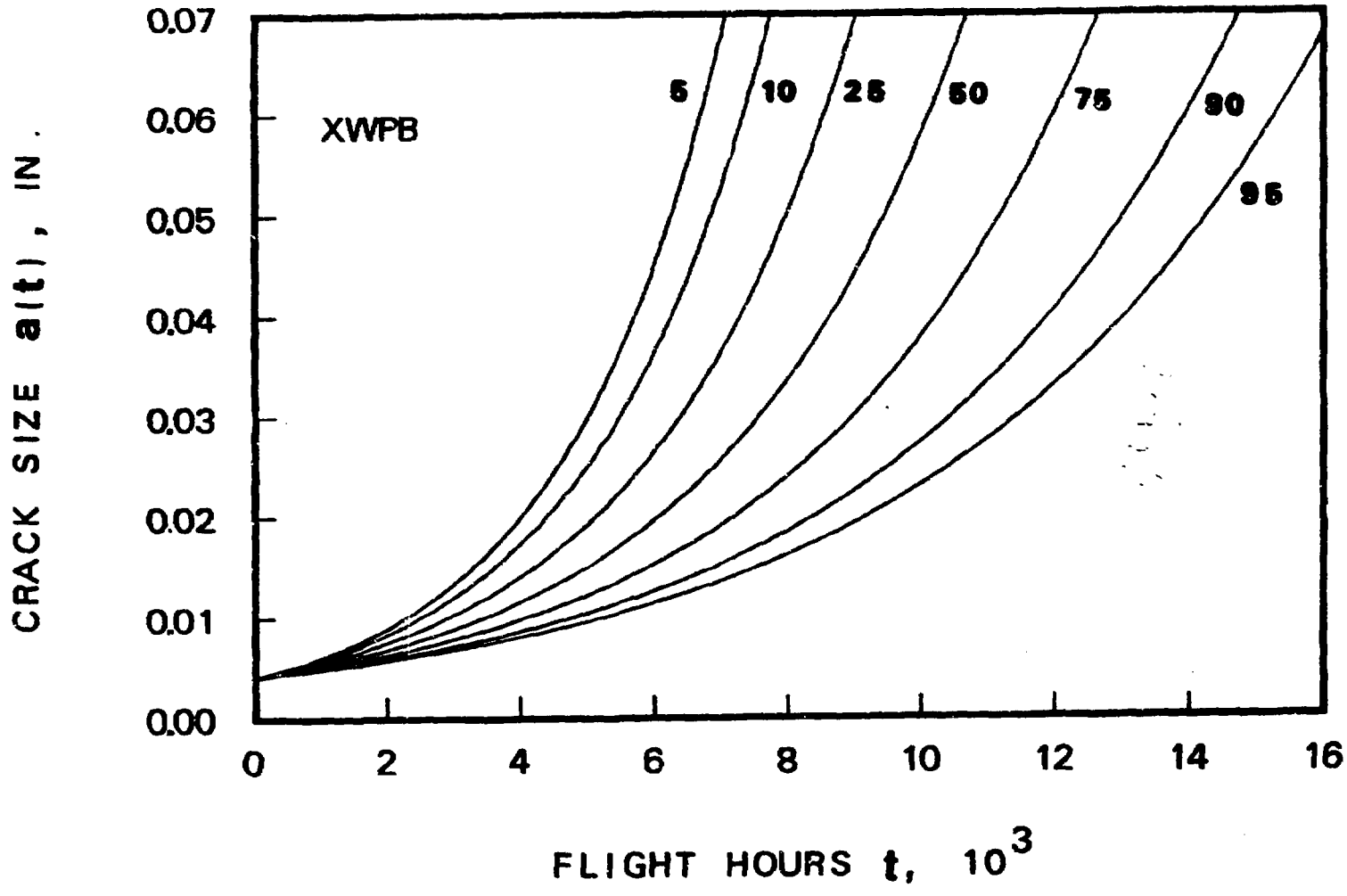

Figure 20: Percentiles of Crack Size a(t) as Function of Service Time t Based on Lognormal Random Variable Model for XWPB Fastener Holes.

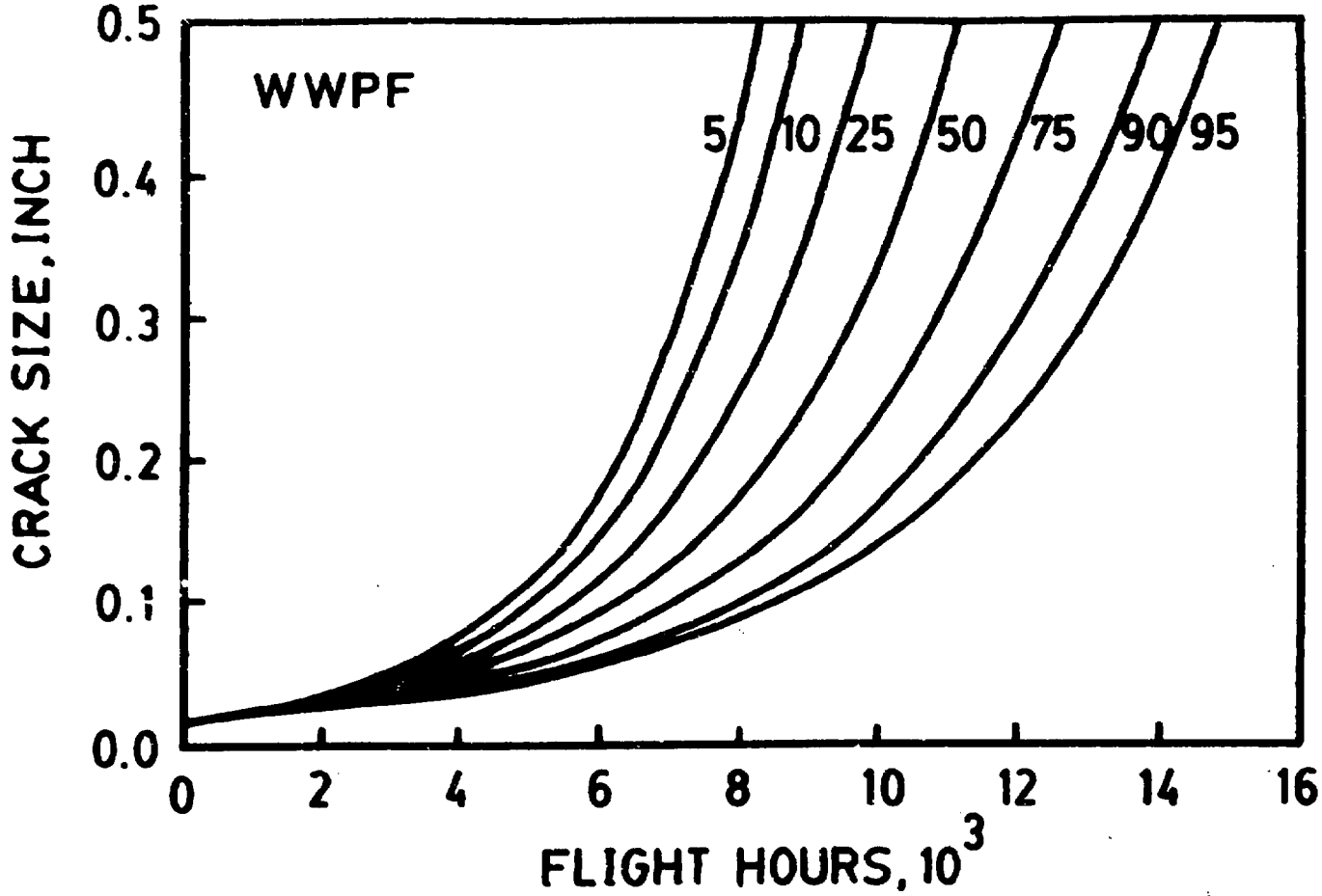

Figure 21: Percentiles of Crack Size a(t) as Function of Service Time t Based on Lognormal Random Variable Model for WWPF Fastener Holes

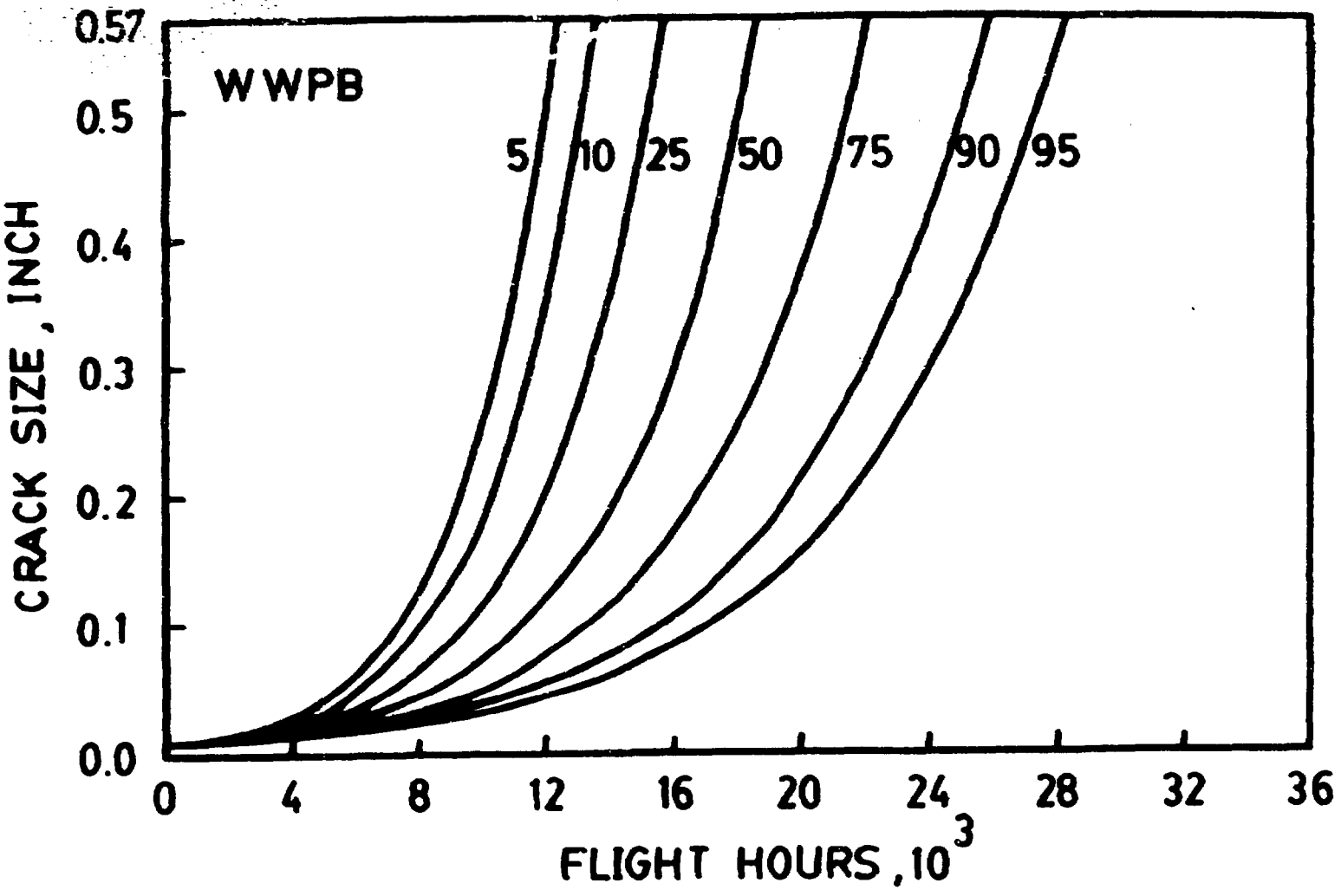

Figure 22: Percentiles of Crack Size a(t) as Function of Service Time t Based on Lognormal Random Variable Model for WWPB Fastener Holes

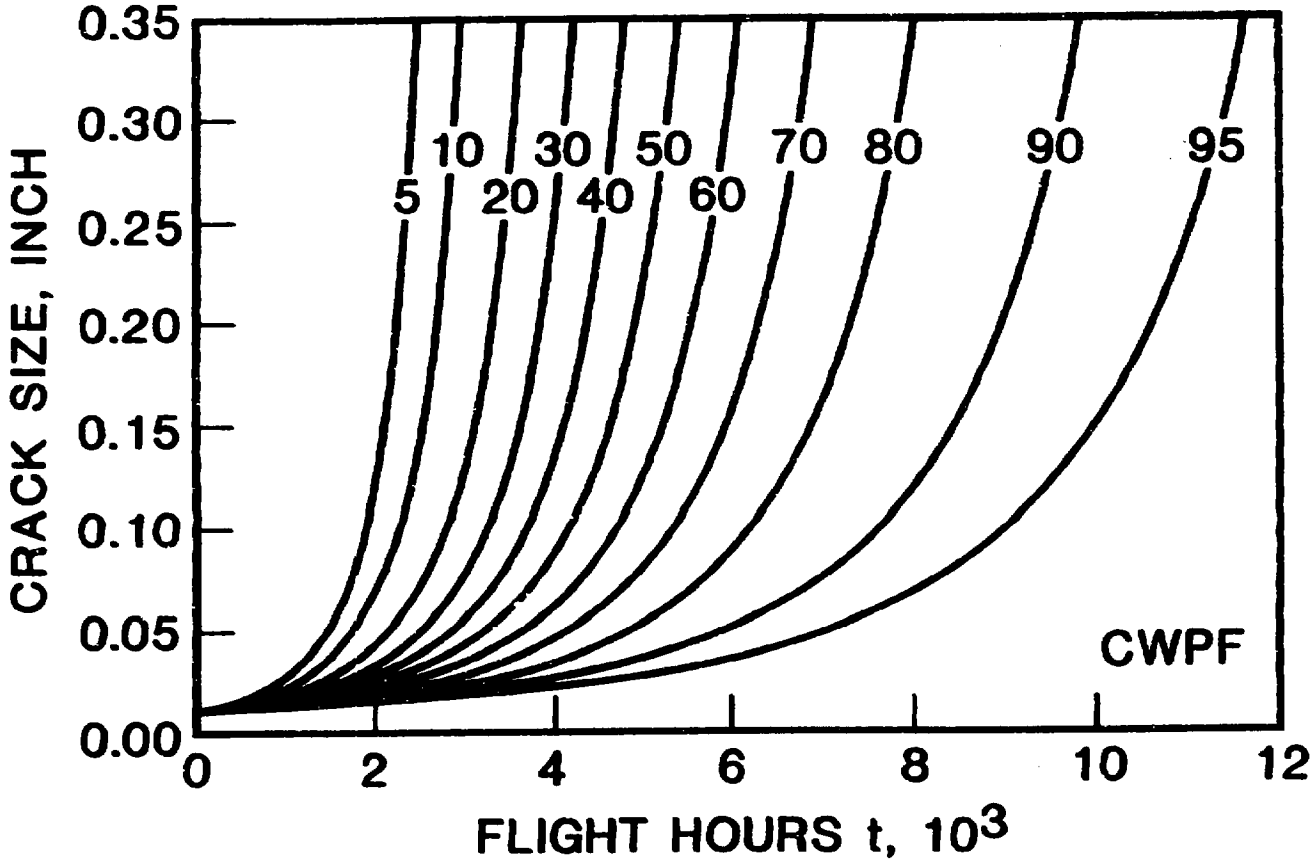

Figure 23: Percentiles of Crack Size a(t) as Function of Service Time t Based on Lognormal Random Variable Model for CWPF Fastener Holes

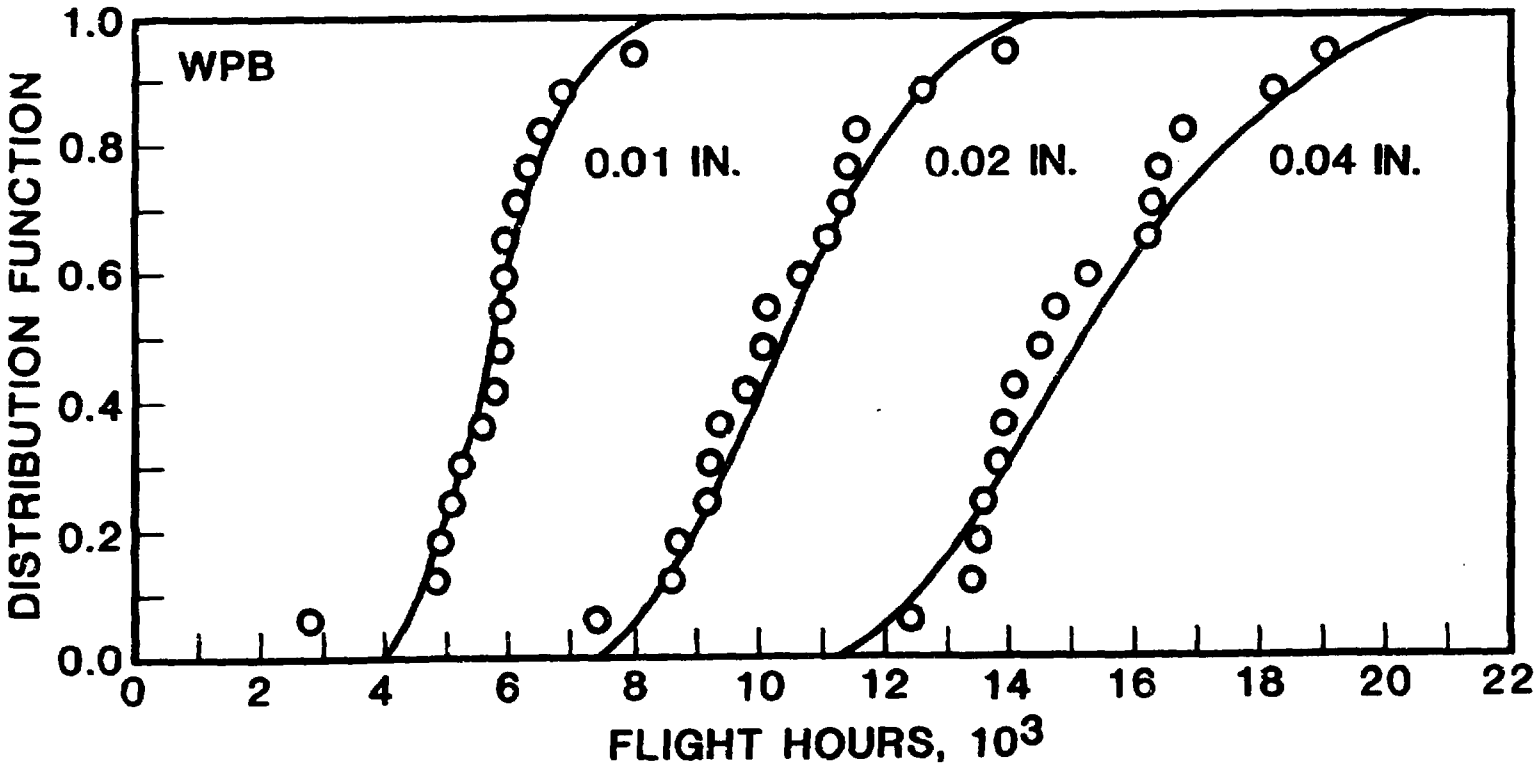

Figure 24: Correlation Between Lognormal Random Variable Model and Test Results for the Distirbution of Time to Reach Crack Sizes 0.01, 0.02 and 0.04 Inch for WPB Fastener Holes.

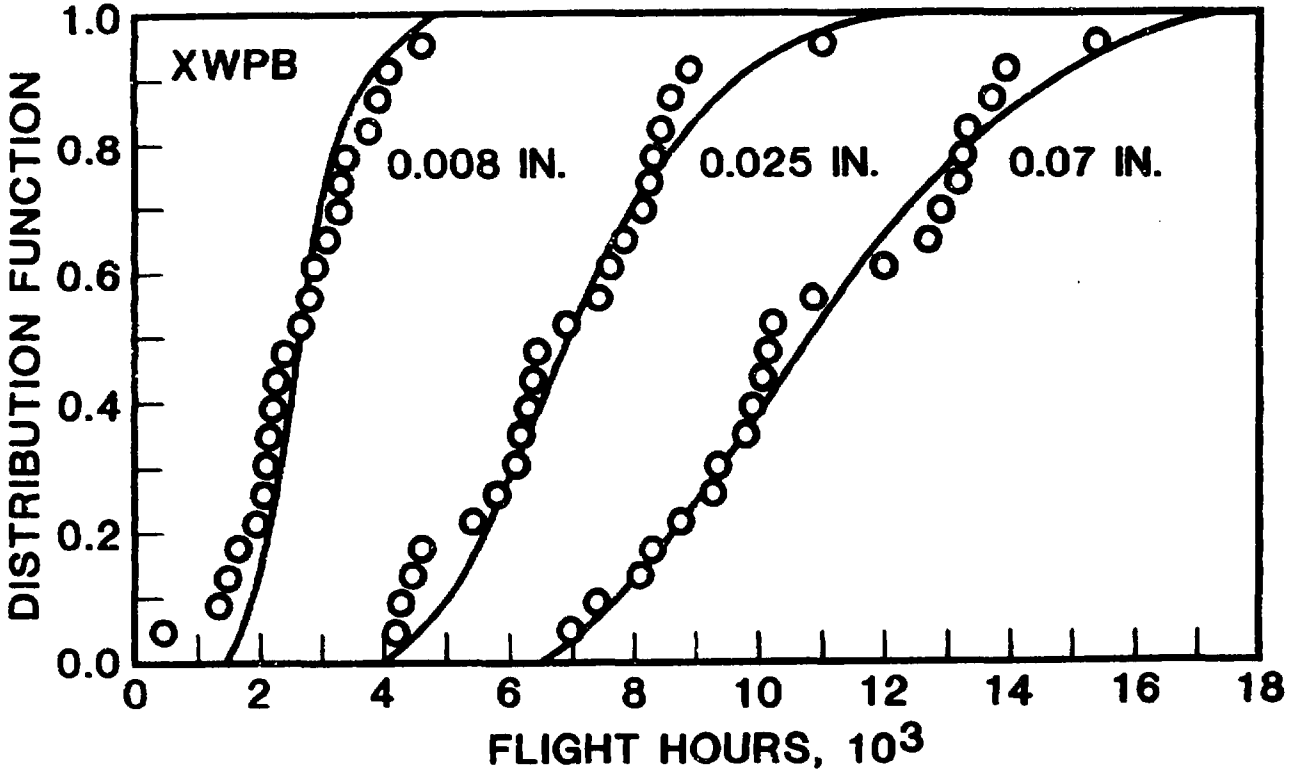

Figure 25: Correlation Between Lognormal Random Variable Model and Test Results for the Distribution of Time to Reach Crack Sizes 0.008, 0.025 and 0.07 Inch for XWPB Fastener Holes.

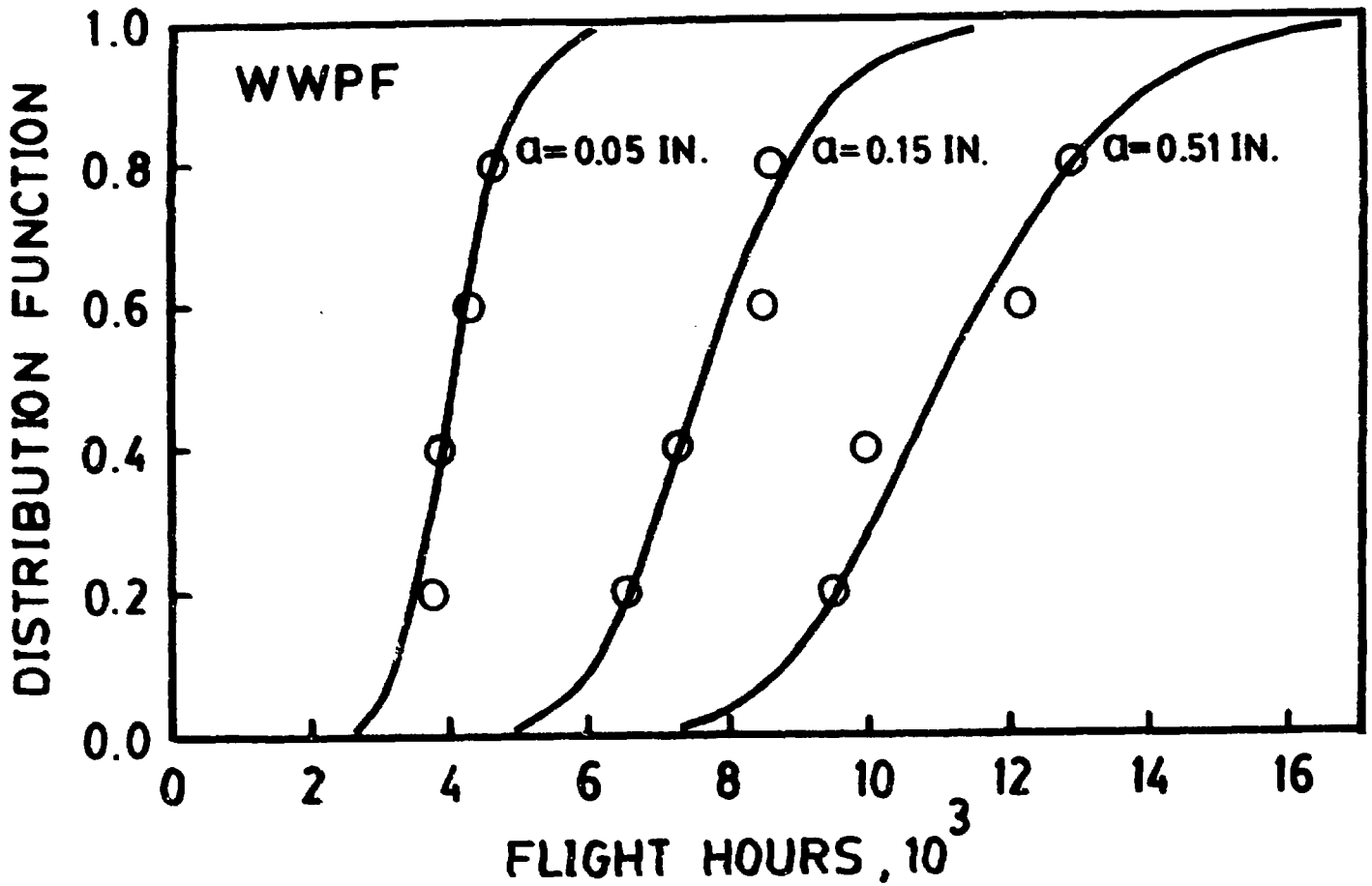

Figure 26: Correlation Between Lognormal Random Variable Model and Test Results for the Distribution of Time to Reach Crack Sizes 0.05, 0.15 and 0.51 Inch for WWPF Fastener Holes.

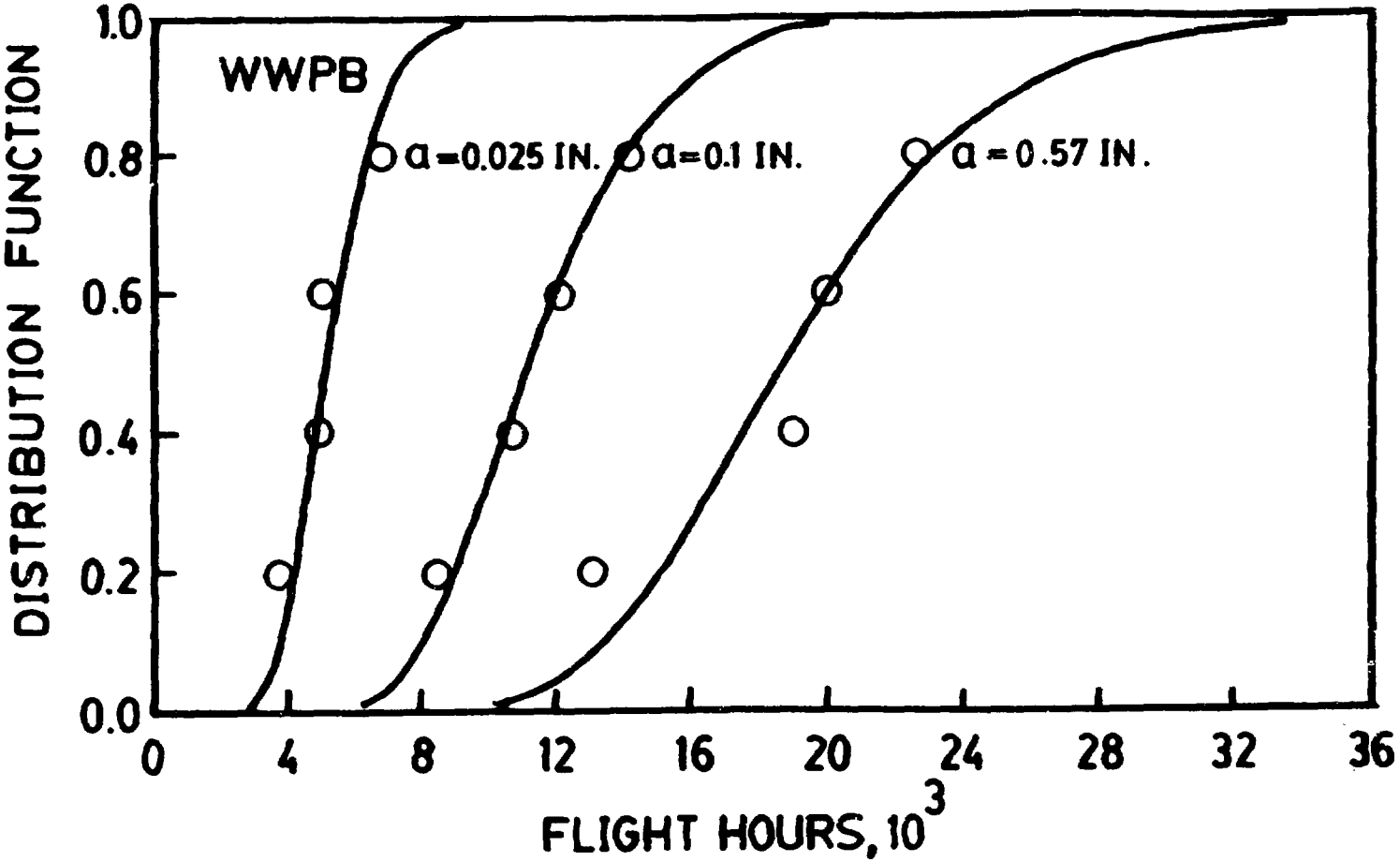

Figure 27: Correlation Between Lognormal Random Variable Model and Test Results for the Distribution of Time to Reach Crack Sizes 0.025, 0.1 and 0.57 Inch for WWPB Fastener Holes

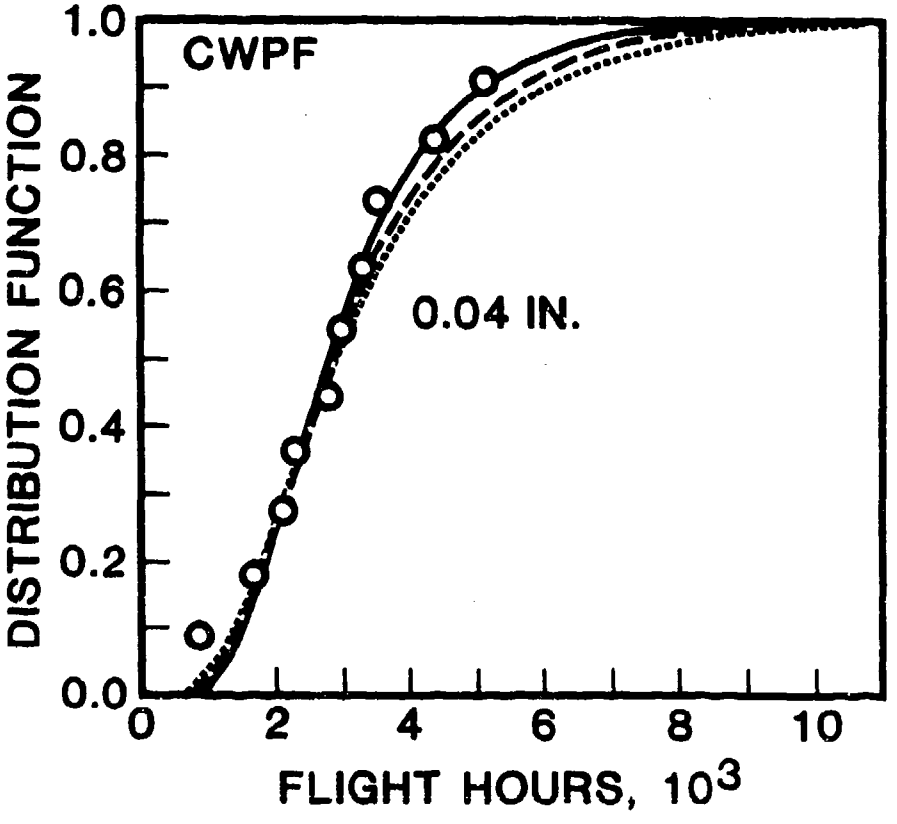

Figure 28(a): Correlation Between Lognormal Random Variable Model and Test Results for the Distribution of Time to Reach 0.04 Inch Crack for CWPF Fastener Holes.

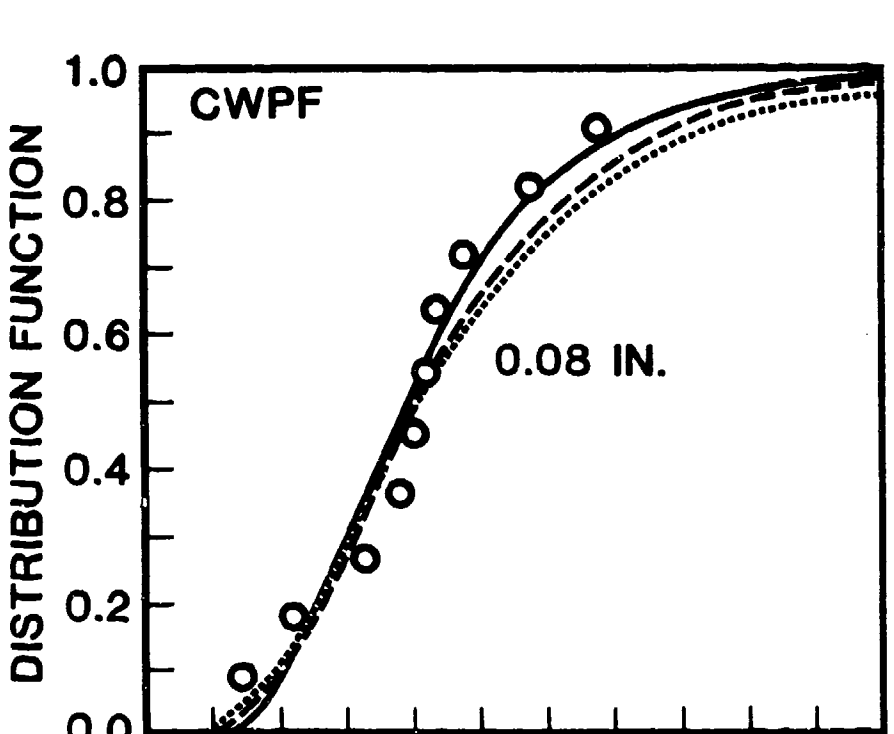

Figure 28(b): Correlation Between Lognormal Random Variable Model and Test Results for the Distribution of Time to Reach 0.08 Inch Crack for CWPF Fastener Holes.

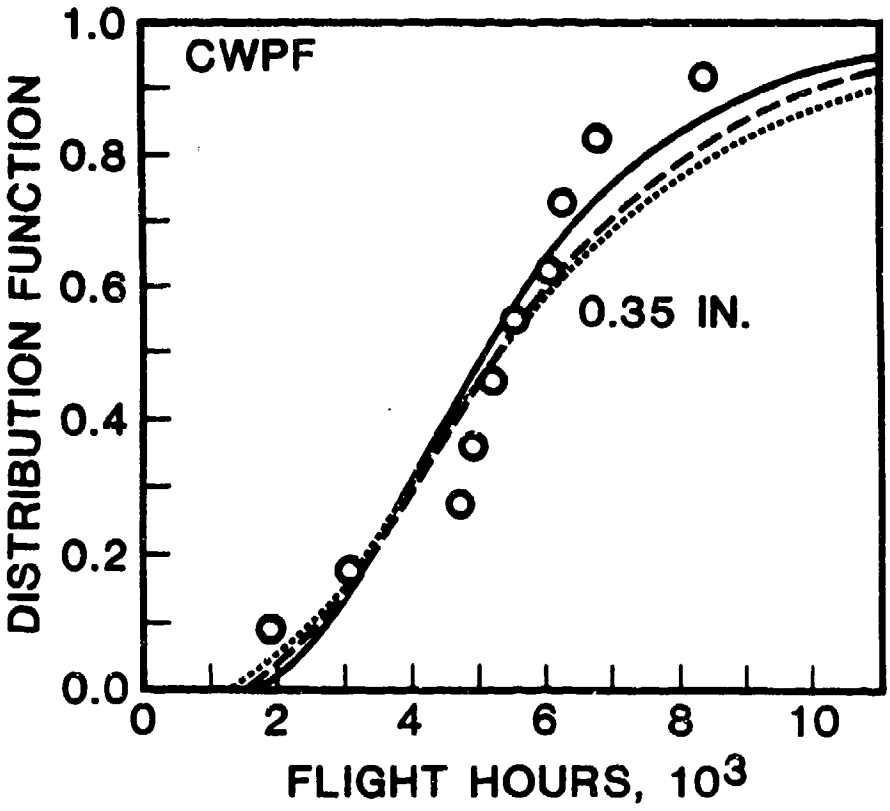

Figure 28(c): Correlation Between Lognormal Random Variable Model and Test Results for the Distribution of Time to Reach 0.35 Inch Crack for CWPF Fastener Holes.

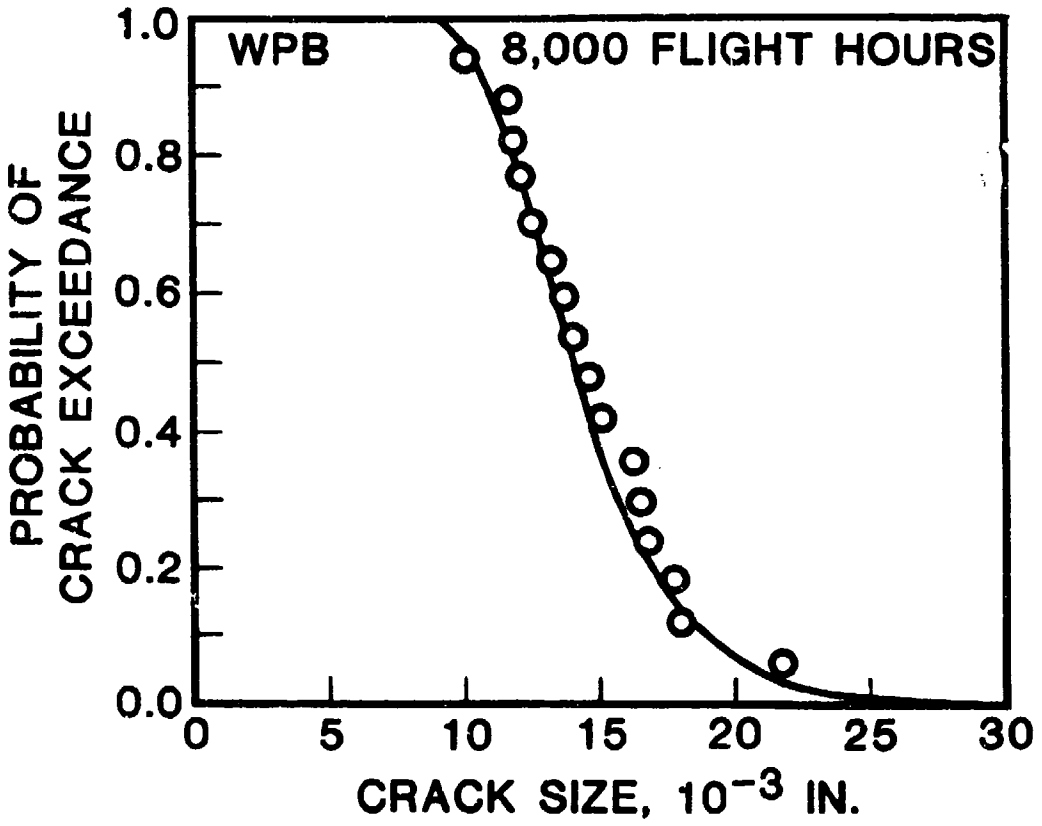

Figure 29: Correlation Between Lognormal Random Variable Model and Test Results for the Probability of Crack Exceedance at 8,000 Flight Hours for WPB Fastener Holes.

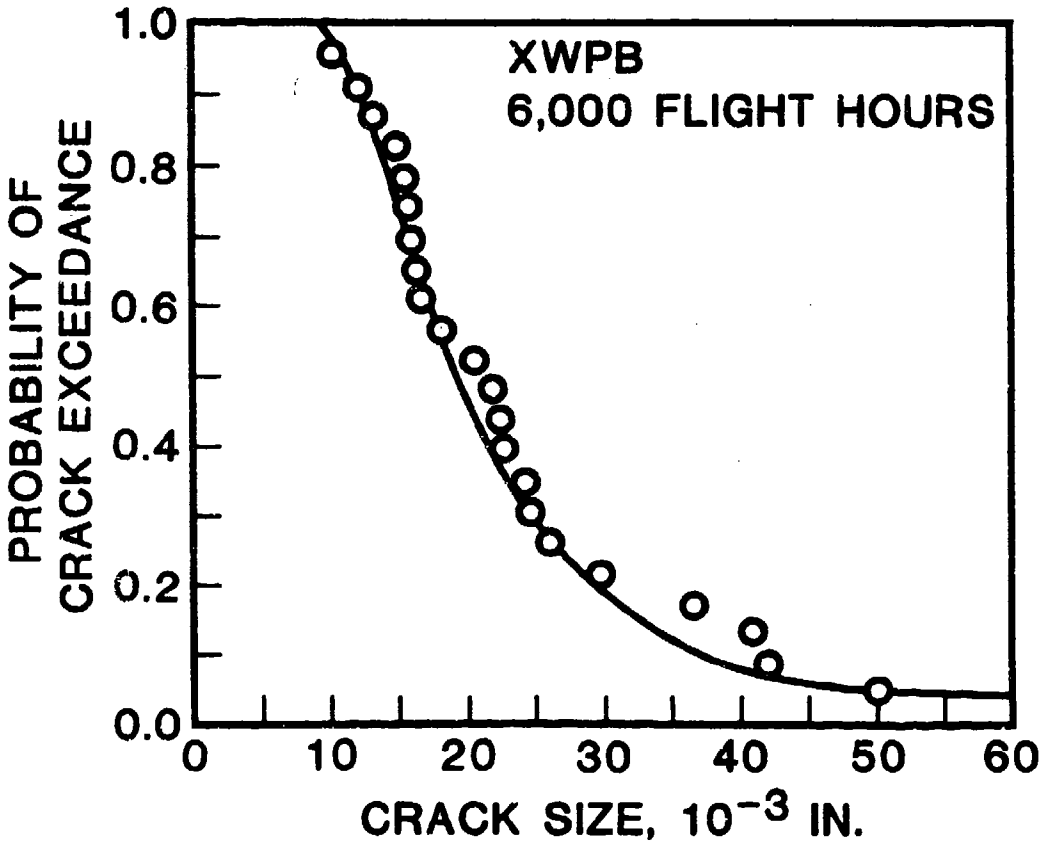

Figure 30: Correlation Between Lognormal Random Variable Model and Test Results for the Probability of Crack Exceedance at 6,000 Flight Hours for XWPB Fastener Holes.

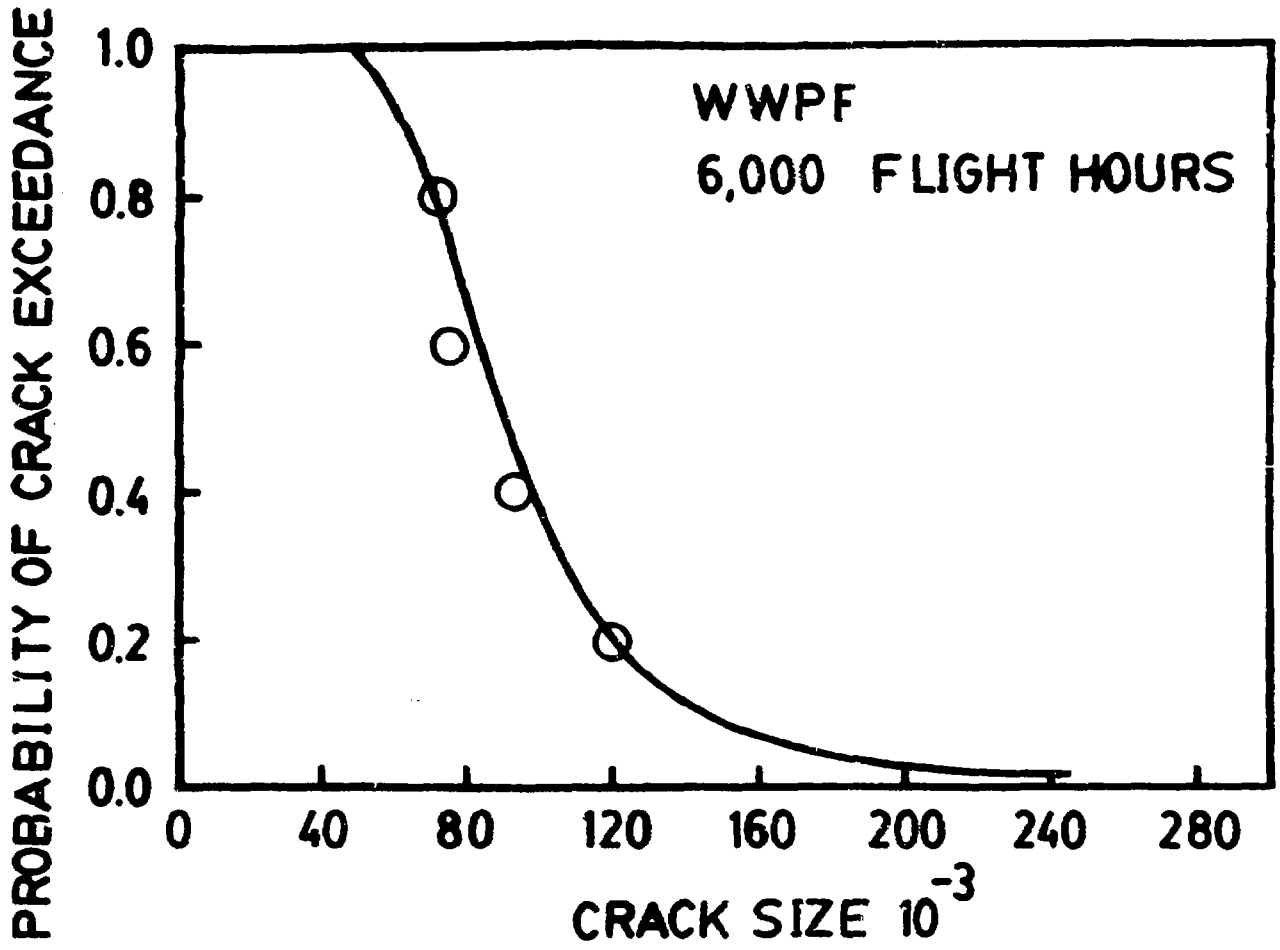

Figure 31: Correlation Between Lognormal Random Variable Model and Test Results for the Probability of Crack Exceedance at 6,000 Flight Hours for WWPF Fastener Holes

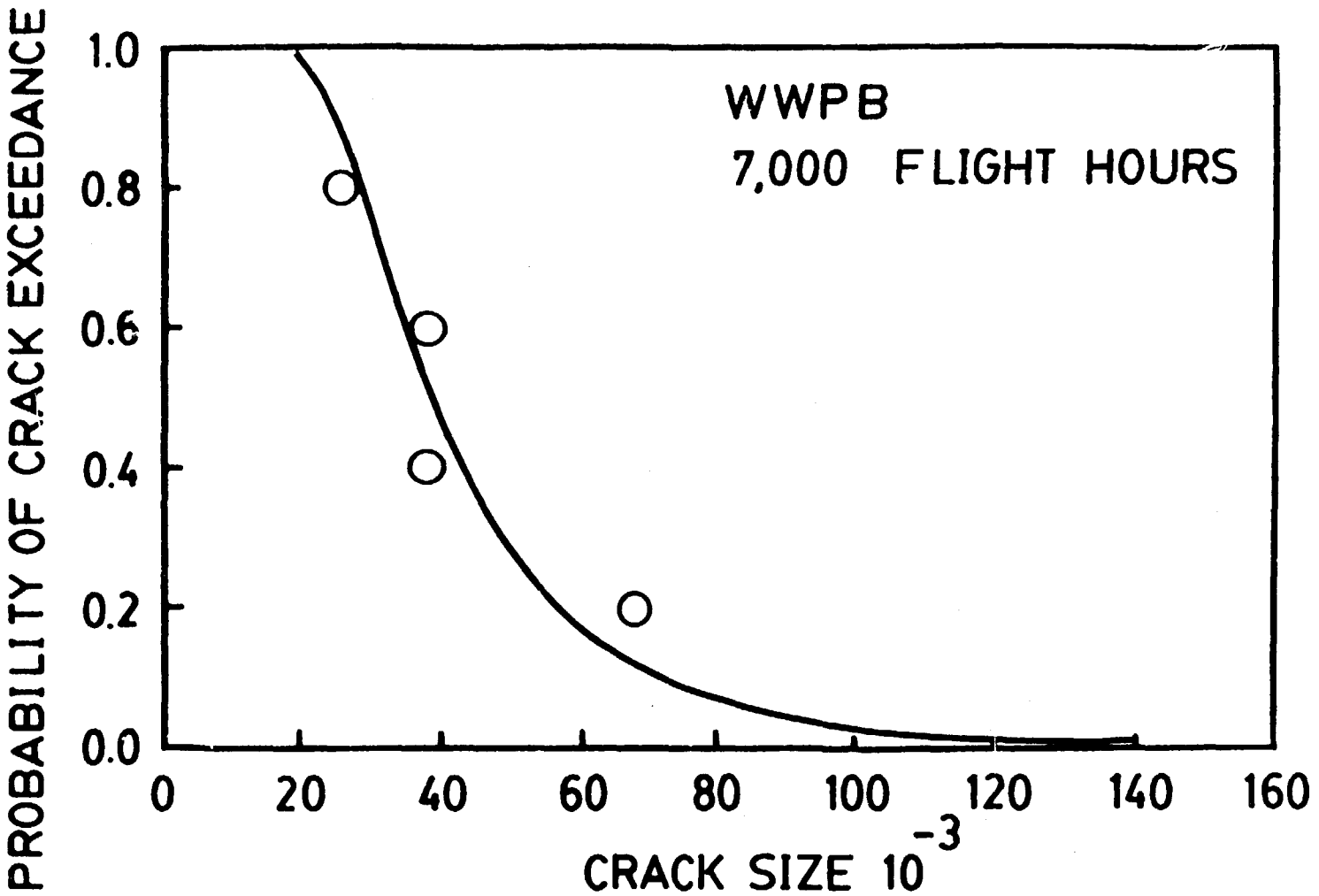

Figure 32: Correlation Between Lognormal Random Variable Model and Test for the Probability of Crack Exceedance at 7,000 Flight Hours for WWPB Fastener Holes

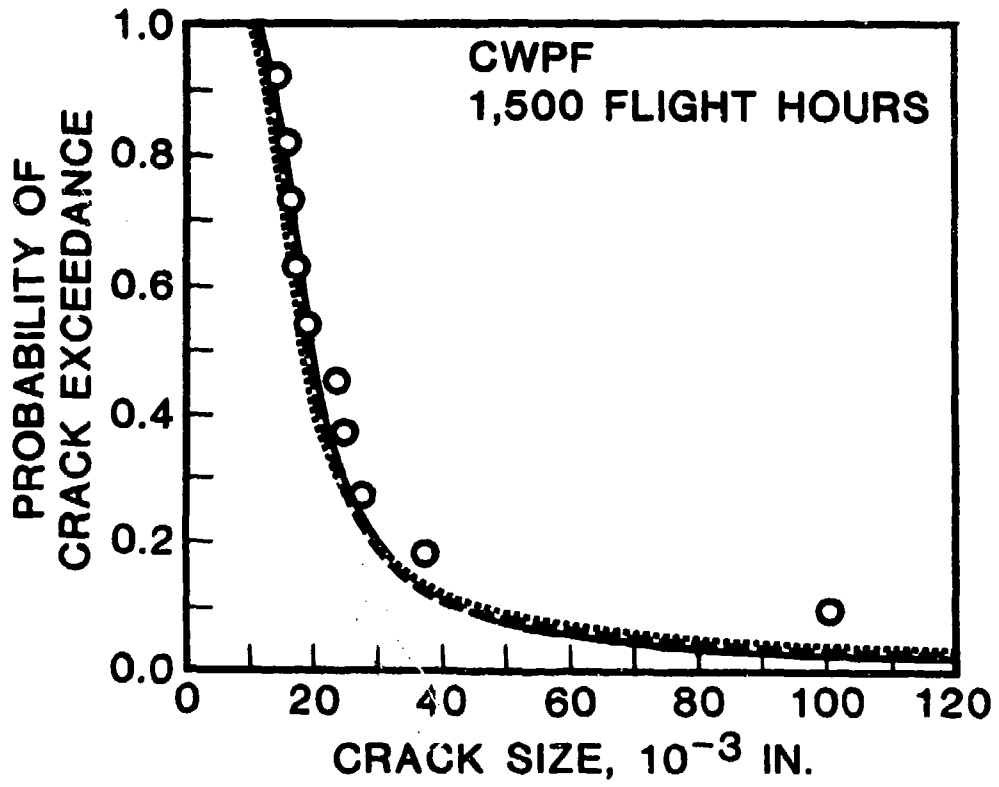

Figure 33: Correlation Between Lognormal Random Variable Model and Test Results for the Probability of Crack Exceedance at 1,500 Flight Hours for CWPF Fastener Holes.

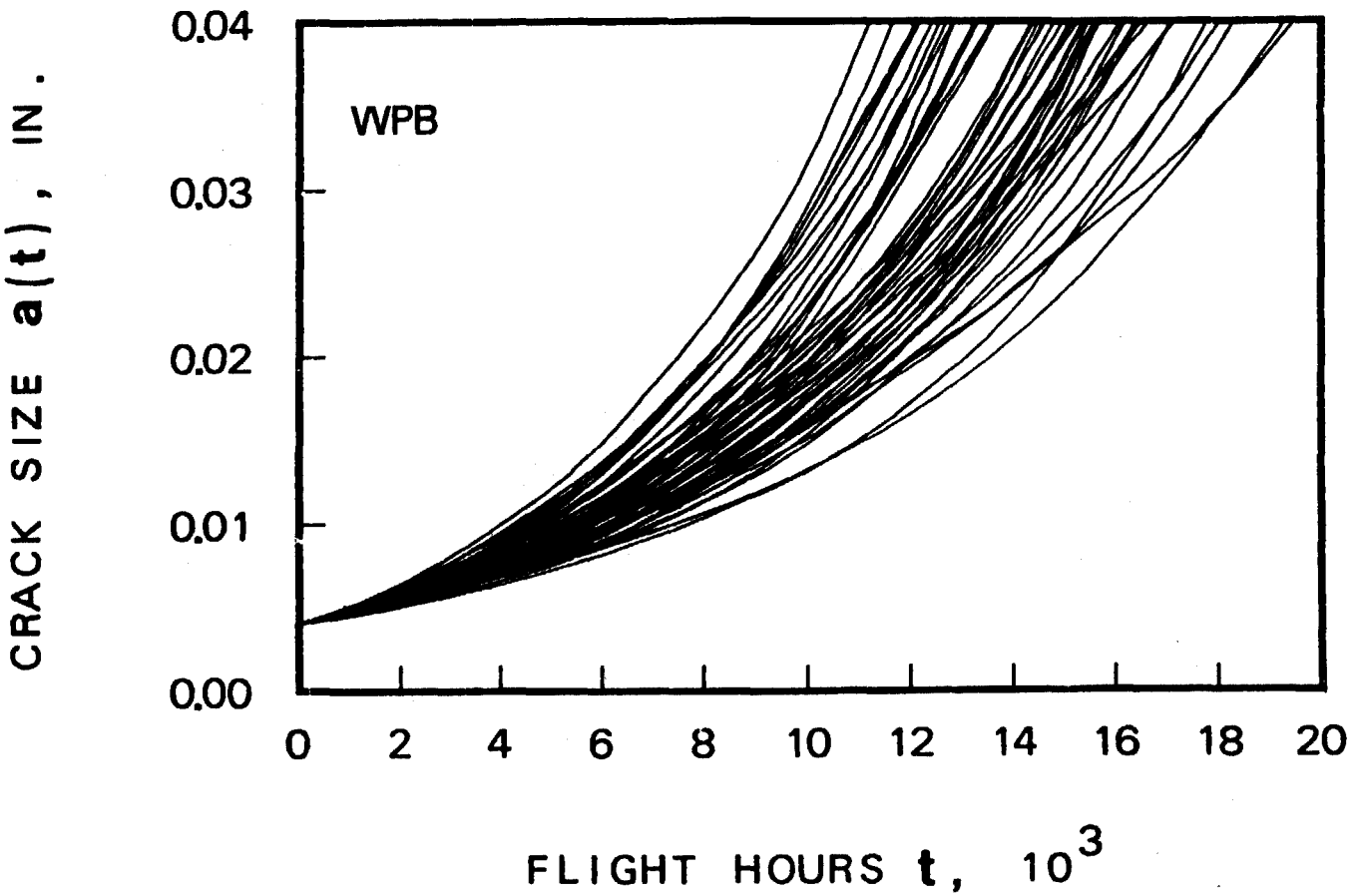

Figure 34: Simulated Sample Functions of Crack Size Versus Service for WPB Fastener Holes; ζ^{-1} = 6,670 Flight Hours.

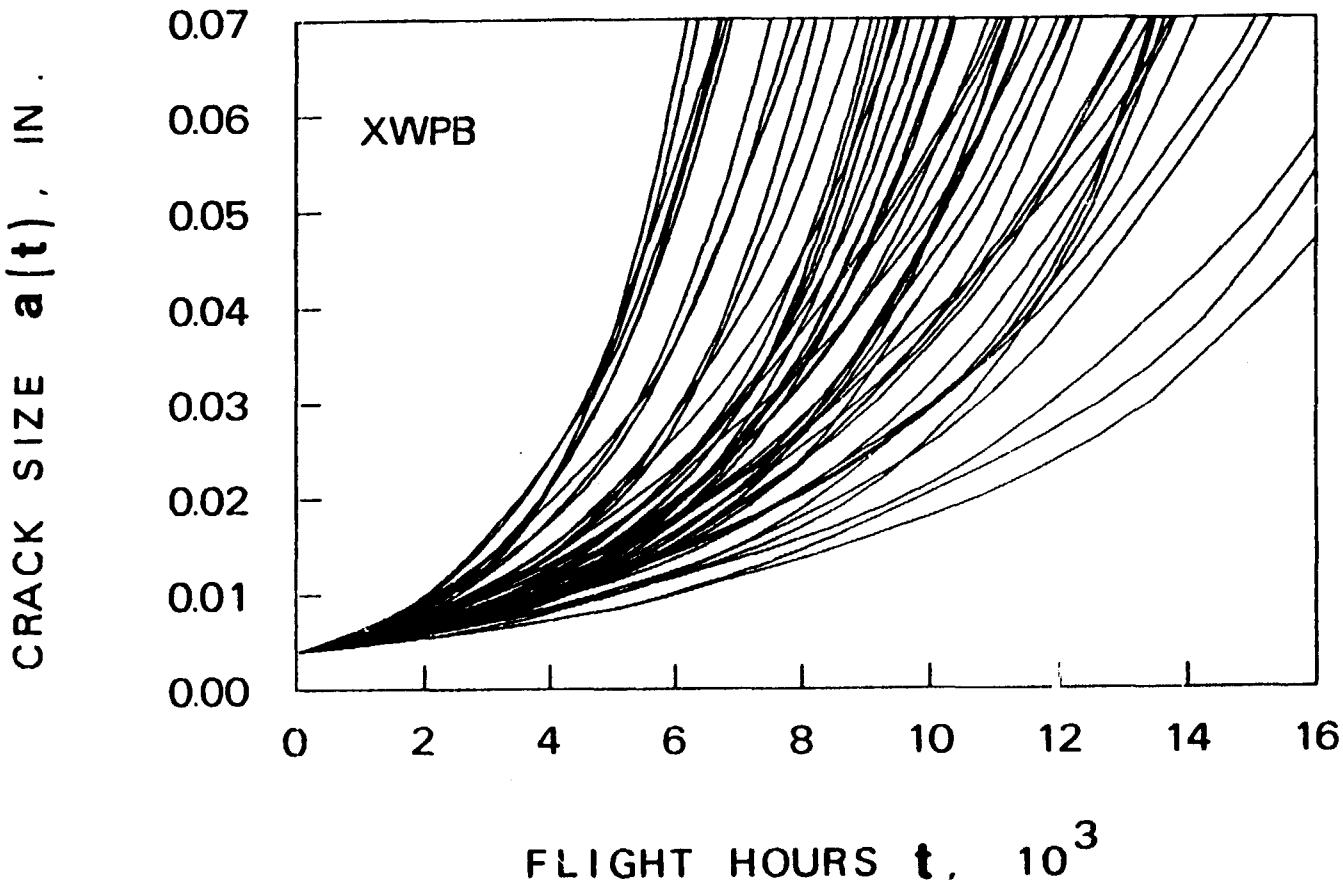

Figure 35: Simulated Sample Functions of Crack Size versus Service Time for XWPB Fastener Holes; ξ^{-1}=10,000 Flight Hours

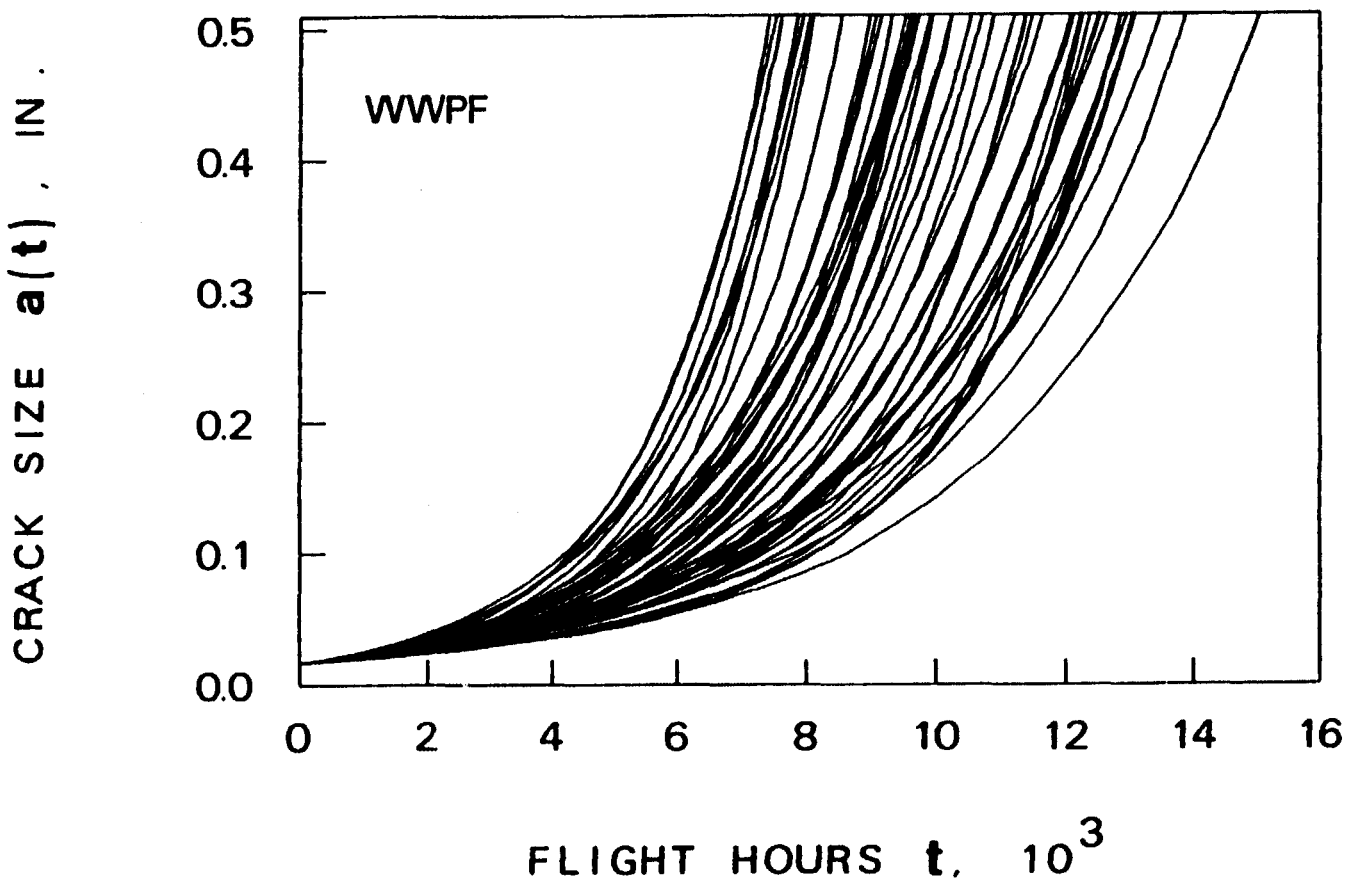

Figure 36: Simulated Sample Functions of Crack Size versus Service Time for WWPF Fastener Holes; ξ^{-1}=8,330 Flight Hours

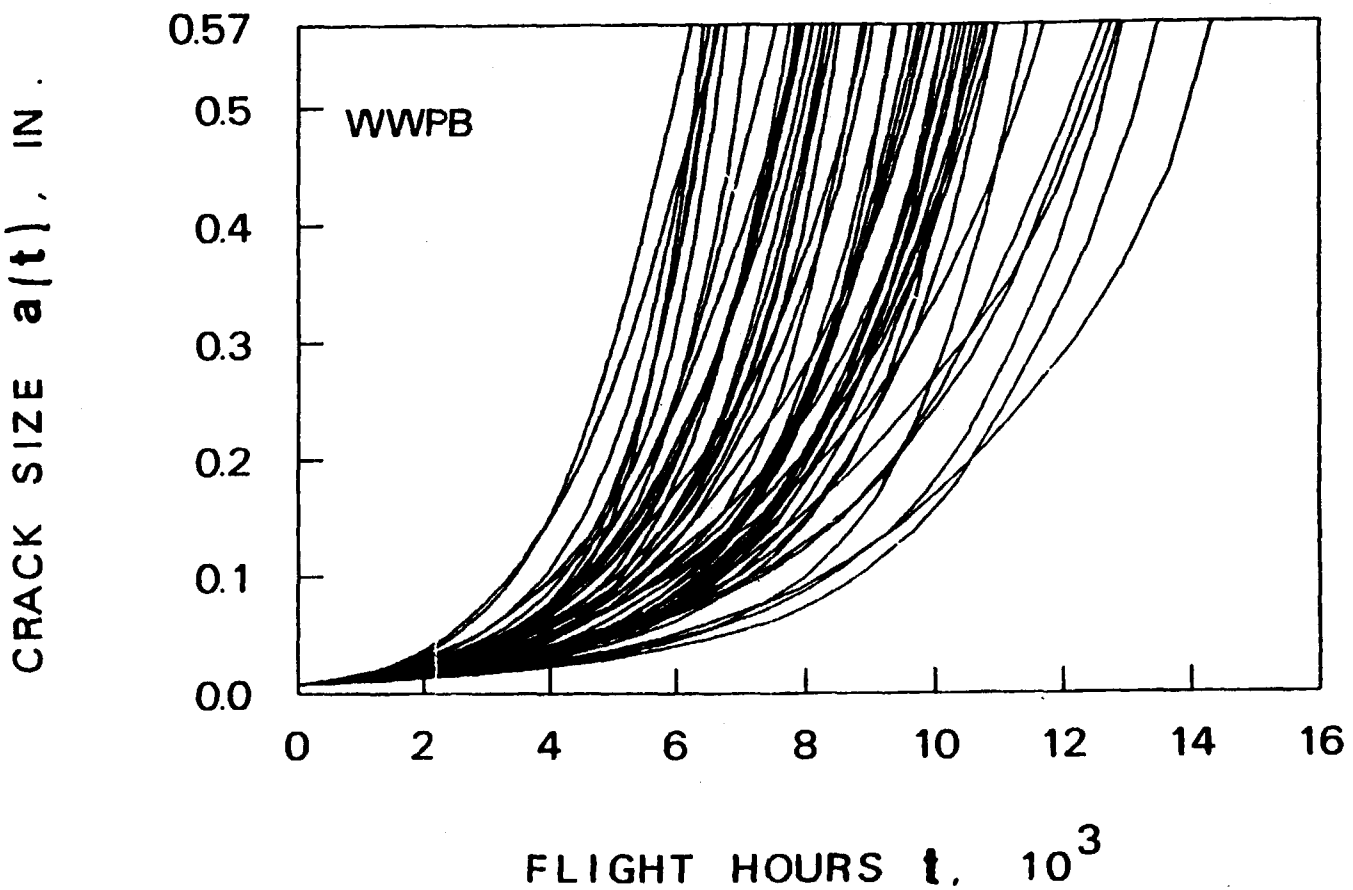

Figure 37: Simulated Sample Functions of Crack Size versus Service Time for WWPB Fastener Holes; ξ^{-1} =11,100 Flight Hours

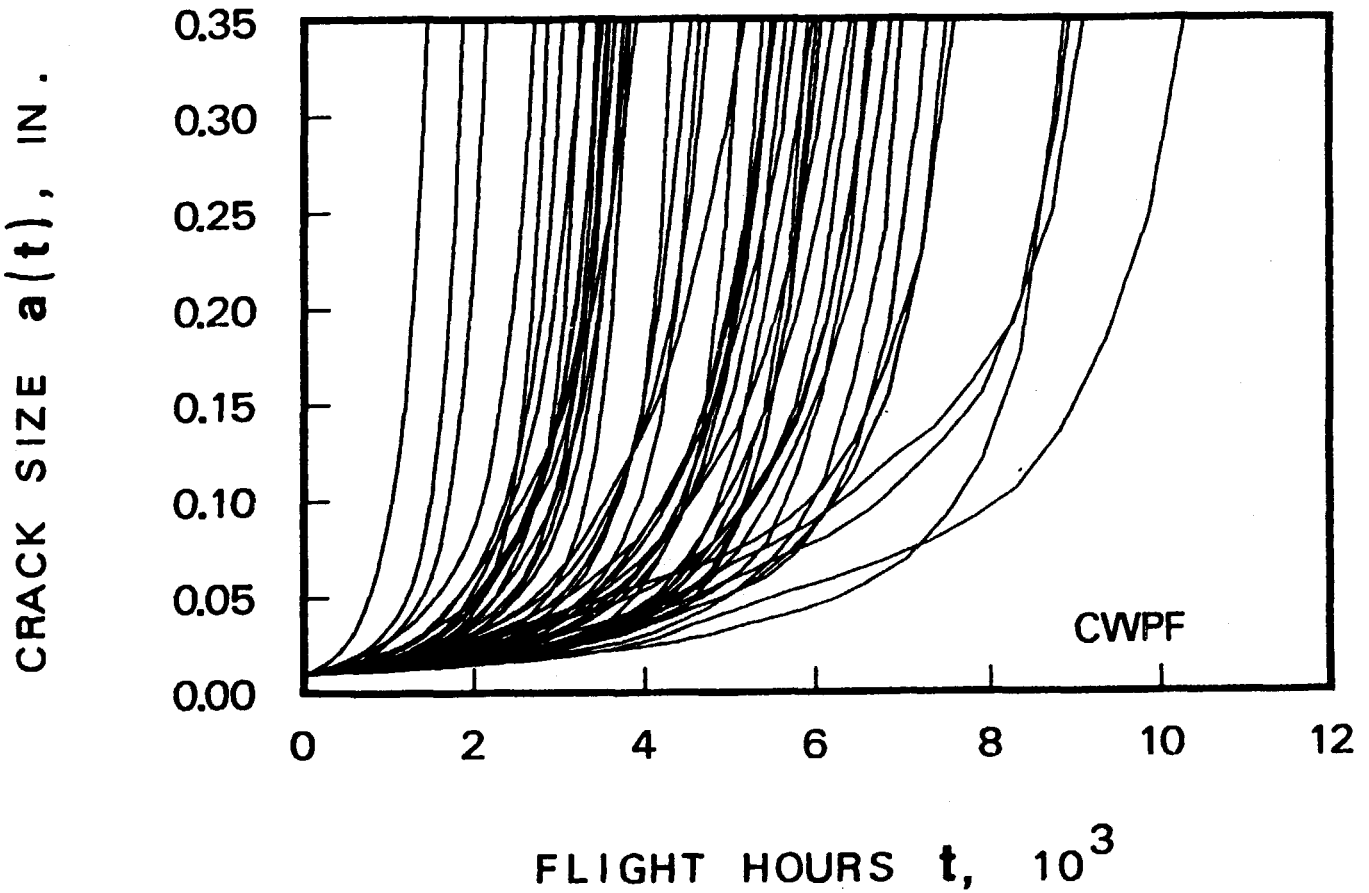

Figure 38: Simulated Sample Functions of Crack Size Versus Service Time for CWPF Fastener Holes; ξ^{-1} = 2,860 Flight Hours.

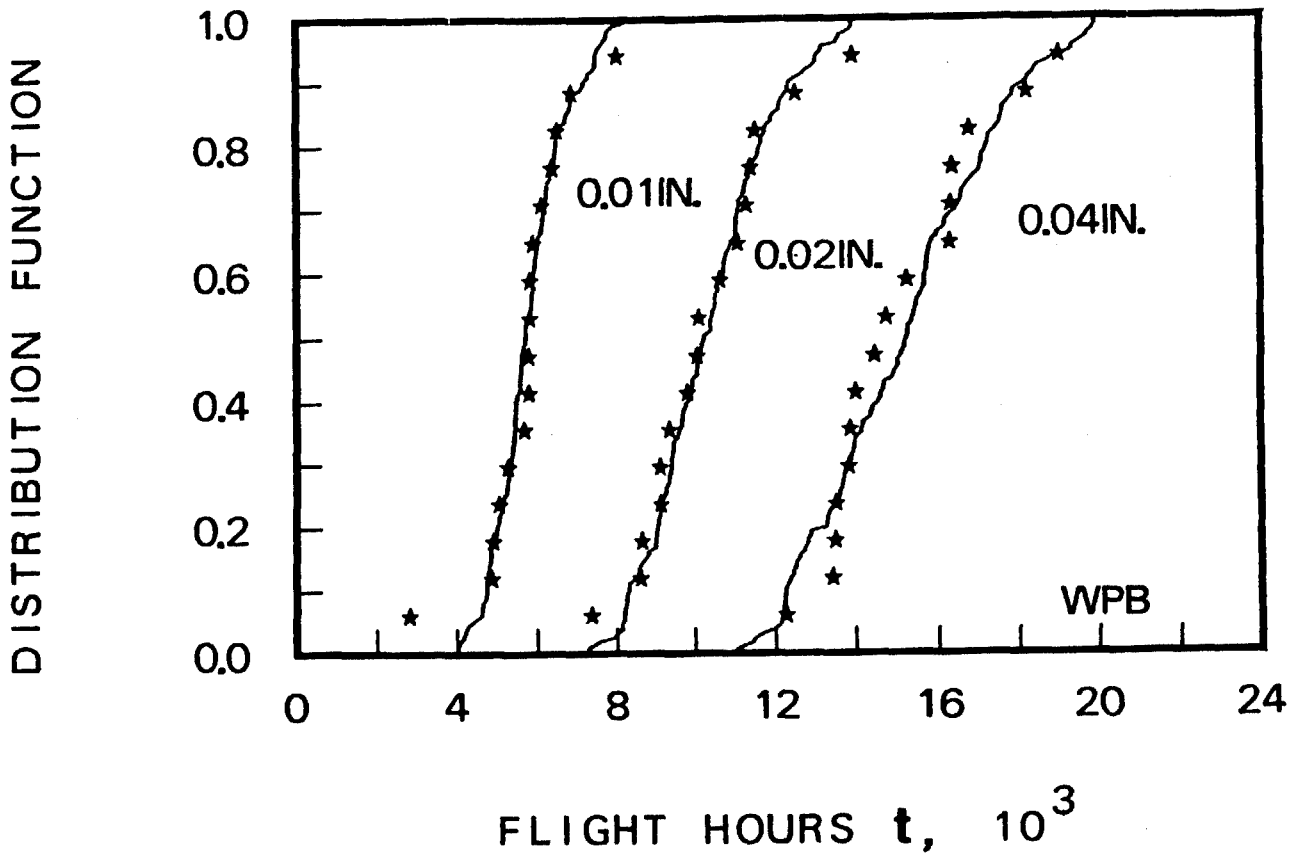

Figure 39: Correlation Between Lognormal Random Process Mode and Test Results for the Distribution of Time to Reach Crack Sizes 0.01, 0.02 and 0.04 Inch for WPB Fastener Holes.

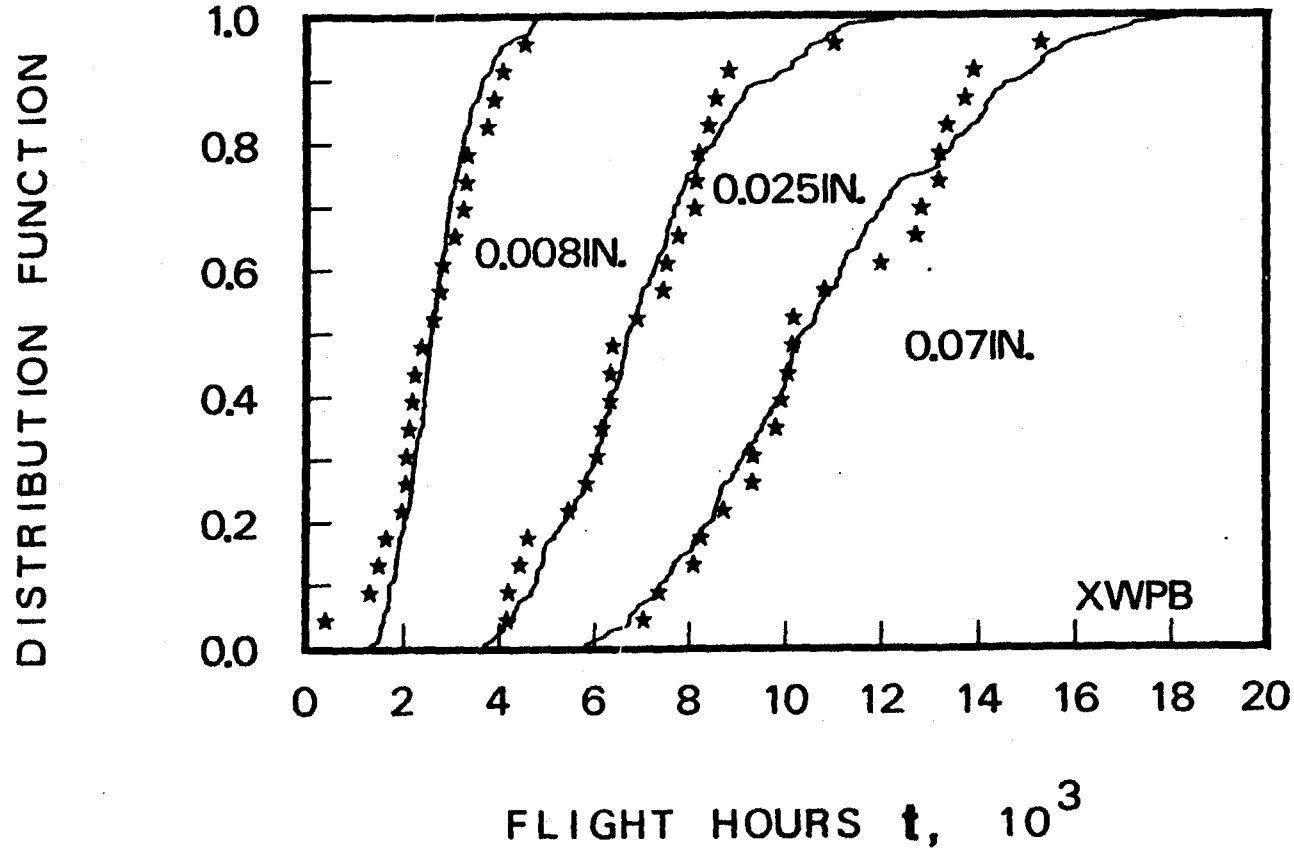

Figure 40: Correlation Between Lognormal Random Process Model and Test Results for the Distribution of Time to Reach Crack Sizes 0.008, 0.025 and 0.07 Inch for XWPB Fastener Holes.

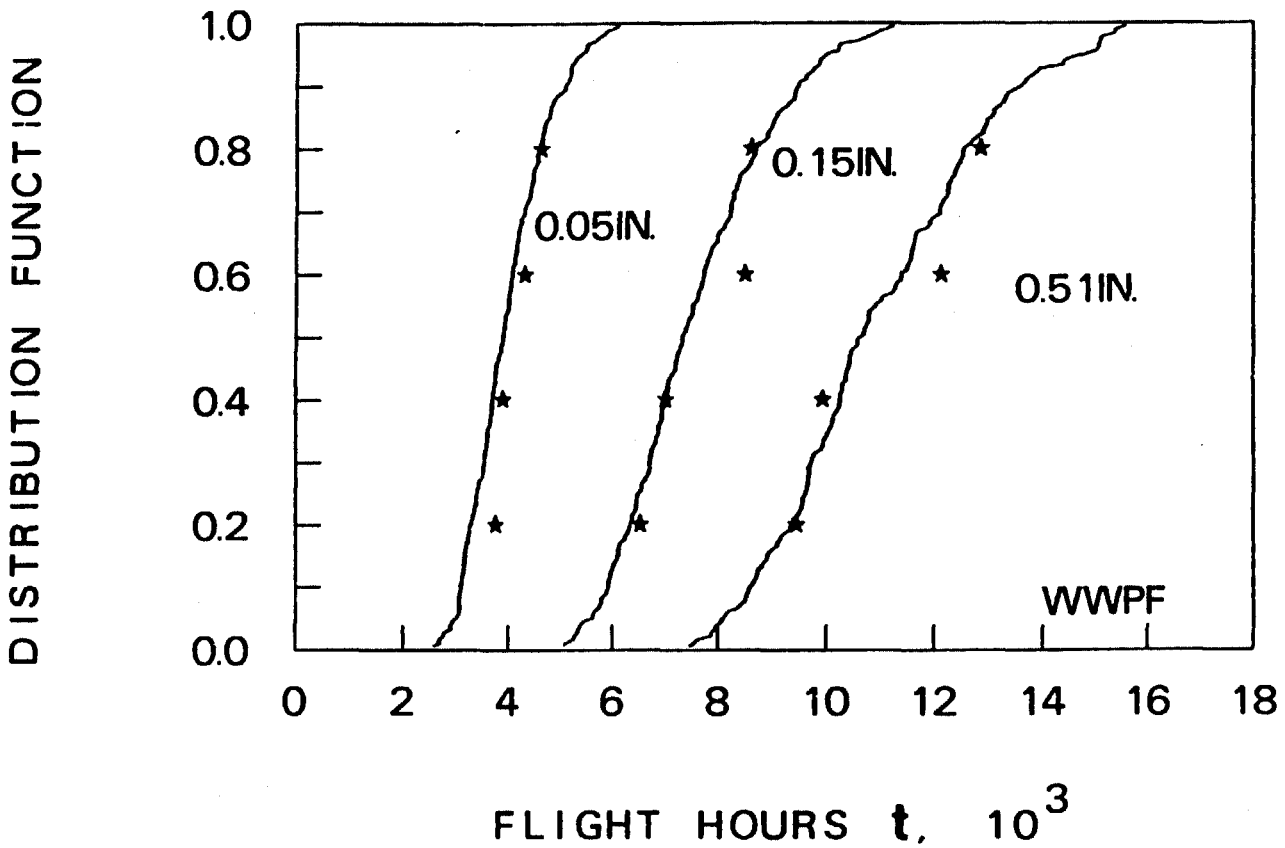

Fig. 41: Correlation Between Lognormal Random Process Model and Test Results for the Distribution of Time to Reach Crack Sizes 0.05, 0.15 and 0.51 Inch for WWPF Fastener Holes.

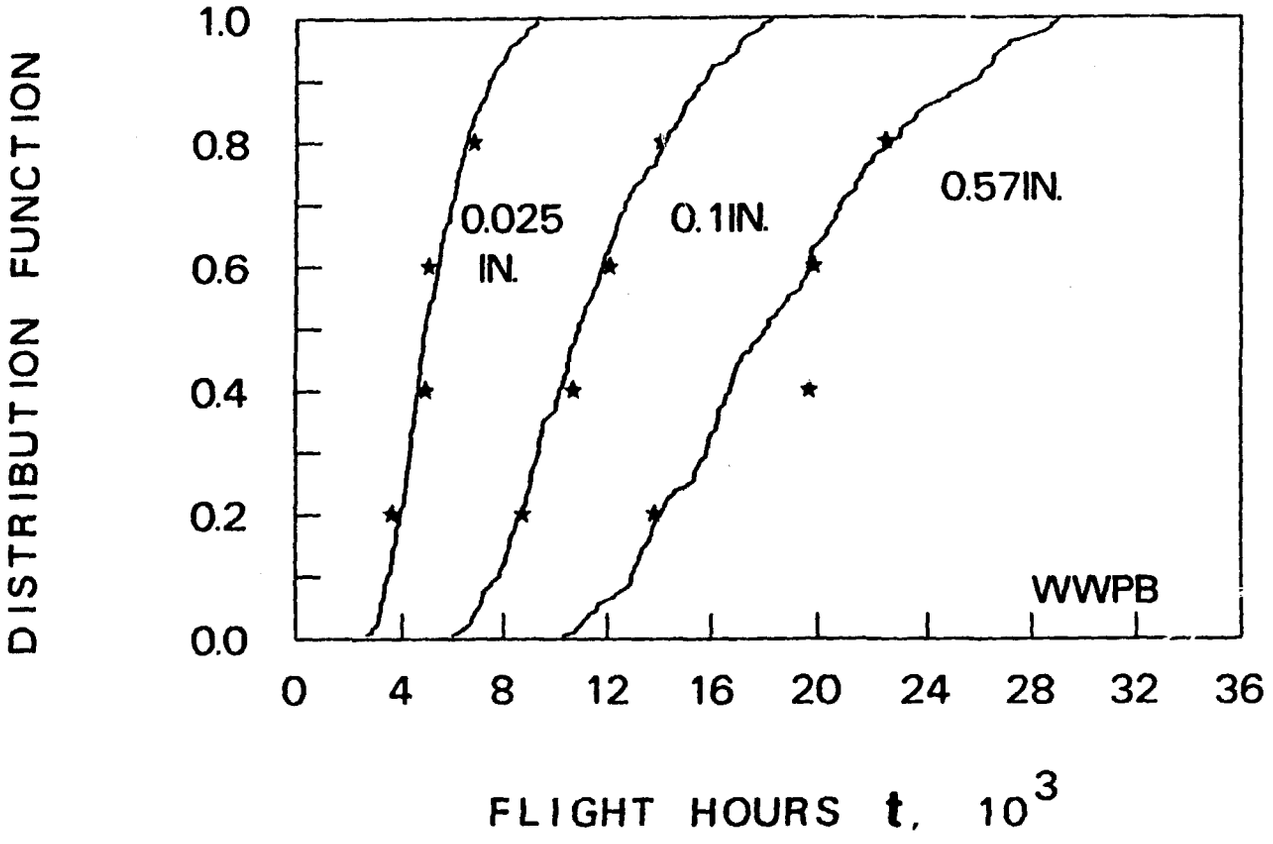

Fig. 42: Correlation Between Lognormal Random Process Model and Test Results for the Distribution of Time to Reach Crack Sizes 0.025, 0.1 and 0.57 Inch for WWPB Fastener Holes.

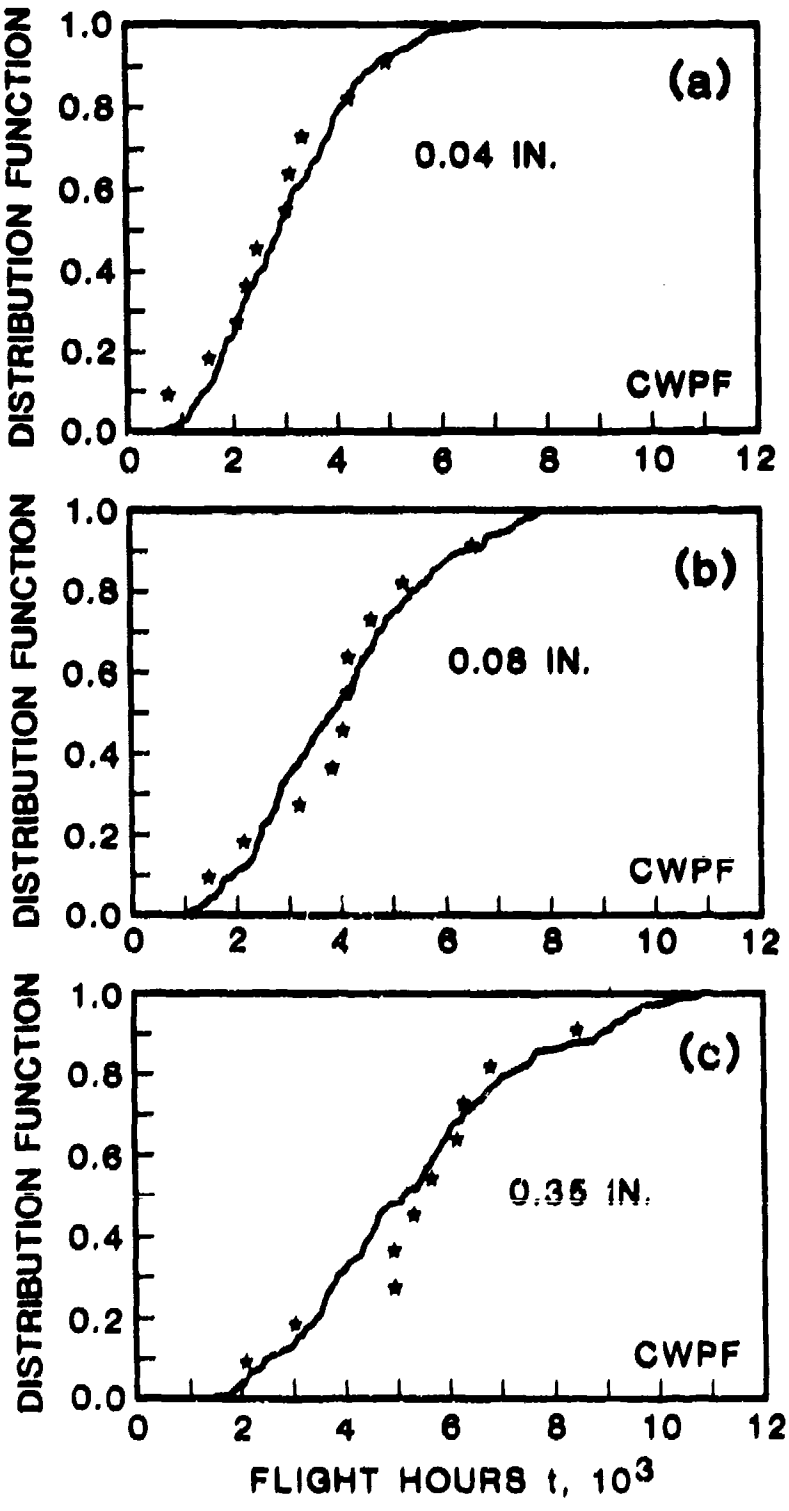

Figure 43: Correlation Between Lognormal Random Process Model and Test Results for the Distribution of Time to Reach crack size a_1 for CWPF Fastener Holes: (a) a_1 = 0.04 Inch, (b) a_1 = 0.08 Inch, and (c) a_1 = 0.35 Inch.

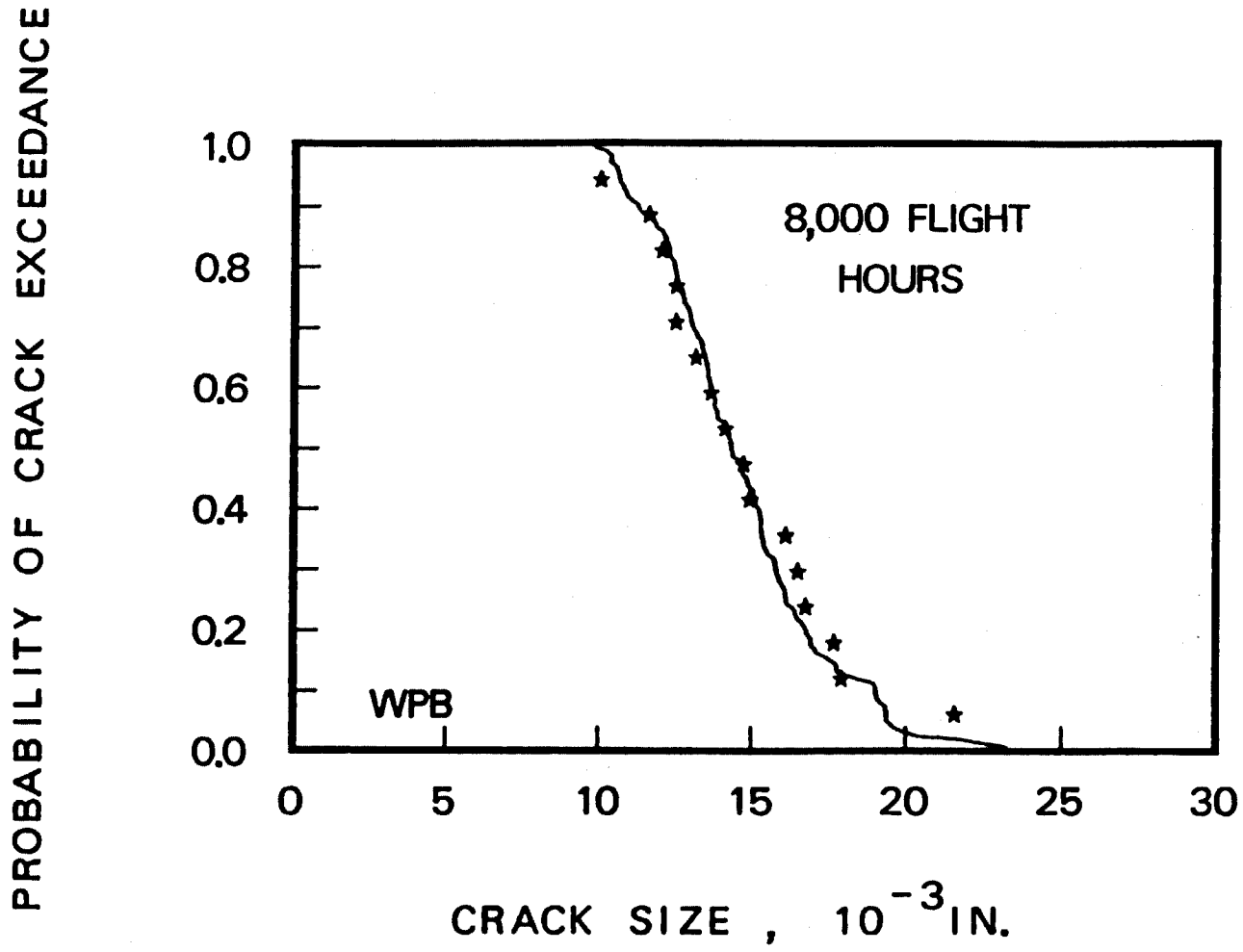

Figure 44: Correlation Between Lognormal Random Process Model and Test Results for the Probability of Crack Exceedance at 8,000 Flight Hours for WPB Fastener Holes.

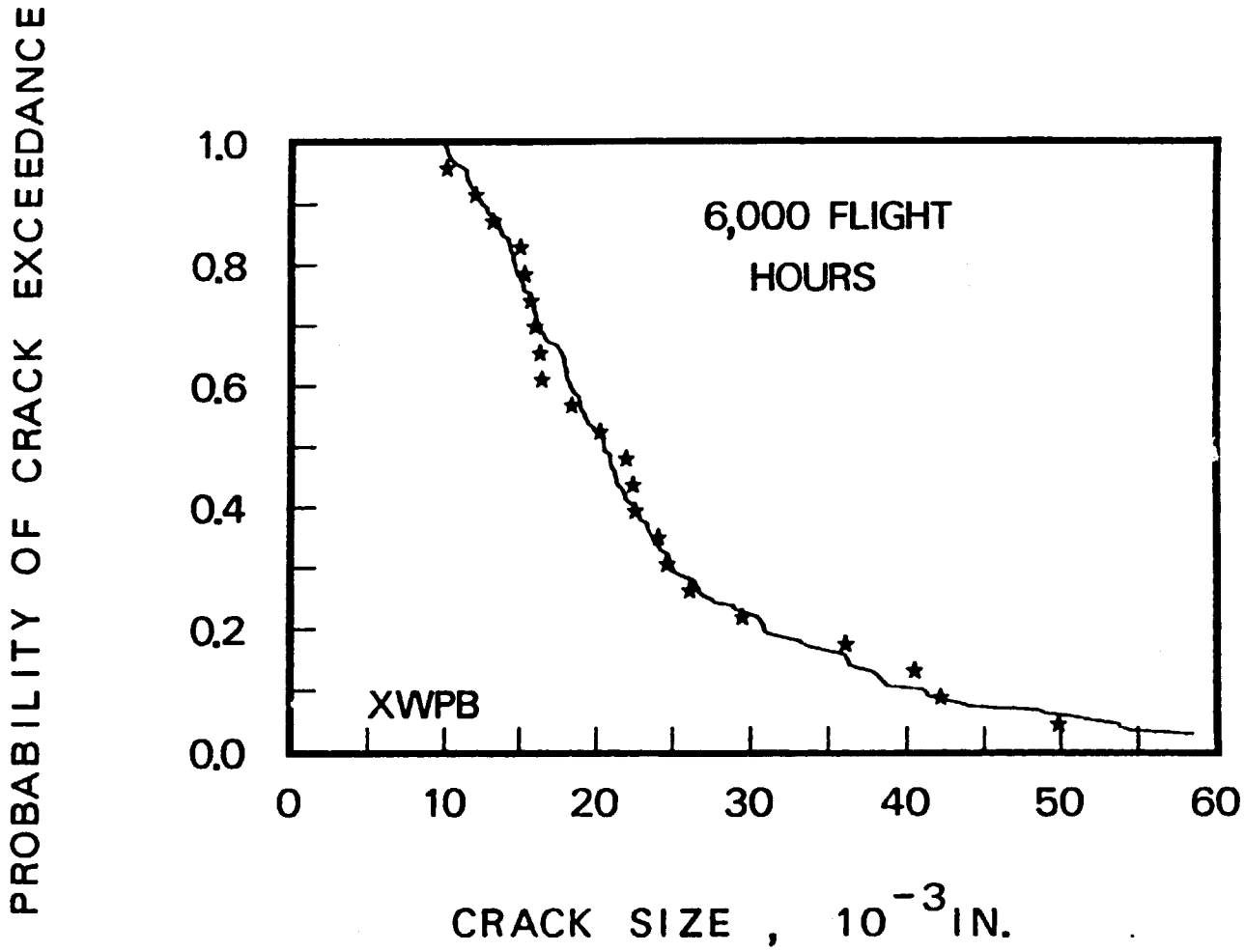

Figure 45: Correlation Between Lognormal Random Process Model and Test Results for the Probability of Crack Exceedance at 6,000 Flight Hours for XWPB Fastener Holes.

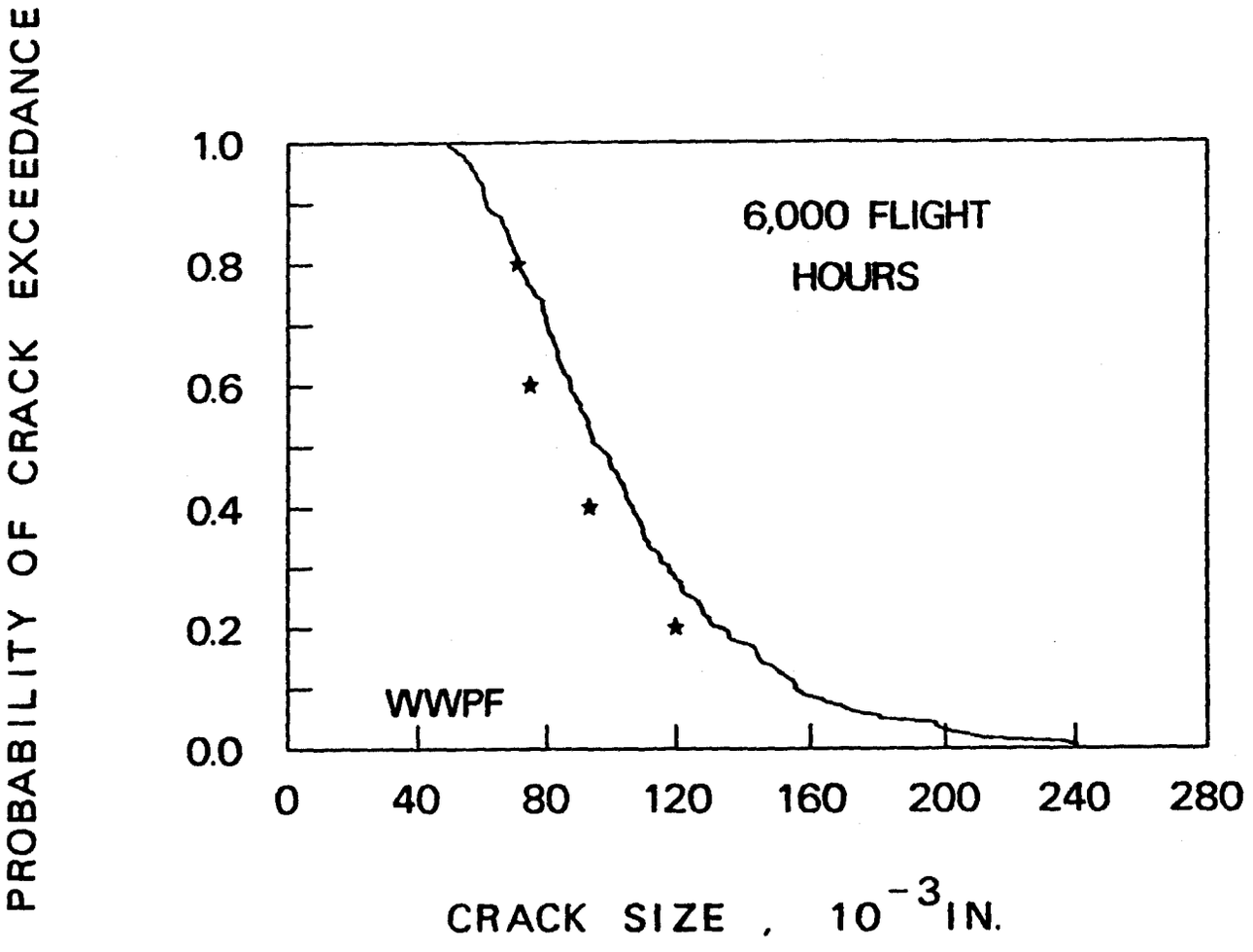

Fig. 46: Correlation Between Lognormal Random Process Model and Test Results for the Probability of Crack Exceedance at 6,000 Flight Hours for WWPF Fastener Holes

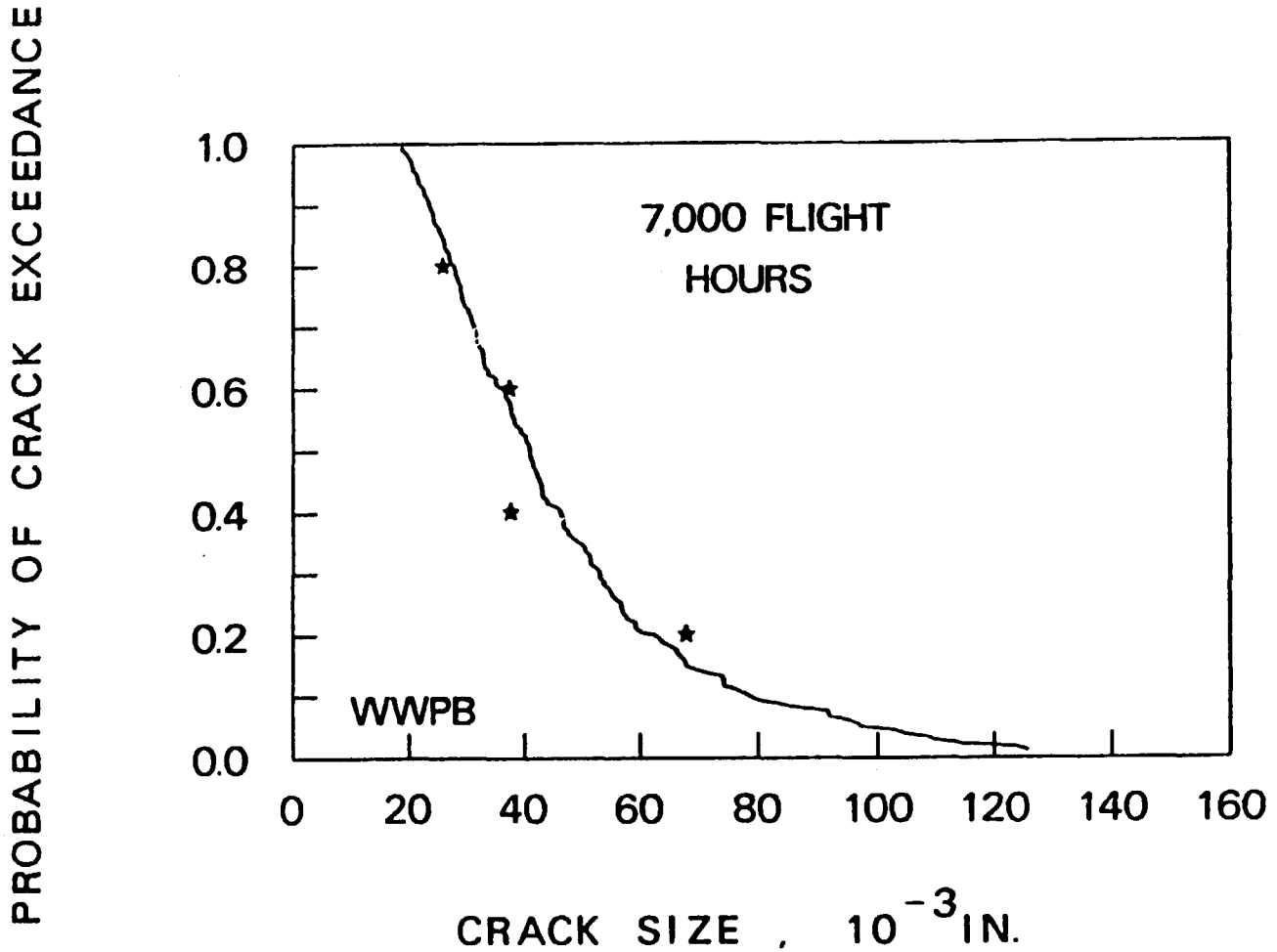

Fig. 47: Correlation Between Lognormal Random Process Model and Test Results for the Probability of Crack Exceedance at 7,000 Flight Hours for WWPB Fastener Holes

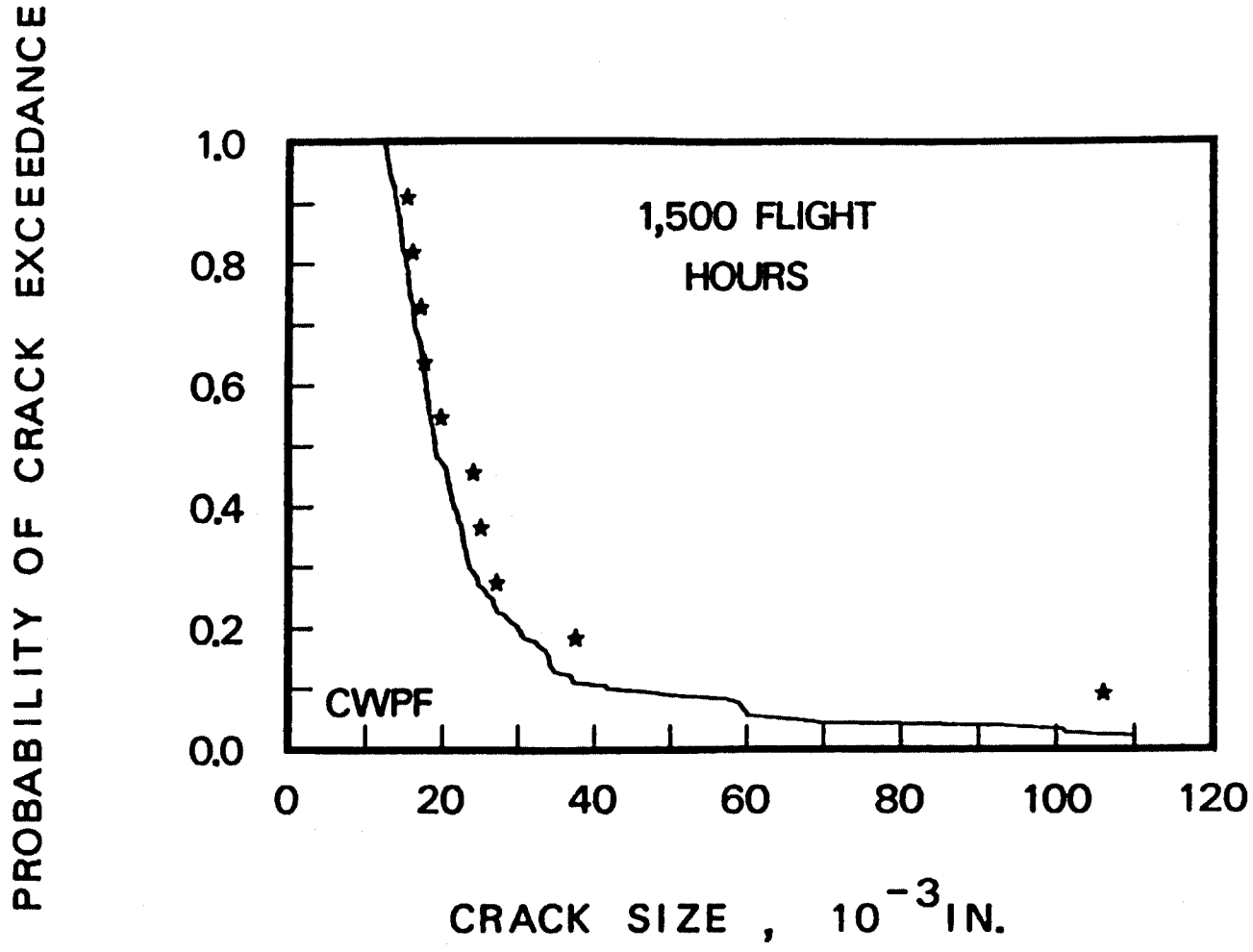

Figure 48: Correlation Between Lognormal Random Process Model and Test Results for the Probability of Crack Exceedance at 1,500 Flight Hours for CWPF Fastener Holes.

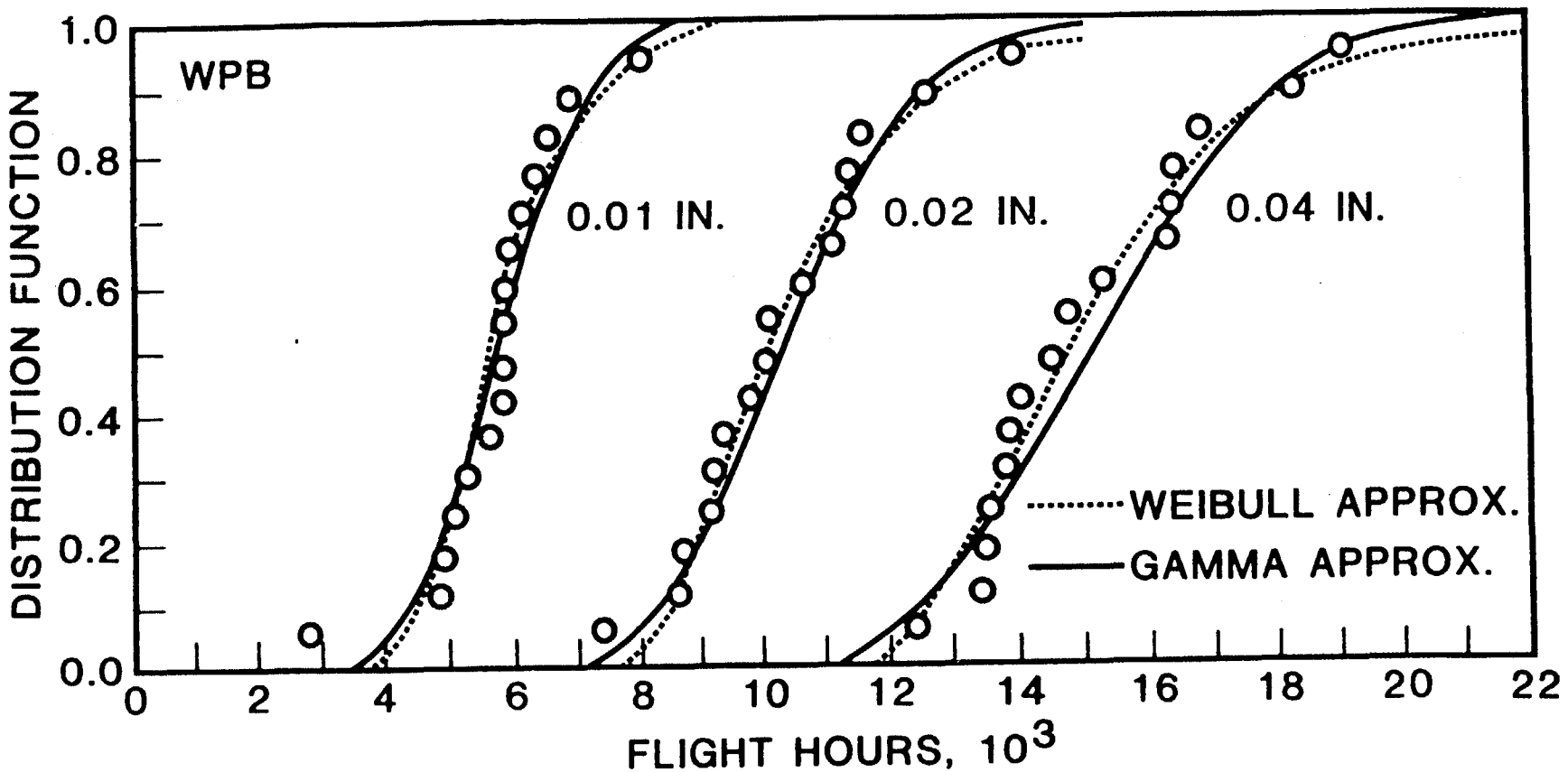

Figure 49(a): Correlation Between Second Moment Approximations and Experimental Results for the Distribution of Time to Reach Crack Sizes of 0.01, 0.02 and 0.04 Inch for the WPB Fastener Holes; Weibull and Gamma Approximation.

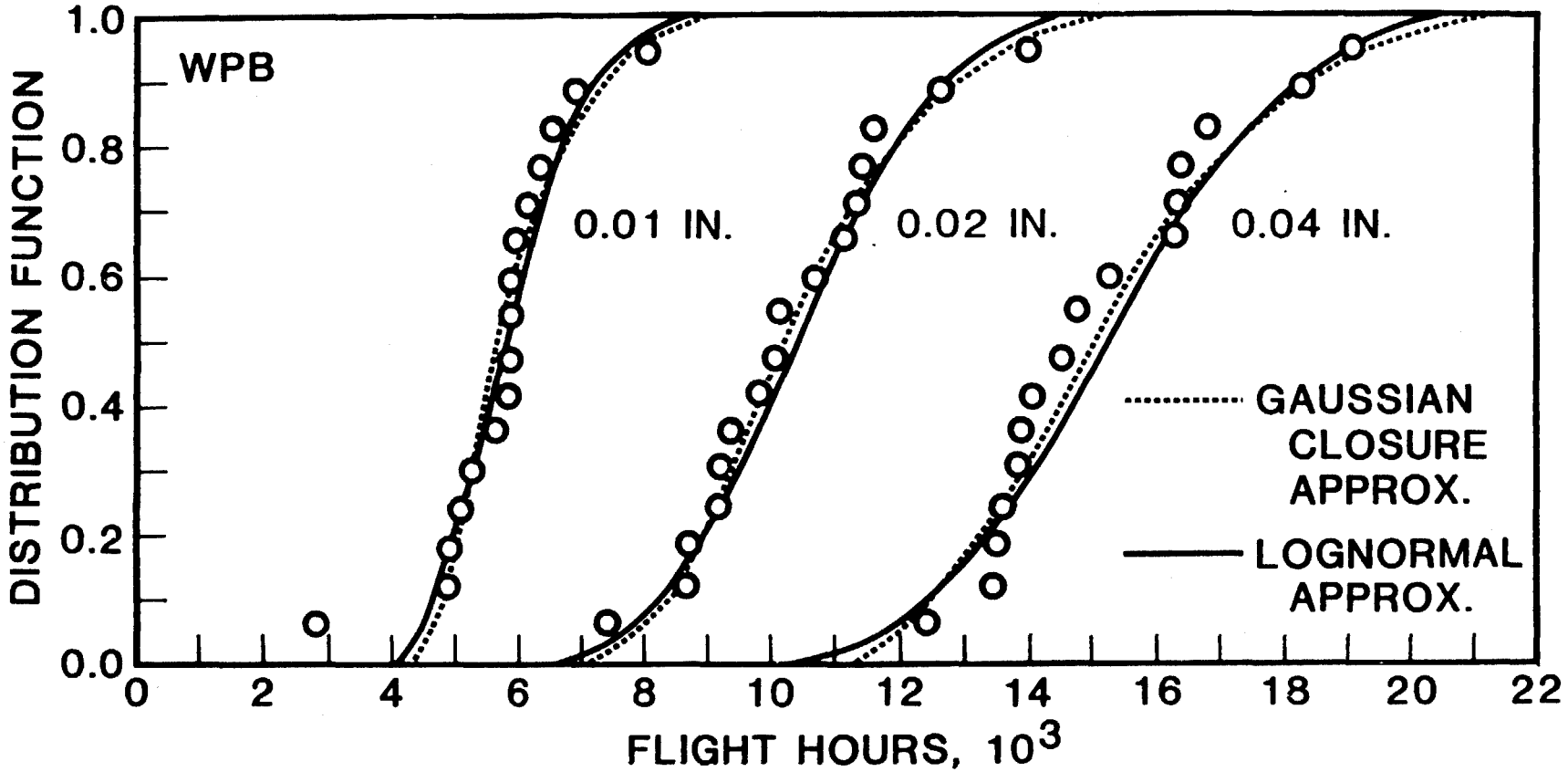

Figure 49(b): Correlation Between Second Moment Approximations and Experimental Results for the Distribution of Time to Reach Crack Sizes of 0.01, 0.02 and 0.04 Inch for WPB Fastener Holes; Gaussian Closure and Lognormal Approximations.

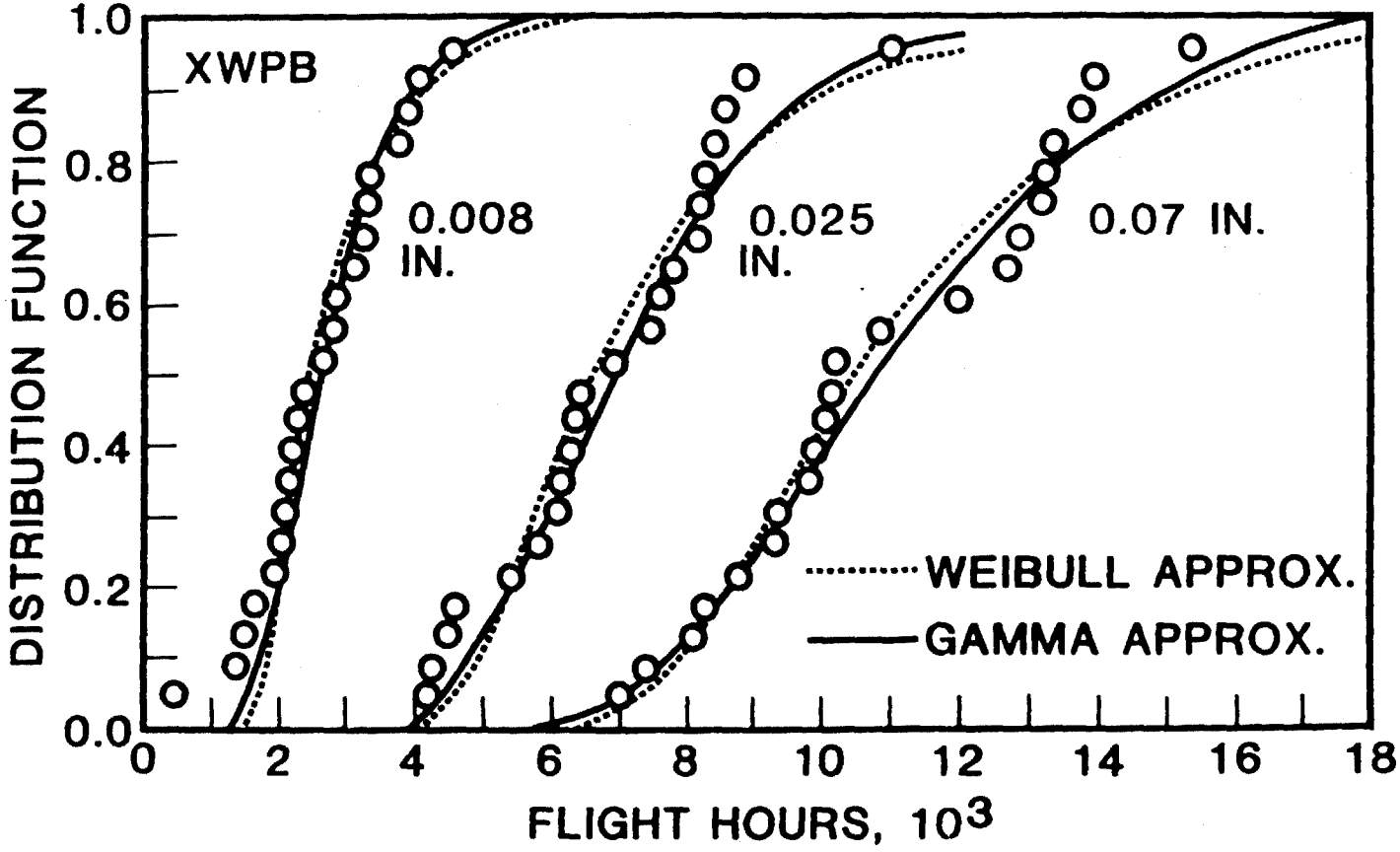

Figure 50(a): Correlation Between Second Moment Approximations and Experimental Results for the Distribution of Time to Reach Crack Sizes of 0.008, 0.025 and 0.07 Inch for XWPB Fastener Holes; Weibull and Gamma Approximations.

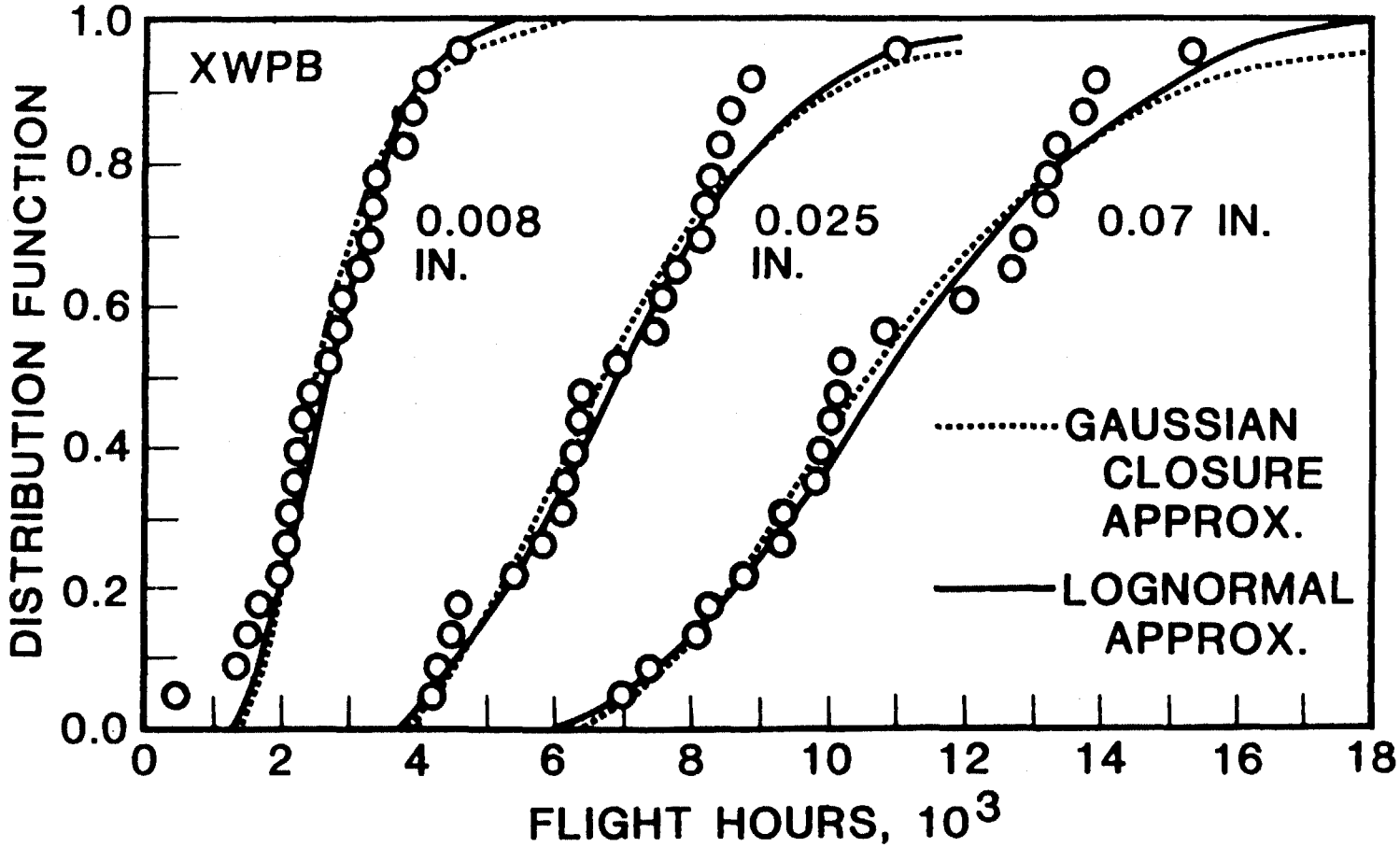

Figure 50(b): Correlation Between Second Moment Approximations and Experimental Results for the Distribution of Time to Reach Crack Sizes of 0.008, 0.025 and 0.07 Inch for XWPB Fastener Holes; Gaussian Closure and Lognormal Approximations.

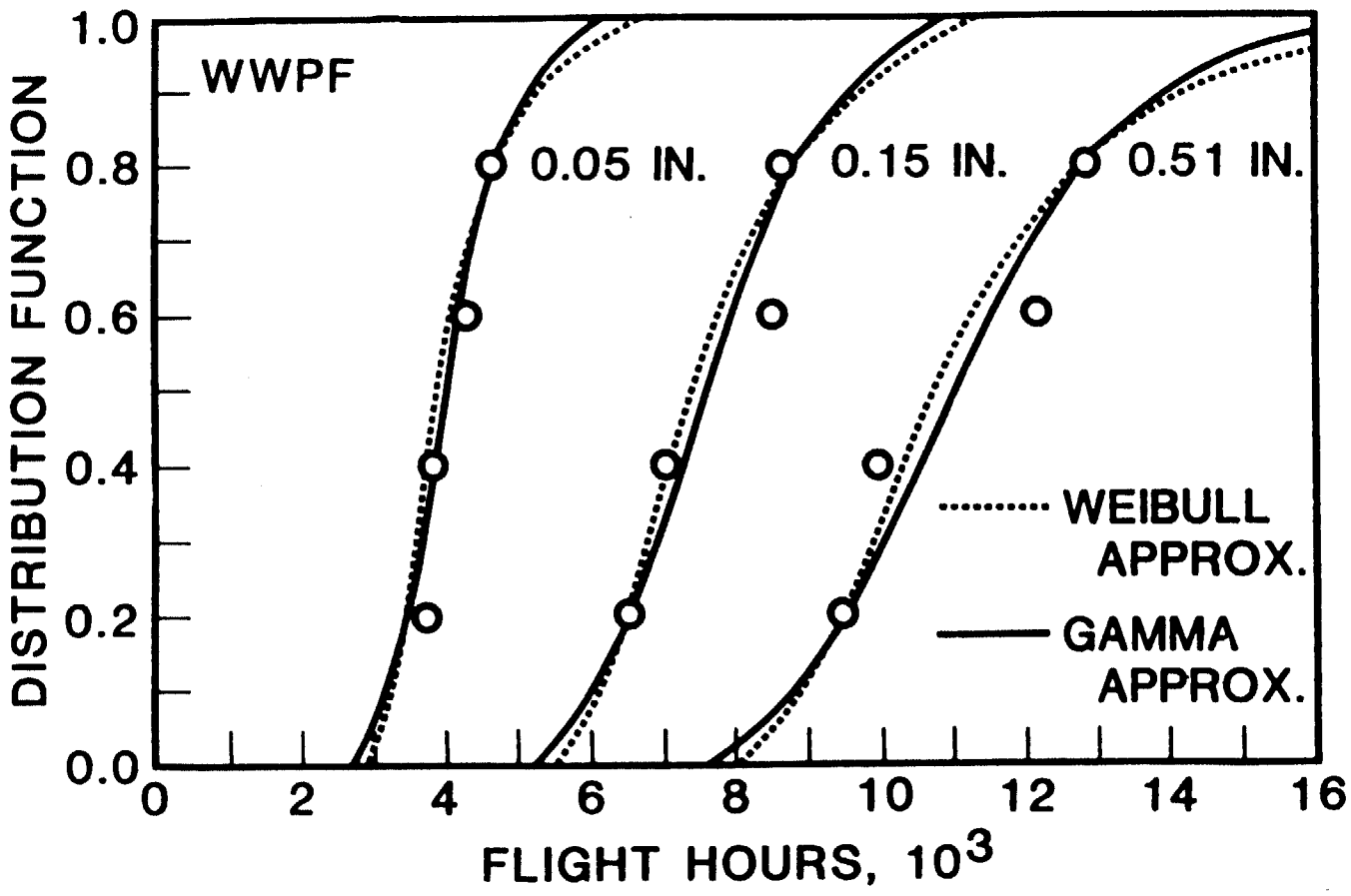

Figure 51(a): Correlation Between Second Moment Approximations and Experimental Results for the Distribution of Time to Reach Crack Sizes of 0.05, 0.15 and 0.51 Inch for WWPF Fastener Holes; Weibull and Gamma Approximations.

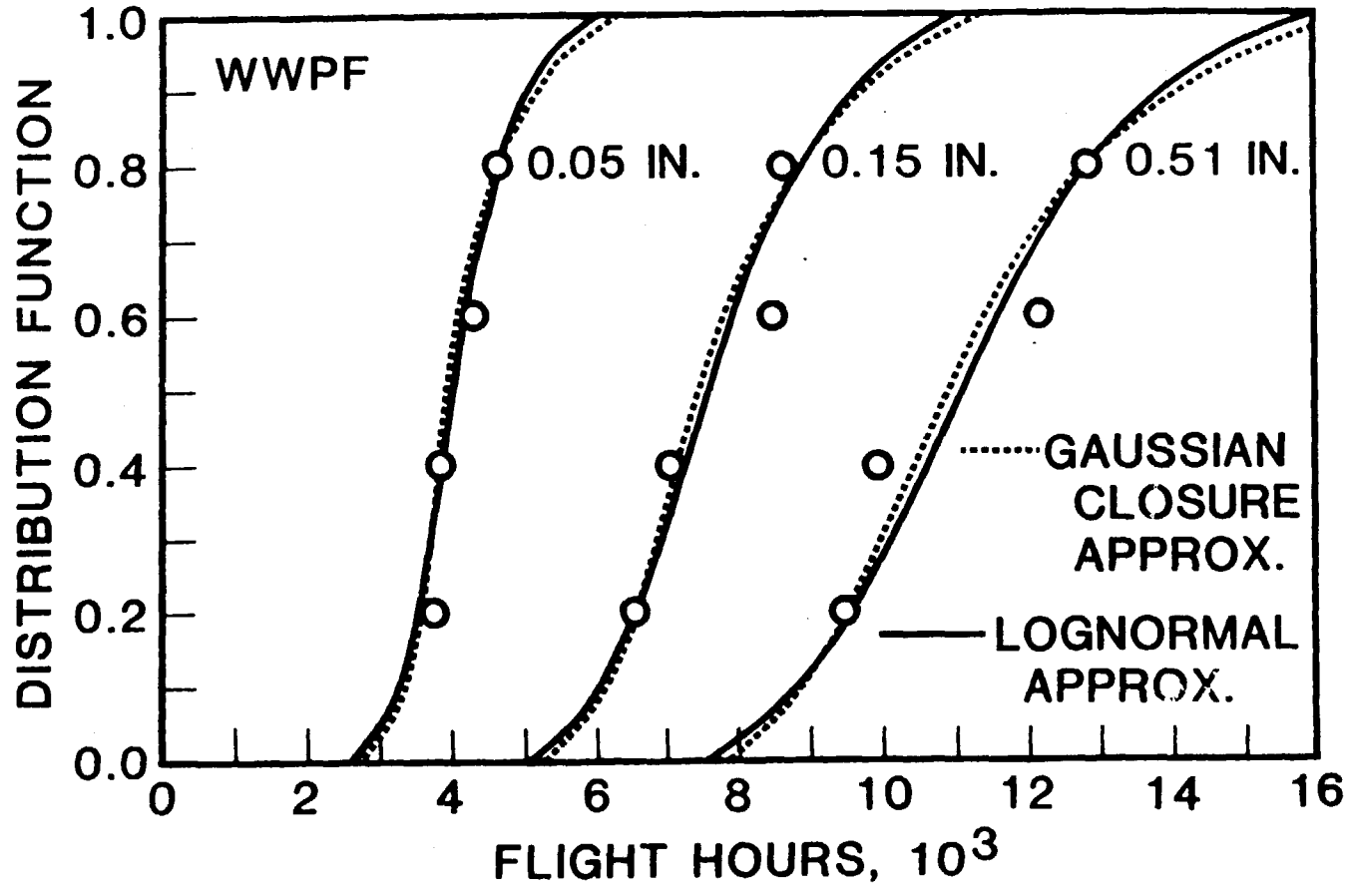

Figure 51(b): Correlations Between Second Moment Approximations and Experimental Results for the Distribution of Time to Reach Crack Sizes of 0.05, 0.15 and 0.51 Inch for WWPF Fastener Holes; Gaussian Closure and Lognormal Approximations.

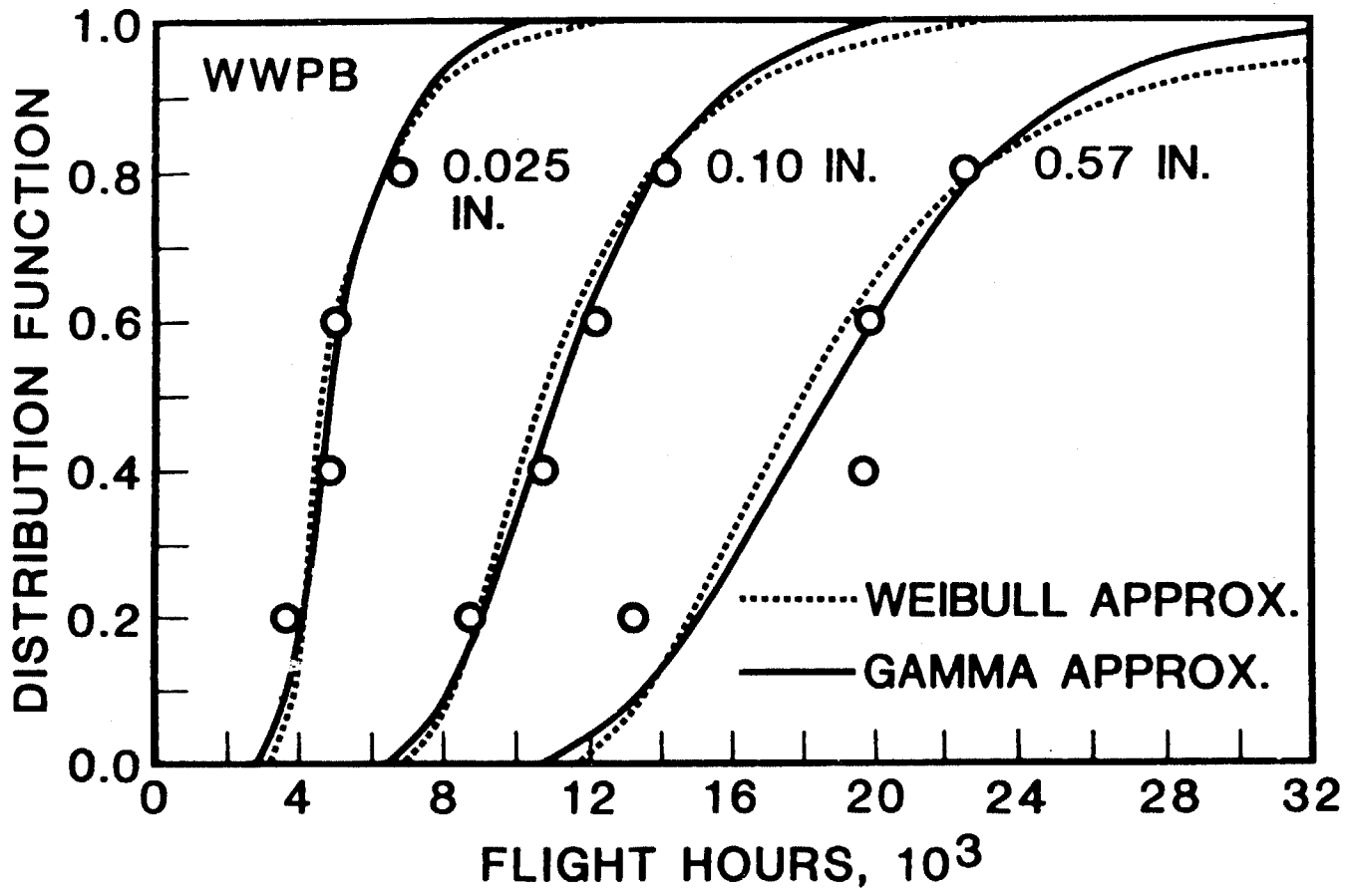

Figure 52(a): Correlation Between Second Moment Approximations and Experimental Results for the Distribution of Time to Reach Crack Sizes of 0.025, 0.01 and 0.57 Inch for WWPB Fastener Holes; Weibull and Gamma Approximations

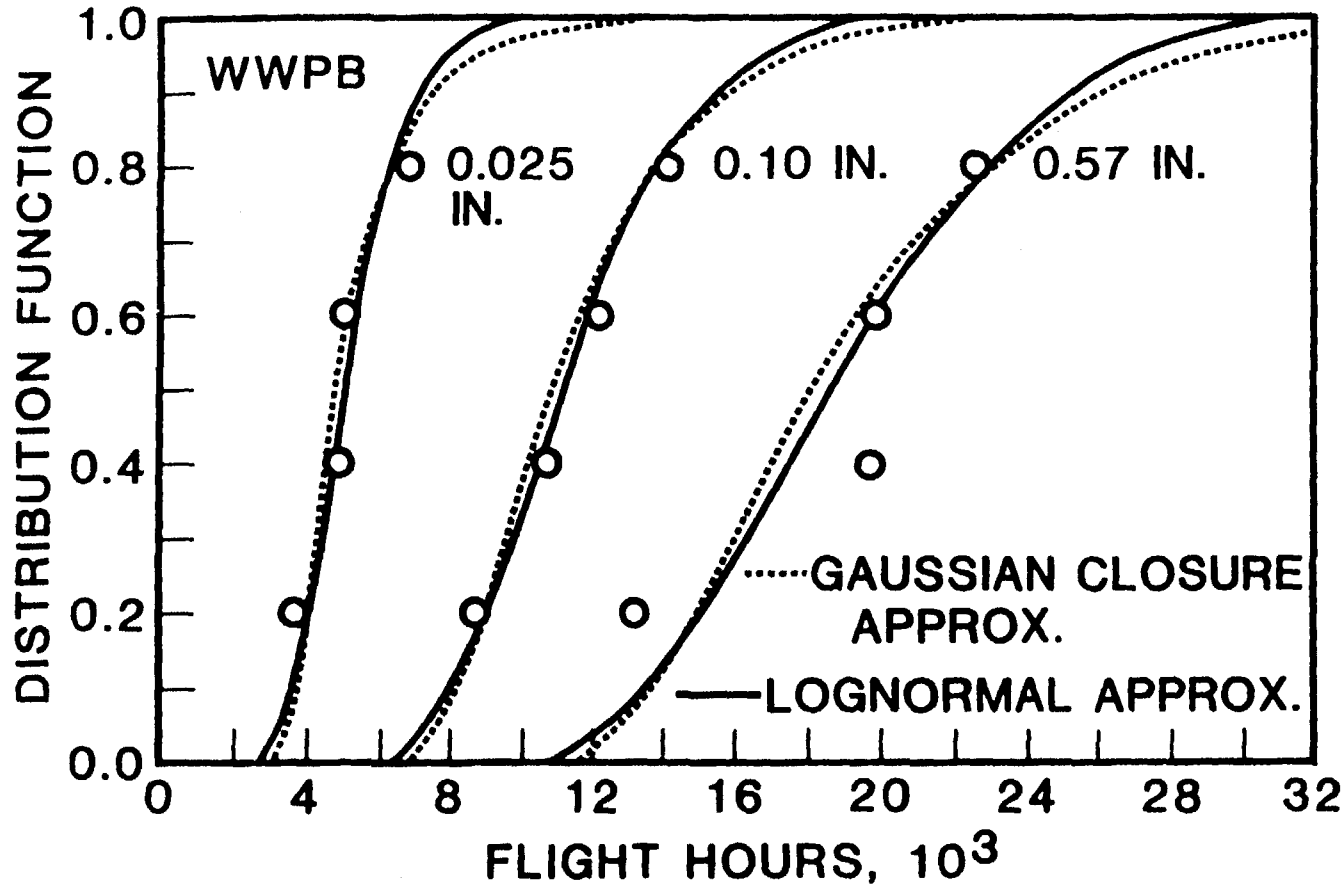

Figure 52(b): Correlation Between Second Moment Approximations and Experimental Results for the Distribution of Time to Reach Crack Sizes of 0.025, 0.01 and 0.57 Inch for WWPB Fastener Holes; Gaussian Closure and Lognormal Approximations.

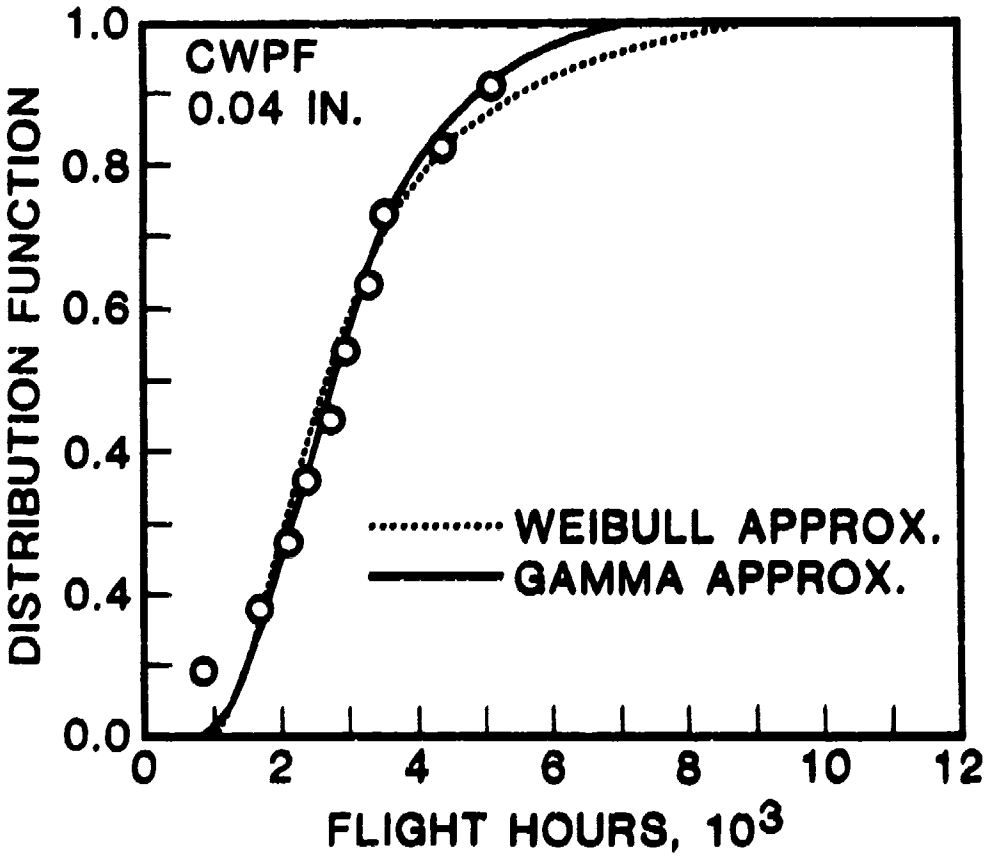

Figure 53(a-1): Correlation Between Second Moment Approximations and Experimental Results for the Distribution of Time to Reach Crack Size of 0.04 Inch for CWPF Fastener Holes; Weibull and Gamma Approximations.

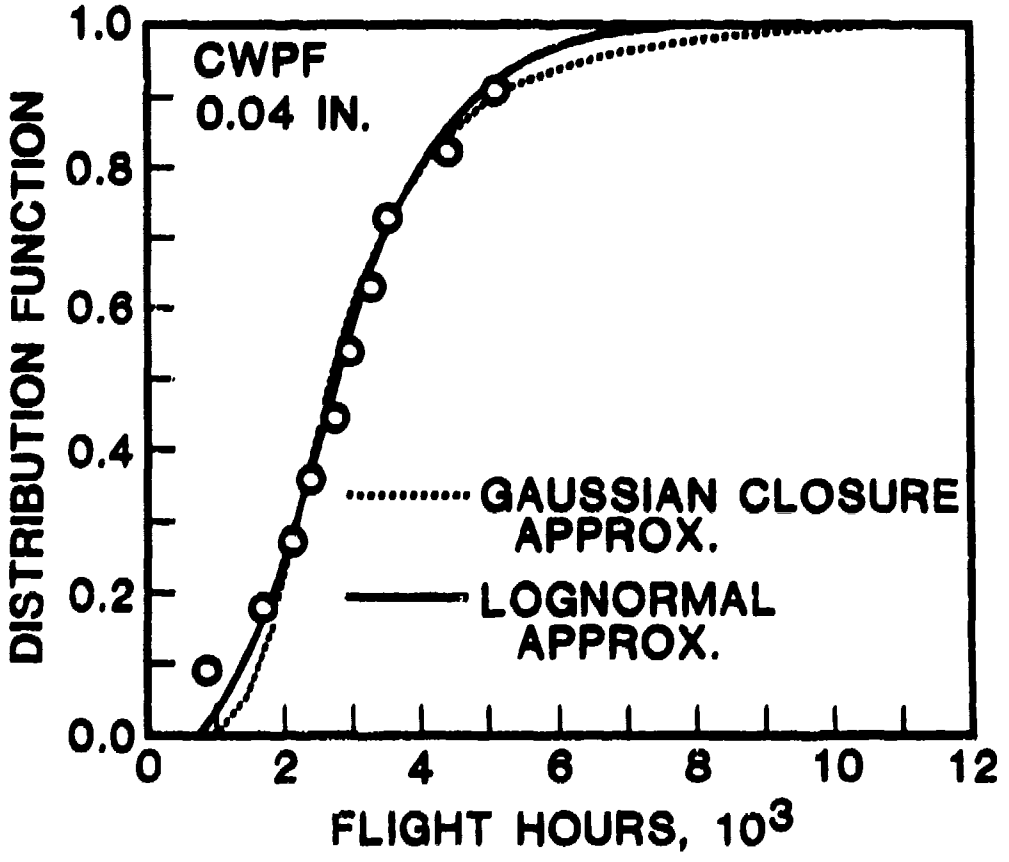

Figure 53(b-1): Correlation Between Second Moment Approximations and Experimental Results for the Distribution of Time to Reach Crack Size of 0.04 Inch for CWPF Fastener Holes; Gaussian Closure and Lognormal Approximations.

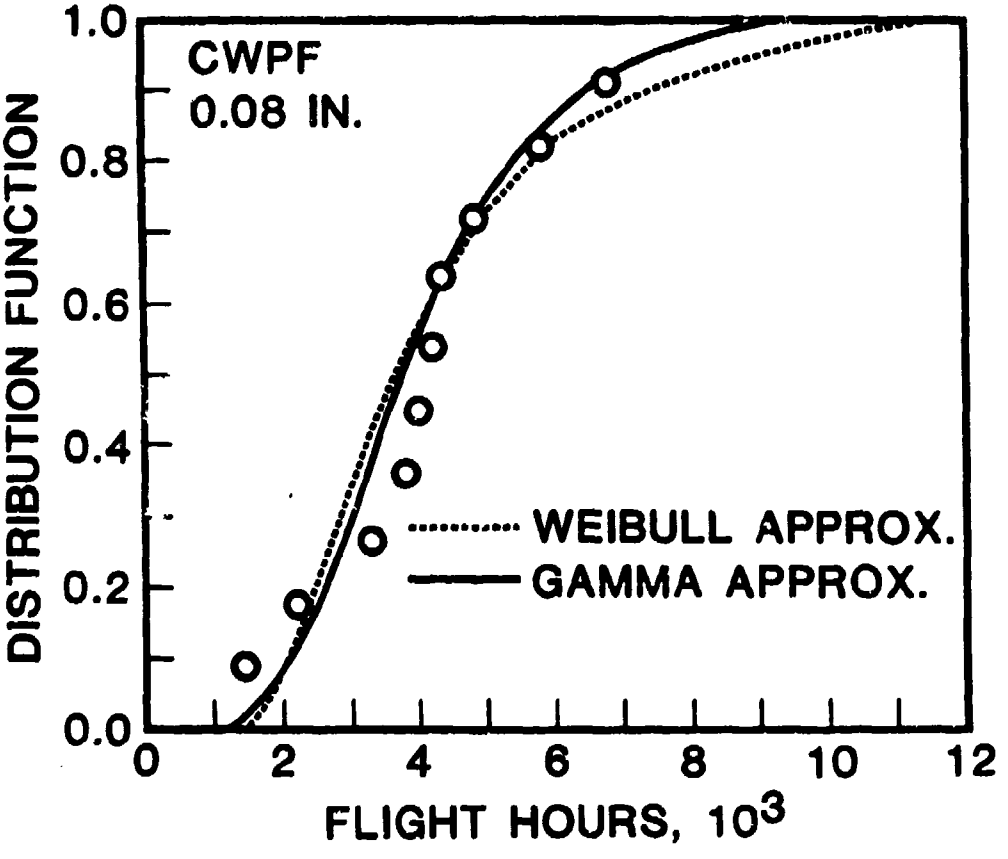

Figure 53(a-2): Correlation Between Second Moment Approximations and Experimental Results for the Distribution of Time to Reach Crack Size of 0.08 Inch for CWPF Fastener Holes: Weibull and Gamma Approximations.

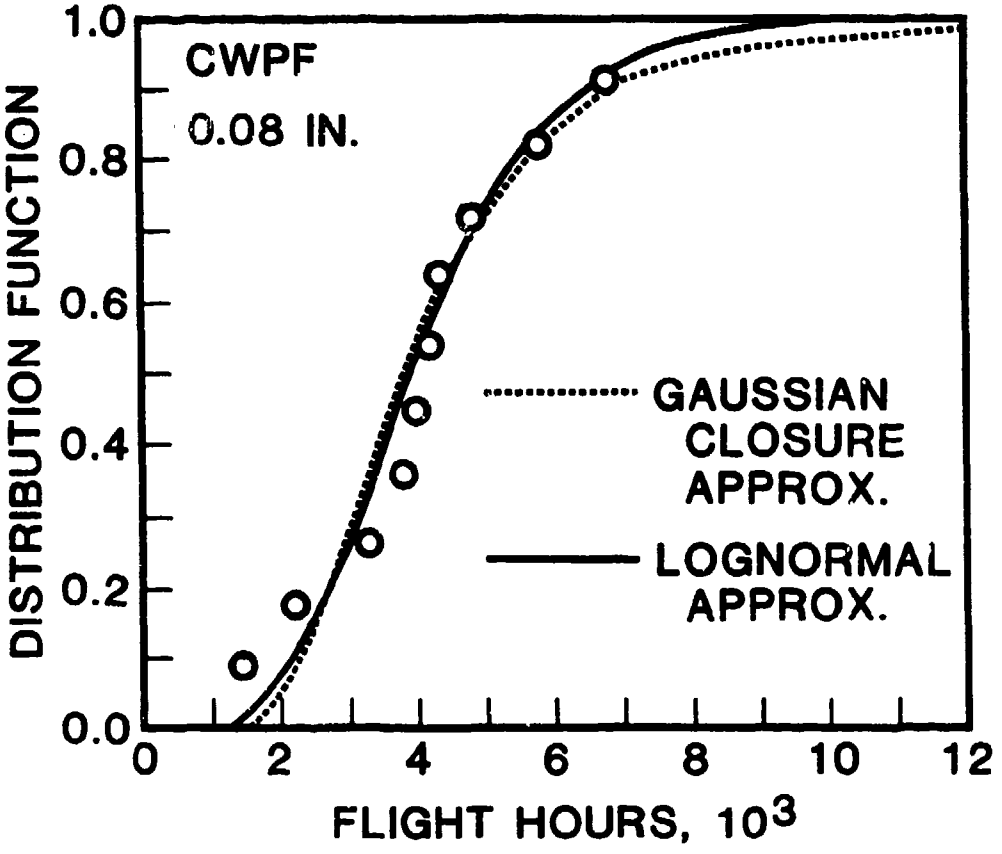

Figure 53(b-2): Correlation Between Second Moment Approximations and Experimental Results for the Distribution of Time to Reach Crack Size of 0.08 Inch for CWPF Fastener Holes; Gaussian Closure and Lognormal Approximations.

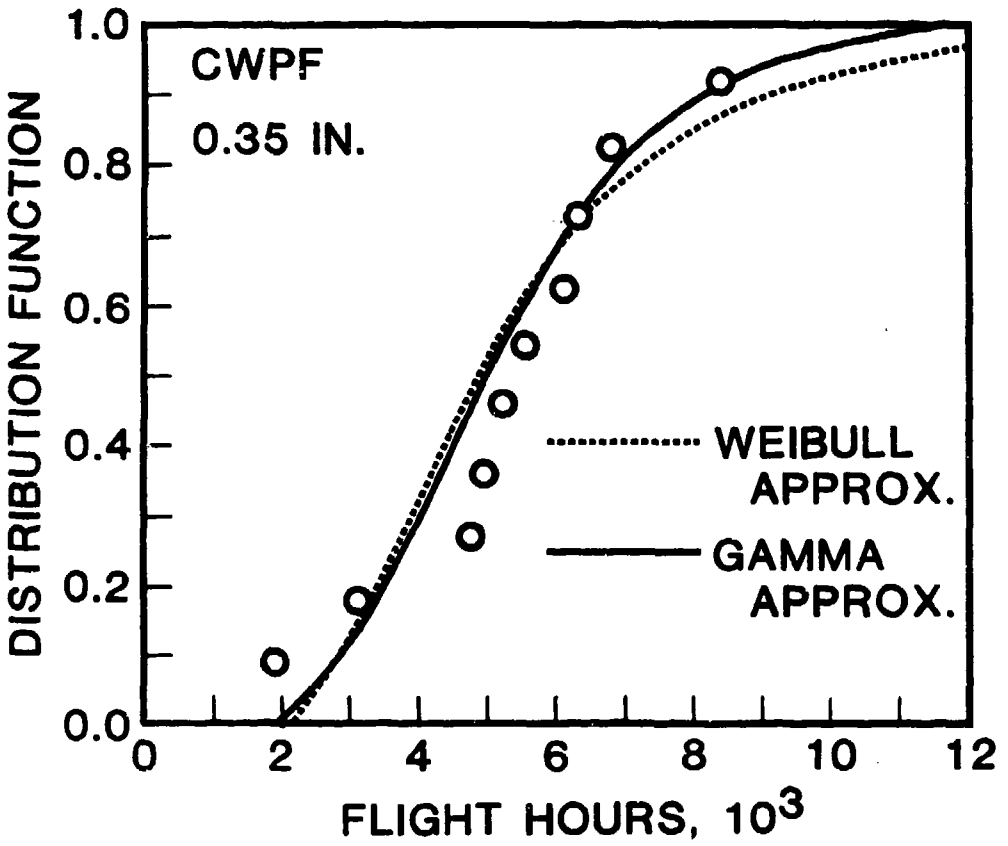

Figure 53(a-3): Correlation Between SEcond Moment Approximations and Experimental Results for the Distribution of Time to Reach Crack Size of 0.35 Inch for CWPF Fastener Holes; Weibull and Gamma Approximations.

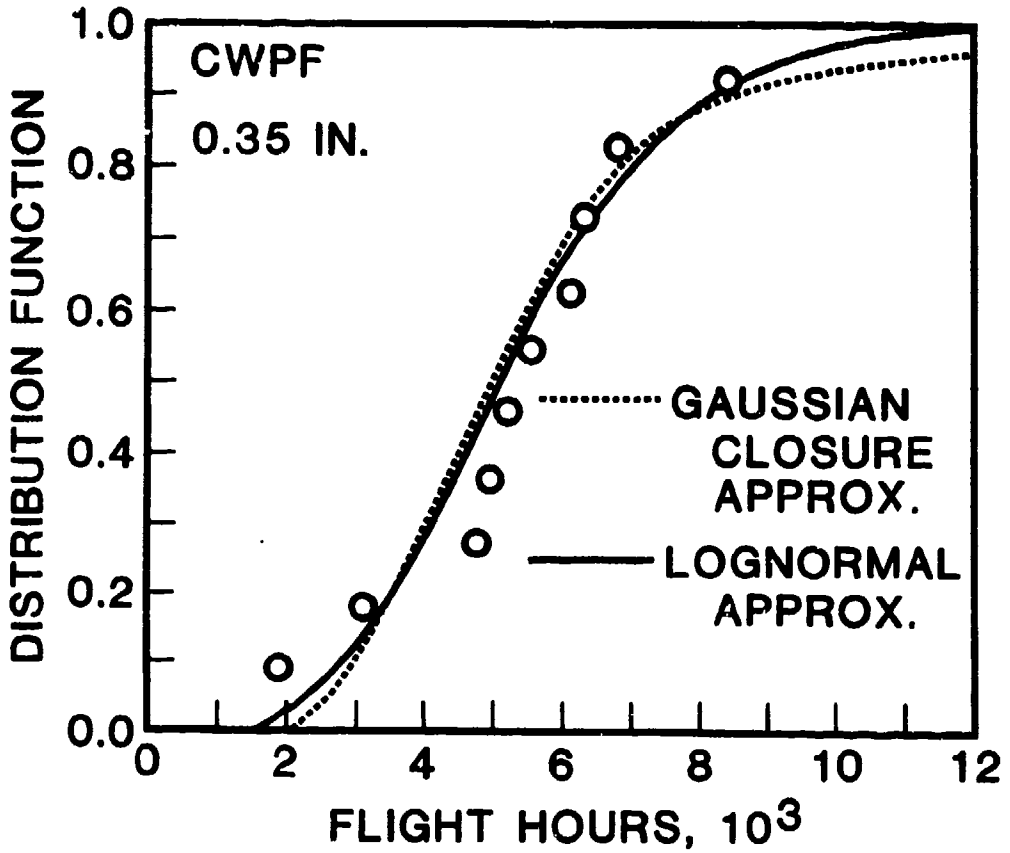

Figure 53(b-3): Correlation Between Second Moment Approximations and Experimental Results for the Distribution of Time to Reach Crack Size of 0.35 Inch for CWPF Fastener Holes; Gaussian Closure and Lognormal Approximations.

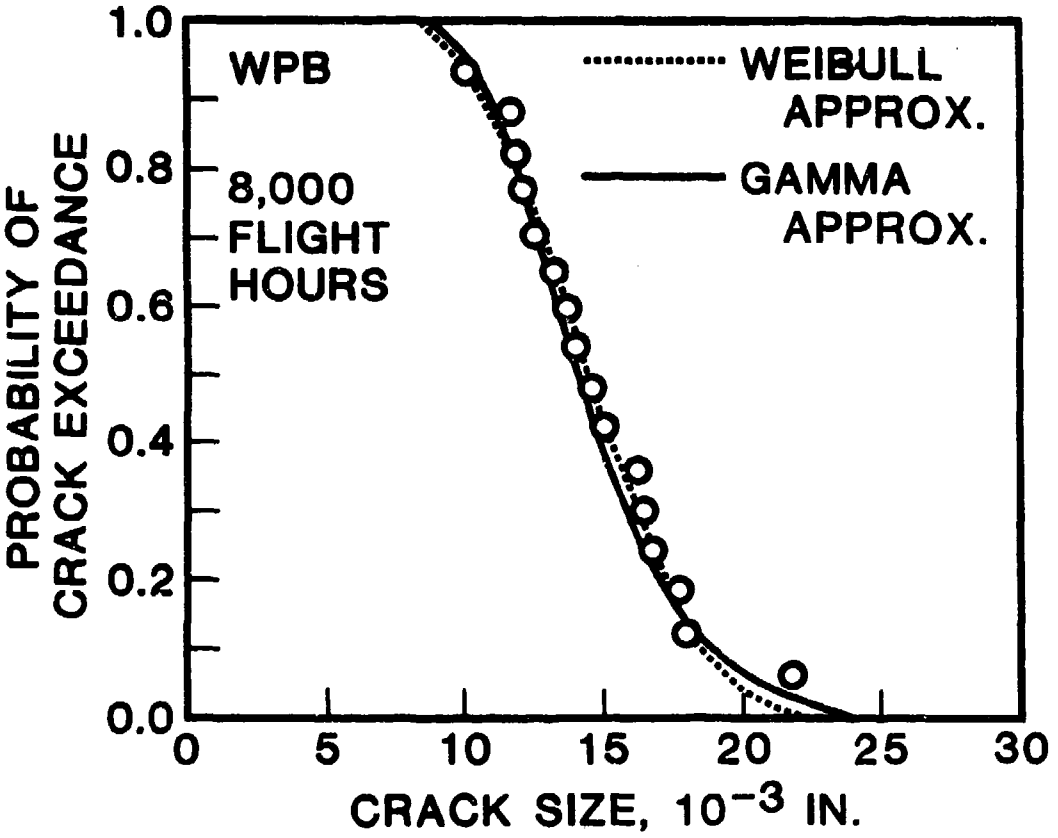

Figure 54(a): Correlation Between Second Moment Approximations and Experimental Results for the Probability of Crack Exceedance at 8,000 Flight Hours for WPB Fastener Holes; Weibull and Gamma Approximations.

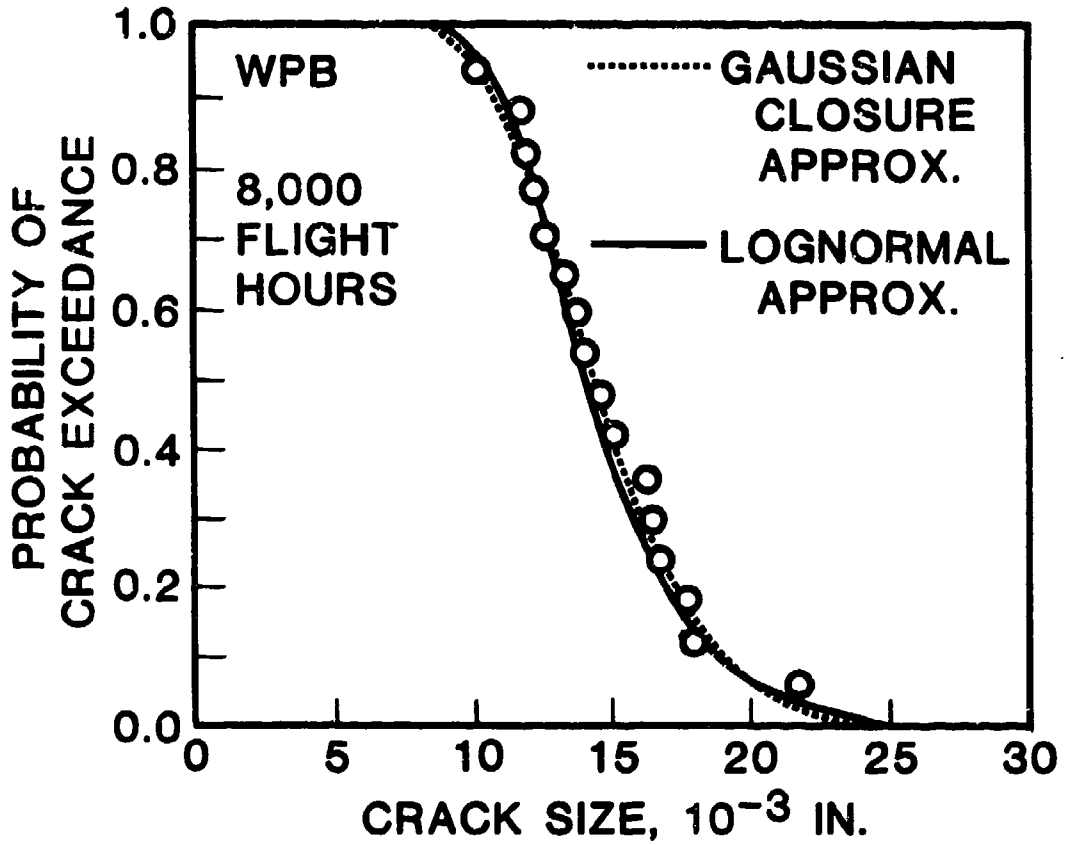

Figure 54(b): Correlation Between Second Moment Approximations and Experimental Results for the Probability of Crack Exceedance at 8,000 Flight Hours for WPB Fastener Holes; Gaussian Closure and Lognormal Approximations.

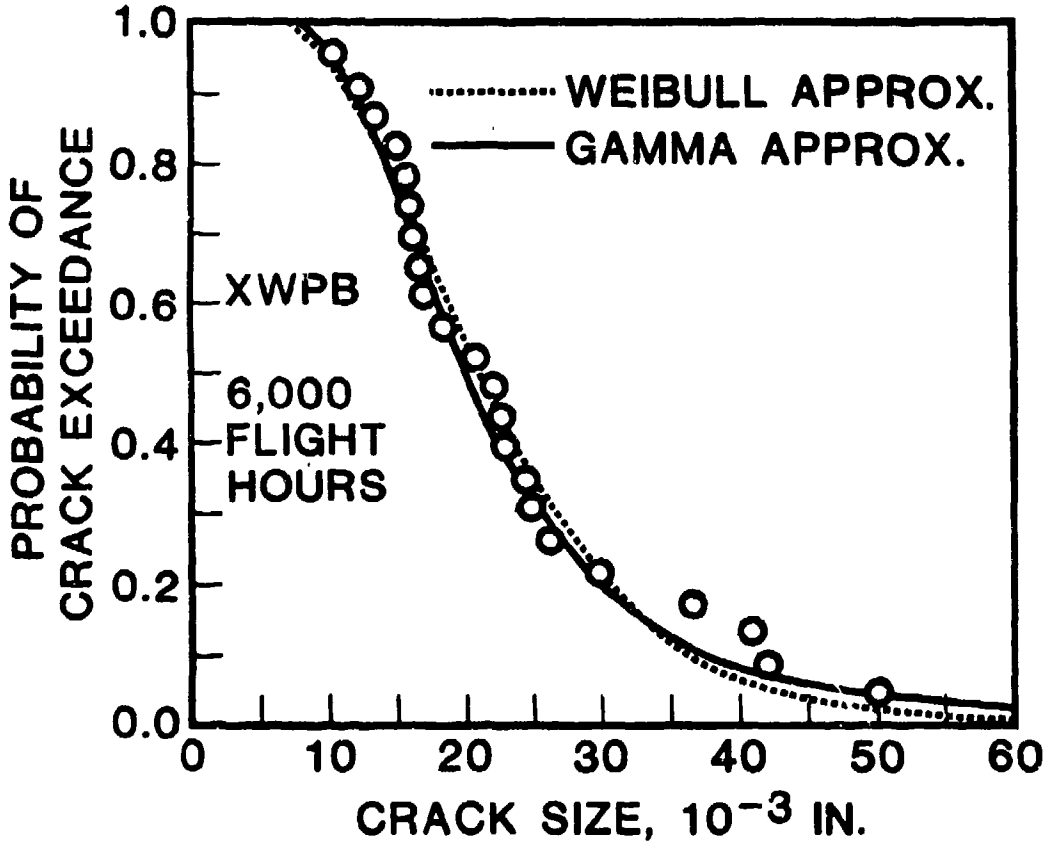

Figure 55(a): Correlation Between Second Moment Approximations and Experimental Results for the Probability of Crack Exceedance at 6,000 Flight Hours for XWPB Fastener Holes; Weibull and Gamma Approximations.

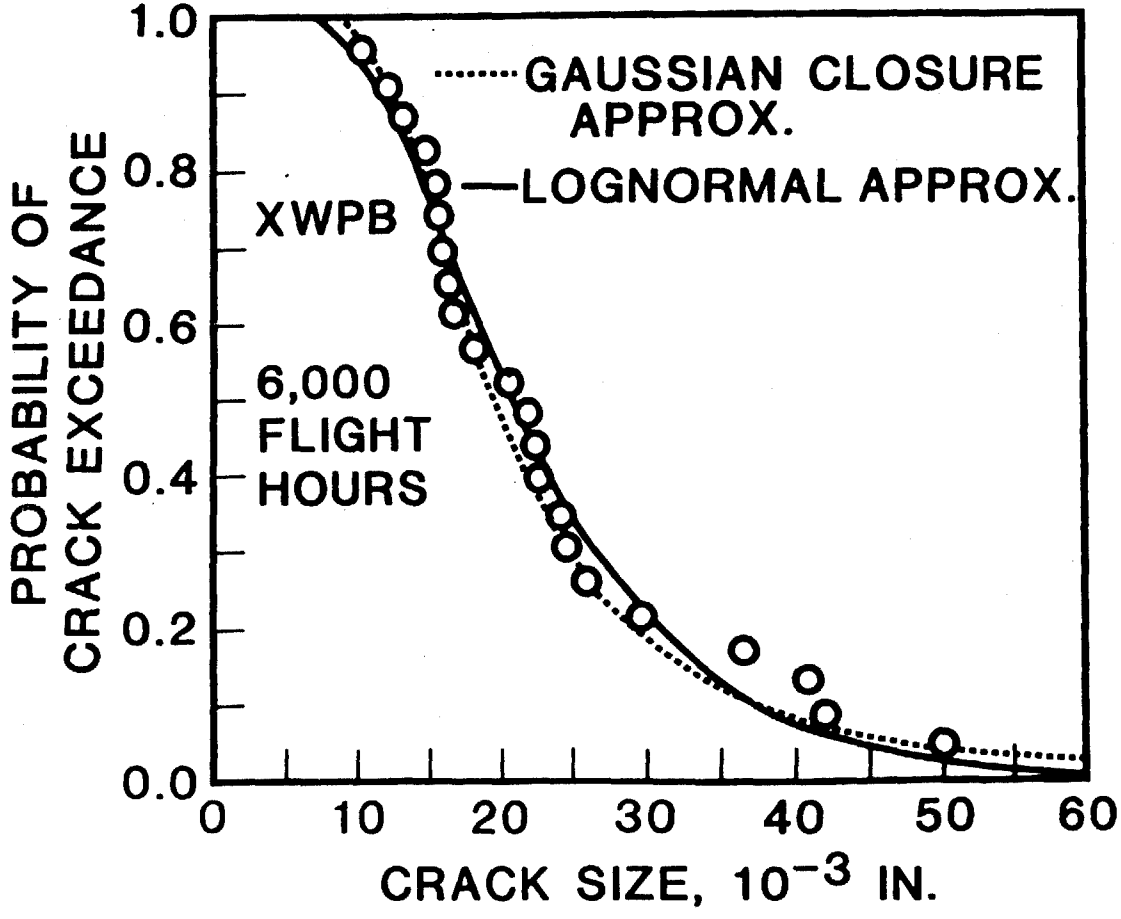

Figure 55(b): Correlation Between Second Moment Approximations and Experimental Results for the Probability of Crack Exceedance at 6,000 Flight Hours for XWPB Fastener Holes; Gaussian Closure and Lognormal Approximations.

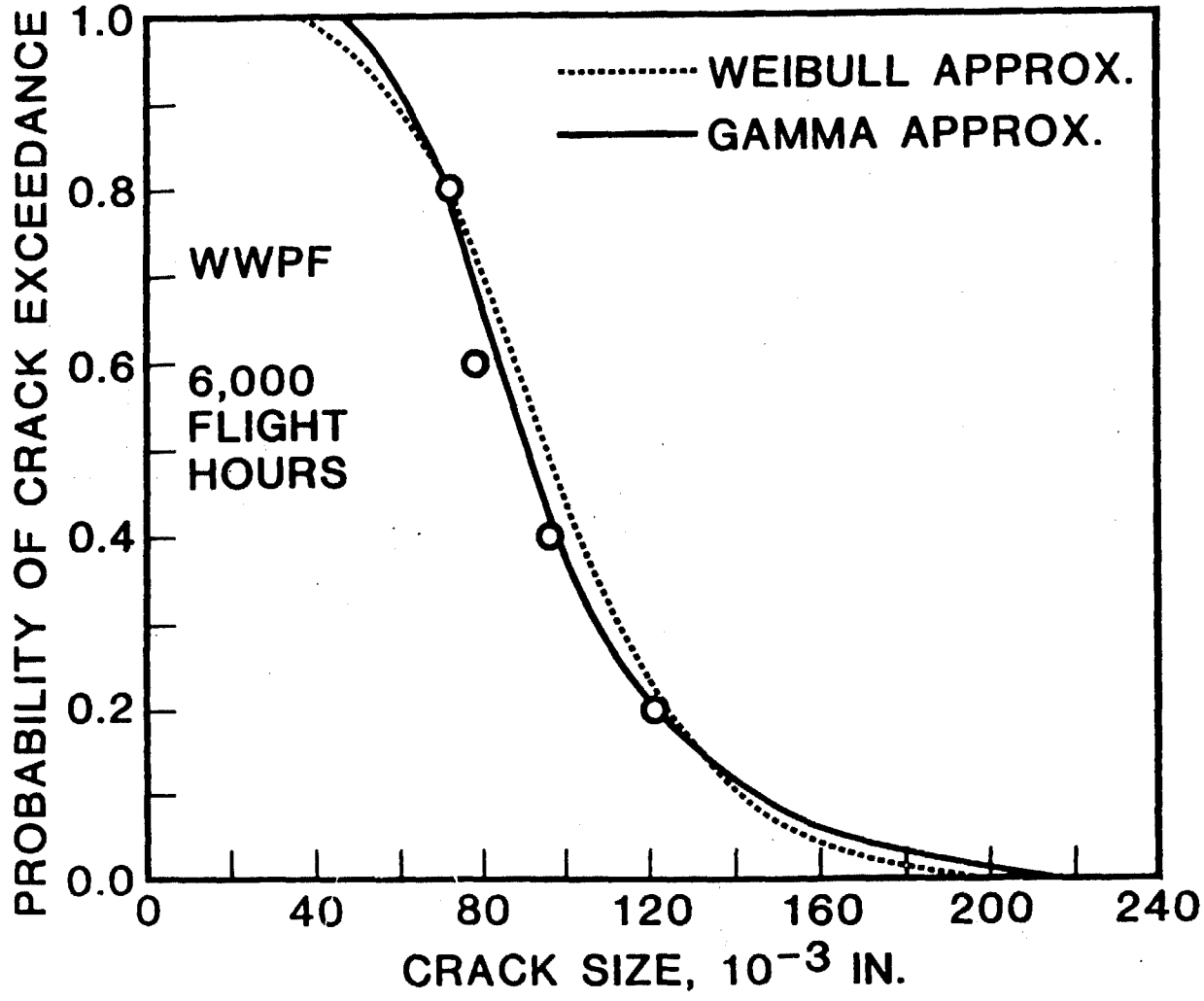

Figure 56(a): Correlation Between Second Moment Approximations and Experimental Resutls for the Probability of Crack Exceedance at 6,000 Flight Hours for WWPF Fastener Holes; Weibull and Gamma Approximations.

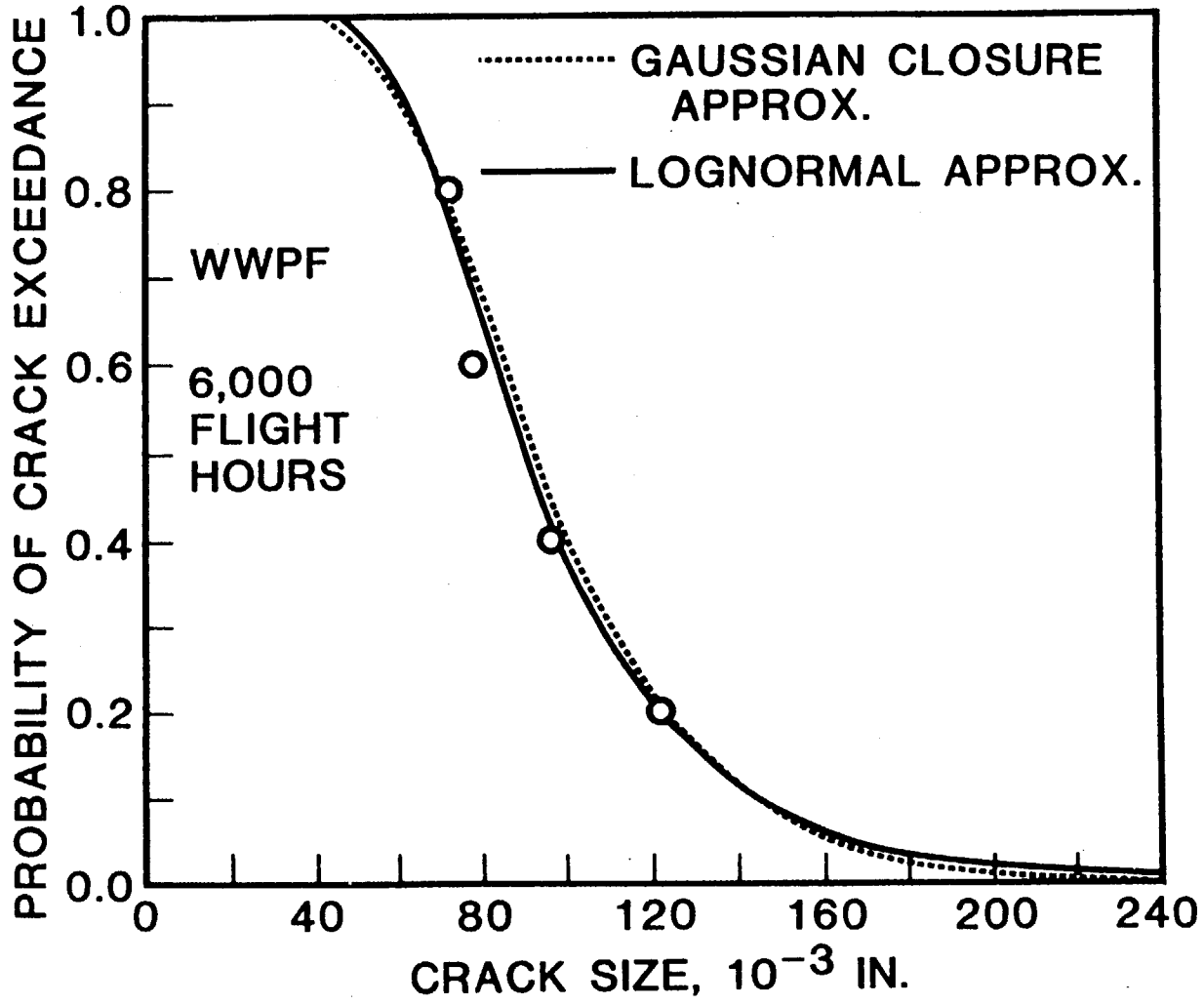

Figure 56(b): Correlation Between Second Moment Approximations and Experimental Results for the Probability of Crack Exceedance at 6,000 Flight Hours for WWPF Fastener Holes; Gaussian Closure and Lognormal Approximations.

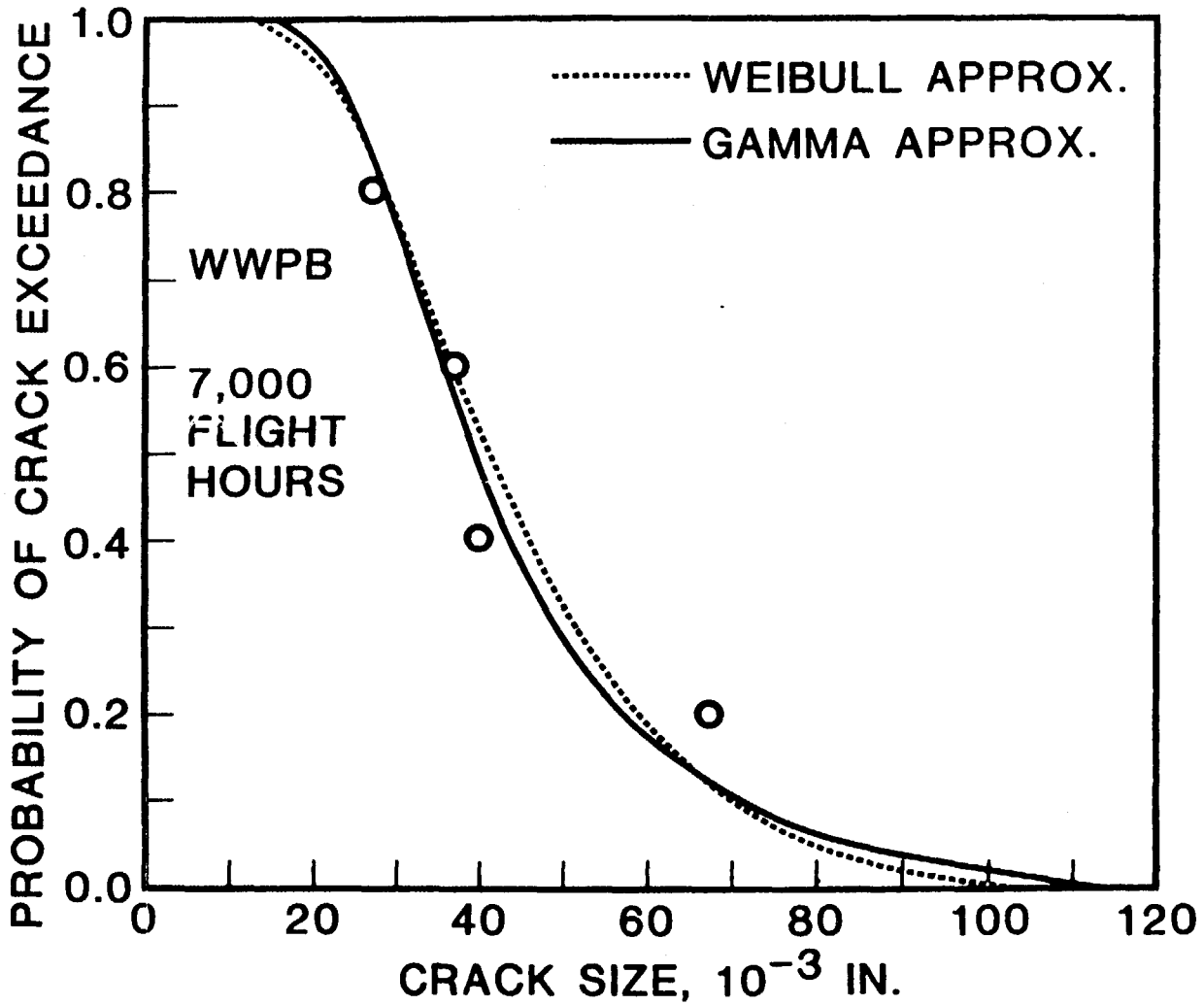

Figure 57(a): Correlation Between Second Moment Approximations and Experimental Results for the Probability of Crack Exceedance at 7,000 Flight Hours for WWPB Fastener Holes; Weibull and Gamma Approximations.

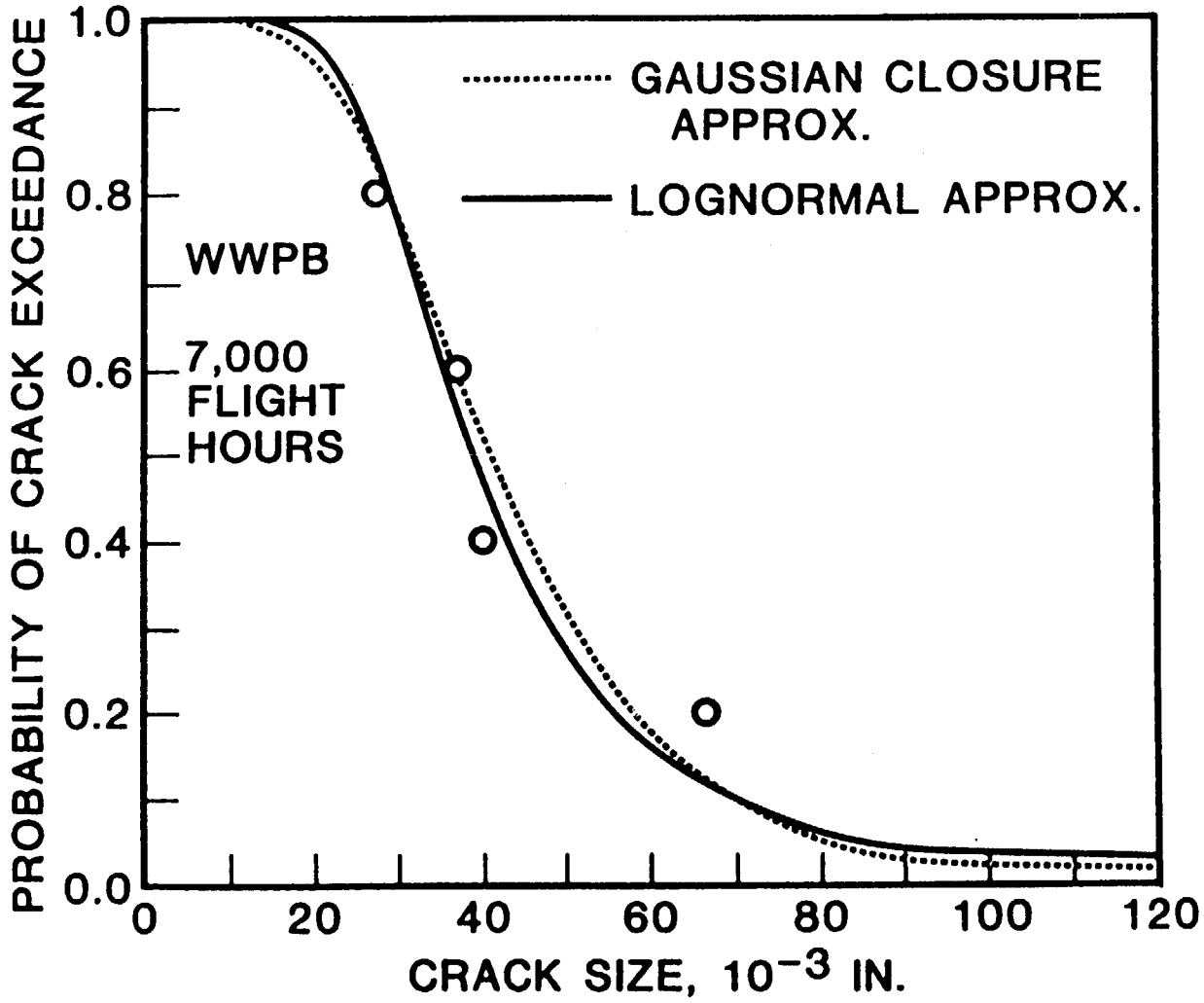

Figure 57(b): Correlation Between Second Moment Approximations and Experimental Results for the Probability of Crack Exceedance at 7,000 Flight Hours for WWPB Fastener Holes; Gaussian Closure and Lognormal Approximations.

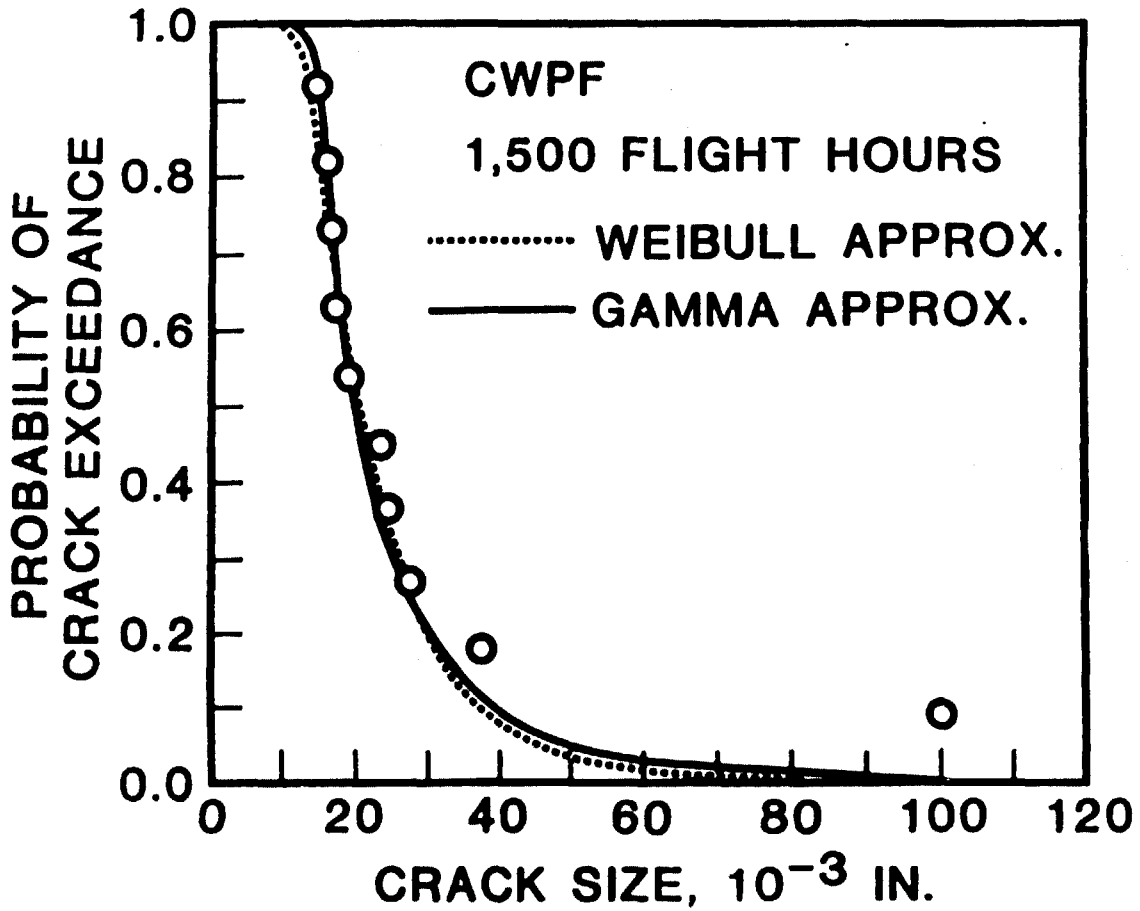

Figure 58(a): Correlation Between Second Moment Approximations and Experimental Results for the Probability of Crack Exceedance at 1,500 Flight Hours for CWPF Fastener Holes; Weibull and Gamma Approximations.

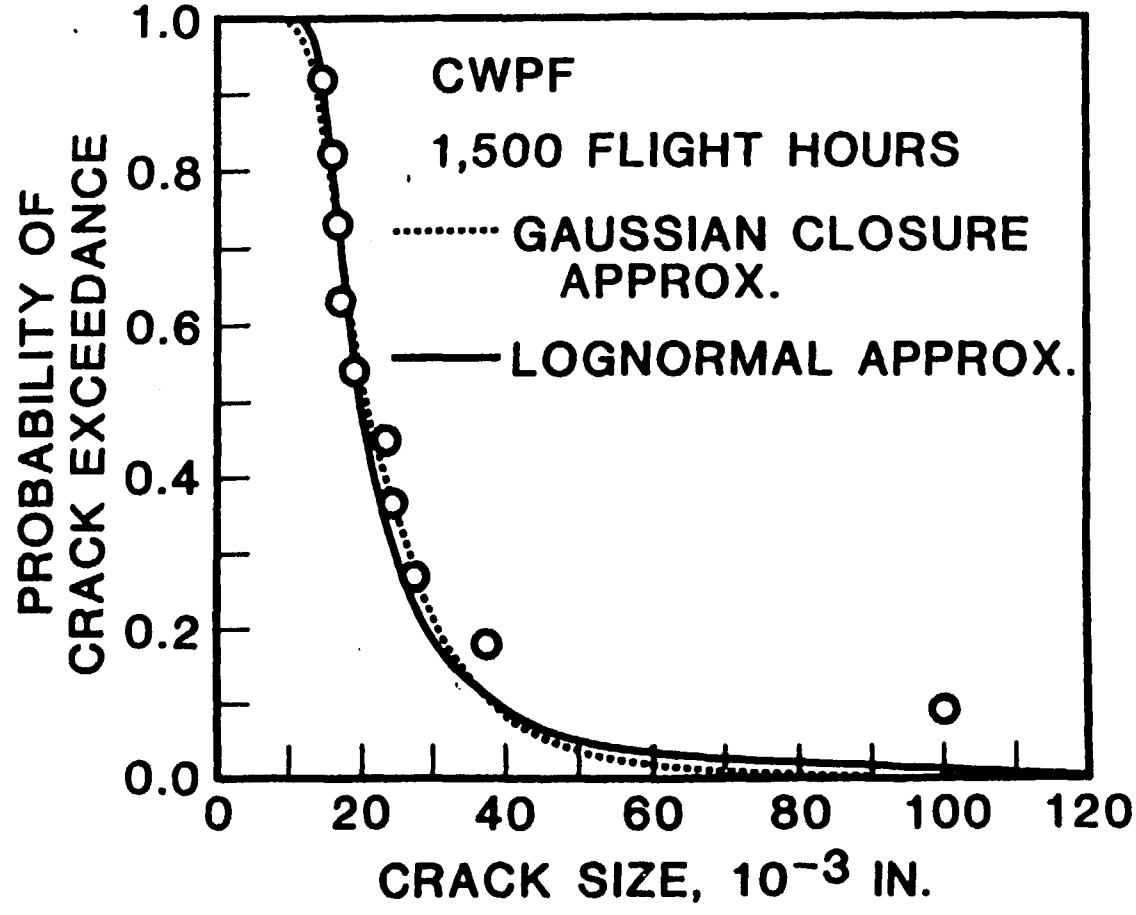

Figure 58(b): Correlation Between Second Moment Approximations and Experimental Results for the Probability of Crack Exceedance at 1,500 Flight Hours for CWPF Fastener Holes; Gaussian Closure and Lognormal Approximations.

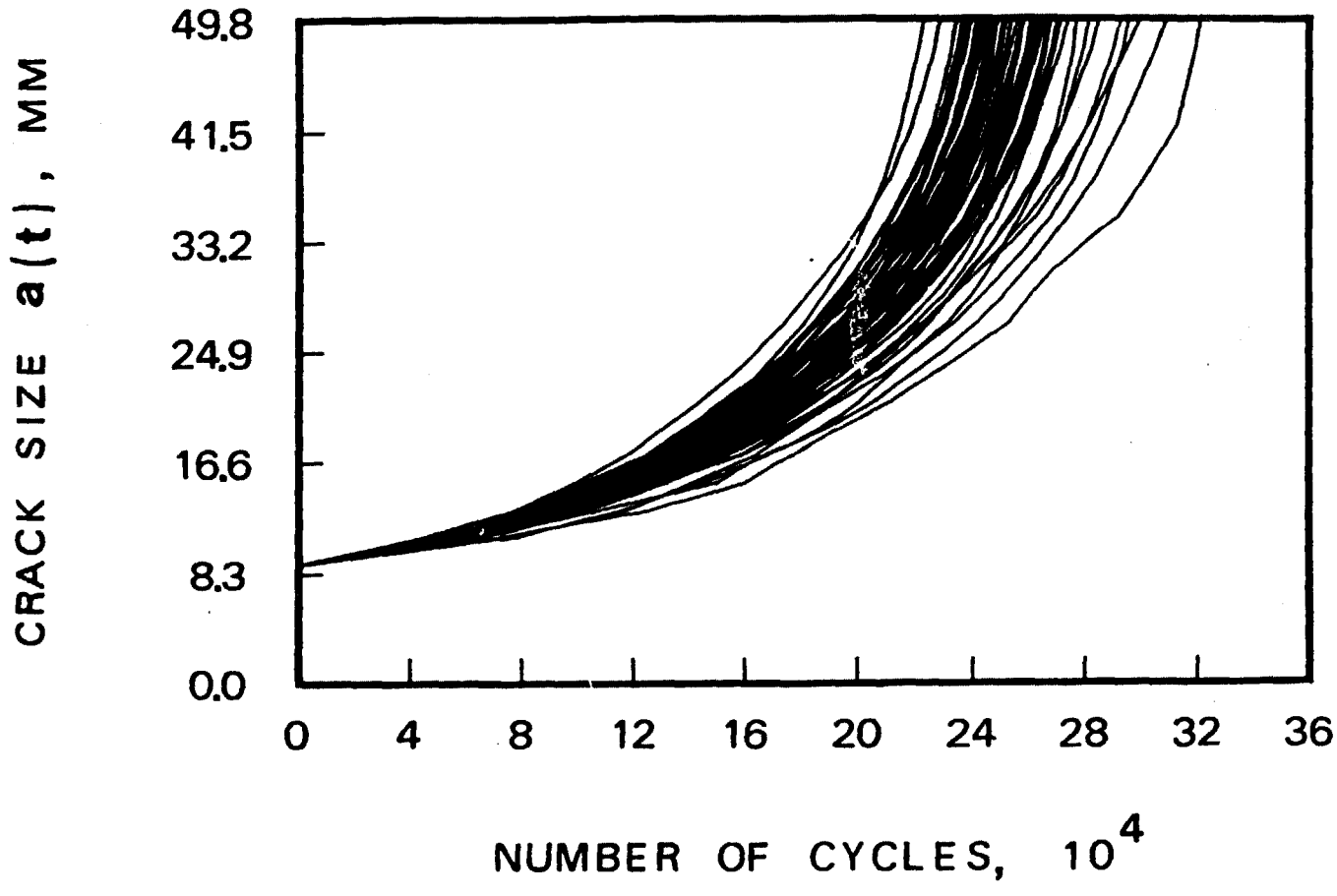

Figure 59: Crack Propagation Time Histories of Center-Cracked Specimens.

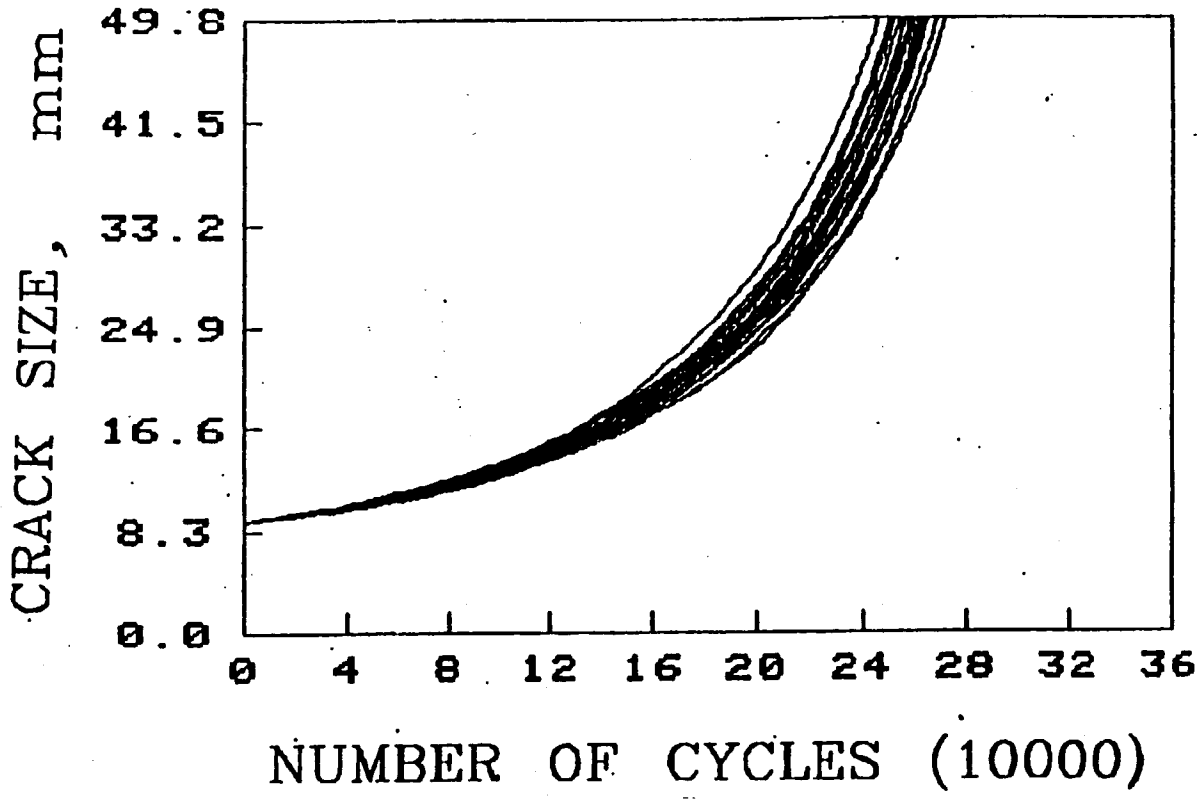

Figure 60: Simulated Crack Propagation Time Histories for Center-Cracked Specimens Based on White Noise Process Model.

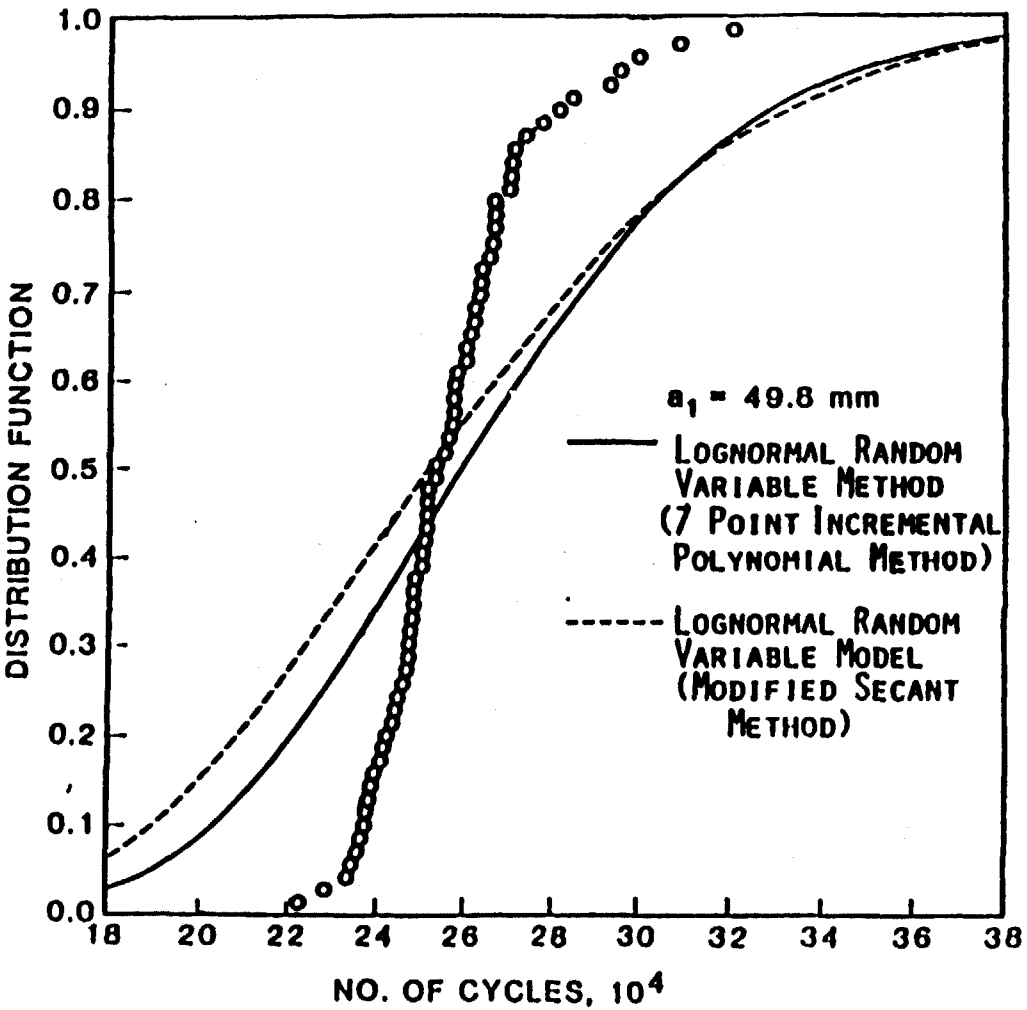

Figure 61(a): Correlation Between Lognormal Random Variable Model and Experimental Results for Distribution of Number of Load Cycles to Reach Half Crack Length 21 mm for Center-Cracked Specimens.

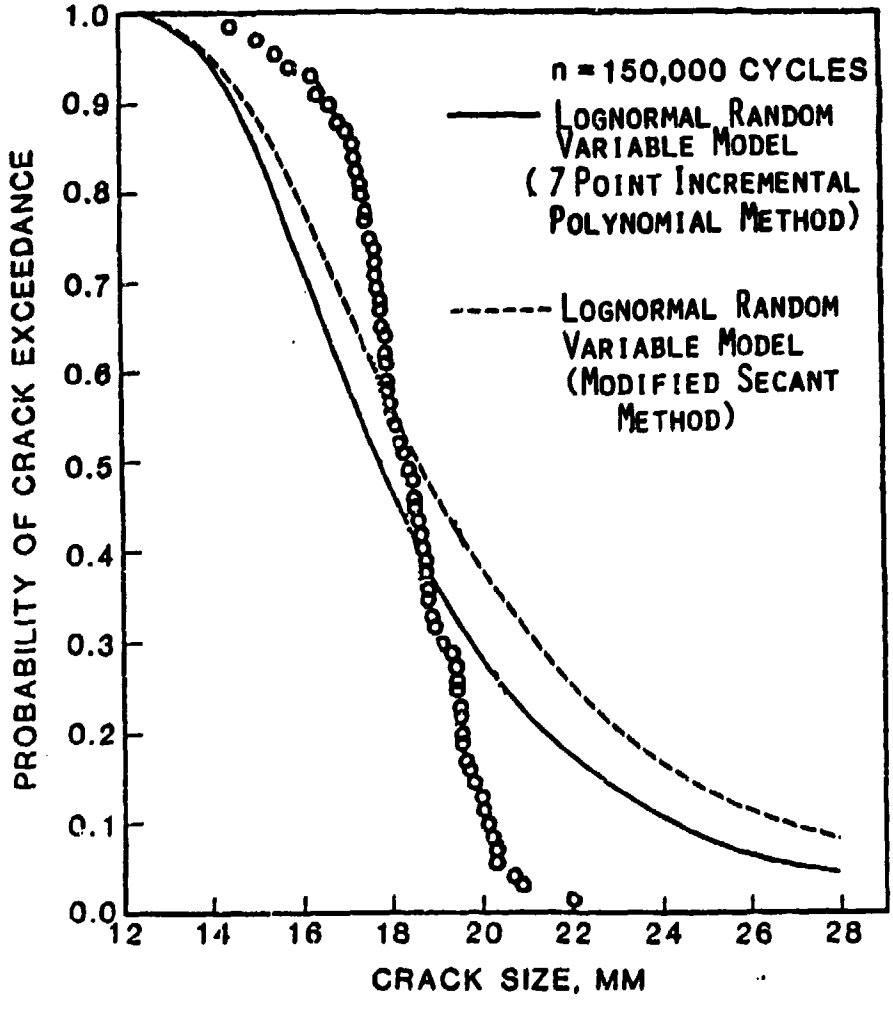

Figure 61(b): Correlation Between Lognormal Random Variable Model and Experimental Results for Distribution of Number of Load Cycles to Reach Half Crack Length 49.8 mm for Center-Cracked Specimens.

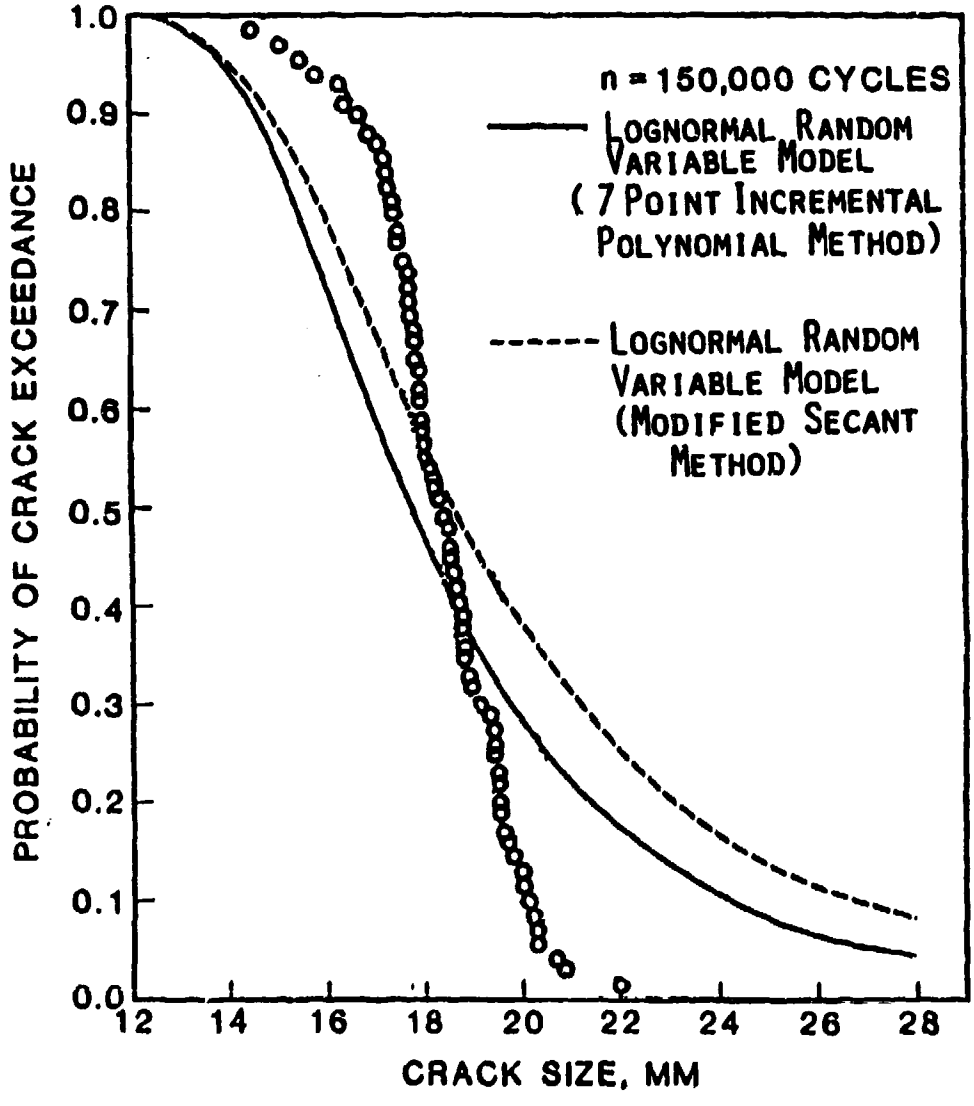

Figure 62: Correlation Between Lognormal Random Variable Model and Experimental Results for Probability of Crack Exceedance at 150,000 Cycles for Center-Cracked Specimens.

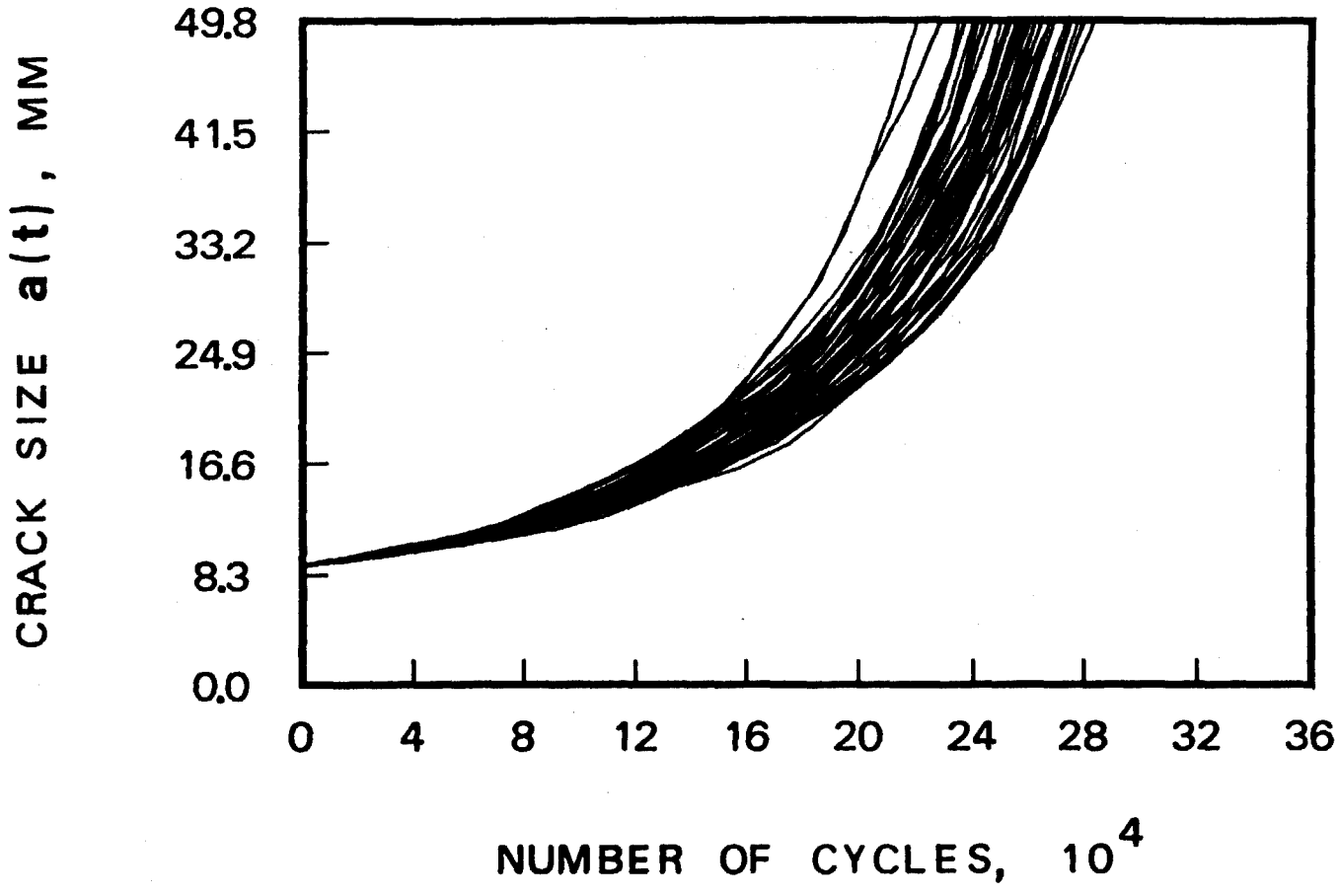

Figure 63: Simulated Crack Propagation Time Histories for Center-Cracked Specimens Based on Lognormal Random Process Model.

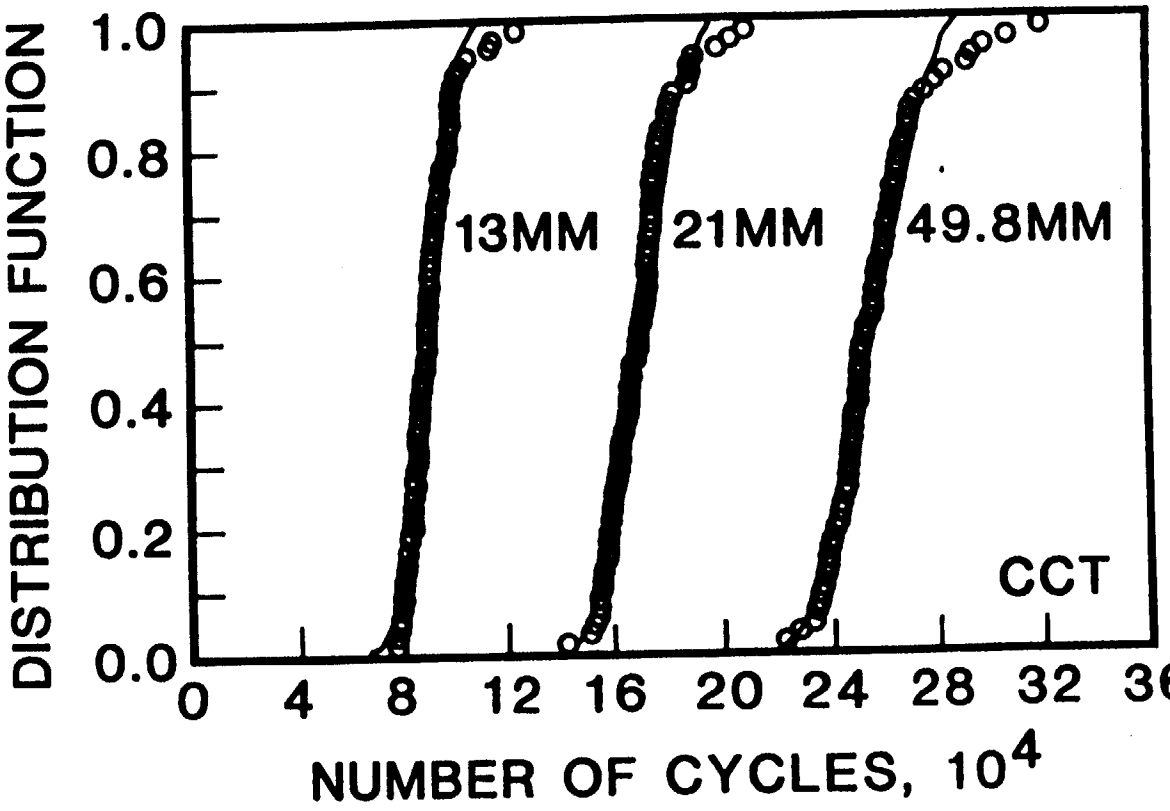

Figure 64: Correlation Between Lognormal Random Process Model and Experimental Results for Distribution of Number of Load Cycles to Reach Half Crack Lengths 13, 21, and 49.8 mm for Center-Cracked Specimens.

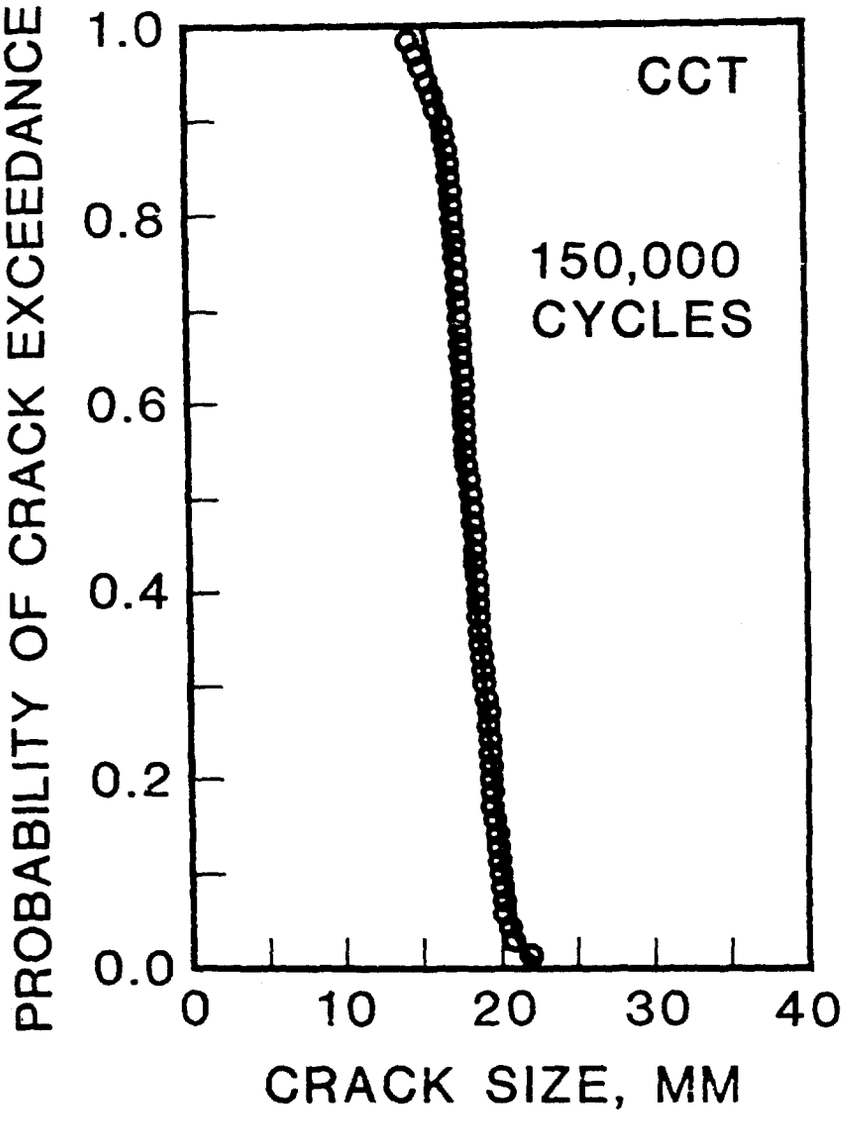

Figure 65: Correlation Between Lognormal Random Process Model and Experimental Results for Probability of Crack Exceedance at 150,000 Cycles for Center-Cracked Specimens.

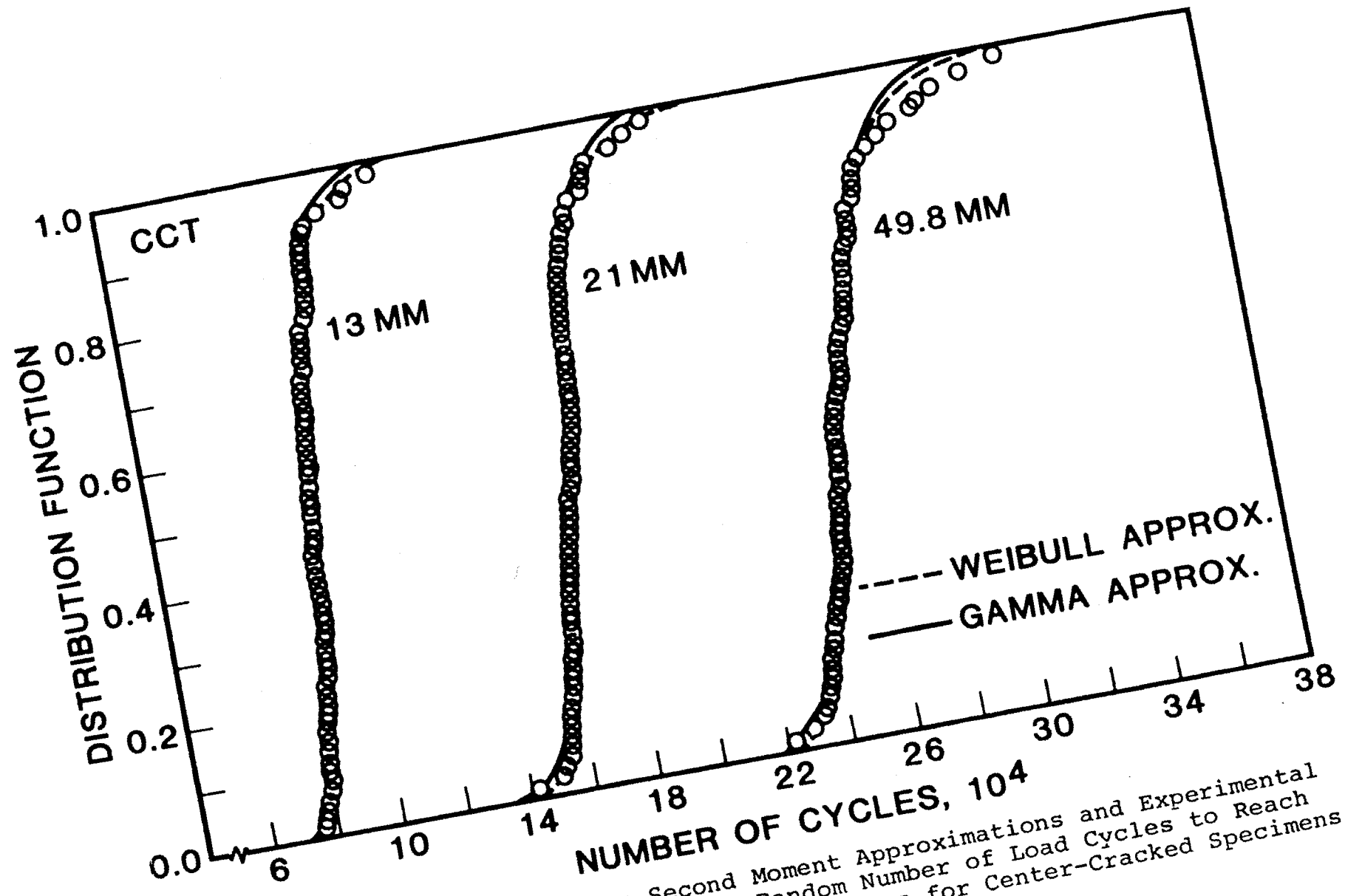

Figure 66(a): Correlation Between Second Moment Approximations and Experimental Results for Distribution of Random Number of Load Cycles to Reach Half Crack Lengths 13, 21, and 49.8 mm for Center-Cracked Specimens; Weibull and Gamma Approximations.

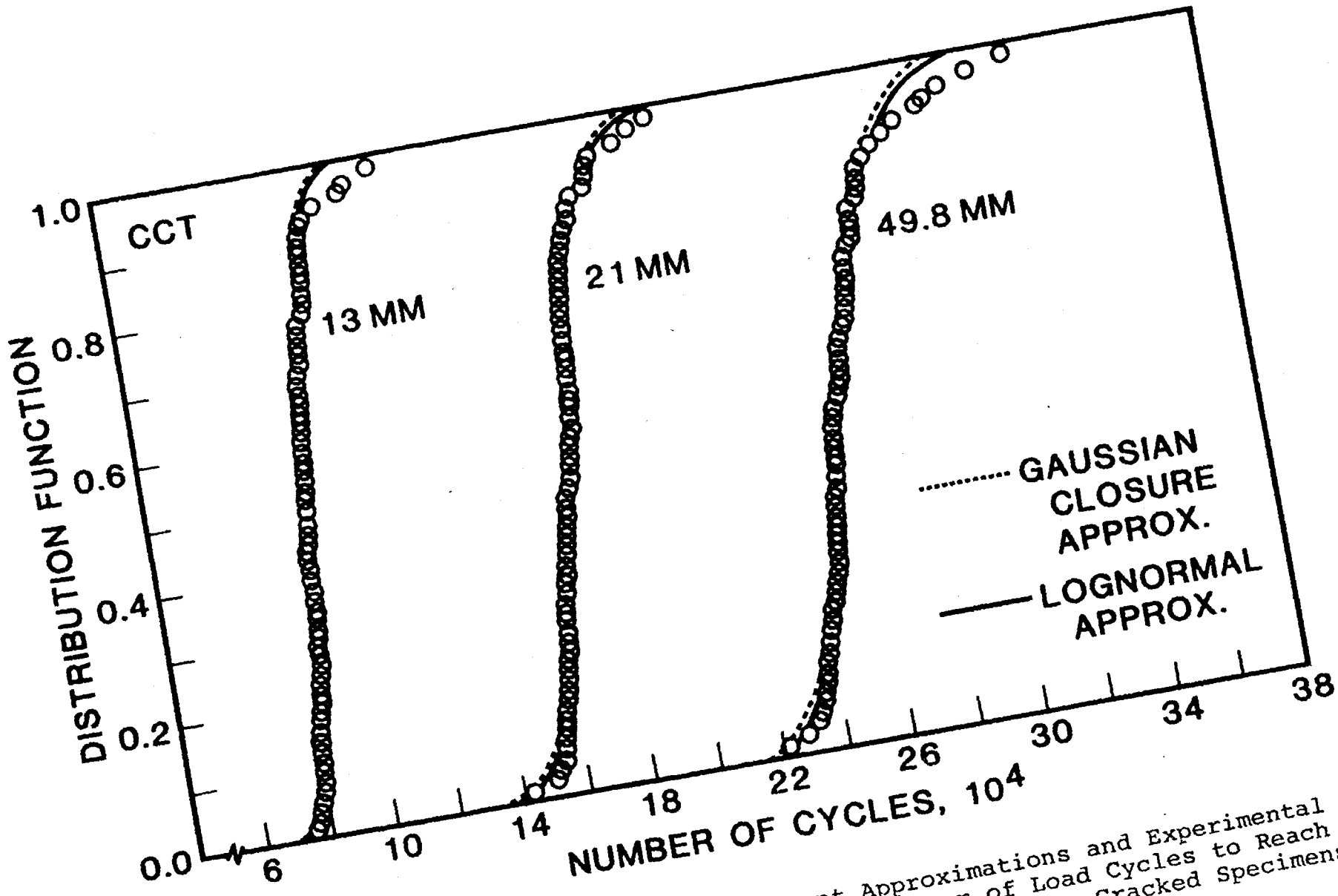

Figure 66(b): Correlation Between Second Moment Approximations and Experimental Results for Distribution of Random Number of Load Cycles to Reach Half Crack Lengths 13, 21 and 49.8 mm for Center-Cracked Specimens; Gaussian Closure and Lognormal Approximations.

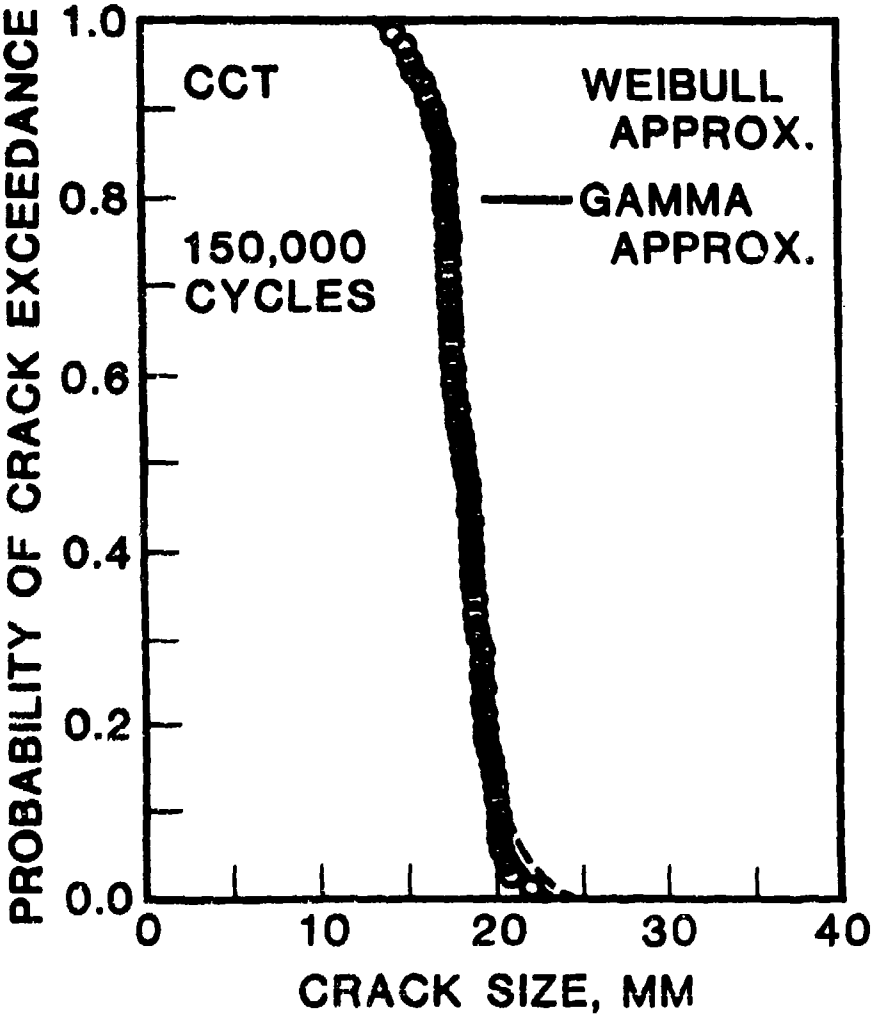

Figure 67(a): Correlation Between Second Moment Approximations and Experimental Results for Probability of Crack Exceedance after 150,000 Load Cycles for Center-Cracked Specimens; Weibull and Gamma Approximations.

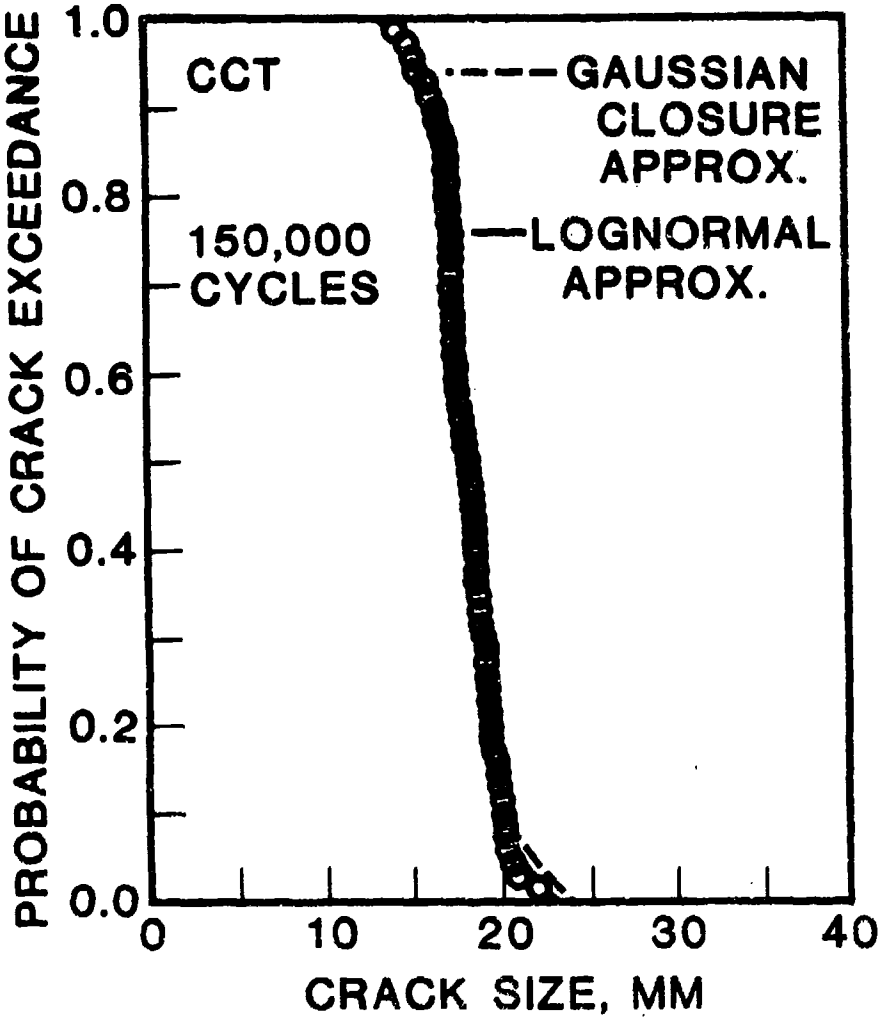

Figure 67(b): Correlation Between Second Moment Approximations and Experimental Results for Probability of Crack Exceedance After 150,000 Load Cycles for Center-Cracked Specimens; Gaussian Closure and Lognormal Approximations.

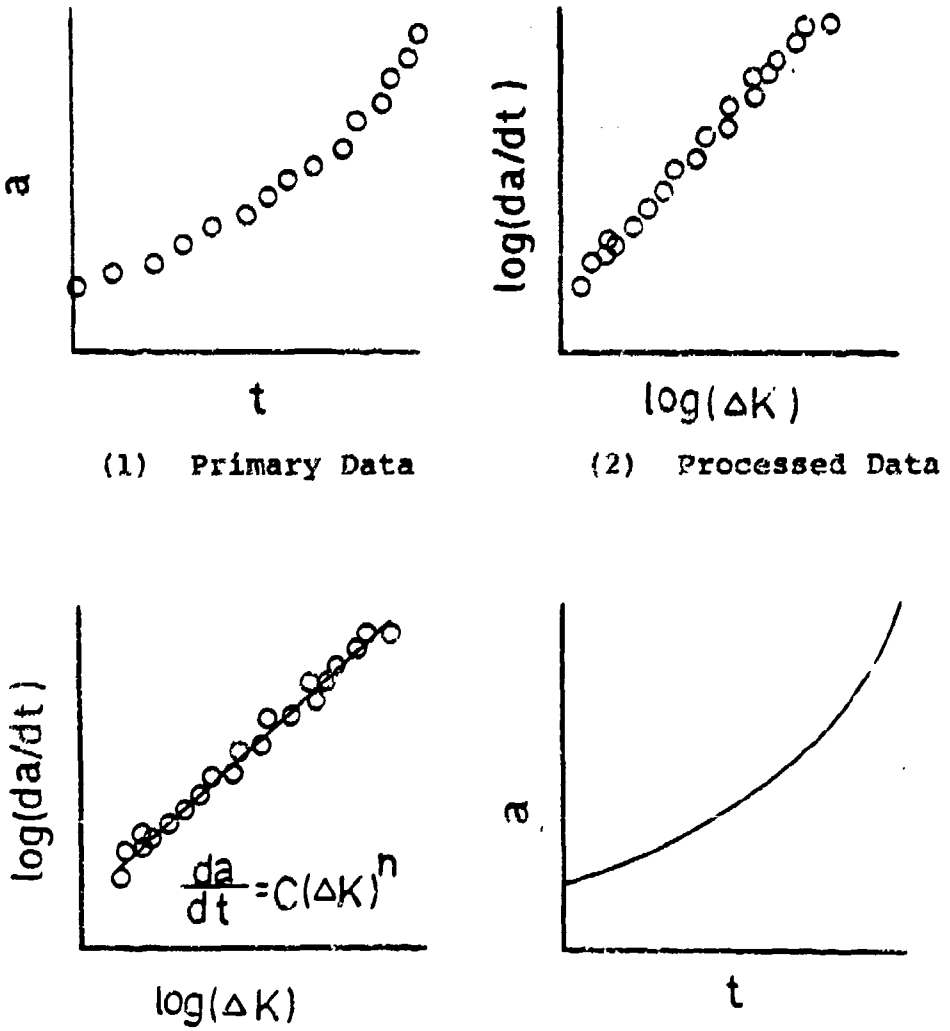

(1) Primary Data (2) Processed Data

(3) Empirical Modeling (4) Prediction

Figure 68: Schematic Illustration for Deterministic Crack Growth Analysis.

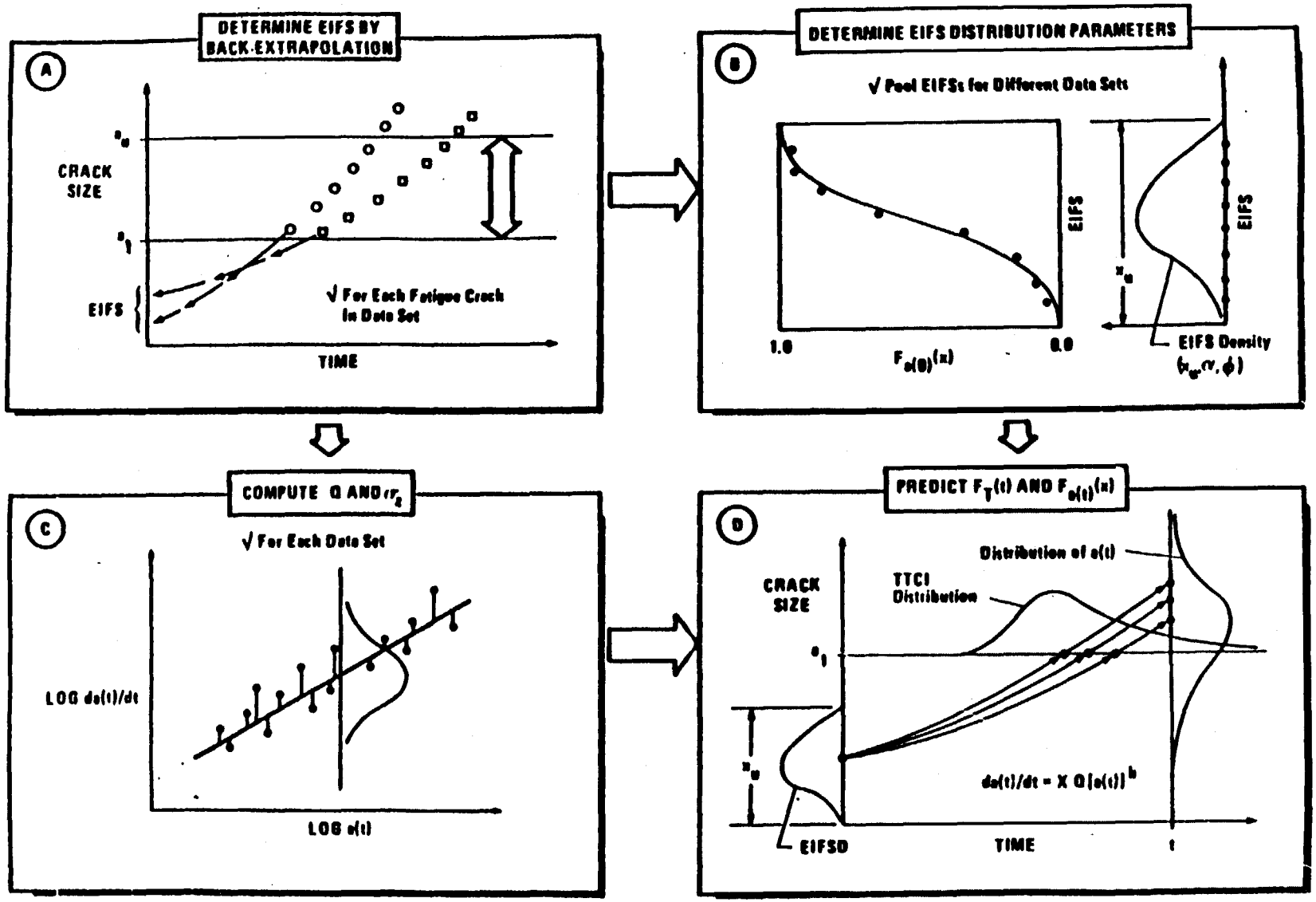

Figure 69: Essential Elements of the Stochastic Crack Growth Approach.

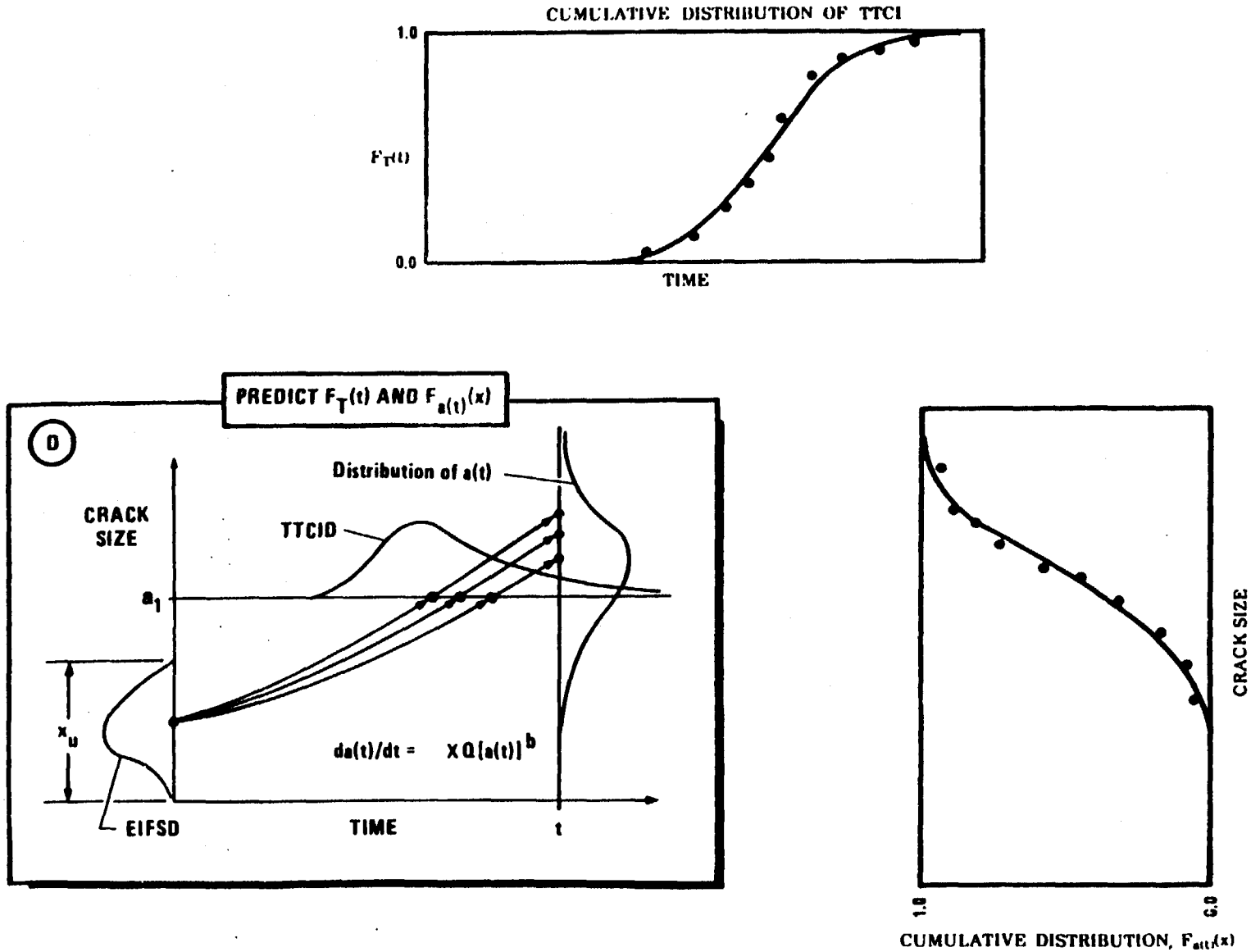

Figure 70: Stochastic Crack Growth of EIFSD

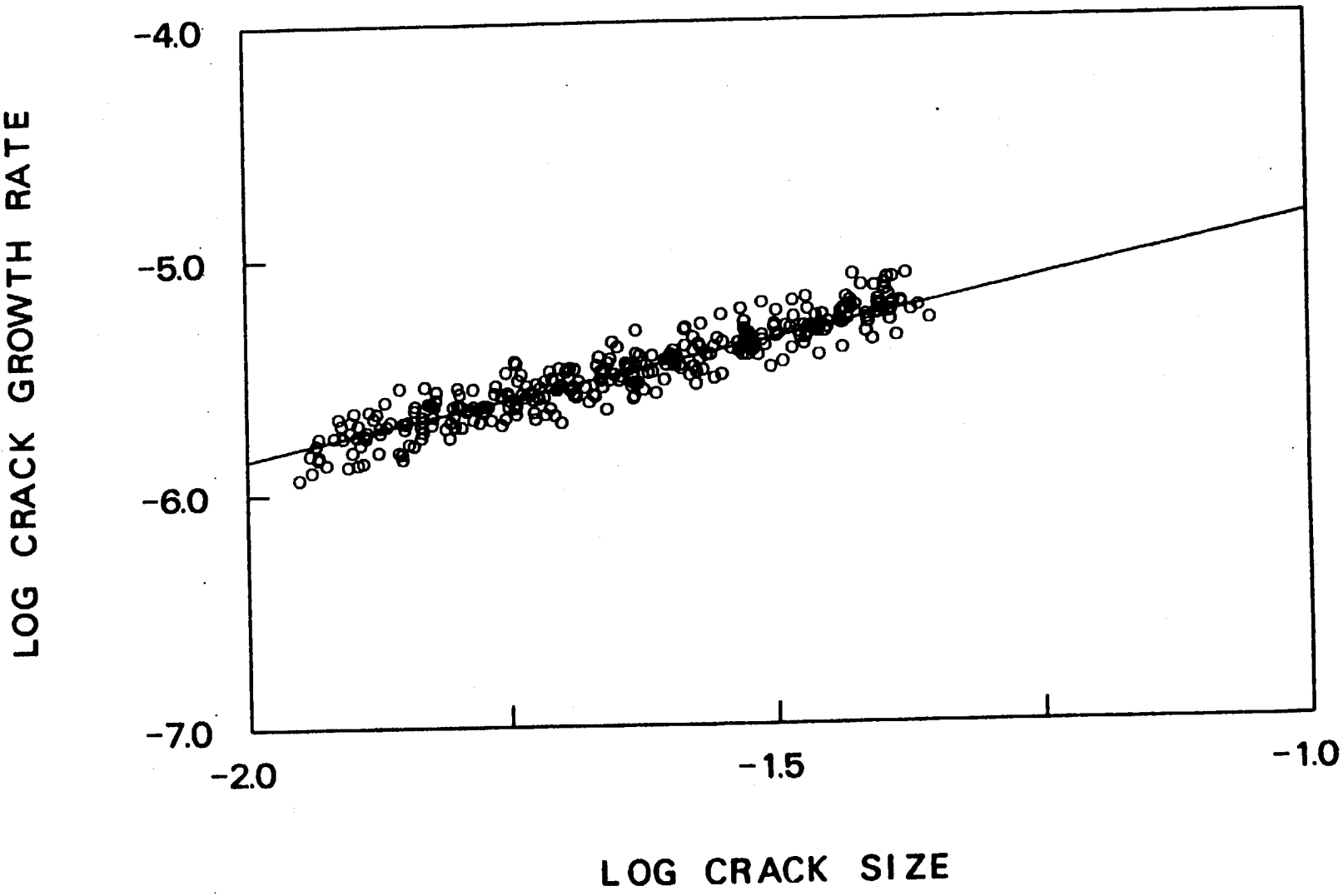

Figure 71: Log Crack Growth Rate Versus Log Crack Size for WPF Data Set

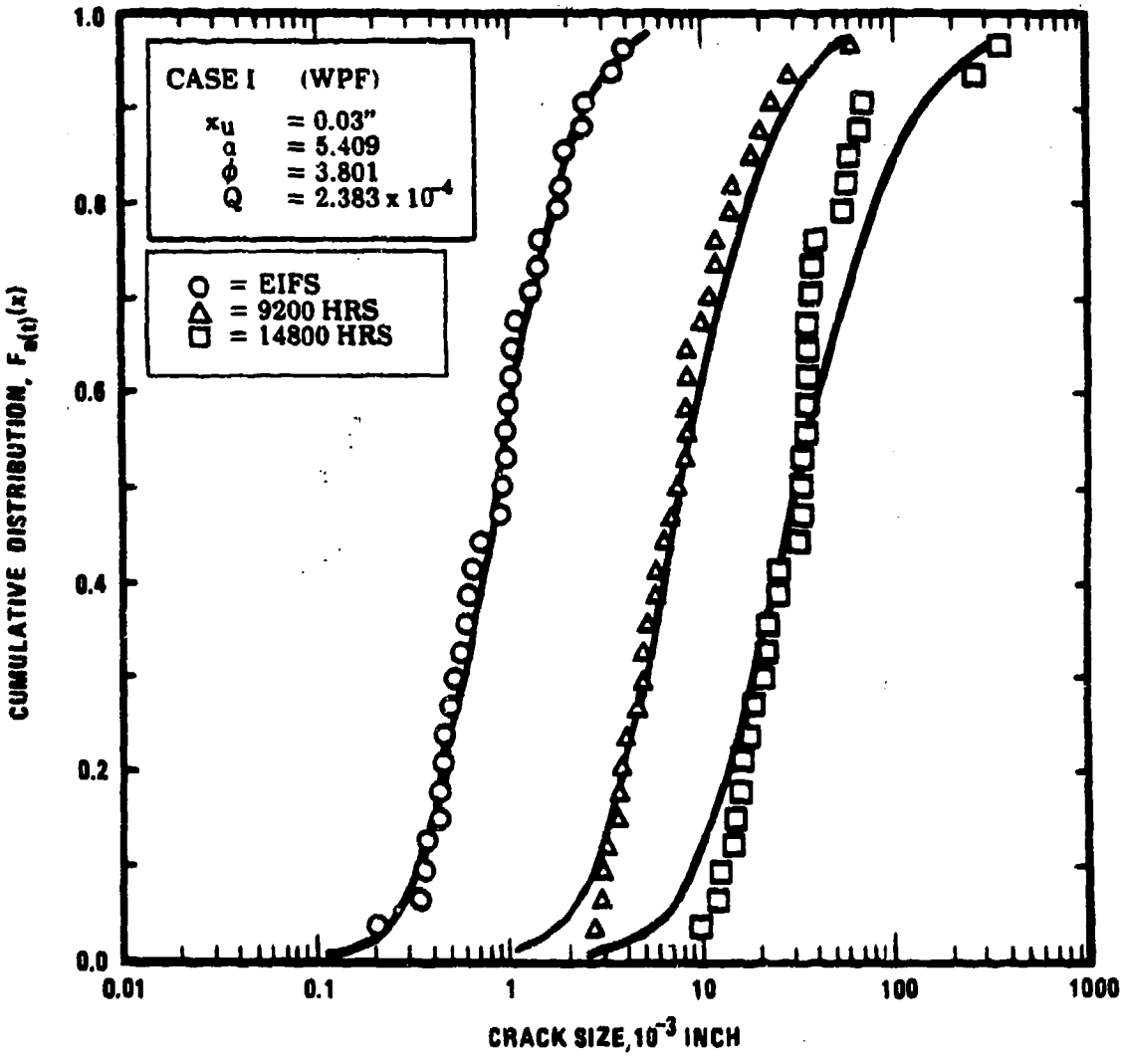

Figure 72: Correlation Between Predictions and Test Results for the Cumulative Distribution of Crack Size at 9200 and 14,800 Flight Hours for WPF Data Set (Case I: EIFSs for WPF; Un-normalized Q Value)

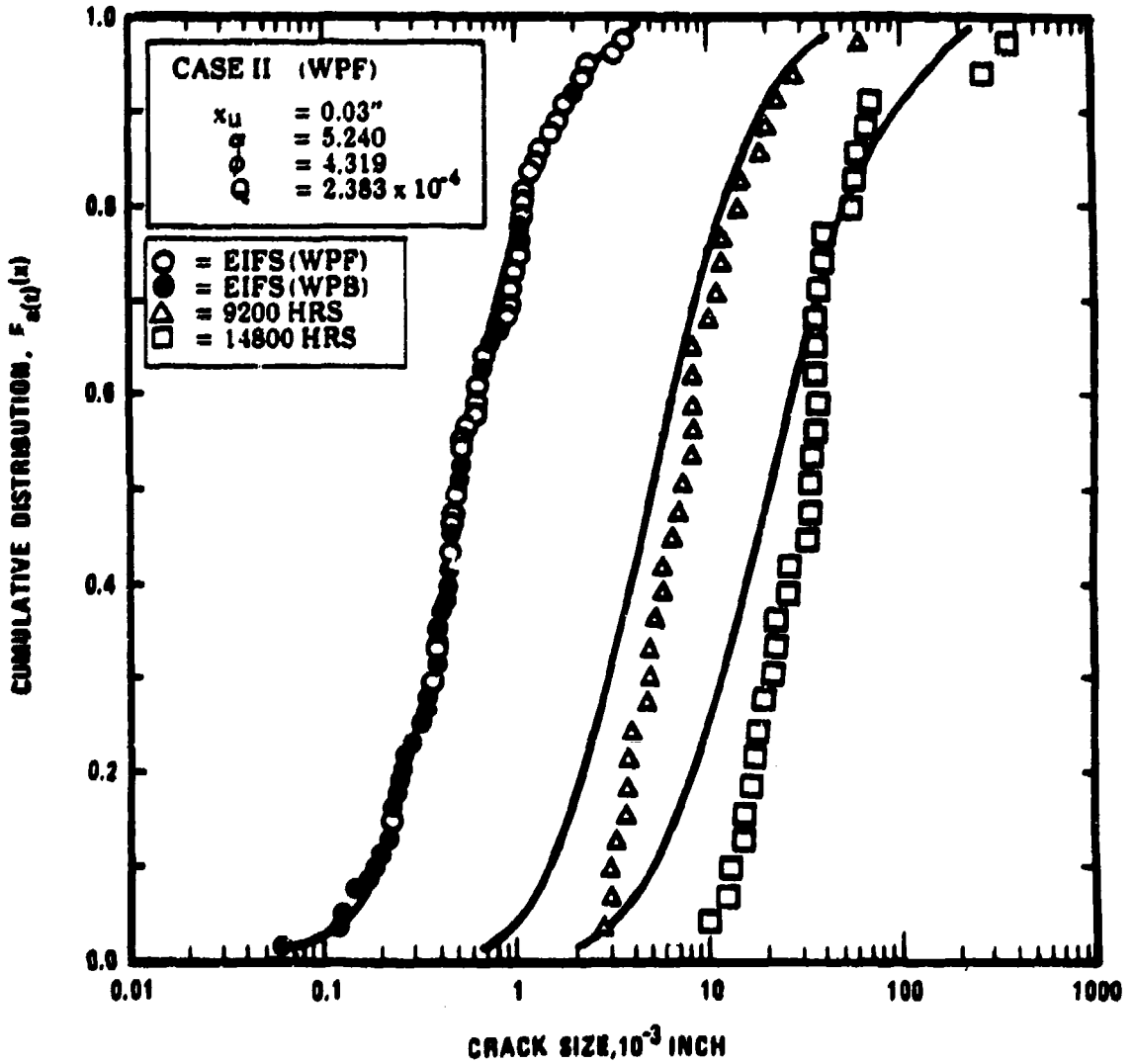

Figure 73: Correlation Between Predictions and Test Results for the Cumulative Distribution of Crack Size at 9200 and 14,800 Flight Hours for WPF Data Set (Case II: Pooled EIFSs for WPF + WPB; Un-normalized Q Value)

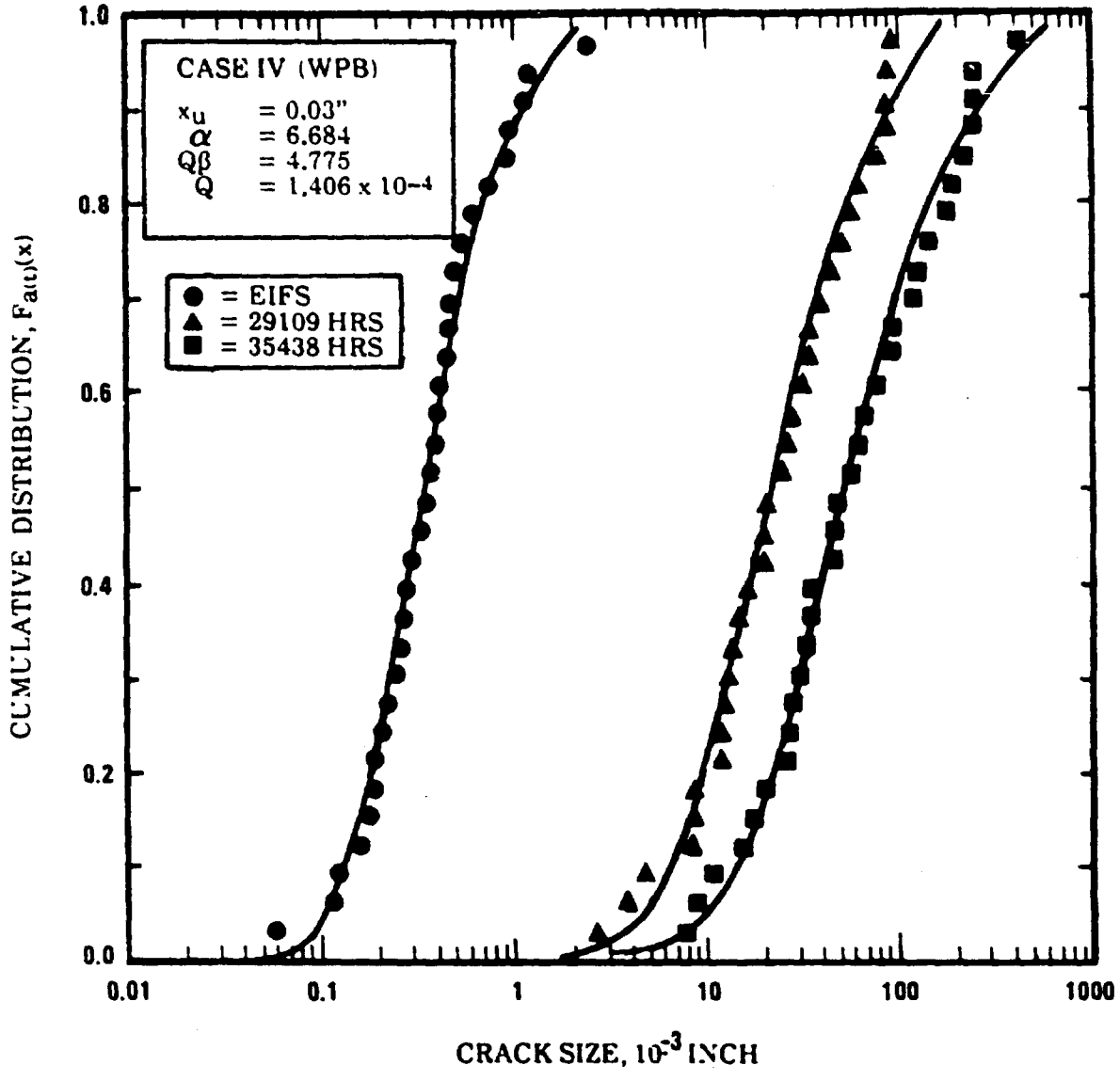

Figure 75: Correlation Between Predictions and Test Results for the Cumulative Distribution of Crack Size at 29,109 and 35,438 Flight Hours for WPB Data Set (Case IV: EIFSs for WPB; Un-normalized Q Value)

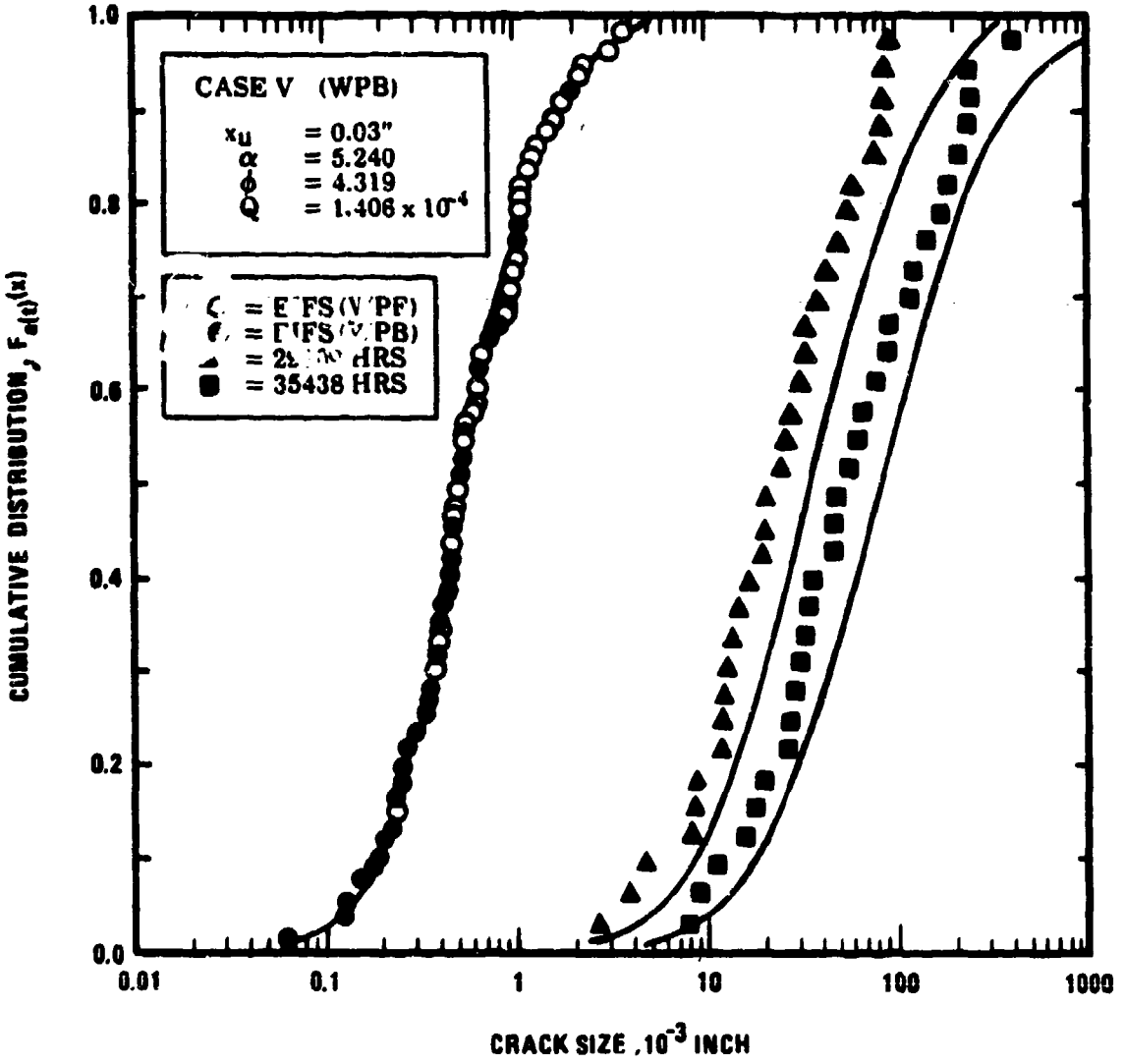

Figure 76: Correlation Between Predictions and Test Results for the Cumulative Distribution of Crack Size at 29,109 and 35,438 Flight Hours for WPB Data Set (Case V: Pooled EIFSs for WPF + WPB; Un-normalized Q Value)

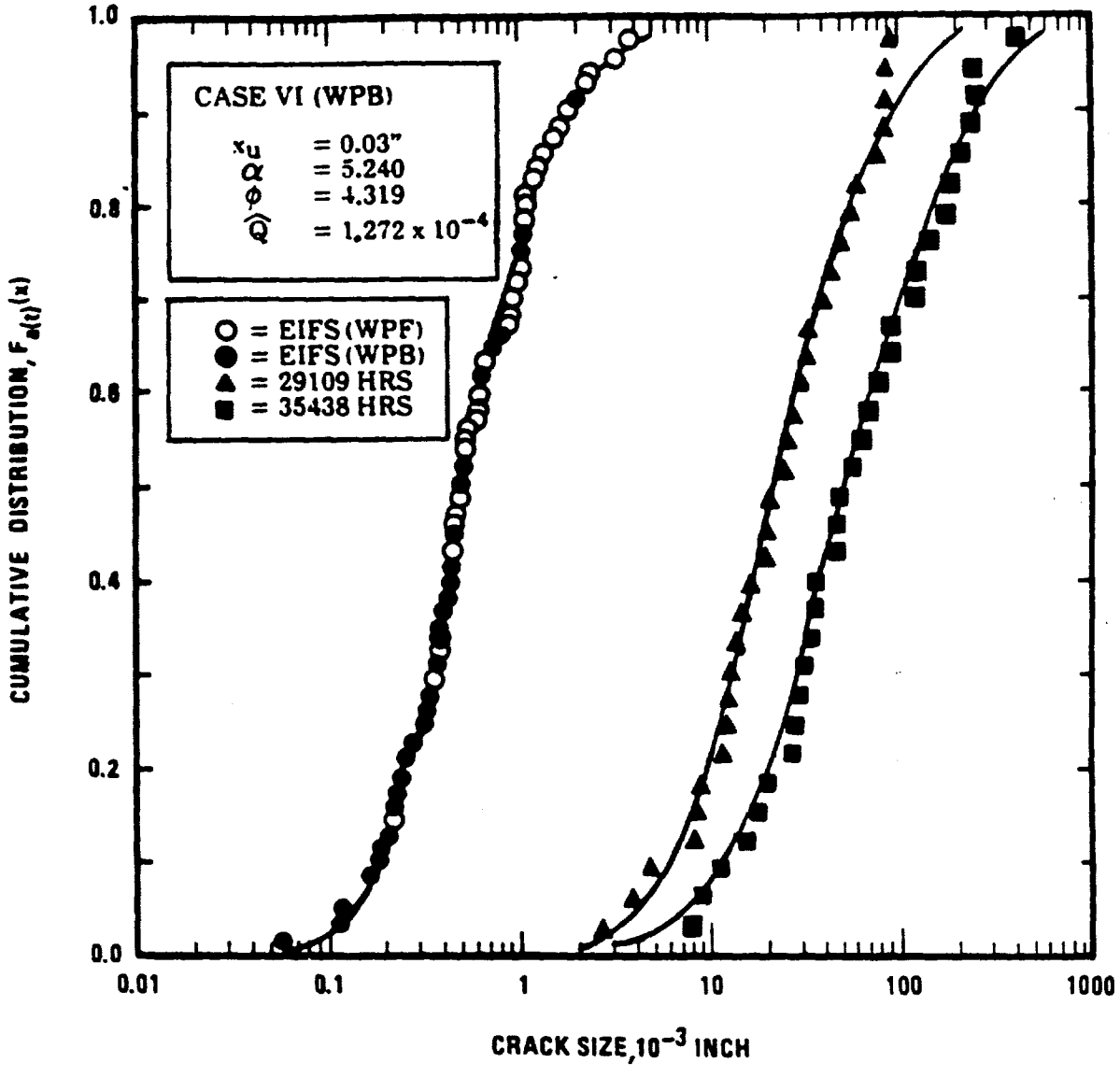

Figure 77: Correlation Between Predictions and Test Results for the Cumulative Distribution of Crack Size at 29109 and 35438 Flight Hours for WPB Data Set (Case VI: Pooled EIFSs for WPF + WPB; Normalized Q Value)

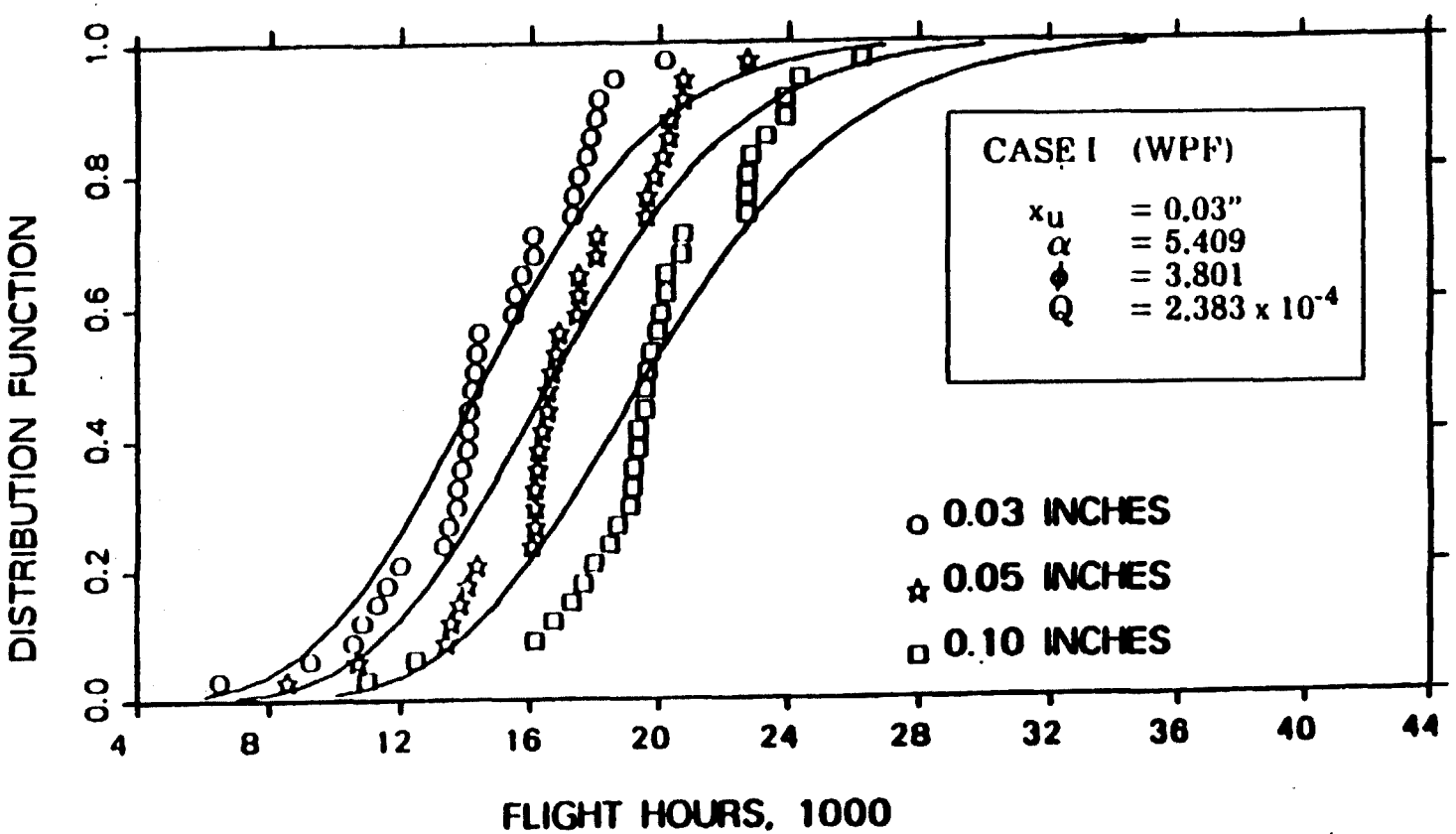

Figure 78: Correlation Between Predictions and Test Results for Cumulative Distribution of Time-to-Crack-Initiation at 0:03", 0.05", and 0.10" for WPF Data Set (Case I: EIFSs for WPF; Un-normalized Q Value)

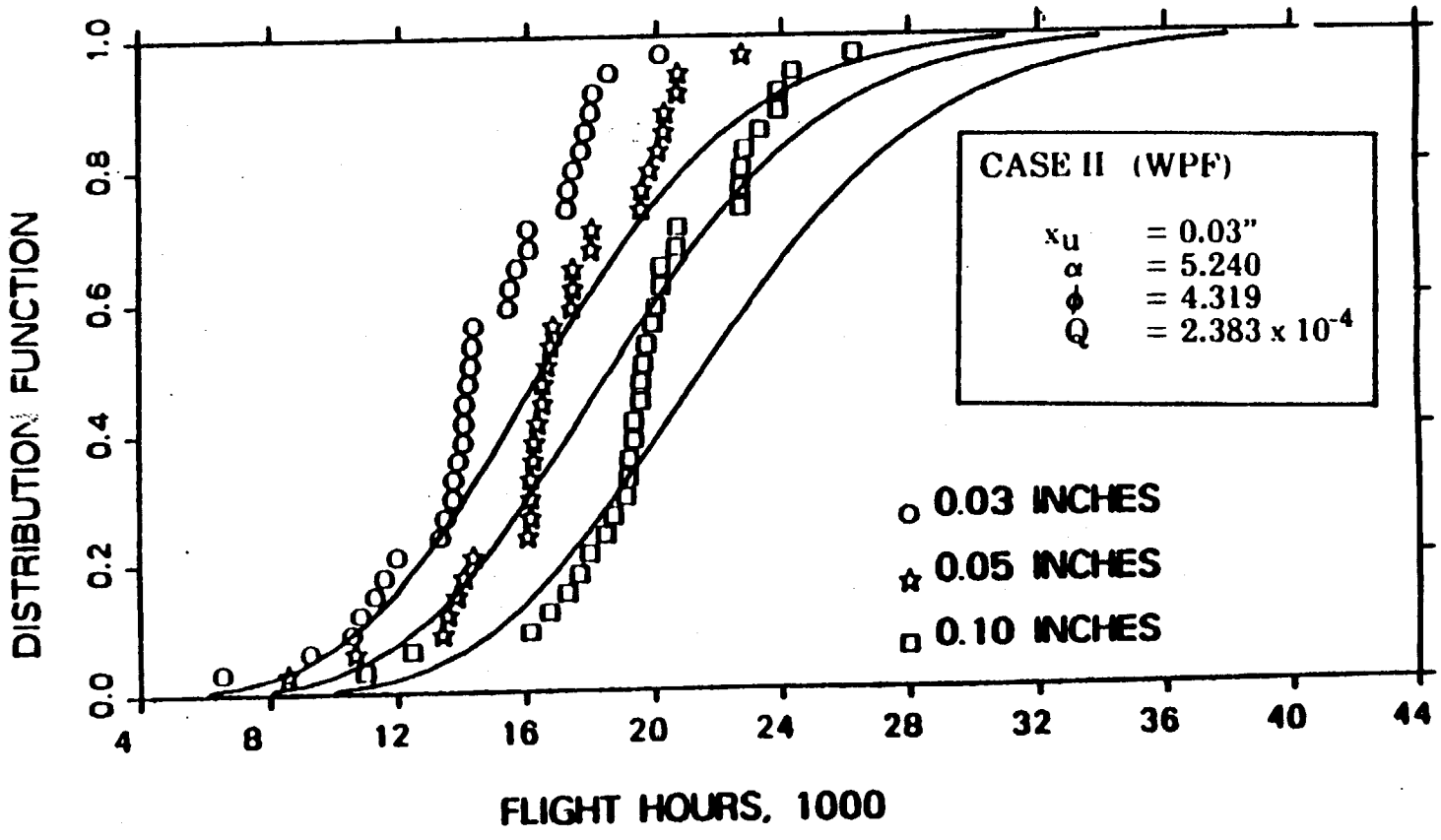

Figure 79: Correlation Between Predictions and Test Results for Cumulative Distribution of Time-to-Crack-Initiation at 0.03", 0.05", and 0.10" for WPF Data Set (Case II: Pooled EIFSs for WPF + WPB; Un-normalized Q Value)

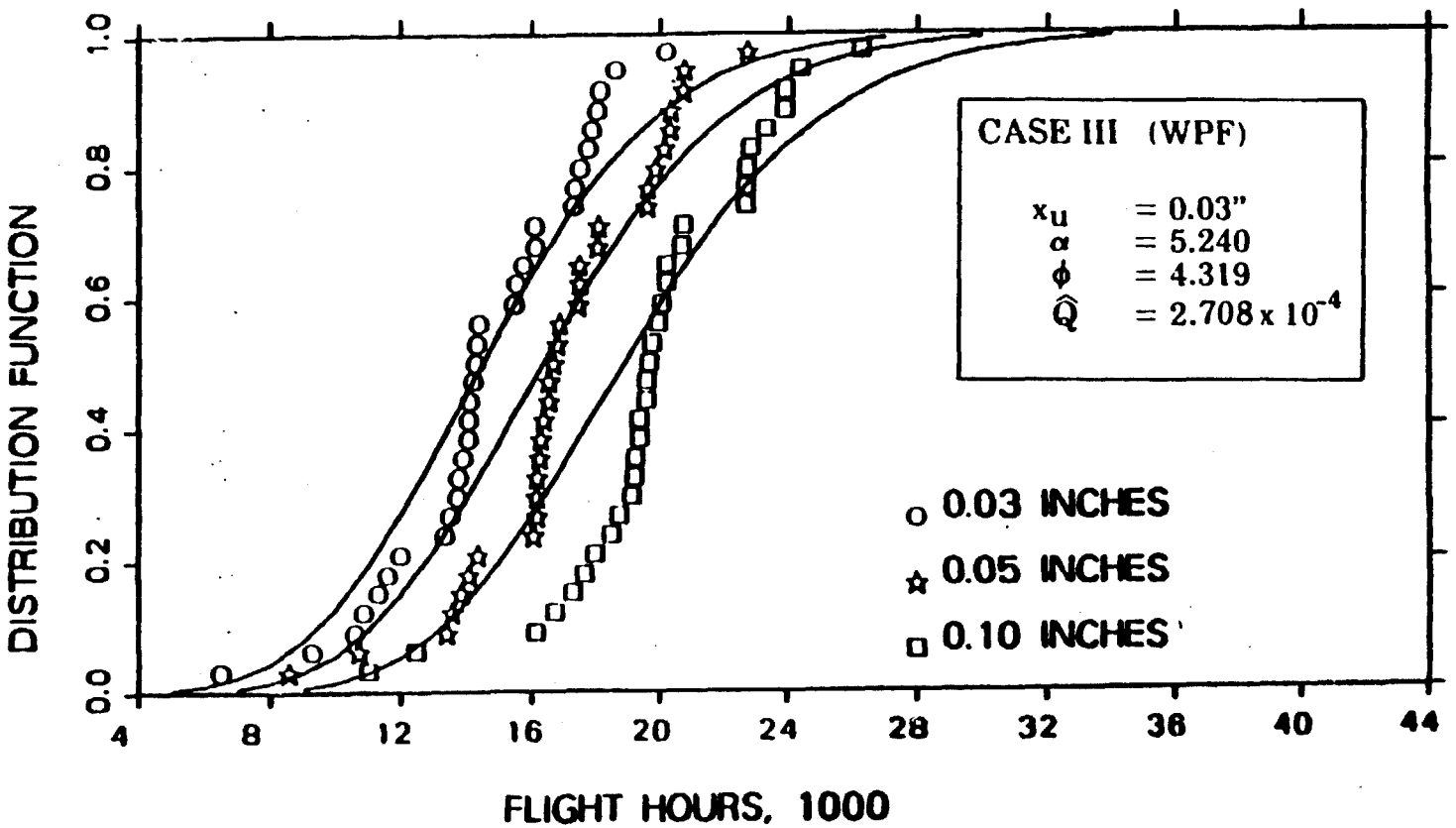

Figure 80: Correlation Between Predictions and Test Results for Cumulative Distribution of Time-to-Crack-Initiation at 0.03", 0.05", and 0.10" for WPF Data Set (Case III: Pooled EIFSs for WPF + WPB; Normalized Q Value)

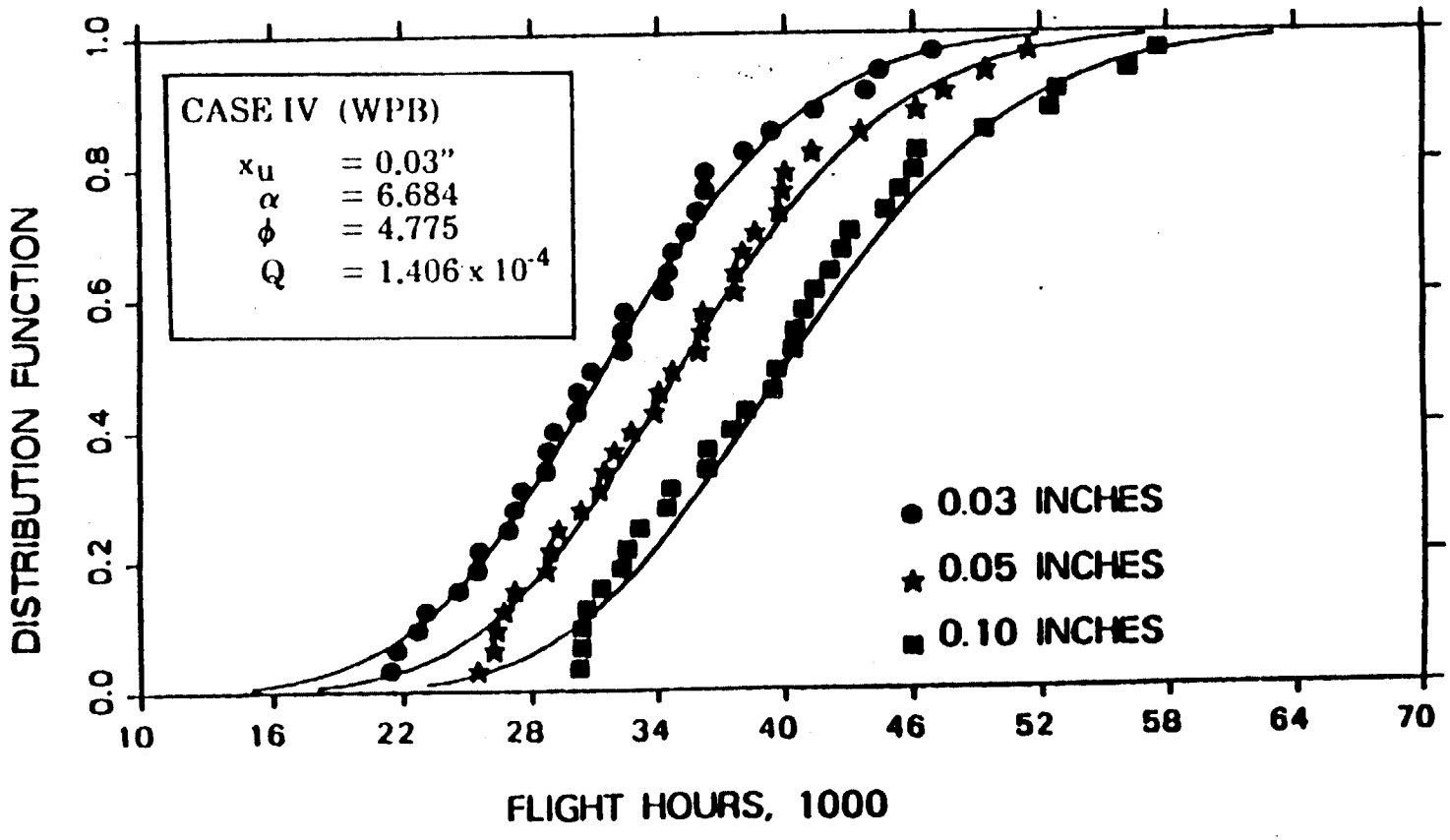

Figure 81: Correlation Between Predictions and Test Results for Cumulative Distribution of Time-to-Crack-Initiation at 0.03", 0.05", and 0.10" for WPB Data Set (Case IV: EIFSs for WPB; Un-normalized Q Value)

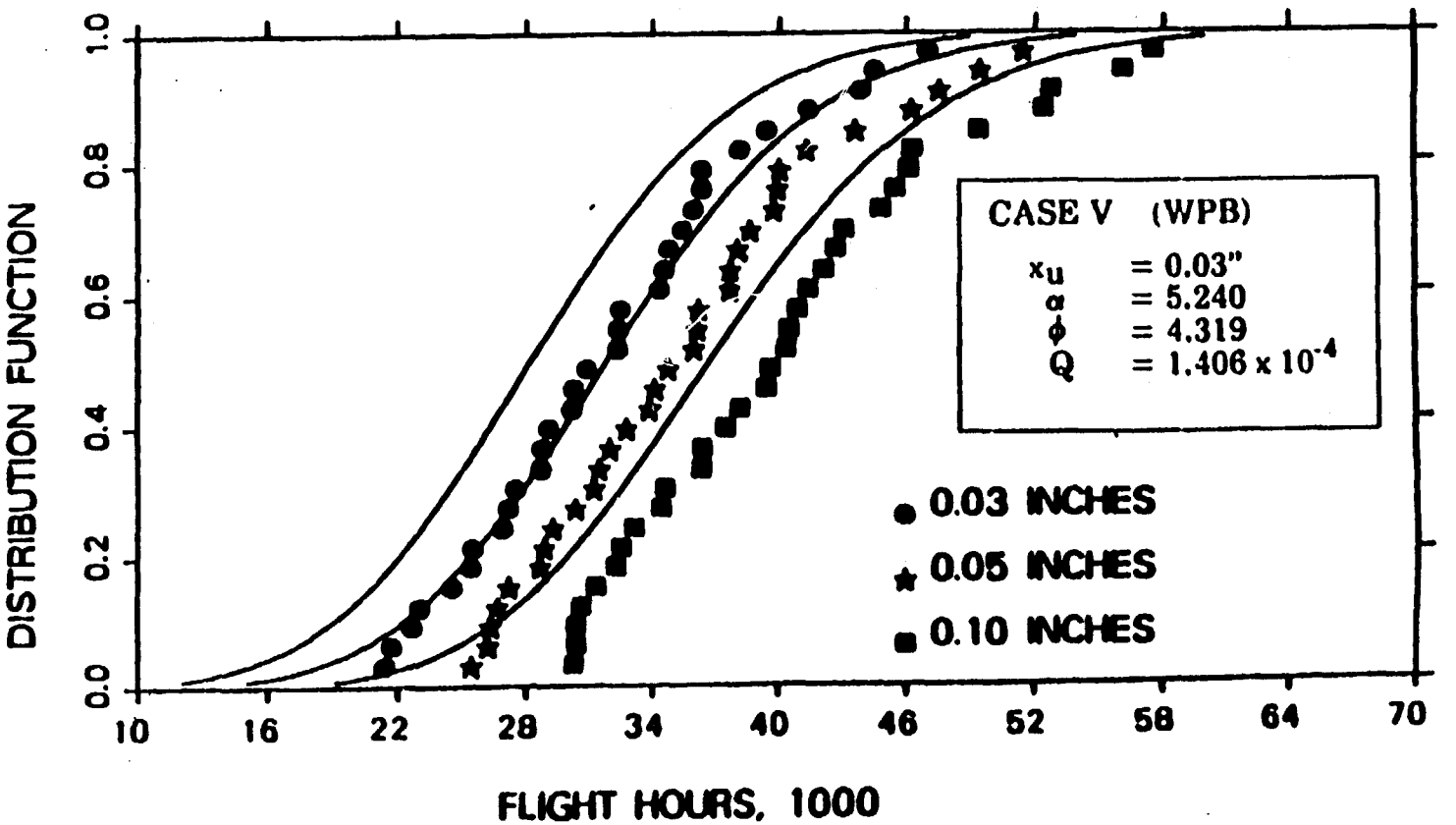

Figure 82: Correlation Between Predictions and Test Results for Cumulative Distribution of Time-to-Crack-Initiation at 0.03", 0.05", and 0.10" for WPB Data Set (Case V: EIFSs for WPF + WPB; Un-normalized Q Value)

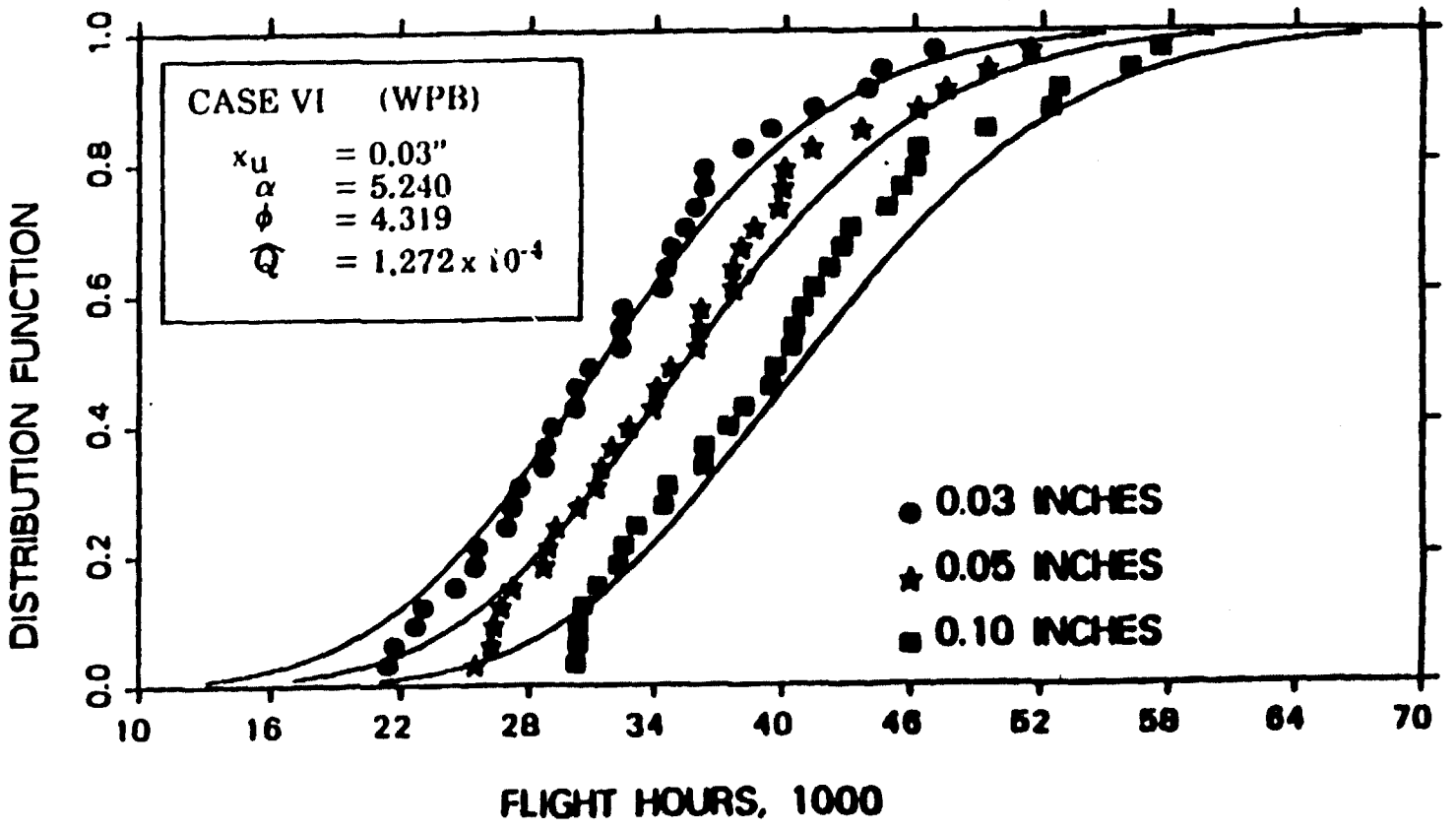

Figure 83: Correlation Between Predictions and Test Results for Cumulative Distribution of Time-to-Crack-Initiation at 0.03", 0.05", and 0.10" for WPB Data Set (Case VI: Pooled EIFSs for WPF + WPB; Normalized Q Value)

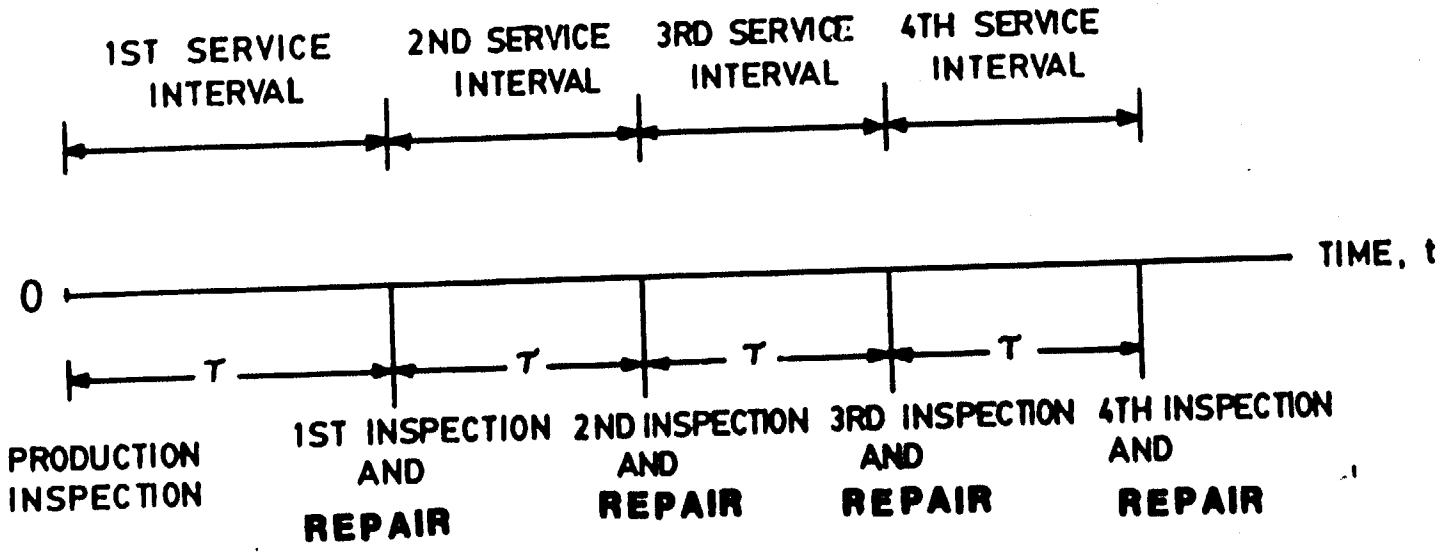

Figure 84: Scheduled Inspection Maintenance.

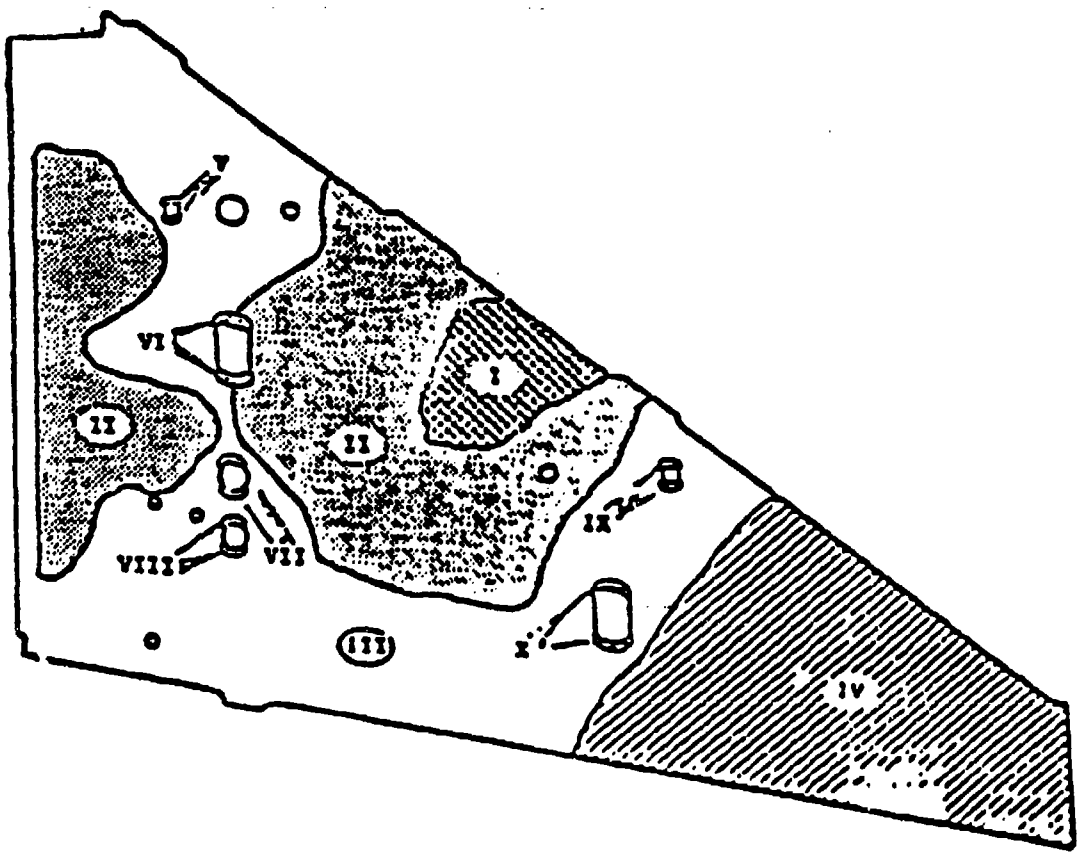

Figure 85: Stress Zones for F-16 Lower Wing Skin

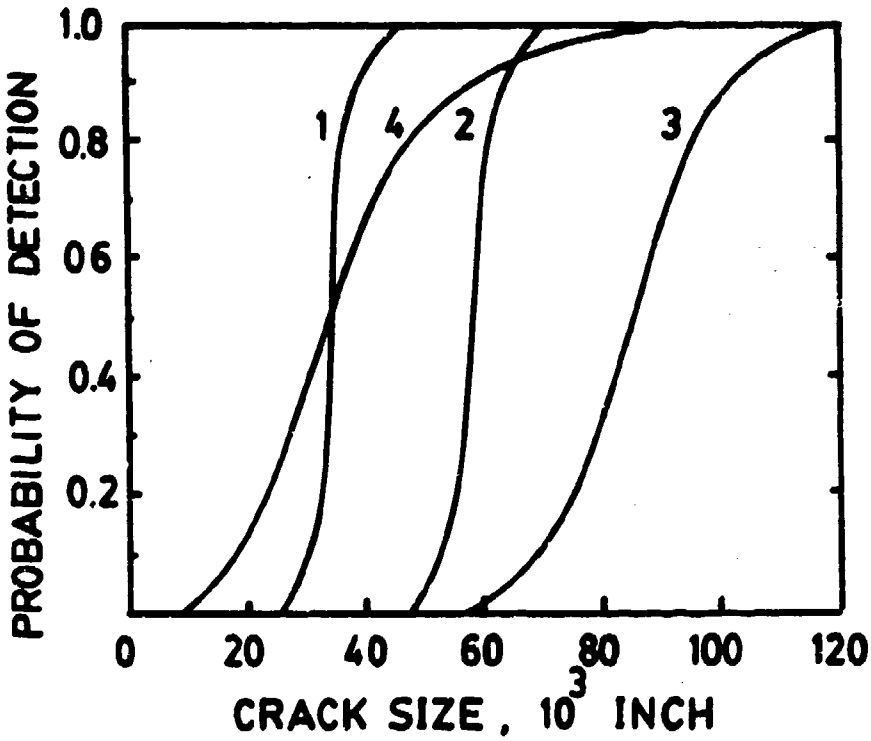

Figure 86: Various POD Curves for NDE System.

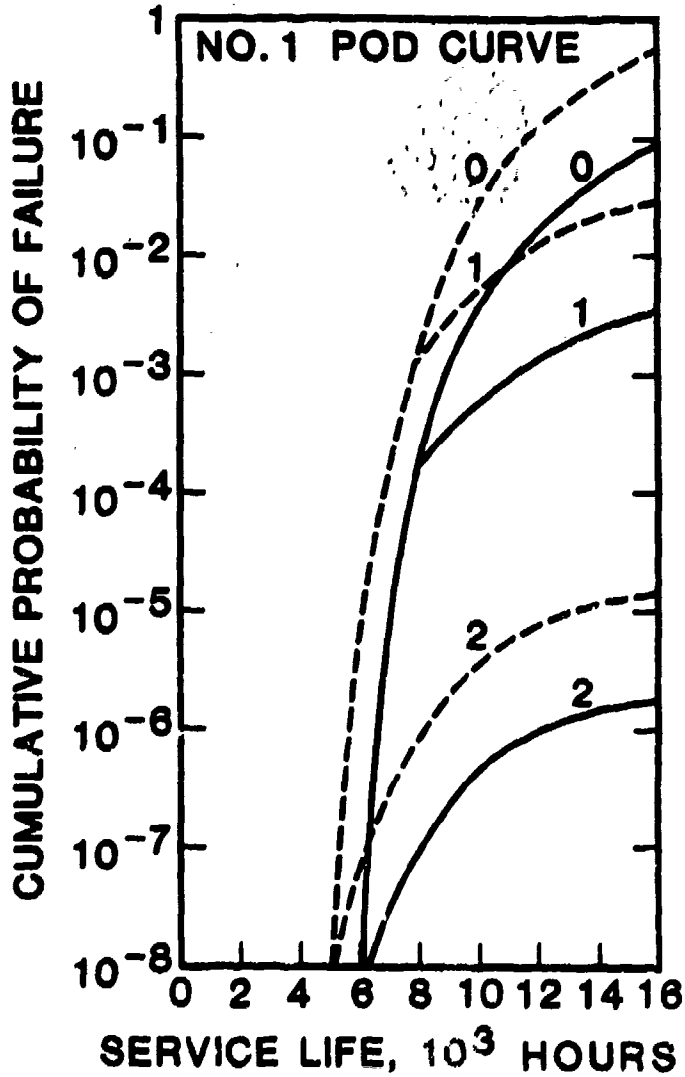

Figure 87: Cumulative Probability of Failure for F-16 Lower Wing Skin Component Using No. 1 POD Curve.

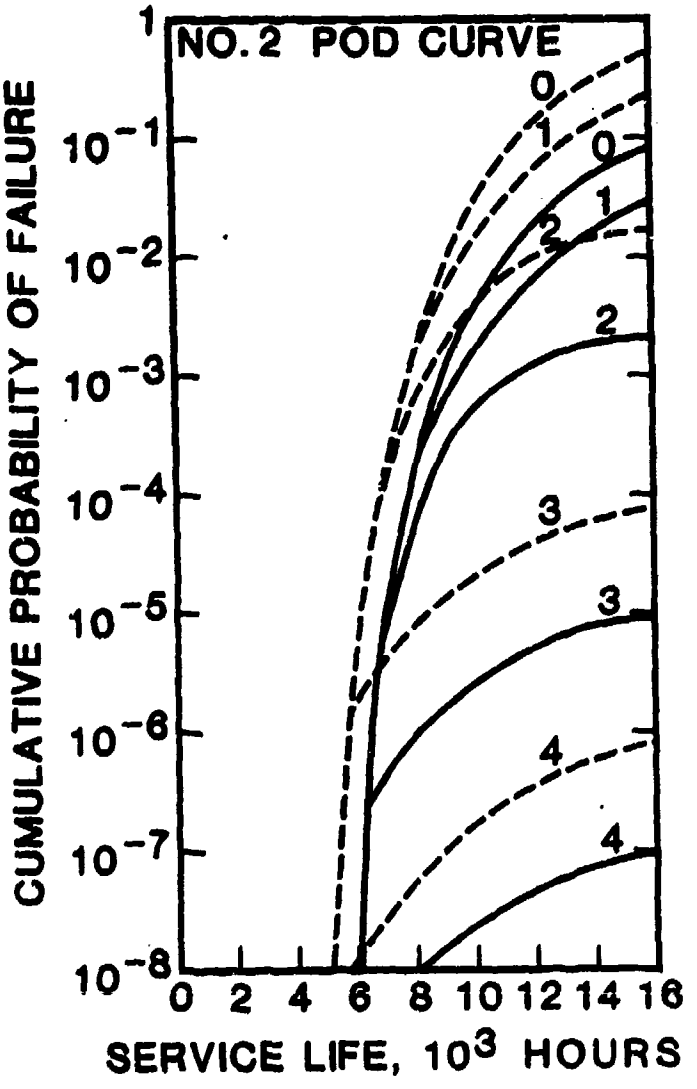

Figure 88: Cumulative Probability of Failure for F-16 Lower Wing Skin Component Using No. 2 POD Curve.

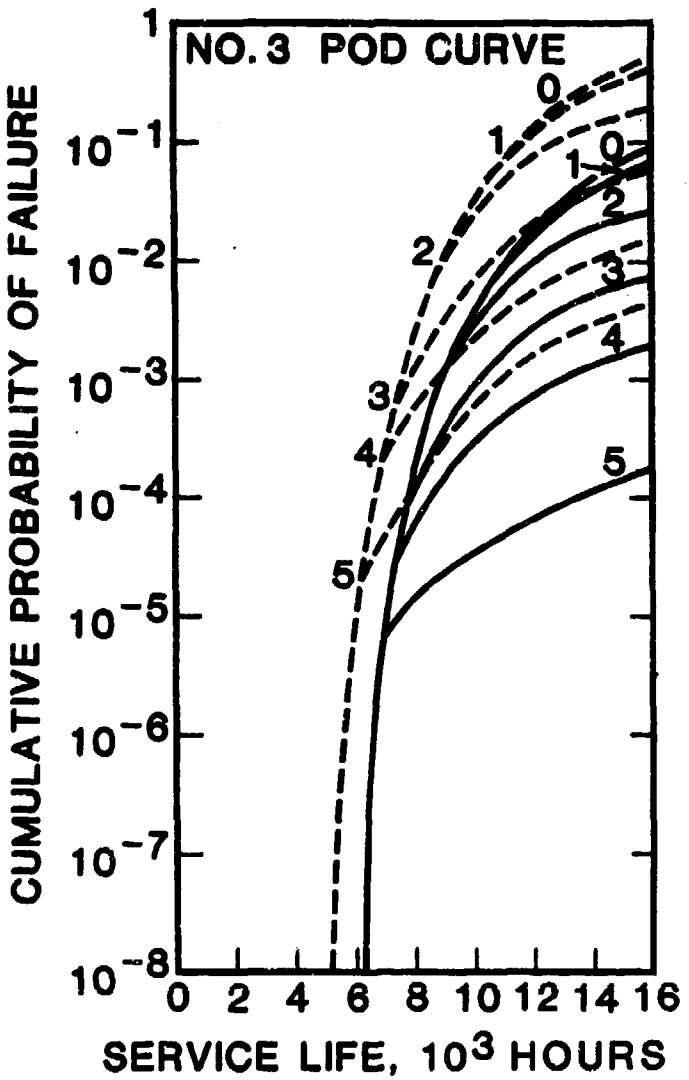

Figure 89: Cumulative Probability of Failure for F-16 Lower Wing Skin Component Using No. 3 POD Curve.

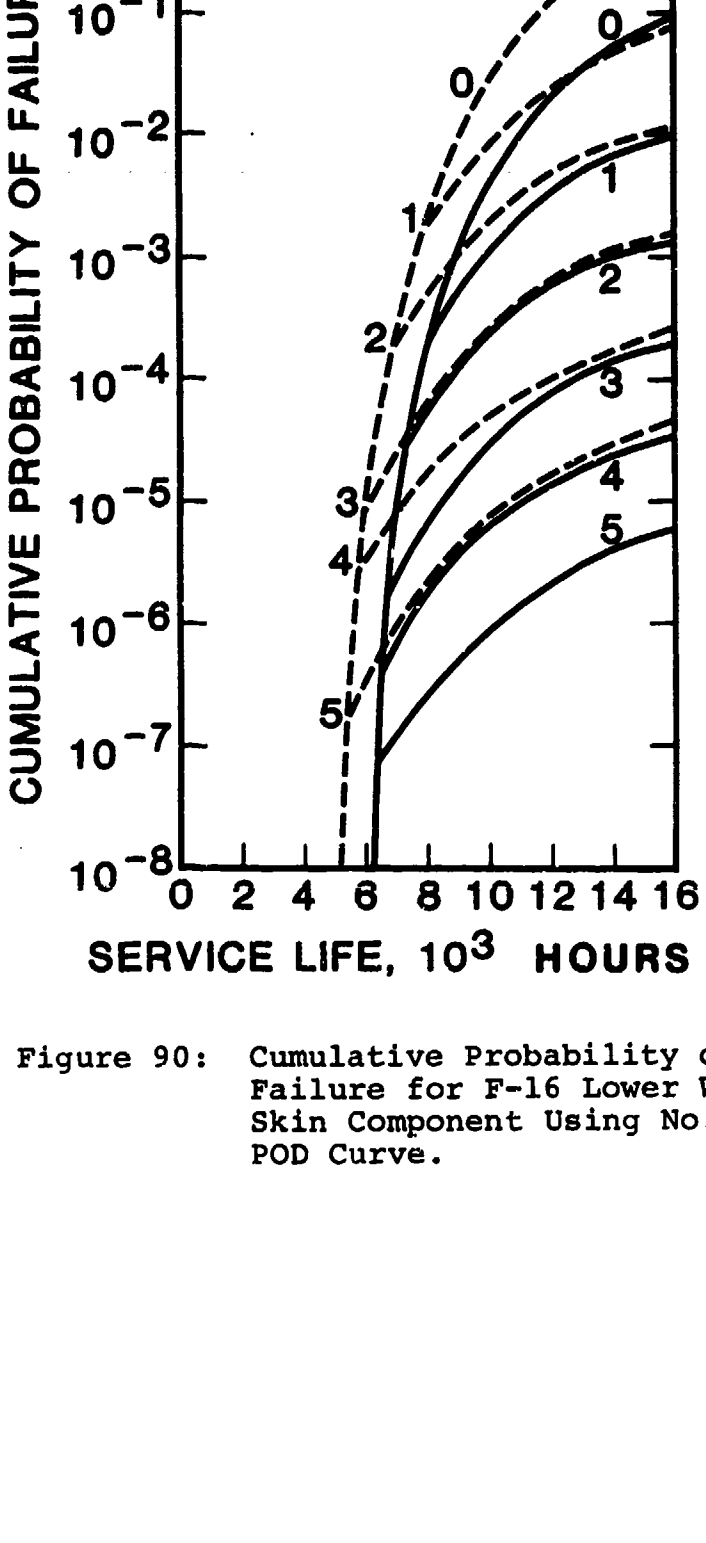

Figure 90: Cumulative Probability of Failure for F-16 Lower Wing Skin Component Using No. 4 POD Curve.

REFERENCES

1. Rudd, J. L., "Air Force Damage Tolerance Design Philosophy," Damage Tolerance of Metallic Structures: Analysis Methods and Applications, ASTM STP 842, J. B. Chang and J. L. Rudd, Eds., American Society for Testing and Materials, 1984, pp. 134-141.

2. "Aircraft Structural Integrity Program, Airplane Requirements," MIL-STD-1530A, Air Force Aeronautical Systems Division, Wright-Patterson Air Force Base, OH, Dec. 1975.

3. "Airplane Damage Tolerance Requirements," MIL-A-83444, Air Force Aeronautical Systems Division, Wright-Patterson Air Force Base, OH, July 1974.

4. MIL-A-8867B, "Airplane Strength and Rigidity Ground Tests," Air Force Aeronautical Systems Division, Wright-Patterson Air Force Base, OH, 22 August, 1975.

5. MIL-A-8866B, "Airplane Strength, Rigidity and Reliability Requirements; Repeated Loads and Fatigue," Air Force Aeronautical Systems Division, Wright-Patterson Air Force Base, OH, August 1975.

6. Manning, S. D. and Yang, J. N., "USAF Durability Design Handbook: Guidelines for Analysis and Design of Durable Aircraft Structures," Air Force Wright Aeronautical Laboratories, Technical Report AFWAL-TR-83-3027, Wright-Patterson Air Force Base, OH, January 1984.

7. Virkler, D.A., Hillberry, B. M., and Goel, P.K., "The Statistical Nature of Fatigue Crack Propagation," Journal of Engineering Materials and Technology, ASME, Vol. 101, 1979, pp. 148-153.

8. Virkler, D. A., Hillberry, B. M., and Goel, P. K., "The Statistical Nature of Fatigue Crack Propagation," Air Force Flight Dynamics Laboratory, Technical Report AFFDL-TR-78-43, Wright-Patterson Air Force Base, OH, 1978.

9. Oh, K. P., "A Diffusion Model for Fatigue Crack Growth," Proc. R. Soc. Lond. A367, 1979, pp. 47-58.

10. Kozin, F. and Bogdanoff, J.L., "A Critical Analysis of Some Probabilistic Models of Fatigue Crack Growth," Engng. Fracture Mech., 14, 1981, pp. 59-81.

11. Kozin, F. and Bogdanoff, J. L., "On the Probabilistic Modeling of Fatigue Crack Growth," Engng. Fracture Mech., 18 (3), 1983, pp. 623-632.

12. Bogdanoff, J. L. and Kozin, F., "Probabilistic Models of Fatigue Crack Growth-II," Engng. Fracture Mech., 20 (2), 1984, pp. 255-270.

13. Kozin, F. and Bogdanoff, J. L., "Probabilistic Fatigue Crack Growth and Design," ASME Failure Prevention and Reliability Conference, Dearborn, MI, 1983.

14. Hovey, P. W., Gallagher, J. P., and Berens, A.P., "Estimating the Statistical Properties of Crack Growth for Small Cracks," Engng. Fracture Mech., Vol. 18, No. 2, 1983, pp. 285-294.

15. Yang, J.N., "Statistics of Random Loading Relevant to Fatigue," Journal of Engineering Mechanics Division, ASCE, Vol. 100, No. EM3, June, 1974, pp. 469-475.

16. Yang, J. N., Salivar, G. C., and Annis, C. G., "Statistical Modeling of Fatigue Crack Growth in a Nickel-Based Super-alloy," Journal of Engineering Fracture Mechanics, Vol. 18, No. 2, June 1983, pp. 257-270.

17. Yang, J. N., and Donath, R.C., "Statistical Crack Growth of a Superalloy Under Sustained Loads," Journal of Materials and Technology, ASME, Vol. 106, Jan. 1984, pp. 79-83.

18. Lin, Y.K. and Yang, J. N., "On Statistical Moments of Fatigue Crack Propagation," Journal of Engineering Fracture Mechanics, Vol. 18, No.2, June 1983, pp. 243-256.

19. Lin, Y.K. and Yang, J.N., "A Stochastic Theory of Fatigue Crack Propagation," Proc. AIAA/ASME/ASCE/AHS Structures, Structural Dynamics and Materials Conf., May 2-4, 1983, Lake Tahoe, AIAA Paper No. 93-0978 CP, pp. 552-562 (Part 1); also AIAA Journal, Vol. 23, No. 1, Jan. 1985, pp. 117-124.

20. Lin, Y.K., Wu, W.F., and Yang, J.N., "Stochastic Modeling of Fatigue Crack Propagation," in Probabilistic Methods in Mechanics of Solids and Structures, edited by S. Eggwertz and N.C. Lind, Springer-Verlag, Berlin, Jan. 1985, pp. 559-568.

21. Yang, J.N. and Donath, [illegible] "Statistical Fatigue Crack Propagation in Fastener Hole Unde[illegible] Loading," Proc. AIAA/ASME/ASCE/AHS 24th Structures, Stru[illegible]gs and Materials Conf., May 2-4, 1983, Lake Tahoe, Al[illegible] 93-0808 CP, pp. 15-21 (Part 2); Journal of Aircraft, AIAA, Vol. 2[illegible]o. 12, Dec. 1983, pp. 1028-1032.

22. Yang, J.N. and Chen, [illegible] "Fat[illegible]iability of Gas Turbine Engine Components Under So[illegible]ection Maintenance," Proc. AIAA/ASME/ASCE/AHS 25th S[illegible]ructural Dynamics and Materials Conference, Palm Springs, [illegible],0-420, AIAA Paper No. 84-0850; Journal of Aircraft, AIAA, Vol. 22, No. 5, May 1985, pp. 415-422.

23. Yang, J.N. and Chen, S., "An Exploratory Study of Retirement-for-Cause for Gas Turbine Engine Components," Proc. AIAA/SAE/ASME 20th Joint Propulsion Conf., June 1984, Cincinnati, AIAA Paper No. 84-1220; to appear in Journal of Propulsion and Power, AIAA, Oct. 1985.

24. Yang, J.N. and Chen, S., "Fatigue Reliability of Structural Components Under Scheduled Inspection and Repair Maintenance," in Probabilistic Methods in Mechanics of Solids and Structures, edited by S. Eggwertz and N.C. Lind, Springer-Verlag, Berlin, Jan. 1985, pp. 103-110.

25. Yang, J.N., Salivar, G.C., and Annis, C.G., "Statistics of Crack Growth in Engine Materials - Vol. 1: Constant Amplitude Fatigue Crack Growth at Elevated Temperatures," Air Force Wright Aeronautical Laboratories, Technical Report AFWAL-TR-83-4040, Wright-Patterson Air Force Base, OH, June 1982.

26. Yang, J.N., et al., "Statistics of Crack Growth in Engine Materials - Vol. 2: Spectrum Loading and Advanced Technique," Air Force Wright Aeronautical Laboratories, Technical Report AFWAL-TR-83-4040, Wright-Patterson Air Force Base, OH, February 1984.

27. Itagaki, H. and Shinozuka, M., "Application of the Monte Carlo Technique to Fatigue-Failure Analysis Under Random Loading," Probabilistic Aspect of Fatigue, ATM-STP 511, 1972, pp. 168-184.

28. Yang, J.N., Manning, S.D., Rudd, J.L., and Hsi, W.H., "Stochastic Fatigue Crack Propagation in Fastener Holes," Proc. of 26th AIAA/ASME/ASCE/AHS Structures, Structural Dynamics and Materials Conf., Florida, April 1985, pp. 225-233, AIAA paper No. 85-0666; Journal of Aircraft, AIAA, Vol. 22, No. 9, Sept. 1985, pp. 810-817.

29. Hudak, S.J., Jr., Saxena, A., Bucci, R.J., and Malcolm, R.C., "Development of Standard Methods of Testing and Analyzing Fatigue Crack Growth Rate Data," AFML-TR-78-40, Air Force Materials Laboratory, May 1978.

30. Clark, W.G., Jr. and Hudak, S.J., Jr., "Variability in Fatigue Crack Growth Rate Testing," ASTM E-24.04.01 Task Group Report, Sept. 1974.

31. Wei, R.P., Wei, W., and Miller, G.A., "Effect of Measurement Precision and Data-Processing Procedures on Variability in Fatigue-Crack Growth-Rate Data," J. Testing and Evaluation, Vol. 7, No. 2, March 1979.

32. Ostergaard, D.F., Thomas, J.R., and Hillberry, B.M., "Effect of the Δa Increment on Calculating da/dN from a Versus N Data," Fatigue Crack Growth Measurement and Data Analysis, ASTM STP 738, American Society for Testing and Materials, 1981.

33. Ostergaard, D.F. and Hillberry, B.M., "Characterization of Variability in Fatigue Crack Propagation Data," ASTM STP 798, 1983, American Society for Testing and Materials, pp. 97-115.

34. Clark, W.G., Jr. and Hudak, S.J., Jr., Journal of Testing and Evaluation, Vol. 3, No. 6, 1975, pp. 454-476.

35. Fong, J.T. and Dowling, N.E., "Analysis of Fatigue Crack Growth Rate Data from Different Laboratories," Fatigue Crack Growth Measurement and Data Analysis, ASTM STP 738, 1981, pp. 171-193.

36. Dowling, N.E. and Walker, H., "Fatigue Crack Growth Rate Testing of Two Structural Steels," SAE Transaction, Society of Automotive Engineers, 1979, Paper 790459. Computer program for implementing incremental polynomial methods.

37. Miller, M.S. and Gallagher, G.P., "An Analysis of Several Fatigue Crack Growth Rate Descriptions," Measurement and Data Analysis, ASTM-STP 738, 1981, pp. 205-251.

38. Hoeppner, D.W. and Krupp, W.E., "Prediction of Component Life by Application of Fatigue Crack Knowledge," Engng. Fracture Mech., Vol. 6, 1974, pp. 47-70.

39. Yusuff, S., "Propagation Laws of Fatigue Cracks," Proceedings of AIAA/ASME 10th Structures, Structural Dynamics and Material Conference, New Orleans, LA, 14-16 April 1969, pp. 429-437.

40. Bluham, J.I., "Crack Propagation Laws," in Fracture Mechanics of Aircraft Structure, AGARD-AG-176, January 1974, pp. 95-109.

41. Paris, P.C. and Erdogan, F., "A Critical Analysis of Crack Propagation Laws," J. of Basic Engineering, Trans ASME, Series D, 85, No. 3, 1963.

42. Forman, R.G., Kearny, V.E. and Engle, R.M., "Numerical Analysis of Crack Propagation in Cyclic Loaded Structures," J. of Basic Engr., Trans. ASME, September 1967, pp. 459-464.

43. Yang, J.N., "Statistical Estimation of Economic Life for Aircraft Structures," Proc. of AIAA/ASME/ASCE/AHS 20th Structures, Structural Dynamics and Materials Conf., 1979, pp. 238-240; also Journal of Aircraft, AIAA, Vol. 17, No. 7, July 1980, pp. 528-535.

44. Yang, J.N. and Manning, S.D., "Distribution of Equivalent Initial Flaw Size," Proc. Reliability and Maintainability Conf., Jan. 1980, pp. 112-120.

45. Rudd, J.L., Yang,J.N., Manning, S.D., and Garver, W.R., "Durability Design Requirements and Analysis for Metallic Airframe," in Design of Fatigue and Fracture Resistant Structures, ASTM-STP 761, American Society for Testing and Materials, 1982, pp. 133-151.

46. Rudd, J.L., Yang, J.N., Manning, S.D., and Yee, B., "Probabilistic Fracture Mechanics Analysis Methods of Structural Durability," AGARD Specialists Conf. No. 328, Behavior of Short Cracks in Airframe Components, Sept. 19-24, 1982, Toronto, Canada, pp. 10-1 to 10-23.

47. Rudd, J.L., Yang, J.N., Manning, S.D., and Yee, G.W., "Damage Assessment of Mechanically Fastened Joints," Proc. of 9th U.S. Congress of Applied Mechanics, June 21-25, 1982.

48. Noronha, P. J., et al., "Fastener Hole Quality," Vols. I and II, Air Force Flight Dynamics Lab., AFFDL-TR-78-206, Wright-Patterson Air Force Base, OH, 1978.

49. Gordon, D.E., et al., "Development of Fatigue and Crack Propagation Design and Analysis Methodology in a Corrosive Environment, Vol. IV - Phase II Test and Fractographic Results," Naval Air Development Center, Report No. NADC-83126-60-Vol IV, August 1984.

50. Crandell, S.H. and Mark, W.D., Random Vibration in Mechanical Systems, Academic Press, New York, 1974.

51. Lin, Y.K. Probabilistic Theory of Structual Dynamics, R.E. Krieger Publishing Co. N.Y. 1976.

52. Ang, A.H.S., and Tang, d., Probabilistic Concepts in Engineering Planning and Design, Vol. 1: Basic Principles, John Wiley & Sons, Inc. New York, 1975.

53. Hahn, G.J., and Shapiro, S.S., Statistical Models in Engineering, John Wiley & Sons, Inc., New York, 1967.

54. Yang, J.N., "On the Normality and Accuracy of Simulated Random Processes," Journal of Sound and Vibration, Vol. 16, No. 13, 1973, pp. 417-428.

55. Yang, J.N., "Simulation of Random Envelope Processes," Journal of Sound and Vibration, Vol. 21, No. 1, 1972, pp. 73-85.

56. Manning, S.D., Yang, J.N., Shinozuka, M., and Garver, W.R., "Durability Methods Development, Volume I - Phase I Summary," Air Force Flight Dynamics Lab., AFFDL-TR-79-3118, September 1979.

57. Manning. S.D., Flanders, M.A., Garver, W.R., and Kim, Y.H., "Durability Methods Development, Volume II, Durability Analysis: State of the Art Assessment," Air Force Flight Dynamics Lab., AFFDL-TR-79-3118, September 1979.

58. Pendley, B.J., Henslee, S.P., and Manning, S.D., "Durability Methods Development, Volume III, Structural Durability Survey: State-of-the-Art Assessment," Air Force Flight Dynamics Lab., AFFDL-TR-79-3118, September 1979.

59. Shinozuka, M., "Durability Methods Development, Volume IV - Initial Quality Representation, " Air Force Flight Dynamics Lab., AFFDL-TR-79-3118, September 1979.

72. Eggwertz,S., and Lindsjo, G., "Influence of Detected Crack Length at Inspections on Probability of Fatigue Failure of Wing Panel," Tech. Note HU-1745, Part 2, ICAF No. 834, 1975.

73. Davidson, J.R., "Reliability After Inspection", in Fatigue of Composite Materials, ASTM STP-569. 1975, pp. 323-334.

74. Davidson, J.R., "Reliability and Structural Integrity," 10th Anniversary Meeting of The Society of Engineering Science, Rayleigh, N.C. 1973.

75. Yang, J.N., and Trapp, W.J., "Reliability Analysis of Aircraft Structures Under Random Loading and Periodic Inspection", AIAA Journal, Vol. 12, No. 12, 1974, pp. 1623-1630.

76. Yang, J.N. and Trapp, W.J., "Inspection Frequency Optimization for Aircraft Structures Based on Reliability Analysis," Journal of Aircraft, AIAA, Vol. 12, No. 5, 1975, pp. 494-496.

77. Yang, J.N.," Reliability Analysis of Structures Under Periodic Proof Test in Service," AIAA Journal, Vol. 14, No. 9, September 1976, pp. 1225-1234.

78. Yang, J.N., "Optimal Periodic Proof Test Based on Cost-Effective and Reliability Criteria," AIAA Journal, Vol. 15, No.3, March 1977, pp. 402-409.

79. Yang, J.N. and Donath, R.C., "Improving NDE Capability Through Multiple Inspections With Application to Gas Turbine Engine," Air Force Wright Aeronautical Lab., Tech. Report AFWAL-TR-82-4111, WPAFB, OH, August 1982.

80. Berens, A.P. and Hovey, P.W., "Evaluation of NDE Reliability Characterization," Air Force Wright Aeronautical Lab. Report AFWAL-TR-81-4160, WPAFB, OH, Nov. 1981.

81. Yang, J.N., "Statistical Estimation of Service Cracks and Maintenance Cost for Aircraft Structures," Journal of Aircraft, AIAA, Vol. 13, No. 12, Dec. 1976, pp. 929-937.

82. Lincoln, J.W., "Risk Assessment of an Ageing Military Aircraft," Proc. AIAA/ASME/ASCE/AHS 25th Structures, Structural Dynamics and Materials Conf., AIAA paper No. 84-0851-CP, 1984.